THEORETICAL STUDY OF THERMAL REARRANGEMENTS OF 2-ALKYLIDENECYCLOPENTA-1,3-DIYL BIRADICALS

A THESIS SUBMITTED TO
THE GRADUATE SCHOOL OF NATURAL AND APPLIED SCIENCES
OF
MIDDLE EAST TECHNICAL UNIVERSITY

BY

UĞUR BOZKAYA

IN PARTIAL FULFILLMENT OF THE REQUIREMENTS
FOR
THE DEGREE OF DOCTOR OF PHILOSOPHY
IN
CHEMISTRY

JUNE 2011

Approval of the thesis:

THEORETICAL STUDY OF THERMAL REARRANGEMENTS OF 2-ALKYLIDENECYCLOPENTA-1,3-DIYL BIRADICALS

submitted by **UĞUR BOZKAYA** in partial fulfillment of the requirements for the degree of **Doctor of Philosophy in Chemistry Department, Middle East Technical University** by,

Prof. Dr. Canan Özgen _____
Dean, Graduate School of **Natural and Applied Sciences**

Prof. Dr. İlker Özkan _____
Head of Department, **Chemistry**

Prof. Dr. İlker Özkan _____
Supervisor, **Chemistry Department, METU**

Examining Committee Members:

Prof. Dr. Şakir Erkoç
Physics Department, METU _____

Prof. Dr. İlker Özkan
Chemistry Department, METU _____

Prof. Dr. Lemi Türker
Chemistry Department, METU _____

Assist. Prof. Dr. M. Fatih Danışman
Chemistry Department, METU _____

Dr. Yavuz Dede
Chemistry Department, Gazi University _____

Date: _____

I hereby declare that all information in this document has been obtained and presented in accordance with academic rules and ethical conduct. I also declare that, as required by these rules and conduct, I have fully cited and referenced all material and results that are not original to this work.

Name, Last Name: UĞUR BOZKAYA

Signature :

ABSTRACT

THEORETICAL STUDY OF THERMAL REARRANGEMENTS OF
2-ALKYLIDENECYCLOPENTA-1,3-DIYL BIRADICALS

Bozkaya, Uğur
Ph.D., Department of Chemistry
Supervisor : Prof. Dr. İlker Özkan

June 2011, 205 pages

Thermal rearrangements of Berson TMMs have been investigated. For this purpose, the potential energy surface of the singlet **S** state has been explored to test Benson's Schemes 1-2 (Figure 1.10 and 1.11). It is verified that the enyne **9c** plays a central role in connecting the two portions of the reaction path (Berson Schemes 1 and 2). Connectivity of successive minima on a given surface has been verified by intrinsic reaction coordinate (IRC) computations. Density functional theory (DFT) and multiconfiguration self consistent field (MCSCF) methods have been employed for these purposes. Further, single point coupled-cluster singles and doubles with perturbative triples (CCSD(T)) energy computations have been carried out at optimized DFT or MCSCF geometries. All transition states (TS) connecting each neighboring minimum have been located in the proposed mechanisms. It is concluded that the proposed mechanisms are confirmed by the theoretical calculations. The computed activation energy and enthalpy of reaction values are in good agreement with the available experimental values, only differing by a few kcal mol^{-1}.

Keywords: Trimethylenemethane, TMM, Berson TMM, Biradical, DFT, MCSCF, CCSD

ÖZ

2-ALKİLİDENSİKLOPENTA-1,3-DİİL BİRADİKALERİNİN TERMAL ÇEVRİLMELERİNİN TEORİK ÇALIŞMASI

Bozkaya, Uğur
Doktora, Kimya Bölümü
Tez Yöneticisi : Prof. Dr. İlker Özkan

Haziran 2011, 205 sayfa

Berson TMM lerinin termal çevrilmeleri incelendi. Bu amaç doğrultusunda, Bersonun 1 ve 2 nolu mekanizmalarını test etmek için singlet **S** halinin potansiyel enerji yüzeyi araştırıldı. Enin **9c** molekülünün reaksiyonun iki kısmını birbirine bağlayıcı merkezi bir rol oynadığı doğrulandı. Ardışık minimumların bağlantıları doğal reaksiyon koordinatı (IRC) hesaplamalarıyla doğrulandı. Yoğunluk fonksiyoneli teorisi (DFT) ve çoklu konfigürasyonlarda SCF (MCSCF) yöntemi bu amaç için kullanıldı. Ayrıca, optimize DFT ya da MCSCF geometrilerinde CCSD(T) düzeyinde tek nokta hesaplamaları yapıldı. Önerilen mekanizmalardaki komşu minimumları birbirine bağlayan bütün geçiş halleri bulundu. Hesaplanan reaksiyon ve aktivasyon enerjileri mevcut deneysel sonuçlarla uyum içindedir, sadece bir kaç kcal/mol fark vardır.

Anahtar Kelimeler: Trimetilenmetan, TMM, Berson TMM, Biradikal, DFT, MCSCF, CCSD

To my wife Tuğba...

ACKNOWLEDGMENTS

I would like to express my sincere appreciation to Prof. Dr. İlker Özkan for his continuous advice, criticism, support, and guidance thought this research. I am deeply impressed by his scientific point of view, criticism, and interpretation.

I would like to thank to Prof. Dr. Tuncer Çaykara for his advice and guidance since I was an undergraduate student.

I would like to thank to Prof. Dr. Lemi Türker for his helps, suggestions, and comments.

I would like to thank to Prof. Dr. Şakir Erkoç for his helps, suggestions, and comments.

I would like to thank to Assist. Prof. Dr. M. Fatih Danışman for his helps, suggestions, and comments.

I thank to all past and present members of the Computational Chemistry Laboratory for their friendship and moral support. Especially, Dr. Yavuz DEDE is gratefully acknowledged.

I would like to thank the Scientific and Technological Research Council of Turkey (TÜBİTAK) for supporting my scientific studies at the University of Georgia and Middle East Technical University.

TABLE OF CONTENTS

LIST OF TABLES

TABLES

LIST OF FIGURES

FIGURES

CHAPTER 1

INTRODUCTION

During the last forty five years, the thermal chemistry of the C_6H_8 chemical system have been investigated in considerable detail. Portions of the ground state electronic potential energy surface (PES) of the system has been explored experimentally using thermolyses techniques. Several of the minima on the PES correspond to interesting biradical intermediates, one of which is a trimethylenemethane (TMM) derivative. Below is a brief overview of the thermal isomerizations of the parent TMM molecule, and many different species belonging to the C_6H_8 system.

1.1 Parent Trimethylenemethanes (TMM)

It is rare in hydrocarbon chemistry to encounter intermediates that are kinetically stable, and yet can not be represented by classical resonance structures due to their lacking at least one bond from the number predicted by standard rules of valence. Because of this they are called non-Kekule molecules [1-3]. Reactive intermediates arising from substituted methylenecyclopropanes (MCP) are such molecules, often referred to as trimethylenemethanes (TMMs) [4-8]. Bonding pattern of TMM is shown below.

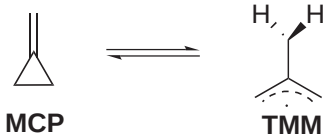

Figure 1.1: Ring opening reaction of MCP leading to (orthogonal) TMM.

Trimethylenemethane (TMM) is one of the most popular organic intermediates which has

been studied both experimentally [9-21] and theoretically [22-47]. Experimental identification of TMM from the photolysis of 4-methylene-1-pyrazoline was reported by Dowd [9] in 1966. The electron spin resonance (ESR) spectrum of TMM indicated that the ground state of TMM is triplet. The confirmation of the triplet ground state was accomplished in 1976 [10].

1.1.1 Methylenecyclopropane Degenerate Rearrangement

A number of experimental studies were carried out in order to investigate methylenecyclopropane degenerate rearrangements [3]. Methylenecyclopropane (MCP) is surprisingly stable upon heating. However, at temperatures above 150 °C, substituted MCPs exhibit a degenerate isomerization which interchanges ring and exomethylene carbons, a reaction which would appears to involve the trimethylenemethane (TMM) biradical

In 1962, Chesick [48] measured the activation energy for the reversible isomerization of 2-methyl-MCP to ethylidenecyclopropane (Figure 1.2) as 40.4 kcal mol^{-1}. In a 1986 study, LeFevre and Crawford [49] determined that the activation energy and enthalpy for the isomerization of dideuteriomethylenecyclopropane to methylenecyclopropane-2,2-d_2 (Figure 1.3) as 41.2±0.8 and 40.5±0.8 kcal mol^{-1}, respectively.

Figure 1.2: Isomerization of 2-methyl-MCP to ethylidenecyclopropane.

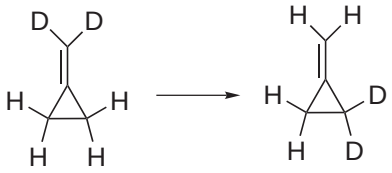

Figure 1.3: Dideuteriomethylenecyclopropane to methylenecyclopropane-2,2-d_2.

1.1.2 The Electronic Structure of Parent TMMs

The simple Hückel method predicts a triplet ground state for TMM as long as its electronic structure is characterized by two degenerate frontier molecular orbitals (FMO's) (Figure 1.4).

For planar D_{3h} geometry, ground state of TMM is $^3A_2'$. If one retains planar D_{3h} geometry, but descends the point group to be C_{2v}, the ground state will be designed as $^3B_2$. Occupation of two degenerate orbitals will yield several different singlet states. One of these states is formed by double occupation of one of two degenerate orbitals to create a planar closed-shell singlet, which can be stabilized by a Jahn-Teller [50] distortion. Another is formed by occupation of two degenerate orbitals separately in order to create a planar open-shell singlet, which can be stabilized by a different Jahn-Teller distortion. Finally, a 90° rotation of one methylene group yields a C_{2v} structure. This picture is summarized in Figure 1.5.

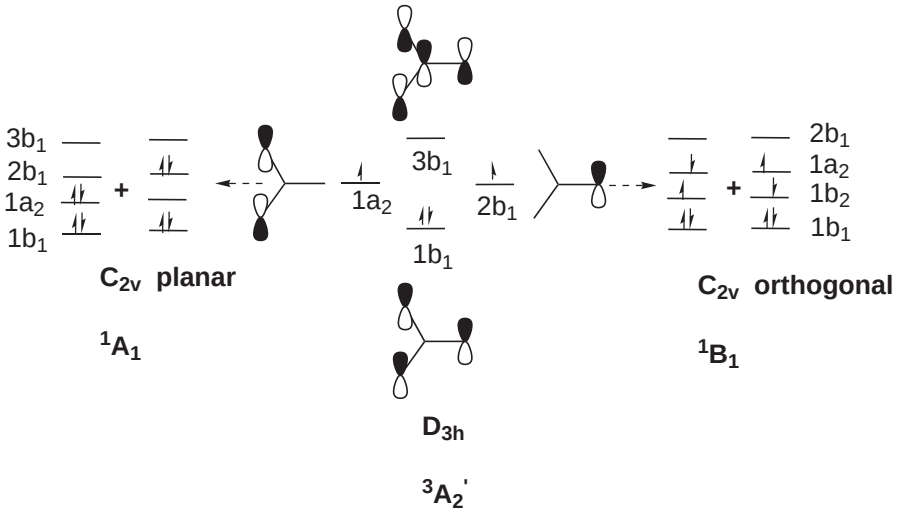

Figure 1.4: The π-system of TMM and the electronic configurations of the three lowest states. C_{2v} labels are used at the ground state equilibrium geometry (D_{3h}) of the triplet state, where the $1a_2$ and $2b_1$ orbitals are two degenerate e' components. Two different distortions can lift the degeneracy between these orbitals (and the two lowest excited states, i.e., $^1A_1$ and $^1B_1$). One is a C_{2v} distortion, which leaves the molecule planar, whereas another involves a 90° rotation of one of the CH_2 groups. The former distortion stabilizes the $1a_2$ orbital and the closed-shell $^1A_1$ singlet state (shown on the left) whereas the latter favors the $2b_1$ orbital and the open-shell $^1B_1$ singlet state (shown on the right). Note that at the orthogonal C_{2v} geometry, the b_1 and b_2 labels interchange.

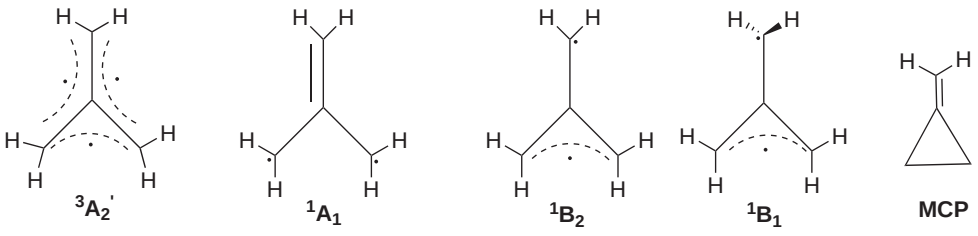

Figure 1.5: Qualitative structures of TMMs and MCP.

A great deal of theoretical computations have been carried out in order to predict relative energies and define nature of each TMM whether it is a minimum or a transition state or whatever. Most of early computations [22-38] predicted that both $^1B_1$ and $^1A_1$ states are minima on the potential energy surface, and that $^1B_1$ state is lower in energy than $^1A_1$ state. Borden and Davidson [26] estimated that the planar $^1B_2$ state is a transition state for the pseudorotation of the $^1A_1$ state. Furthermore, Davis and Goddard [24] predicted that the $^1B_2$ state is unstable with respect to rotation of one of the methylene units to form a stable, nonplanar $^1B_1$ state. Therefore, the $^1B_2$ state of TMM is a maximum in two coordinates on the potential energy surface (a "*mountain top*"). The computations of Borden [41] at the (4*e*,4*o*)MCSCF/6-31G* level of theory suggest that $^1A_1$ TMM is a saddle point that connects two equivalent C_2 states. Each C_2 state is a transition state that exchanges the out-of-plane methylene with a planar methylene in the $^1B_1$ state. However, the imaginary frequency at this level of theory is only 70*i*. At the (10*e*,10*o*)MCSCF/cc-pVTZ levels of theory, Cramer's computations [38] estimated that $^1A_1$ state is a minimum, $^1B_1$ state is a transition structure. The eigenvector that is associated with this frequency pyramidalizes the rotated methylene. Cramer was able to find a minimum for pyramidalized structure. The extent of pyramidalization is small only 10° away from C_{2v} geometry.

The energy difference between the singlet and triplet states of TMM (the "*singlet-triplet splitting*") has been of considerable interest. Dowd's experiments [12, 13] indicated that the energy separation between lowest singlet and triplet states was 7.8±0.3 kcal mol^{-1}. In that experiment Dowd measured the temperature dependence of the rate of disappearance of the ESR signal for the matrix isolated triplet biradical. If it is assumed that the rate determining step for the signal loss is intersystem crossing, then the measured activation energy can be equated with the singlet-triplet splitting. However, early computational studies [22-37] predicted the energy difference between the $^3A_2'$ and $^1B_1$ states to be 15-20 kcal mol^{-1}. Cramer's computations [38] at the (10*e*,10*o*)CASPT2N/cc-pVTZ level suggested that the energy difference between the $^3A_2'$ and $^1B_1$ states was 16.1 kcal mol^{-1}, and $^1B_1$ state was 3 kcal mol^{-1} lower in energy than $^1A_1$ state. Thus, Dowd's experiments led to a disagreement between experimental and theoretical results. A number of theoretical studies was carried out to understand the controversy. Davidson [32] pointed out that the experimentally measured value of 7.8±0.3 kcal mol^{-1} may not correspond to singlet-triplet splitting of $^3A_2'$ and $^1B_1$ state. Instead, the disappearance of the ESR signal may be arising from the closure to MCP by crossing of the

triplet to the singlet surface.

Photoelectron spectroscopy (PS) of the TMM radical anion has suggested that $^1A_1$ state lies 16.1 kcal mol^{-1} above the triplet ground state. The $^1B_1$ state was not observed in the photoelectron spectrum due to the fact that Frank-Condon overlap was insufficient to observe $^1B_1$ state spectroscopically [19-21].

1.2 Berson Trimethylenemethanes (Berson-TMMs)

Due to their unusual electronic structures, TMM derivatives have been extensively studied both experimentally [2,4-8,31,51-61] and theoretically [30, 45, 62, 63]. In particular spectroscopic and chemical experiments with monocyclic TMM derivatives by Berson's group at Yale University have been instrumental in raising our understanding of TMMs to a high level [6-8]. The singlet-triplet energy splitting (ΔE_{S-T}) of other TMMs have not been experimentally measured. However, thermochemical estimates indicate that the singlet-triplet energy spacing in TMM derivatives does not differ by more than several kcal mol^{-1} from that in the parent TMM [6].

1.2.1 Singlet-Triplet Energy Splitting of Berson TMMs

Berson *et al.* [54] published their experimental estimation of singlet-triplet energy separation for 2-isopropylidenecyclopenta-1,3-diyl (**1c**) (Figure 1.6 on the next page), a TMM derivative, in 1982. They suggested that the singlet biradical (**1c**) was 13.3 kcal mol^{-1} higher in energy than compound (**3c**). Since triplet (**1c**) is more stable than compound (**3c**) due to the high ring strain in the latter, the singlet-triplet energy separation was estimated as $\geq$ 13.3 kcal mol^{-1}, which was in poor agreement with their previously reported experimental value of $<$ 3.5 kcal mol^{-1} [64]. Dixon and co-workers [30] computed that singlet-triplet splitting between $^3B_2$-$^1B_1$ states of 2-methylenecyclopenta-1,3-diyl (**1a**) is 15.2 kcal mol^{-1}, and $^1A_1$ state is 6.0 kcal mol^{-1} lower in energy than $^1B_1$ state at (4*e*,4*o*)MCSCF/STO-3G level.

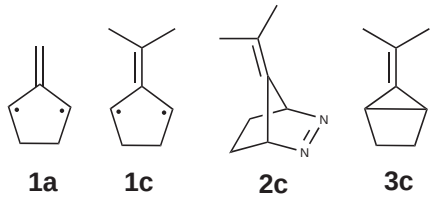

Figure 1.6: Structures of molecules **1a**, **1c**, **2c**, and **3c**.

1.2.2 Generation of Berson TMMs

Both singlet and triplet **1c** can be generated from azoalkane **2c** via thermal and photochemical denitrogenation, respectively [8,52-56] (Figure 1.7). The triplet species is readily observed by ESR spectroscopy [56]. Its reactions with olefins are stereorandom. In the absence of olefins it dimerizes [6, 8, 52, 53, 55]. These observations suggest that the molecule in its triplet state reacts by two successive bond-forming steps. Characterization of the singlet species has been more difficult since it has no ESR spectrum. Its reactions with olefins appear to be stereospecific and this suggests an intermediate with singlet-paired electron spins, which in turn gives cycloadducts by forming two bonds in a concerted manner. Structural rearrangements and stereomutations (geometrical isomerizations) of TMMs are usually formulated with the singlet state of **1c**.

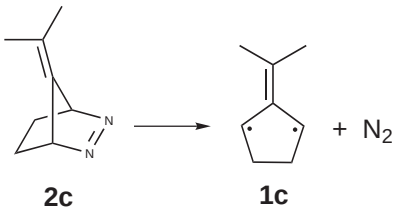

Figure 1.7: Rearrangement of **2c** to **1c**.

1.2.3 Thermal Rearrangements of Berson TMMs

Figure 1.9 on the next page shows the qualitative structures for products of vacuum pyrolysis of azoalkane **2c** and enyne **9c**. Figures 1.10 and 1.11 depict the proposed mechanisms [51] for formation of the majority of the species in Figure 1.9. Since the azoalkane **2c** has a singlet ground state, it is known that the biradical **1c** is formed in its singlet **S** state.

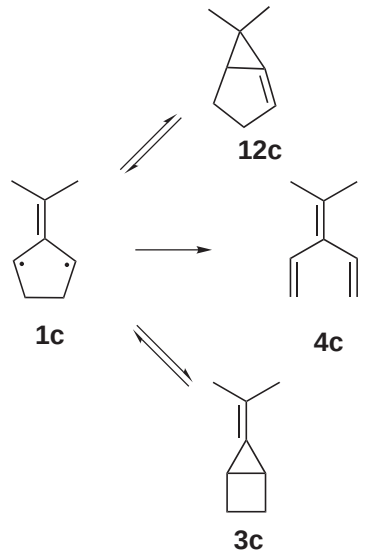

Figure 1.8: Rearrangements of **1c** to **3c**, **4c**, and **12c**.

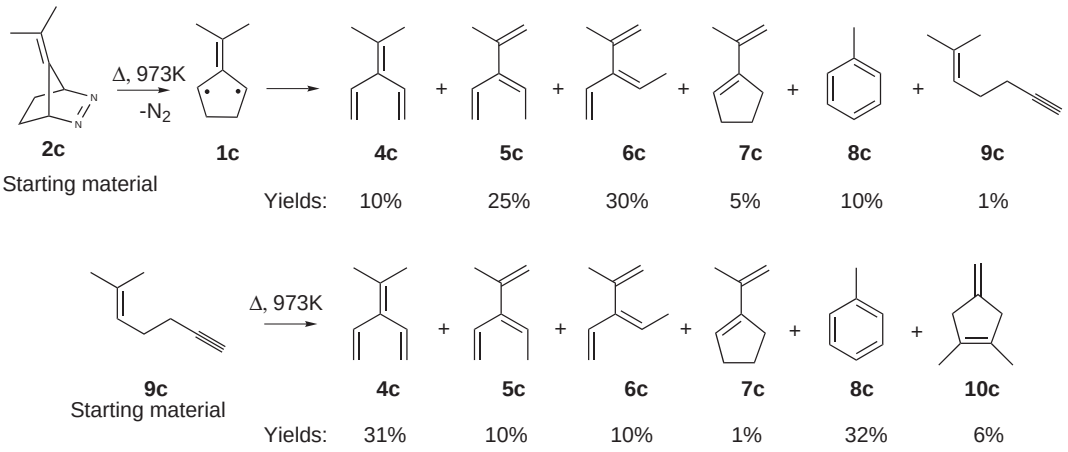

Figure 1.9: Products of flash vacuum pyrolysis of diazene **2c** and enyne **9c** from Berson.

1.3 Several Related Reactions

1.3.1 Formation of Methyelenecyclopentenes

Huntsman *et al.* [65-67] carried out the interconversion of 1-hexen-5-yne (**9a**) and 1,2,5-hexatriene (**14a**) and observed that methelenecyclopentenes (**10a** and **11a**) were formed at the expense of the triene (Figure 1.12 on the next page). They also estimated the activation energy as 32.7 kcal mol^{-1} for the rearrangement of **9a** to **14a**. Further, Huntsman *et al.* predicted an

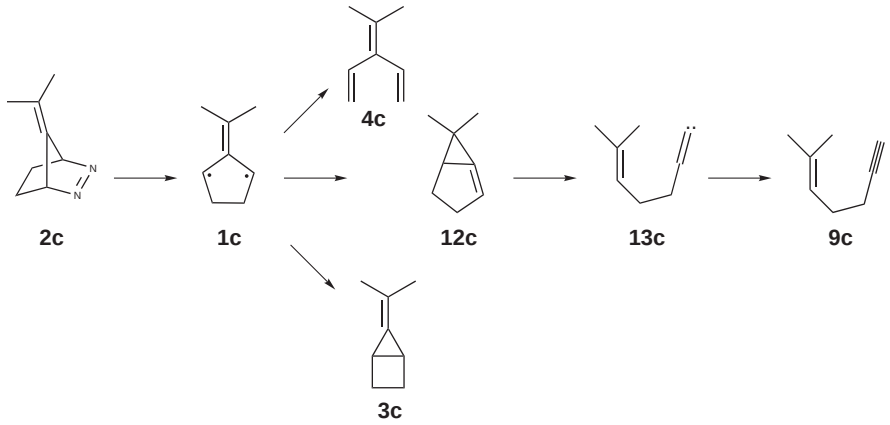

Figure 1.10: Berson's Scheme 1.

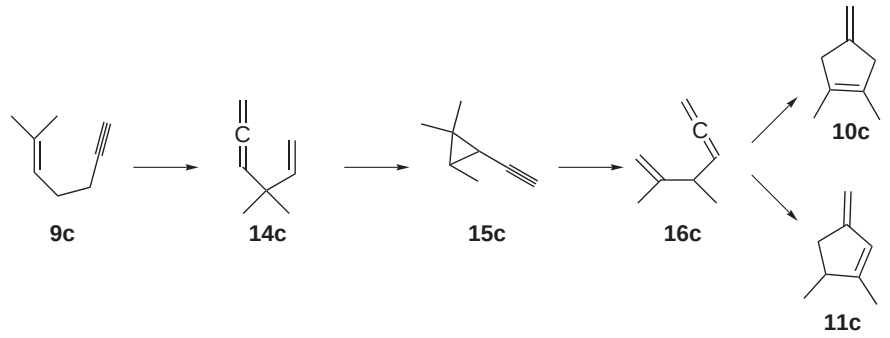

Figure 1.11: Berson's Scheme 2.

activation energy of 37.2 kcal mol^{-1} for the rearrangement of **14a** to **10a** and **11a**. Moreover, they observed that the ratio of methelenecyclopentenes are [**11a**]/[**10a**]=1.27 (Table 1.1 on the next page).

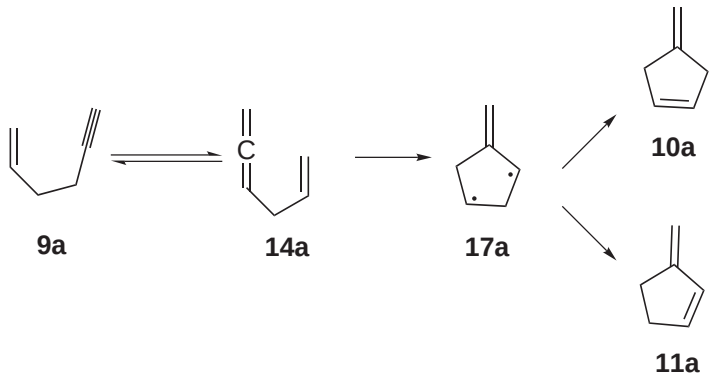

Figure 1.12: Huntsman's Mechanism.

Table 1.1: Huntsman's results.

Temperature (°C)	Contact Time (s)	**9a**	**14a**	**10a**	**11a**
340	62	29	65	2	3
340	130	24	62	6	8
340	150	20	50	13	17
385	62	10	22	30	38

In a 1988 study, Andrews and Baldwin [68] observed that pyrolysis of 2-methylenebicyclo[2.1.0]-pentane (**27a**) at 253 °C yields **14a**, **10a**, and **11a** with the ratio of [**11a**]/[**10a**]=1.4, which is consistent with Huntsman *et al.*'s predictions (Figure 1.13). Andrews and Baldwin predicted that the activation energy for the conversion of **27a** to products was 36 kcal mol^{-1}, which was estimated by a gas-chromatographic method.

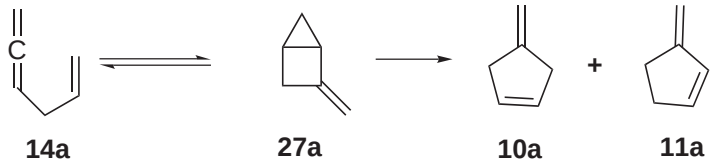

Figure 1.13: Baldwin's Mechanism.

In 1989, Roth *et al.* [69] determined the activation energies for the three reactions in the pyrolysis of 2-methylene bicyclo[2.1.0]pentane (Figure 1.13) as 36.5 (**27a** → **14a**), 35.8 (**27a** → **10a**), and 35.8 kcal mol^{-1} (**27a** → **11a**).

1.3.2 Hopf Mechanism

Hopf *et al.* investigated the thermal rearrangements of *cis*- and *trans*-1-ethynyl-2-methylene cyclopropane (**15a**) in a flow system with 35 s residence times at high temperatures (340-530 °C) (Figure 1.14) [70-72]. They observed that the *cis* and *trans* isomers were in equilibrium, but the *cis* isomer undergoes a homo-1,5-hydrogen shift to form **14a**. In their experiments, methelenecyclopentenes **10a** and **11a** were also formed. They also observed that the ratio of methelenecyclopentenes are [**11a**]/[**10a**]=1.3 which is consistent with Huntsman *et al.*'s and Andrews and Baldwin's predictions. Moreover, it is proposed that **14a** undergoes to a 1,3-hydrogen shift to form 1,3,5-hexatriene (**21a**), which was not observed, but its electrocyclization product, 1,3-cyclohexadiene (**22a**) was isolated. In addition to these products, the benzene (**24a**) molecule was observed at high temperatures (Table 1.2).

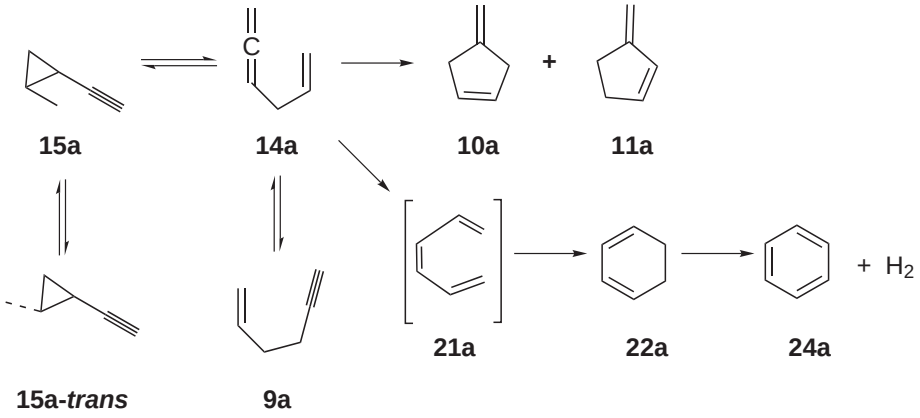

Figure 1.14: Mechanism suggested by Hopf.

Table 1.2: Hopf's results.

Temperature (°C)	%Conversion	**14a**	**11a**	**10a**	**9a**	**22a**	**24a**
340	67	58	4	3	20	15	0
370	74	46	9	5	20	20	0
530	100	0	38	29	0	30	3

1.3.3 Bicyclo[3.1.0]hexene to 1,3- and 1,4-Cyclohexadiene

In 1966, Ellis and Frey [73] carried out high temperature thermal rearrangement of bicyclo[3.1.0]hexene (**20a**), and observed that **20a** rearranges to 1,3- and 1,4-cyclohexadiene, **22a** and **23a** (Figure 1.15). They estimated the activation energies for these reactions as 50.2 kcal mol^{-1}.

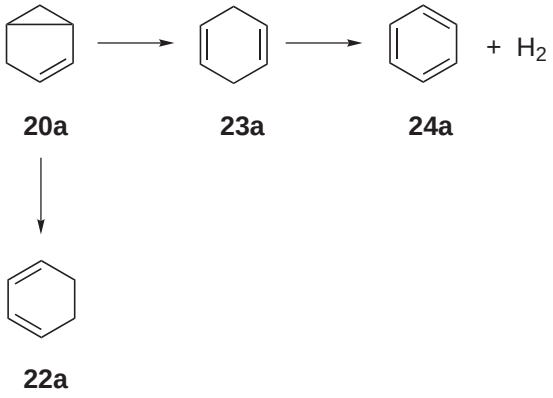

Figure 1.15: Ellis's Mechanism.

1.3.4 1,3- and 1,4-Cyclohexadiene to Benzene

1,4-cyclohexadiene (**23a**) undergoes dehydrogenation reaction to give benzene (**24a**) with the activation energy of 42.7 kcal mol^{-1} [73] (Figure 1.16). This reaction occurs via a *syn* elimination by a retro Diels-Alder like mechanism [74]. However, 1,3-cyclohexadiene (**22a**) decomposes to **24a** only at very low pressures (< 0.04 torr) with the activation energy of 61.7 kcal mol^{-1} [75, 76, 77].

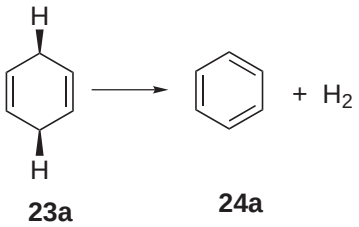

Figure 1.16: Decomposition of 1,4-cyclohexadiene to benzene

1.3.5 An Alternative Path to Formation of Cyclohexadienes

In a 1988 study, Huntsman *et al.* [78] proposed an alternative path to formation of 1,3- and 1,4-cyclohexadiene (**22a** and **23a**) (thus to benzene, **24a**) via bicyclo[3.1.0]hexene, **20a** (Figure 1.17). According to this mechanism methylenecyclopentenes (**10a** and **11a**) first rearrange to biradicalic intermediates (**18a** and **19a**). These biradicalic intermediates then form the bicyclo[3.1.0]hexene (**20a**). Then, **20a** rearranges to cyclohexadienes **22a** and **23a** (Figure 1.15 on the previous page).

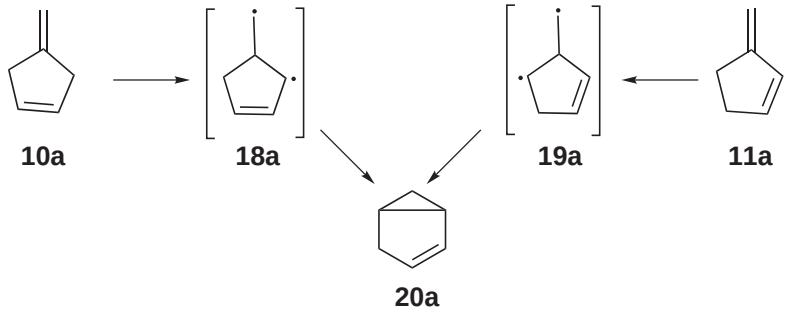

Figure 1.17: Proposed mechanism for the formation of **20a** from **10a** and **11a**.

1.3.6 Vinylmethylenecyclopropane Route to 3-Methylenecyclopentene (11a)

In a 1968 study, Shields *et al.* [79] synthesized the 2-vinylmethylenecyclopropane and reported its thermal rearrangement to 3-methylenecyclopentene (**11a**) (Figure 1.18). This reaction is closely related to vinylcyclopropane rearrangement [3]. Later, Billups *et al.* [80] determined the activation energy as 25.8 kcal mol^{-1}.

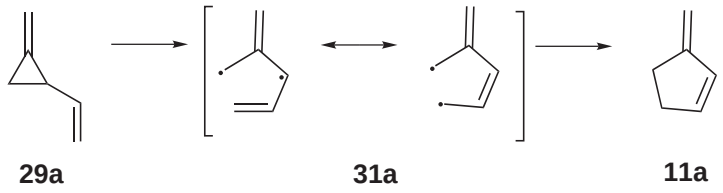

Figure 1.18: Rearrangement of **29a** to **11a**.

1.4 The Object of Study

The object of the proposed study is to carry out a comprehensive theoretical investigation of the thermal rearrangements of TMMs (Figure 1.9 on page 7) by quantum mechanical computations. The potential energy surface of the singlet **S** state has been explored to test Benson's Schemes 1-2 (Figures 1.10 and 1.11 on page 8). It is verified that the enyne **9c** plays a central role in connecting the two portions of the reaction path (Berson Schemes 1 and 2). Connectivity of successive minima on a given surface is confirmed by intrinsic reaction coordinate (IRC) computations. Density functional theory (DFT) and multiconfiguration self consistent field (MCSCF) methods are employed for these purposes. The MCSCF method is required for the singlet biradicals due to the well-known spin contamination problem associated with unrestricted DFT or *ab initio* methods. Further, single point frozen-core CCSD(T) energy computations are carried out at optimized DFT or MCSCF geometries. To reduce the cost of computations somewhat, initially a model of TMMs with two less CH_3 group is taken as shown below, Figure 1.19.

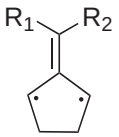

1a (R_1,R_2 = H)

Figure 1.19: Model of TMMs with two less CH_3 groups than Berson TMMs.

CHAPTER 2

THEORETICAL BACKGROUND OF THE COMPUTATIONAL METHODS EMPLOYED

Computational chemistry is a branch of chemistry which uses principles of theoretical chemistry and computer science to solve chemical problems. It uses the results of quantum chemistry, which is integrated into efficient computer programs, to predict the structures and properties of atoms and molecules. Nowadays, computational methods are widely used for the understanding of the chemical phenomena such as chemical bonding, molecular spectra, reactivity, and various other fundamental chemical problems. Depending on the desired chemical accuracy, it is possible to obtain important results even for macromolecules using computational methods. However, the most challenging issue is the choice of the computational method that will be employed to achieve the results with satisfactory quality. In the following sections, computational methods will be discussed starting from basic ideas to much more sophisticated techniques.

2.1 The Born-Oppenheimer Approximation

For a molecule consisting of n electrons and M nuclei, the Schrödinger equation [81] is

$$\hat{H}\,\Psi \;=\; E\,\Psi \tag{2.1}$$

where E is the total energy of the molecule, and $\hat{H}$ is the Hamiltonian operator

$$\hat{H} \;=\; \hat{T}_e \;+\; \hat{T}_N \;+\; \hat{V} \tag{2.2}$$

In this expression $\hat{T}_e$ is the kinetic energy operator of the electrons, $\hat{T}_N$ is that for the nuclei, and V is the potential energy of interaction among the electrons and the nuclei. Using atomic

units, the explicit expressions for these operators are:

$$\hat{T}_e = -\frac{1}{2} \sum_{i}^{n} \nabla_i^2 \tag{2.3}$$

$$\hat{T}_N = -\frac{1}{2} \sum_{A}^{M} \frac{1}{m_A} \nabla_A^2 \tag{2.4}$$

$$\hat{V} = -\sum_{i}^{n} \sum_{A}^{M} \frac{Z_A}{r_{iA}} + \sum_{i}^{n} \sum_{j>i}^{n} \frac{1}{r_{ij}} + \sum_{A}^{M} \sum_{B>A}^{M} \frac{Z_A Z_B}{R_{AB}} \tag{2.5}$$

where n is the total number of the electrons, M is the total number of the nuclei, Z_A is the atomic number of nucleus A, m_A is the mass of nucleus A in units of m_e, r_{ij} is the distance between i^{th} and j^{th} electrons, r_{iA} is the distance between i^{th} electron and A^{th} nucleus, and R_{AB} is the distance between A^{th} and B^{th} nuclei.

The molecular Hamiltonian can be written as

$$\hat{H} \;=\; \hat{H}_e \;+\; \hat{T}_N \tag{2.6}$$

where $\hat{H}_e = \hat{T}_e + \hat{V}$ is called the electronic Hamiltonian. It describes the motion of the electrons in the field of nuclei with fixed positions in space.

The molecular Schrödinger equation [Eq.(2.1)] is universally solved within the Born Oppenheimer approximation [82-85]. The procedure starts by assuming that Ψ of Eq.(2.1) can be written as a product of an electronic function ψ_e and a function of nuclear positions, ψ_N.

$$\Psi(r, R) \;=\; \psi_e(r)\psi_N(R) \tag{2.7}$$

where r and R collectively denote the set of variables of the electrons and the nuclei, respectively. The functions ψ_e and ψ_N are determined in two consecutive steps. One first solves the electronic Schrödinger equation at a specified nuclear configuration R (*i.e.* a given geometrical arrangement of the nuclei in space, or equivalently, a given "geometry" of the molecule).

$$\hat{H}_e \, \psi_e \;=\; E_e \, \psi_e \tag{2.8}$$

and obtains the electronic wavefunction ψ_e and the associated energy E_e for the electronic state of interest. Both ψ_e and E_e have a parametric dependence on the nuclear positions R. For a nonlinear molecule with M nuclei, specification of the molecular geometry R requires

values of $3M - 6$ independent variables. It is necessary to repeat solving Eq.(2.8) for many different geometries of the molecule, and thus obtain $E_e(R)$ as a function of the geometrical structure. The electronic energy $E_e(R)$, a function of $3M - 6$ nuclear variables, is called *the electronic potential energy surface* (PES). Since Eq.(2.8) is known to have many solutions, a molecule has a corresponding number of different electronic states and their associated PESs. Fortunately, thermal reactions can be adequately explained on the basis of the lowest energy (ground) PES. In the following, PES refers to the ground electronic state.

The chemically interesting regions on the PES, as a function of R, are the minima and first order saddle points. In general, the PES of a polyatomic molecule will have several local minima and saddle points. The minima on the PES correspond to the various isomers (or the conformers) the molecules may have, and the saddle points correspond to the transition structures (TS) in isomerization or dissociation reactions.

The gradient $\mathbf{g}$ of E_e is the vector of first derivatives of E_e with respect to the nuclear variables, whereas the Hessian, $\mathbf{F}$, is the square matrix of second derivatives. At a stationary geometry R_0 on the PES, $\mathbf{g} = \mathbf{0}$; and this condition is used in the numerical procedure for the actual determination of R_0. The nature of a given R_0 is then identified by the eigenvalues of the Hessian $\mathbf{F}$ evaluated at the computed geometry R_0, (the force constant matrix). A stationary geometry R_0 is classified as a saddle point of order k, where k is the number of negative eigenvalues of $\mathbf{F}$. Thus, a geometry R_0 is a local minimum on the PES if all eigenvalues of $\mathbf{F}$ are positive (*i.e.* $k = 0$); it is a first order saddle point (TS) if $\mathbf{F}$ has one and only one negative eigenvalue ($k = 1$), *etc*. The vibrational frequencies of a species (an isomer, a conformer, or a TS) associated with R_0 are related to the eigenvalues of $\mathbf{F}$ by a square-root relation so that negative eigenvalues of $\mathbf{F}$ correspond to imaginary frequencies. Thus, an equivalent description of the nature of R_0 may be made by stating the number of imaginary vibrational frequencies, as is very commonly done in literature.

In the second step of the Born-Oppenheimer approximation, the electronic PES is used as the vibrational potential energy function in finding $\psi_N(R)$ of Eq.(2.7) near a given stationary geometry R_0, by solving the Schrödinger equation for the motion of the nuclei.

$$[\hat{T}_N + E_e(R)]\,\psi_N = E\,\psi_N \tag{2.9}$$

Defining $V(R) = E_e(R) - E_e^\circ$, where $E_e^\circ = E_e(R_0)$ is the electronic energy of the stationary

structure in consideration, Eq.(2.9) may be rewritten as:

$$[\hat{T}_N + V(R)]\,\psi_N = E_N\,\psi_N \tag{2.10}$$

where $E_N = E - E_e^\circ$ is the total energy associated with the motion of the nuclei alone. In Eq.(2.10) the nuclear kinetic energy operator $\hat{T}_N$, and hence the function ψ_N is a function of all $3M$ variables of the nuclei, whereas $V(R)$ is a function of only $3M-6$ (or $3M-7$ for a TS) variables. By an appropriate choice of the $3M$ variables, solution of Eq.(2.10) can be simplified. Thus one takes 3 variables as the center of mass coordinates (C.M.) of the nuclei, and 3 angle variables describing rigid rotations of the nuclear framework R_0 in the three-dimensional space. The remaining $3M-6$ variables that $V(R)$ depends on describe the vibrational motion of the molecule. With this selection of the variables, ψ_N of Eq.(2.10) is (approximately) factorized: $\psi_N = \psi_t\psi_r\psi_v$, where ψ_t is the translational wavefunction depending only on the 3 C.M. coordinates, ψ_r is the rotational wavefunction depending on 3 angles, and ψ_v is the vibrational wavefunction of $3M-6$ (or $3M-7$ for a TS) variables. Substitution of the product function into Eq.(2.10) gives a Schrödinger equation for ψ_t and associated translational energy E_t, another equation for ψ_r and the rotational energy E_r, and finally a third equation for ψ_v and the vibrational energy E_v. The total energy of the nuclear motion is: $E_N = E_t + E_r + E_v$. Combining all of the foregoing results, the Born-Oppenheimer prescription of the molecular wavefunction and the total energy for geometries in the vicinity of R_0 are:

$$\Psi = \psi_e\psi_t\psi_r\psi_v \tag{2.11}$$

$$E = E_e^\circ + E_t + E_r + E_v \tag{2.12}$$

According to Eq.(2.12), the ground state energy associated with the stationary geometry R_0 is

$$E_0 = E_e^\circ + ZPVE \tag{2.13}$$

where the zero-point vibrational energy, $ZPVE$, is the lowest allowed value of E_v. In the *harmonic approximation*, it is given by

$$ZPVE = \frac{h}{2}\sum_i \nu_i \tag{2.14}$$

where h is the Planck's constant and the sum is over $3M-6$ or $3M-7$ vibrational frequencies depending on whether R_0 is a minimum or a TS, respectively. The energy E_0 is called the *ZPVE corrected energy* of the molecule at stationary geometry R_0.

2.2 Methods of Computing the Electronic Energy of a Molecule

The computational bottleneck in the Born-Oppenheimer procedure is the determination of the PES. Since the nineteen-thirties much effort has been devoted in search of computationally feasible approaches towards finding reasonably accurate solutions of the electronic Schrödinger equation, Eq.(2.8). Some of these methods are outlined below.

2.2.1 The Variational Principle

In variational methods, the exact wavefunction is approximated by a trial function and the approximate energy is obtained by the expectation value of Hamiltonian operator using the trial wavefunction [83].

$$\widetilde{E}_0 = \frac{\langle \widetilde{\Psi} | \hat{H} | \widetilde{\Psi} \rangle}{\langle \widetilde{\Psi} | \widetilde{\Psi} \rangle} \tag{2.15}$$

where $\widetilde{\Psi}$ is the trial function and $\widetilde{E}_0$ is the approximate ground state energy.

The *variation principle* for the ground state states that the approximate ground state energy is always higher than the exact ground state energy.

$$E_0 \leq \widetilde{E}_0 \tag{2.16}$$

where E_0 is the exact energy.

The approximate energy indicates the quality of the wavefunction. The lower the energy, the more accurate is the wavefunction. This statement forms the main idea of variational methods: take a trial wavefunction which depends on some parameters, and then minimize the energy with respect to those parameters.

$$\frac{\partial \widetilde{E}_0}{\partial \mathbf{c}} = 0 \tag{2.17}$$

where $\mathbf{c}$ is a set of variational parameters such as the molecular orbital coefficients *etc.*.

2.2.2 The Hartree-Fock Theory

The simplest wavefunction which satisfies the antisymmetry requirement (Pauli exclusion principle) [86, 87] for a n-electron system is the *Slater determinant* [83, 88].

$$\Phi(x_1, x_2, ..., x_n) = \frac{1}{\sqrt{n!}} \begin{vmatrix} \phi_1(x_1) & \phi_2(x_1) & ... & \phi_n(x_1) \\ \phi_1(x_2) & \phi_2(x_2) & ... & \phi_n(x_2) \\ ... & ... & ... & ... \\ \phi_1(x_n) & \phi_2(x_n) & ... & \phi_n(x_n) \end{vmatrix} \tag{2.18}$$

where $\{\phi_i(x_j)\}$ are the spin orbitals. Swapping two rows of Slater determinant changes the sign of the determinant, and this corresponds to exchanging the coordinates of two electrons. Thus, Slater determinants satisfy the antisymmetry condition. The Hartree-Fock (HF) theory [83,89-94] uses a single Slater determinant as a trial function for an n-electron system, and determines the best spin orbitals ϕ_i via the variation principle. The HF orbitals are obtained by

$$\hat{f}\phi_i = \varepsilon_i\phi_i \tag{2.19}$$

where $\hat{f}$ is called the Fock operator and ε_i is the energy of i^{th} spin-orbital. Eq.(2.19) is not an ordinary eigenvalue equation because the Fock operator itself contains the unknown molecular orbitals (MOs). Thus, such an equation should be solved by an iterative procedure. The iterative procedure for solving the Hartree-Fock equations is called *self-consistent field* (SCF) method.

In Eq.(2.18), the Slater determinant is constructed from the spin molecular orbitals ϕ_i. Spin molecular orbitals are the product of space molecular orbitals with a spin function ($\phi = \varphi\alpha$ or $\phi = \varphi\beta$). Spin orbitals are denoted by $\phi(x)$, where x consists of spatial and spin variables ($x = r, s$), while spatial MOs are denoted by $\varphi(r)$.

For computational efficiency it is convenient to use spin-adapted formalisms [95]. For a molecule with even number of electrons, if all spatial orbitals are doubly occupied, the wave-function is a closed-shell singlet state, and the corresponding Hartree-Fock formalism is called *restricted Hartree-Fock* (RHF). The RHF formalism yields reasonable results for the equilibrium geometry, whereas at stretched geometries it is unreliable and usually gives wrong dissociation curves.

On the other hand, if different spatial orbitals are used for α and β electrons, the corresponding Hartree-Fock formalism is called *unrestricted Hartree-Fock* (UHF) [96]. One can use the UHF formalism for both closed- and open-shell molecules. The UHF method gives the

same solution as the RHF method for closed-shell singlet molecules at equilibrium geometry. However, at stretched geometries UHF provides lower energies than RHF, and gives qualitatively correct dissociation curves. The most important disadvantage of the UHF method is that UHF wavefunction is not an eigenfunction of $\hat{S}^2$ operator. This situation leads to a problem called *spin contamination* which means that the wavefunction includes contributions from higher-lying spin multiplicities.

For open-shell systems the RHF analogue of Hartree-Fock formalism is called *restricted-open Hartree-Fock* (ROHF). It is generally used for high-spin open-shell cases such as doublets, triplets, *etc.*. In the ROHF formalism the same spatial orbital set is used for both α and β electrons except those electrons occupying open-shell orbitals. The advantage of ROHF formalism over UHF is that the ROHF wavefunction is an eigenfunction of $\hat{S}^2$ operator; thus there is no spin-contamination problem.

2.2.3 Atomic Orbital Basis Sets

Basis set expansion approach is one of the most basic tools of modern quantum chemistry [83,91,97-99]. The main idea is expanding the unknown MOs in terms of a *basis set* of atomic orbitals (AOs). In other words, the MOs are expressed as a linear combination of atomic orbitals (LCAO).

$$\varphi = \sum_{\mu}^{AO} c_\mu \chi_\mu \tag{2.20}$$

where $\{\chi_\mu\}$ are AOs, and $\{c_\mu\}$ are the MO expansion coefficients.

If the basis set is complete then the expansion of Eq.(2.20) is exact. However, in practice finite basis sets are used for the expansion. As the basis set size gets larger, the number of variational parameters (c_μ) increases. Hence, the variational flexibility increases as the basis set becomes more complete. Thus, the computed energy will be more accurate as basis set gets larger.

Two types of AO basis sets are commonly used in quantum chemistry. These are the *Slater type orbitals* (STOs) [100] and *Gaussian type orbitals* (GTOs) [101]. The general form of GTOs is [97]

$$\chi^{GTO}_{\zeta,n,l,m}(r,\theta,\phi) = N Y_l^m(\theta,\phi) r^{2n-2-l} e^{-\zeta r^2} \tag{2.21}$$

where N is a normalization constant, $Y_l^m(\theta, \phi)$ is the spherical harmonic, and ζ is the basis function exponent. The exponent ζ defines the spatial width of a basis function. Large ζ gives a tight function, while small ζ gives a diffuse function.

After deciding on the basis set type, the most important matter is the number of basis functions that will be used. If one basis function is used for each occupied atomic orbital of a given atom, the corresponding molecular basis set is called the *minimal basis set*. Further, when two basis functions are used for each AO the resulting basis set is called *double-ζ basis set* (DZ). Similarly, if one uses three basis functions for each AO the corresponding basis set is called *triple-ζ basis set* (TZ). For chemical bonding the *valence* electrons play more important roles than the *core* electrons. Therefore, it is reasonable to use 2, 3, *etc.* basis functions only for valence orbitals in order to reduce computational efforts. Such basis sets are called *split valence basis sets*.

A further attempt to improve the basis set is addition of *polarization* functions to basis sets. Polarization functions are AOs with higher angular momenta then those of the valence AOs [83, 94]. Another important improvement for basis sets is the addition of *diffuse* functions. Diffuse functions have small exponents which keep the electrons far away from the nucleus. Such functions are necessary especially in the presence of loosely bound electrons, and properties that depend on wavefunction tail. More specifically, diffuse functions are important for the computations of anions, Rydberg states, very electronegative atoms (such as F), polarizabilities, and binding energies of Van der Waals complexes [97-99,102,103]. Diffuse functions are generally denoted by + signs in basis set acronyms.

The most commonly used basis sets are the Pople basis sets developed by Pople's group [104-110], and popularized by the GAUSSIAN program written by the same group [111]. STO-nG basis sets are minimal basis sets in which n primitive GTOs are contracted to mimic the behavior of a STO. Pople's split-valence double-ζ basis set is called 6-31G. Similarly, 6-311G denotes Pople's split-valence triple-ζ basis set. The 6-31G(d) or 6-31G* basis is constructed by adding one d-type polarization function to 6-31G basis for heavy atoms. The 6-31G(d,p) or 6-31G** basis is constructed from the 6-31G* basis by adding one p-type polarization function for the H atoms. Further, 6-31+G basis set is constructed from the 6-31G basis by adding diffuse s and p functions for heavy atoms. Similarly, 6-31++G basis set is constructed from the 6-31G basis by adding diffuse s and p functions for heavy atoms and a diffuse s

function for the H atom [97-99].

Dunning pointed out that basis sets optimized at the Hartree-Fock level are not the optimal choice for correlated levels. The *correlation consistent* basis sets are optimized at CISD level [112-116]. cc-pVXZ basis sets denote Dunning correlation-consistent, polarized valence, X-ζ basis sets (X=D,T,Q,5,6). The aug-cc-pVXZ basis set denotes that one set of diffuse functions is added to cc-pVXZ basis set. The cc-pCVXZ basis set denotes Dunning correlation-consistent, polarized core and valence basis sets [98]. The Dunning basis sets are designed to converge smoothly toward the complete (infinite) basis set limit, and are widely used for basis set extrapolation procedures (*focal point analysis*) [117-122].

2.2.4 Electron Correlation Methods

The Hartree-Fock theory is inherently an independent-electron theory. The Slater determinant, Φ, of Eq.(2.18) is essentially a product of spin orbitals (which is antisymmetrized to obey the Pauli exclusion principle; or equivalently, symmetry-adapted so as to belong to the antisymmetric representation of the permutation (symmetric) group). The electronic Hamiltonian $\hat{\mathbf{H}}_\mathbf{e}$, on the other hand, is not separable because of the electron-electron repulsion terms $V_{ee} = \sum 1/r_{ij}$ in Eq.(2.5). The spin-restricted Hartree-Fock energy,

$$E_{RHF} = \langle \Phi | \hat{\mathbf{H}}_\mathbf{e} | \Phi \rangle \tag{2.22}$$

takes the contribution of V_{ee} into account only to first order, whereas, by definition, the exact ground state electronic energy E_{exact} includes its effect exactly. The error in the HF energy is called by Löwdin [123] as the (electron) *correlation energy*

$$E_{corr} = E_{exact} - E_{RHF} \tag{2.23}$$

It has been found that while E_{corr} has a substantial magnitude (i.e. much larger than the desired chemical accuracy of 2-3 kcal mol^{-1}), it is rather insensitive to large variations, ΔR, in the molecular geometries except for those R at which one or more Slater determinants have energies near that of the HF determinant, and interact strongly with it. In the latter case, E_{corr} is anomalously high, and the HF method fails badly. Typical examples are singlet states of biradicals and stretched bonds during (homolytic) bond breaking or formation. The problem can be overcome by replacing the HF determinant by a linear combination of the HF Φ and

the few other determinants that interact strongly with Φ. The resulting wavefunction Ψ_{MC} is called a multiconfiguration or a *multi-reference* wavefunction. In the context of the latter terminology, the HF determinant is called a *single-reference* wavefunction. Let the lowest energy obtainable with Ψ_{MC} be E_{MC}. It is clearly lower than E_{RHF} but higher than E_{exact} as can be inferred from the variation principle. The correlation energy can be written as $E_{corr} = (E_{exact} - E_{MC}) + (E_{MC} - E_{RHF})$, thus partitioning it into two qualitatively different types of correlation energy. The contribution $(E_{MC} - E_{RHF})$ is referred to as *nondynamical correlation* energy while $(E_{exact} - E_{MC})$ is called *dynamical correlation* energy [124, 125]. Both contributions are negative in sign. It is the dynamical correlation energy which appears to be weakly sensitive to ΔR. It should be noted that in the absence of degeneracy or near-degeneracy effects, Ψ_{MC} will be dominated by the HF determinant with the consequence that the nondynamical correlation energy will be relatively unimportant as compared with the dynamical one. Also note that if one initially starts directly with Ψ_{MC} (instead of the HF determinant) as a first approximation to the exact wavefunction then one needs to assess only the dynamical correlation energy (i.e. the error in E_{MC}) since the nondynamical correlation energy is already included.

Several techniques are available for the treatment of the electron correlation problem. Correlation methods based on the HF theory are generally called *post*-HF methods. These are configuration interaction (CI), multiconfiguration self consistent field (MCSCF) method, many-body perturbation theory (MBPT), and coupled cluster (CC) theory. Another theory based on electron density rather than wavefunction is called density functional theory (DFT).

2.2.4.1 Configuration Interaction (CI)

One can show that the exact n-electron eigenfunctions of the Hamiltonian operator can be expressed as a linear combination of n-electron Slater determinants [83, 126]. Therefore, the main idea of the CI method is to diagonalize the Hamiltonian operator in a basis of Slater determinants constructed by using the MOs obtained by the SCF procedure [83,94,126-130]. The CI wavefunction can be written as

$$\Psi_{CI} = C_0\Phi_0 + \sum_S C_S\Phi_S + \sum_D C_D\Phi_D + \ldots \tag{2.24}$$

where Ψ_{CI} is the CI wavefunction, Φ_0 is the HF reference determinant, Φ_S and Φ_D are the *singly* and *doubly* excited Slater determinants, and $C_0,\ C_S,\ C_D,\ \ldots$ are the CI expansion

coefficients. The variational minimization leads to the following eigenvalue equation for the CI coefficients

$$\mathbf{HC} = \mathbf{CE} \tag{2.25}$$

where **H** is the Hamiltonian matrix, **E** is a diagonal matrix corresponding to the state energies, and **C** is the CI coefficients matrix.

In principle the CI method gives the exact solution of the n-electron problem. However, in practice we can only use finite basis sets, so CI yields exact solutions within the basis set limit. In other words, with finite basis sets, the CI energy is an upper bound to the exact energy. Further, with m spin orbitals and n electrons the dimension of CI space is

$$dim(CI) = \frac{m!}{n!(m-n)!} \tag{2.26}$$

The above equation (Eq.2.26) indicates that one can perform CI computations only for very small molecules and with very small basis sets. In other words, the CI method is computationally prohibitive.

In order to overcome computational limitations one truncates the CI expansion at various levels. Such approaches are called *truncated CI*. For example, if one only includes double excitations, which are the most important excitations, the resulting method is called *CI doubles* (CID). Similarly, if one only considers both single, which are very important for molecular properties, and double excitations, the resulting method is called *CI singles and doubles* (CISD). However, truncated CI methods suffer from lack of *size-extensivity* which means that the energy of a dimer consisting of non-interacting monomers is not twice of that for the monomer with truncated CI. Nevertheless, one can approximately compensate for this effect by an empirical correction, known as *Davidson correction* [83, 127, 131, 132].

2.2.4.2 Multiconfiguration Self Consistent Field (MCSCF) Method

The Hartree-Fock (HF) orbitals are optimized for a single determinant SCF wavefunction. Thus, these orbitals are not the optimal choice for a truncated CI wavefunction. In the MCSCF method, one uses a CI expansion with a limited number of determinants. The basic idea is simultaneous optimization of both the CI and MO coefficients [83,94,124,133-143].

As previously stated, the MCSCF method is generally preferred for the molecules whose electronic structure cannot be adequately described by the RHF determinant. The most common examples of such systems are molecules having biradicalic character and low-lying excited states. Another example case where MCSCF wavefunction should be used is a bond-breaking process. Although UHF based methods such as UHF, UCISD, UCCSD, *etc.* give a qualitatively correct PES for biradicalic systems, the energy predictions of such methods are unreliable due to high spin-contamination. However, MCSCF wavefunction is an eigenfunction of $\hat{S}^2$ operator, and does not suffer from the spin-contamination problem.

The complete active space SCF (CASSCF) theory is one of the most commonly used MCSCF variant [124, 144, 145]. In CASSCF method, a MCSCF computation performed in a specially chosen *active space* (limited space). The world "complete" means that a full CI computation will be performed in the active space. For this purpose, the full MO space is generally divided into four subspaces: frozen occupieds (FO), active occupieds (ACO), active virtuals (ACV), and frozen virtuals (FV). The combination of the ACO and ACV subspaces constitute the active space. However, the choice of active space is not unique, and different active spaces yield different energies. Therefore, the key feature of CASSCF method is the proper choice of the active space. For the CASSCF method, (*n e*,*m o*)CASSCF notation can be used. Here, *n* is the number of active electrons and *m* is the number of active orbitals. For example, (4*e*,6*o*)CASSCF means a CASSCF computation using 4 active electrons and 6 active orbitals. The active space concept is illustrated in Figure 2.1.

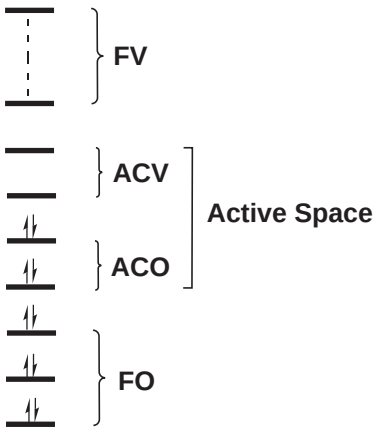

Figure 2.1: Illustration of (4*e*,4*o*)CASSCF active space.

Since the MCSCF method recovers only the nondynamical correlation, a further attempt to

improve the wavefunction is the introduction of multi-reference CI (MRCI) methods. In MRCI method, excitations are performed from the CASSCF reference instead of HF reference. If only double excitations are allowed from a CASSCF reference, the resulting method is called MRCI doubles (MRCID). Similarly, if both single and double excitations are considered the method is called MRCI singles and doubles (MRCISD) [141, 146].

2.2.4.3 Many-Body Perturbation Theory (MBPT)

Another way to include electron correlation is perturbation theory (PT), which is not-variational but size-extensive at each order. The application of PT to a system consisting of many particles is generally called *many-body perturbation theory* (MBPT) [83,94,147-152]. In this theory, the total Hamiltonian of a system is partitioned into two parts: the *unperturbed Hamiltonian* (zeroth order Hamiltonian) and a *perturbation*.

$$\hat{H} = \hat{H}_0 + \hat{V} \tag{2.27}$$

where $\hat{H}$ is the total Hamiltonian, $\hat{H}_0$ is the unperturbed Hamiltonian, and $\hat{V}$ is the perturbation operator. It is assumed that the exact eigenfunctions and eigenvalues of unperturbed Hamiltonian are known but those of the total Hamiltonian are unknown.

$$\hat{H}_0\Phi_0 = E_0\Phi_0 \tag{2.28}$$

$$\hat{H}\Psi = E\Psi \tag{2.29}$$

where Ψ and E are the exact wavefunction and energy, respectively. The exact wavefunction and energy are expressed as infinite summations of contributions of different orders.

$$\Psi = \Phi_0 + \Psi^{(1)} + \Psi^{(2)} + ... \tag{2.30}$$

$$E = E_0 + E^{(1)} + E^{(2)} + ... \tag{2.31}$$

The MBPT method based on the Møller-Plesset (MP) partitioning of $\hat{H}$, and using HF orbitals is called *Møller-Plesset perturbation theory* (MPPT) [147, 153, 154]. In MPPT method, the unperturbed Hamiltonian is chosen as the sum of individual Fock operators. Hence, the zeroth-order energy is the sum of occupied orbital energies, and the zeroth-order wavefunction is the HF wavefunction. Further, the perturbation operator is chosen to be the difference

between the total Hamiltonian and the unperturbed Hamiltonian.

$$\hat{H}_0 = \sum_i \hat{f}(i) \tag{2.32}$$

$$E_0 = \sum_i \varepsilon_i \tag{2.33}$$

$$\hat{V} = \hat{H} - \hat{H}_0 \tag{2.34}$$

In MPPT theory, the HF energy corresponds to the sum of the zeroth and first order corrections. Therefore, MPPT series start with MP2 (MPPT2).

$$E_{HF} = E_0 + E^{(1)} \tag{2.35}$$

Using MPPT approach we can write the second-order energy correction (MP2) more explicitly as follows

$$\Delta E_{MP2} = \frac{1}{4} \sum_i^{occ} \sum_j^{occ} \sum_a^{vir} \sum_b^{vir} \frac{|\langle ij||ab\rangle|^2}{\left(\varepsilon_i + \varepsilon_j - \varepsilon_a - \varepsilon_b\right)} \tag{2.36}$$

where $\langle ij||ab\rangle$ is the antisymmetrized two-electron integral.

The MP2 method is the most economical wavefunction-based method including electron correlation. The major disadvantage of MPPT methods is that it is non-variational. Hence, the predicted energy is not an upper bound to the exact energy and MPPT energy may fall under the exact energy. Another disadvantage is that for MPPT theory analytic evaluation of the energy derivatives are very expensive, even more expensive than truncated CI methods. Thus, geometry optimization and frequency computations are very slow compared to SCF and MCSCF methods.

The standard MPPT methods are based on the HF reference, thus these methods are single-reference methods. However, if one uses a multi-reference wavefunction such as CASSCF wavefunction for a single state, then this method is called multi-reference Møller-Plesset method, and is denoted by MRMP. However, with CASSCF wavefunction the choice of unperturbed Hamiltonian is not unique. Different choices of unperturbed Hamiltonian are possible. In such cases, the computed electronic energies are generally slightly different, but energy differences are consistent with each other. The multi-reference PT (MRPT) method based on Roos and coworkers unperturbed Hamiltonian is denoted by CASPT2 in the literature [155-158]. Another widely used approach is the multiconfiguration quasi-degenerate perturbation theory (MCQDPT) [147, 159]. The MCQDPT method is a multi-state as well as multi-reference PT.

2.2.4.4 Coupled Cluster (CC) Theory

The coupled cluster (CC) theory appears as the most reliable method among the computationally feasible methods for the approximate solution of the electronic Schrödinger equation, and the estimation of molecular properties [83,94,147,149,160-170]. The CC wave function can be written as

$$\Psi_{CC} = e^{\hat{T}}\Phi_0 \tag{2.37}$$

where Φ_0 is the *reference HF determinant* and $\hat{T}$ is the cluster excitation operator. More explicitly, one decomposes the cluster excitation operator into individual components as follows

$$\hat{T} = \hat{T}_1 + ... + \hat{T}_n \tag{2.38}$$

where $\hat{T}_1$ is the single-excitation operator, $\hat{T}_2$ is the double-excitation operator, and $\hat{T}_n$ is the n-tuple excitation operator.

If all excitation operators are considered then the CC wavefunction will be equivalent to the CI wavefunction. However, in practice cluster excitation operators are truncated at some level. For example, if only double excitation operator is included, the method is called CC doubles (CCD), if both single and double excitation operators are included the method is called CC singles and doubles (CCSD). Similarly, if single, double, and triple excitation operators are included the method is called CC singles, doubles, and triples (CCSDT). However, it is expensive to consider the triple excitation operator. Thus instead of full triples, CCSDT, one can consider effects of triple excitations by perturbation theory, and the resulting method is denoted as CCSD(T) [164, 168].

The main advantages of CC are that the CC method provides highly accurate results, and the method is size-extensive even in cases of truncated CC methods as opposed to truncated CI methods. Another advantage of CC theory is that even for truncated CC methods the CC wavefunction includes higher level excited determinants in an approximate way. For example, the CCSD wavefunction includes all singly and doubly excited determinants and includes contribution of higher excited determinants in an approximate manner due to the exponential expansion of cluster operator. However, the CC method is not-variational, thus the CC energy is not an upper bound to the exact energy. Another disadvantage is that for CC theory analytic evaluation of the energy derivatives are very expensive, even comparable with

numerical derivatives [171]. Thus, the geometry optimization and frequency computations are very slow compared to variational methods.

2.2.4.5 Density Functional Theory (DFT)

Roots of density functional theory (DFT) can be traced to as back as 1920s, in the studies of Thomas and Fermi [172, 173]. However, it became a complete and accurate theory with studies of Hohenberg, Kohn, and Sham in 1960s [174-176]. In 1964, Hohenberg and Kohn proved that the *electron density*, $\rho(r)$, can be used as a basic variable for molecular systems with non-degenerate ground states. More explicitly, the ground state energy and all molecular properties are determined uniquely by the electron density and *external potential* (electron-nucleus attraction potential). The proof of this theorem was simple, all that was applied is the minimum energy principle for the ground state energy. The second Hohenberg-Kohn theorem yields a variational principle for the electron density. For a trial electron density the approximate energy is an upper bound for the exact energy. Later, Levy generalized Hohenberg-Kohn theorems for degenerate ground states [176-178]. However, Hohenberg-Kohn theorems do not state how one can express the ground state energy in terms of electron density.

In a 1965 study, Kohn and Sham [175] introduced a practical method for finding the ground state electron density and the energy. In principle, their method was devised for finding the exact results. However, the Kohn-Sham (KS) equations include an unknown functional to be approximated. Thus, the KS equations give approximate results similar to the situation in wavefunction-based methods. In the KS frame, the ground state energy can be written as

$$E[\rho] \quad = \quad T[\rho] \; + \; V_{ne}[\rho] \; + \; J[\rho] \; + \; E_{xc}[\rho] \tag{2.39}$$

where $T[\rho]$ is the kinetic energy functional, $V_{ne}[\rho]$ is the electron-nucleus potential energy functional, $J[\rho]$ is the Coulomb potential energy functional, and $E_{xc}[\rho]$ is the exchange-correlation (XC) functional which is unknown.

The major problem of DFT is the finding of exchange-correlation functional which is unknown as expressed earlier. There are several commonly used approximations which are based on non-interacting *uniform electron gas* model [179-181].

In order to obtain a better functional, a *non-uniform electron gas* behavior should be taken

into account. A first attempt for this purpose considers the exchange and correlation energies as functions of both the electron density and derivatives of the density, $E_{xc}[\rho, \nabla\rho]$. Such approaches are called *generalized gradient approximations* (GGA). The most commonly used exchange functionals based on GGA approach are Perdew's functionals (PW86 and PW91) and Becke's functional (B88), while correlation functionals are Lee, Yang, and Parr's LYP functional, Perdew's P86 and PW91 functionals and Becke's B95 functional [182-193].

A large number of hybrid functionals, which contain a mixture of Hartree-Fock exchange with DFT exchange-correlation, have been suggested in order to further improve the DFT functionals [194, 195]. One of the most commonly used hybrid functionals is B3LYP which consists of Beckes's 3-parameter exchange functional along with Lee, Yang, and Parr's LYP correlation functional. The B3LYP functional is defined by

$$E_{xc}^{B3LYP} = E_x^{LSDA} + (1-a)E_x^{HF} + b\Delta E_x^{B88} + c\Delta E_c^{LYP} \tag{2.40}$$

where $\Delta E_x^{B88} = E_x^{B88} - E_x^{LSDA}$, $\Delta E_c^{LYP} = E_c^{LYP} - E_c^{LSDA}$, and the empirical values of the parameters are: $a = 0.80$, $b = 0.72$, and $c = 0.81$.

Nowadays, DFT methods are very popular among computational chemists although some computational chemist are still viewing them with caution [196-199]. The main advantage of DFT is that DFT is a very economical method compared to wavefunction based correlation methods. Roughly, the computational cost of DFT is as much as that of the HF method. However, the main disadvantage of the DFT is the usage of the empirical functionals to approximate the exact exchange-correlation functionals. Further, there is no systematic way to improve the functionals; thus functionals are generally constructed via empirical fitting of the experimental results. It is not clear how to obtain better results with DFT. Therefore, many functionals are proposed and the number of functionals is continuously growing. One can mix the functionals in many ways and obtain new functionals. Hence, the DFT method is generally not considered as an *ab initio* method.

Another remarkable point is that the DFT method is variational in principle. However in practice, it is non-variational because of the empirical parameters used to approximate the exchange-correlation functional. Thus, DFT energies are not upper bounds to the exact energies, and DFT energies might be lower than the exact energy. Furthermore, DFT methods generally underestimate the total energies by several kcal mol^{-1}, while they provide generally very reasonable molecular properties [97].

2.3 Computational Chemistry Methods Employed in This Work

The computations in this study have mostly been carried out by using GAUSSIAN 03 (RevD.01) program [111], and the GAMESS package [200]. GAUSSIAN 03 is used for the DFT and CC computations, whereas GAMESS is used for the CASSCF and MRMP2 (CASSCF-MP2) computations. For 3-dimensional chemical drawings the CHEMVP program is used [201]. Our Linux PC cluster, *ivc*, of the computational chemistry laboratory is used throughout this research.

Geometry optimizations for the closed-shell and high-spin open-shell molecules are performed with the DFT method (B3LYP functional) using GAUSSIAN 03 program. Vibrational frequencies are computed to characterize each stationary structure as a minimum, TS, or whatever. After locating a TS, intrinsic reaction coordinate (IRC) [202] computations are carried out. In order to improve the computed energies single-point frozen-core CCSD(T) computations are carried out at optimized DFT geometries. In all computations Pople's polarized triple-ζ split valence basis set, 6-311G(d,p), is employed. For biradicals, geometry optimization and frequency computations are performed with the CASSCF method using GAMESS program package. At optimized geometries, single-point MRMP2 computations are carried out to improve the energy values.

In order to obtain a unique energy scale at CCSD(T)/6-311G(d,p) level for biradicals, vertical singlet-triplet energy differences obtained via MRMP2 computations were used with CCSD(T) energies of the corresponding triplet states to obtain final energy of singlet biradicals. This approximation can be formalized by

$$E(^1X) \;=\; E_{CCSD(T)}(^3X) \;+\; E_{MRMP2}(^1X) \;-\; E_{MRMP2}(^3X) \tag{2.41}$$

where X is a biradical and $E(^1X)$ is the final energy of species ^1X.

CHAPTER 3

RESULTS AND DISCUSSION

3.1 Thermal Ring Opening Reaction of Methylenecyclopropane, and the Parent TMM System

Qualitative structure of TMMs and MCP are illustrated in Figure 3.1 on the facing page. Zero-point vibrational energy (ZPVE) corrected relative energies of the parent TMMs are reported in Table 3.1 at CASSCF/6-311G(d,p) and MRMP2/6-311G(d,p) levels. For the parent TMMs an active space which consists of four electrons and four orbitals (4e,4o) have been used for the CASSCF and MRMP2 computations. The MRMP2 computations have been carried out at optimized CASSCF geometries. Initially, the potential energy surface of parent TMM has been studied. Four electronic states of TMM, namely $^3A_2'$ ($^3B_2$ in C_{2v} subgroup), $^1A_1$, $^1B_1$, $^1B_2$ and ground electronic state of MCP have been investigated.

Table 3.1: ZPVE corrected relative energies (in kcal mol^{-1}) of the parent TMM species, MCP, TS (MCP/o$_1$), **conrot** and **disrot** structures with 6-311G(d,p) basis set.

Structure	**(4e,4o)CASSCF**	**(4e,4o)MRMP2**	**(4e,4o)MRCISD**	**CCSD(T)**
triplet	0.0	0.0	0.0	0.0
o$_1$	13.7	14.9	12.7	
s$_1$	17.2	18.0	16.9	
l_1	16.7	16.7		
MCP	−13.0	−16.2	−21.2	−22.5
TS (MCP/o$_1$)	17.2	17.4		
conrot	19.3	20.1		
disrot	18.9	19.6		

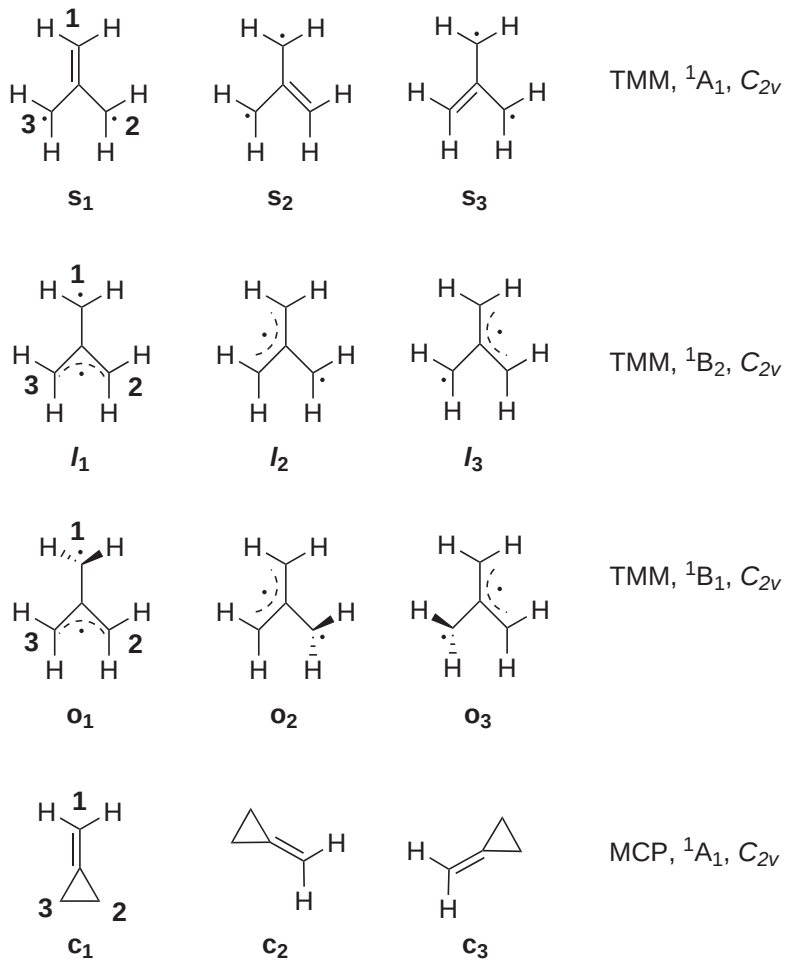

Figure 3.1: Qualitative structures of TMMs and MCP. Definition of abbreviations; **p**: planar, **l**: long planar, **o**: orthogonal methylene group, **c**: cyclopropane ring. In all structures, carbon atoms of methylene groups are labeled by **1**, **2**, and **3** clockwise starting with the top methylene. The subscripts in **1**, **2**, and **3** in $\mathbf{s}_n$, $\boldsymbol{l}_n$, $\mathbf{o}_n$ and $\mathbf{c}_n$ indicate position of the double bond, or the long bond, or the orthogonal methylene.

3.1.1 Triplet TMM

With the CASSCF method we have calculated that the triplet TMM is a minimum on potential energy surface at D_{3h} geometry (state symmetry is $^3A_2'$). In order to construct a relative energy scale for the parent TMMs we use the triplet TMM ($^3A_2'$) as a reference molecule and we set relative energy of the triplet to zero. Therefore, energies of other structures will be given relative to the energy of triplet TMM. Further, in order to obtain relative energy of the MCP we used the RCCSD(T) energy for MCP and UCCSD(T) energy for triplet TMM at optimized CASSCF geometries. Since two π-type active orbitals of TMM will transform

to two σ-type orbitals in MCP, the active space will be somewhat modified. In order to obtain reliable energy differences with the CASSCF method the MOs in the active spaces should be similar. Hence, the CASSCF energy differences between TMMs and MCP may not be reliable. On the other hand, we used the CASSCF and MRMP2 energy differences for biradicalic TMM structures, since the RCCSD(T) method suffers from triplet instabilities [94], while the UCCSD(T) method suffers from high spin contamination for singlet TMMs. The computed geometry of triplet TMM ($^3A_2'$) is shown in Figure 3.2.

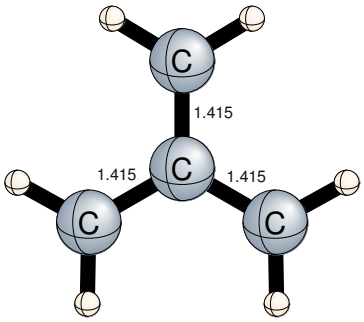

Figure 3.2: Selected interatomic distances (Å) for the triplet TMM (D_{3h}, $^3A_2'$).

3.1.2 Orthogonal TMM

With the CASSCF method the optimum geometry of $\mathbf{o}_1$ ($^1B_1$) structure at C_{2v} symmetry is a transition state, the imaginary frequency is $264i$ cm^{-1}, connecting two equivalent pyramidalized structures. We found a minimum at C_s geometry with slightly pyramidalized (12.9°) methylene group which includes the C_1 atom (see Figure 3.1 on the previous page for numbering of the TMM carbon atoms). The state symmetry of the C_s structure is A''. However, the $\mathbf{o}_1$ (A'') structure is only 0.1 kcal mol^{-1} lower in energy than $\mathbf{o}_1$ ($^1B_1$) with the CASSCF method, whereas $\mathbf{o}_1$ ($^1B_1$) is 0.8 kcal mol^{-1} lower in energy than $\mathbf{o}_1$ (A'') with MRMP2. Therefore, we conclude that pyramidalization is an artifact of CASSCF method, and the actual geometry is C_{2v} ($^1B_1$ structure). The relative energy of the $\mathbf{o}_1$ structure is 13.7 and 14.9 kcal mol^{-1} with the CASSCF and MRMP2 methods, respectively. Both the CASSCF and MRMP2 energies are consistent with the Berson's prediction of singlet-triplet splitting energy ≥ 13.5 kcal mol^{-1}($\Delta E_{ST} \geq 13.5$ kcal mol^{-1}) [6], and also in agreement with Wenthold and co-workers estimate of 13-16 kcal mol^{-1} [20, 21]. Further, in order to show that relative energies of the singlet and triplet states of biradicalics are reliably computed by the CASSCF and MRMP2 meth-

ods, we performed highly expensive MRCISD computations for the parent system. At the MRCISD level the calculated relative energy of $\mathbf{o}_1$ is 12.7 kcal mol^{-1} which is consistent with both the CASSCF and MRMP2 methods. The computed geometries of $\mathbf{o}_1$ ($^1B_1$) and $\mathbf{o}_1$ ($^1A''$) structures are shown in Figure 3.3.

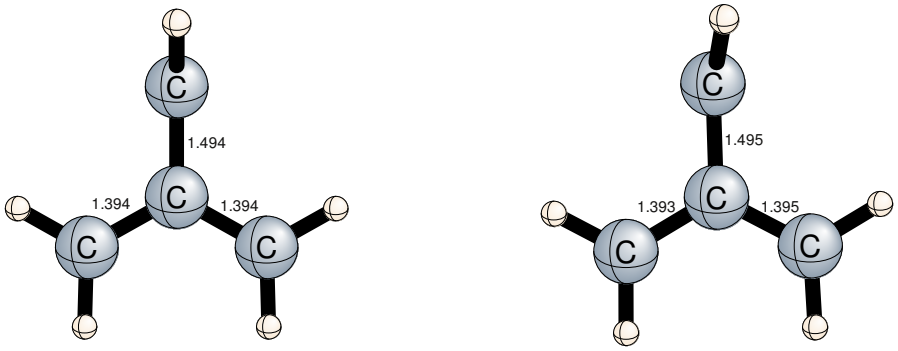

(a) $\mathbf{o}_1$ (C_{2v}, $^1B_1$) (b) $\mathbf{o}_1$ (C_s, $^1A''$)

Figure 3.3: Selected interatomic distances (Å) for $\mathbf{o}_1$ (C_{2v}, $^1B_1$) and $\mathbf{o}_1$ (C_s, $^1A''$) structures.

3.1.3 Planar TMMs

We found that the $\boldsymbol{l}_1$ ($^1B_2$) structure is a third-order saddle point at C_{2v} symmetry with the CASSCF method. Corresponding imaginary frequencies are 655i, 378i and 271i cm^{-1}. The vibrational mode corresponding to imaginary frequency 655i cm^{-1} connects $\mathbf{s}_2$ and $\mathbf{s}_3$ structures by a reaction path which has C_s symmetry. Therefore, this mode will connect $\mathbf{s}_1$ and $\mathbf{s}_3$ structures in $\boldsymbol{l}_2$, while $\mathbf{s}_1$ and $\mathbf{s}_2$ structures in $\boldsymbol{l}_3$. The vibrational mode corresponding to imaginary frequency 378.3i connects two equivalent structures with slightly pyramidalized methylene groups by a reaction path which has C_s symmetry. As stated previously, we conclude that this mode is an artifact of the CASSCF method. The vibrational mode corresponding to imaginary frequency 271.1i yields the orthogonal structure $\mathbf{o}_1$ by a reaction path which has C_2 symmetry. Therefore, this mode will yield the $\mathbf{o}_2$ structure in $\boldsymbol{l}_2$, while the $\mathbf{o}_3$ structure in $\boldsymbol{l}_3$. Relative energy of the $\boldsymbol{l}_1$ ($^1B_2$) structure is 16.7 kcal mol^{-1} at both the CASSCF and MRMP2 levels. The computed geometries of the $\boldsymbol{l}_1$ ($^1B_2$) structure is shown in Figure 3.4 on the next page.

We calculated that the $\mathbf{s}_1$ ($^1A_1$) structure is a minimum on the potential surface at C_{2v} sym-

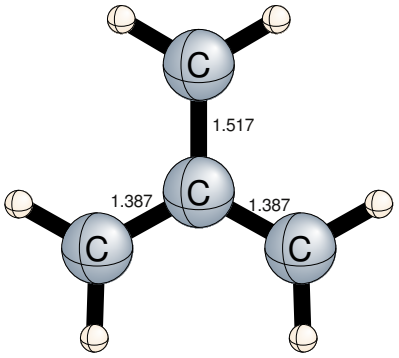

Figure 3.4: Selected interatomic distances (Å) for the $\boldsymbol{l}_1$ (C_{2v}, $^1B_2$) structure.

metry with the CASSCF method. However, we found a transition structure (TS) for a slightly modified $\mathbf{s}_1$ structure at C_1 symmetry, which has the "same" energy with the $\mathbf{s}_1$ ($^1A_1$) structure. This transition structure persists with larger basis sets such as cc-pVTZ. Furthermore, we next considered whether the nature of $\mathbf{s}_1$ structure changes with substituents or not. For this purpose, we investigated the methyl TMM (Me-TMM) and Berson TMMs. For Me-TMM we found only transition structures, and for Berson TMMa we found both a minimum (at C_2 geometry) and a transition structure (at C_{2v} geometry), but the transition structure was lower in energy than the minimum at the CASSCF and MRMP2 levels, and for the Berson TMMc we found a TS at C_2 geometry. Therefore, we conclude that the potential energy surface around the $\mathbf{s}_1$ structure is very flat and the $^1A_1$ state is a transition state in fact. Relative energy of the $^1A_1$ state is 17.2 and 18.0 kcal mol^{-1} at the CASSCF and MRMP2 levels, respectively. Further, at the MRCISD level the calculated relative energy of the $^1A_1$ state of parent TMM is 16.9 kcal mol^{-1} which differs by only 0.3 and 1.1 kcal mol^{-1} from the CASSCF and MRMP2 methods, respectively. The computed geometries of $\mathbf{s}_1$ ($^1A_1$) and $\mathbf{s}_1$ (^1A) structures are shown in Figure 3.5 on the facing page.

Wenthold and co-workers measured the energy difference between the $^1A_1$ and $^3A_2'$ states as 16.1 ± 0.2 kcal mol^{-1}, and the enthalpy of formation for the triplet TMM as 70 ± 3 kcal mol^{-1}. Further, they estimated the energy difference between the $^1B_1$ and $^3A_2'$ states to be 13-16 kcal mol^{-1} [20, 21]. However, observing the $^1A_1$ state by photoelectron spectroscopy does not demonstrate that the $^1A_1$ state is a minimum. With negative ion photoelectron spectroscopy it is possible to study of transition states [20, 21]. In the system under interest, an electron can be used to "lock" the geometry of the anion close to that of a neutral transition state. With

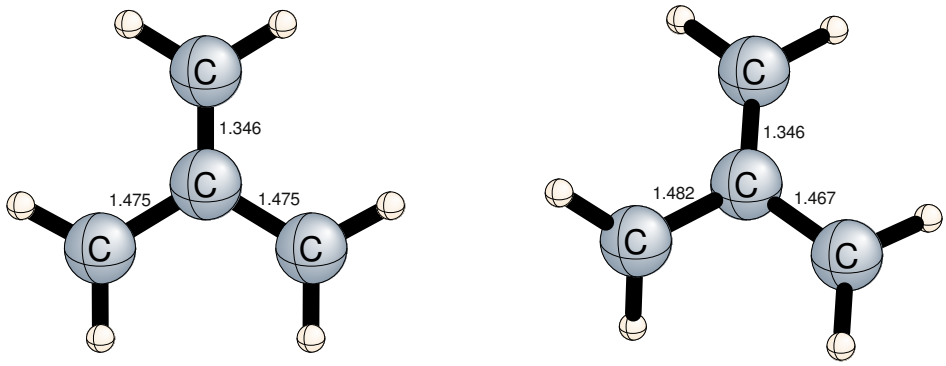

(a) $\mathbf{p}_1$ (C_{2v}, $^1A_1$) (b) $\mathbf{s}_1$ (C_1, ^1A)

Figure 3.5: Selected interatomic distances (Å) for the $\mathbf{s}_1$ (C_{2v}, $^1A_1$) and $\mathbf{s}_1$ (C_1, ^1A) structures.

vertical photodetachment the neutral transition state can be generated, and spectroscopic information on that transition state can be obtained directly from the analysis of photoelectron spectrum [203]. In principle, this approach is very close to that used by Zewail and co-workers [204]. Since geometry of the TMM anion may be close to that of the $^1A_1$ state, it is possible to observe the $^1A_1$ transition state by photoelectron spectroscopy [20, 21]. Furthermore, Wenthold and co-workers [20, 21] stated that "*if the* $^1A_1$ *state is a transition state, it must be in a region of the potential energy surface that is exceptionally flat*". Thus, this interpretation is also consistent with our computational observations.

The $\mathbf{s}_1$ structure is 0.5 and 1.3 kcal mol^{-1} higher in energy than the $\boldsymbol{l}_1$ structure at CASSCF and MRMP2 levels, respectively. However, it is expected that the long planar structure ($\boldsymbol{l}_1$) would be higher in energy than the short planar structure ($\mathbf{s}_1$). Since, the $\mathbf{s}_1$ structure is a minimum, while $\boldsymbol{l}_1$ is a third-order saddle point at CASSCF level, the ZPVE of $\boldsymbol{l}_1$, 49.3 kcal mol^{-1}, is 1.0 kcal mol^{-1} lower than that of $\mathbf{s}_1$, 50.3 kcal mol^{-1}. Hence, if one only consider the electronic energy differences, the relative energy of $\boldsymbol{l}_1$ is 19.7, whereas the relative energy of $\mathbf{s}_1$ is 19.4 kcal mol^{-1} at CASSCF level. Thus, without including ZPVEs, the electronic energy differences are consistent with our expectation. Furthermore, this result also point out that the real nature of the $\mathbf{s}_1$ and $\boldsymbol{l}_1$ structures are not been reflected by the CASSCF method.

3.1.4 Methylenecyclopropane

The MCP ($\mathbf{c}_1$) structure is a minimum on potential surface at C_{2v} geometry with the CASSCF method. Relative energy of MCP is −13.0, −16.2, and −22.5 kcal mol^{-1} at the CASSCF, MRMP2, and CCSD(T) levels, respectively. The experimental value for heat of formation of MCP is 47.9 ± 0.4 kcal mol^{-1} [38, 205], while for triplet TMM is 70 ± 3 kcal mol^{-1} [20, 21]. Thus, the experimental energy of MCP relative to triplet TMM is −22.1 kcal mol^{-1}. At the CASSCF level the computed relative energy of −13.0 kcal mol^{-1} is in poor agreement with the experiment. This result confirms our expectation that the CASSCF energy difference between MCP and triplet TMM is not reliable due to the different active spaces. The MRMP2 method somewhat compensates the inconsistencies arising from the different active spaces, and yields a relative energy of −16.2 kcal mol^{-1} for MCP. But, the MRMP2 relative energy is in error by 5.9 kcal mol^{-1}, which is still not in good agreement with the experiment. However, the CCSD(T) relative energy of −22.5 kcal mol^{-1} is in a very good agreement with experimental value of −22.1 kcal mol^{-1}. Further, at the MRCISD level the calculated relative energy of MCP is −21.2 kcal mol^{-1} which differs by 8.2 and 5.0 kcal mol^{-1} from the CASSCF and MRMP2 methods, respectively, while differs by only 0.4 kcal mol^{-1} from the CCSD(T) results. Consequently, these observations verify our expectation that the CCSD(T) relative energy is more reliable than those of the CASSCF and MRMP2 methods for MCP.

3.1.5 Ring Opening Reaction of Methylenecyclopropane

The relative energy of the transition state which corresponds to ring opening of MCP is computed as 17.2 kcal mol^{-1} and 17.4 kcal mol^{-1} at the CASSCF and MRMP2 levels, respectively. The transition structure forms by an initial cleavage of the C_2–C_3 bond in MCP ($\mathbf{c}_1$) followed by a 90° rotation of only one of the ring methylene groups, in agreement with a suggestion first made by Gajewski [206, 207], and connects MCP to the orthogonal TMM (Figure 3.6 on the next page). The activation energy for ring opening of MCP is computed to be 39.9 kcal mol^{-1} (relative energy of TS at MRMP2 level minus relative energy of MCP at CCSD(T) level, $E_{TS[mrmp2]} - E_{MCP[ccsd(t)]}$. It is in a good agreement with the experimental value of 41.2±0.8 kcal mol^{-1} [49]. Further, we found that the structures corresponding to conrotatory (**conrot**) and disrotatory (**disrot**) ring openings of MCP [32] are mountain tops. Each structure connects MCP to $\mathbf{s}_1$ via vibrational mode corresponding to one of the two imaginary

frequencies, while it connects MCP to $\mathbf{o}_1$ via the vibrational mode corresponding to the other imaginary frequency. The mountain tops have C_2 and C_s geometries, respectively. Relative energy of the **conrot** structure is 19.3 kcal mol^{-1} and 20.1 kcal mol^{-1}, whereas relative energy of the **disrot** structure is 18.9 kcal mol^{-1} and 19.6 kcal mol^{-1} at CASSCF and MRMP2 levels, respectively. The computed geometries of MCP and MCP/o_1 structures are shown in Figure 3.7, while geometries of the **conrot** and **disrot** structures are shown in Figure 3.8 on the next page.

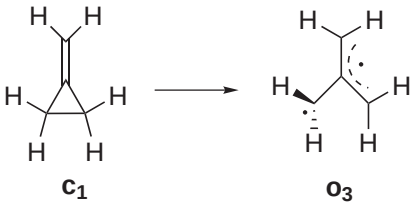

Figure 3.6: Ring opening reaction of methylenecyclopropane.

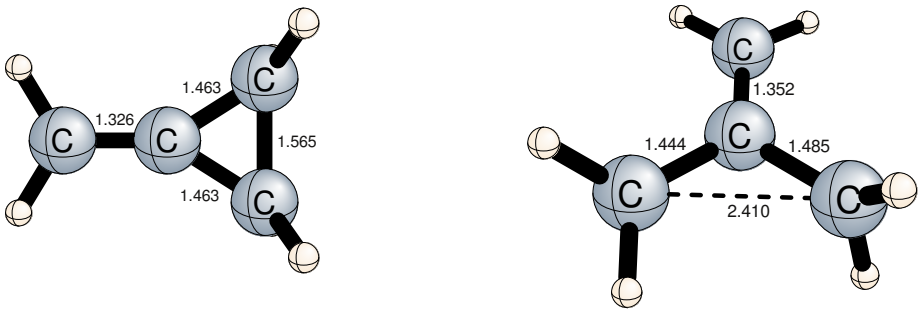

(a) **MCP** (b) **MCP/o$_1$**

Figure 3.7: Selected interatomic distances (Å) for the **MCP** and **MCP/o$_1$** structures.

3.2 Thermal Rearrangements of 2-methylenecyclopenta-1,3-diyl Biradical

3.2.1 Energetics of the Berson TMMa Structures

Qualitative structures of the Berson TMMa stationary points are illustrated in Figure 3.9 on page 41, while ZPVE corrected relative energies are reported in Table 3.2 on the next page. Four electronic states of the Berson TMMa system, namely $^3B_2$, $^1A_1$, $^1B_1$, and $^1B_2$ have been

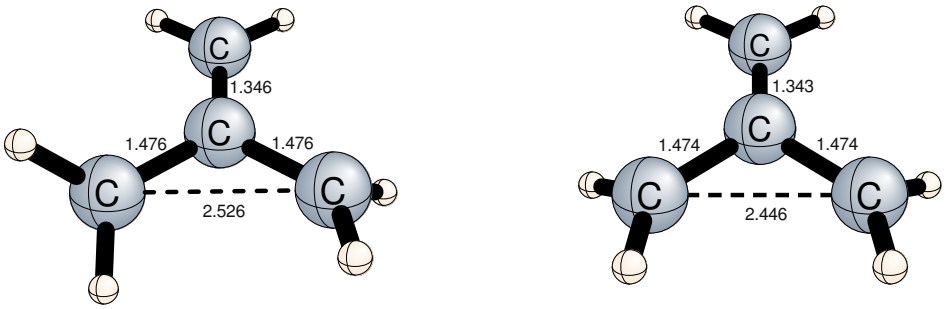

(a) **conrot** (b) **disrot**

Figure 3.8: Selected interatomic distances (Å) for the **conrot** and **disrot** structures.

investigated. An active space of four electrons and four orbitals (4*e*,4*o*) have been used in the CASSCF and MRMP2 computations as in the case of the parent TMMs.

Table 3.2: ZPVE corrected relative energies (in kcal mol^{-1}) of the Berson TMMa structures with 6-311G(d,p) basis set.

Structure	**(4*e*,4*o*)CASSCF**	**(4*e*,4*o*)MRMP2**
1a-T	0.0	0.0
1a-o_1	13.6	14.8
1a-o_2	17.5	17.8
1a-p_1	17.0	16.5
1a-p_2	17.8	18.2
1a-p-l_1	16.7	16.2

3.2.1.1 Triplet TMMa

Using the CASSCF method we found that triplet TMMa, **1a-T** ($^3B_2$), is a minimum on potential energy surface at C_{2v} geometry. In order to construct a relative energy scale for the Berson TMMa structures we used **1a-T** ($^3B_2$) as a reference molecule and we set relative energy of the triplet to zero. Therefore, energies of other structures will be given relative to energy of **1a-T** ($^3B_2$). The computed geometry of the **1a-T** ($^3B_2$) structure is shown in Figure 3.10 on the facing page.

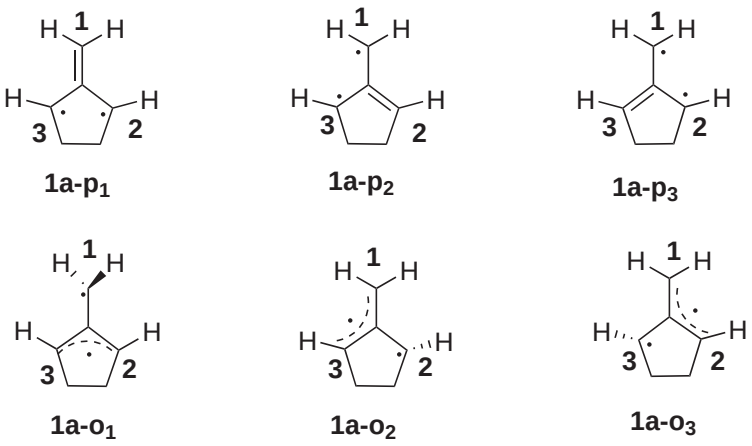

Figure 3.9: Structures in the Berson TMMa system. Abbreviations; **p**: planar, **o**: orthogonal methylene group. In all structures, carbon atoms of methylene groups are labeled by **1**, **2**, and **3** clockwise, starting with the top methylene. The subscripts in $\mathbf{p}_n$ and $\mathbf{o}_n$ indicate position of the double bond or the orthogonal methylene.

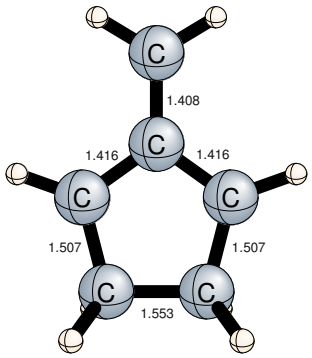

Figure 3.10: Selected interatomic distances (Å) for the **1a-T** (C_{2v}, $^3B_2$) structure.

3.2.1.2 Orthogonal TMMa

At the CASSCF level, the optimum geometry of the **1a-o**$_1$ ($^1B_1$) structure is a transition state. The imaginary frequency is $219.9i$ cm^{-1} and connects two equivalent pyramidalized structures with C_s symmetry. We found a minimum at C_s geometry with a slightly pyramidalized (10.0°) methylene group which includes the C_1 atom (see Figure 3.9 for numbering of the TMMa carbon atoms). The state symmetry of that C_s structure is A''. However, the **1a-o**$_1$ (A'') structure is 0.4 kcal mol^{-1} lower in energy than **1a-o**$_1$ ($^1B_1$) at the CASSCF level, whereas at the MRMP2 level **1a-o**$_1$ ($^1B_1$) is 0.6 kcal mol^{-1} lower in energy than **1a-o**$_1$ (A''). Therefore, we conclude that the pyramidalization is an artifact of the CASSCF method as in case of the

parent TMM system. Relative energy of the **1a-o**$_1$ (A'') structure is 13.6 kcal mol^{-1} and 14.8 kcal mol^{-1} at the CASSCF and MRMP2 levels, respectively.

It should be recalled that in the parent TMM system, the **o**$_1$–triplet energy splitting is 13.7 and 14.9 kcal mol^{-1} at the CASSCF and MRMP2 levels, respectively. Thus, in TMMa system the computed lowest singlet-triplet splitting energies are almost the same as in the parent TMM system, the difference being only 0.1 kcal mol^{-1} at the CASSCF and MRMP2 levels. This fact indicates that the fundamental characteristic of the parent TMM PES is maintained in TMM derivatives and substituents do not change the relative energies significantly.

Furthermore, we again found a slightly pyramidalized minimum structure corresponding to the **1a-o**$_2$ structure at C_1 geometry. Relative energy of the **1a-o**$_2$ structure is 17.5 kcal mol^{-1} and 17.8 kcal mol^{-1} at the CASSCF and MRMP2 levels, respectively. Relative energy of the **1a-o**$_2$ structure is 3.9 and 3.0 kcal mol^{-1} higher than that of the **1a-o**$_1$ (A'') structure at the CASSCF and MRMP2 levels, respectively, due to the ring strain. In orthogonal structures one methylene group tends to be 90° rotated from the plane. However, in the **1a-o**$_2$ structure the ring strain prevents a rotation of 90°. Therefore, the **1a-o**$_2$ structure is higher in energy than **1a-o**$_1$. The computed geometries of the **1a-o**$_1$ ($^1B_1$), **1a-o**$_1$ (A'') and **1a-o**$_2$ structures are shown in Figure 3.11 on the facing page.

3.2.1.3 Planar TMMa

We found two stationary points corresponding to the **1a-p**$_1$ structure. One of them is a transition state at C_{2v} geometry ($^1A_1$) with an imaginary frequency of 83.5i cm^{-1}, and the other is a minimum at C_2 geometry (^1A). The C_{2v} structure is 0.02 kcal mol^{-1}and 0.08 kcal mol^{-1} lower in energy than the C_2 structure at the CASSCF and MRMP2 levels, respectively. Relative energies of the **1a-p**$_1$ ($^1A_1$) and **1a-p**$_1$ (^1A) structures are 17.0 and 16.9 kcal mol^{-1} at the CASSCF level, while the analogous results are 16.5 kcal mol^{-1} and 16.4 kcal mol^{-1} at MRMP2 level, respectively. The calculated relative energies of **1a-p**$_1$ ($^1A_1$) differ by only 0.2 and 1.5 kcal mol^{-1} from its corresponding analogue in the parent TMM system (**s**$_1$) at the CASSCF and MRMP2 levels, respectively. Again, it can be concluded that the major aspects of the parent TMM PES does not change significantly with substituent effects.

Furthermore, for the **1a-p**$_2$ structure we only found a transition structure with an imaginary

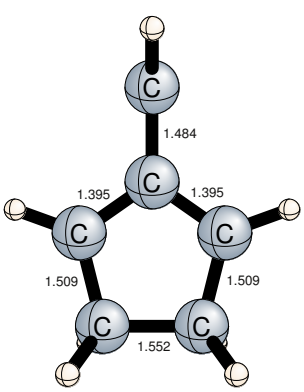

(a) **1a-o**$_1$ (C_{2v}, $^1B_1$)

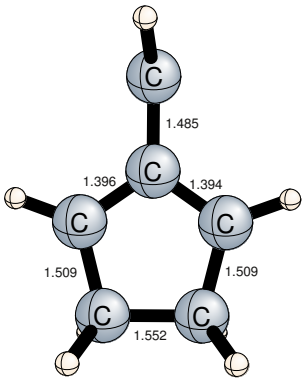

(b) **1a-o**$_1$ (C_s, A'')

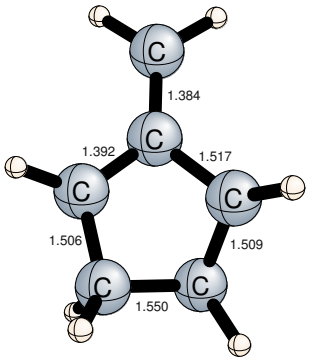

(c) **1a-o**$_2$ (C_1)

Figure 3.11: Selected interatomic distances (Å) for the **1a-o**$_1$ (C_{2v}, $^1B_1$), **1a-o**$_1$ (C_s, A'') and **1a-o**$_2$ (C_1) structures.

frequency of 440.3i cm^{-1} at C_1 geometry. Relative energy of **1a-p**$_2$ is 17.8 kcal mol^{-1} and 18.2 kcal mol^{-1} at the CASSCF and MRMP2 levels, respectively. Since for the **1a-p**$_2$ structure only a TS is found, and for the **1a-p**$_1$ structure relative energy of the TS is lower than that of the minimum, we concluded that the planar structures are TSs. The computed geometries of the **1a-p**$_1$ ($^1A_1$), **1a-p**$_1$ (^1A), and **1a-p**$_2$ structures are shown in Figure 3.12 on the next page.

Moreover, we calculated that the **1a-p-*l***$_1$ ($^1B_2$) structure, which is the analogue of ***l***$_1$ structure of the parent TMM, is a third-order saddle point. Corresponding imaginary frequencies are 573.5i, 366.4i, and 276.7i cm^{-1}. The vibrational mode corresponding to imaginary frequency 573.5i cm^{-1} connects the **1a-p**$_2$ and **1a-p**$_3$ structures by a reaction path which has C_1 symmetry. The vibrational mode corresponding imaginary frequency 366.4i cm^{-1} connects two equivalent pyramidalized planar structures by a reaction path which has C_s symmetry. The mode corresponding to imaginary frequency 276.7i cm^{-1} connects two equivalent **1a-o**$_1$

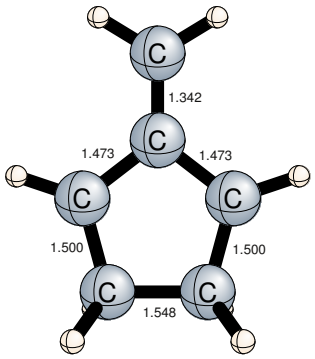

(a) **1a-p**$_1$ (C_{2v}, $^1A_1$)

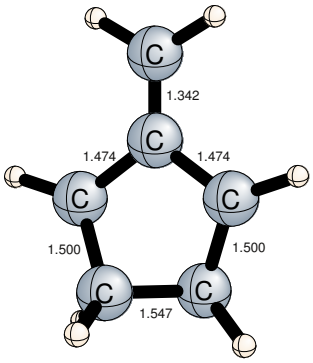

(b) **1a-p**$_1$ (C_2, ^1A)

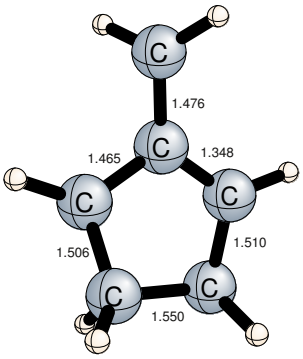

(c) **1a-p**$_2$ (C_1)

Figure 3.12: Selected interatomic distances (Å) for the **1a-p**$_1$ (C_{2v}, $^1A_1$), **1a-p**$_1$ (C_2, ^1A), and **1a-p**$_2$ (C_1) structures.

structures by a reaction path of C_2 symmetry. Relative energies of the **1a-p-*l*$_1$** structure are 16.7 kcal mol^{-1} and 16.2 kcal mol^{-1} at the CASSCF and MRMP2 levels, respectively. Again, relative energy of the long planar structure (**1a-p-*l*$_1$**) is quite close to that of its corresponding analogue in the parent TMM system (***l***$_1$). Relative energies of **1a-p-*l*$_1$** differ by less than 0.5 kcal mol^{-1} from those of ***l***$_1$. The computed geometries of the **1a-p-*l*$_1$** structure is shown in Figure 3.13 on the facing page.

3.2.1.4 Rearrangements Involving Berson TMMa Structures

Initially, formation of biradical **1a** from diazene **2a** has been studied (Figure 3.14 on the next page). Diazene **2a** decomposes to **1a** with a reaction energy of 3.0 kcal mol^{-1}and a barrier of 25.2 kcal mol^{-1}. The computed geometries of diazene **2a** and **2a/1a** structures are shown in

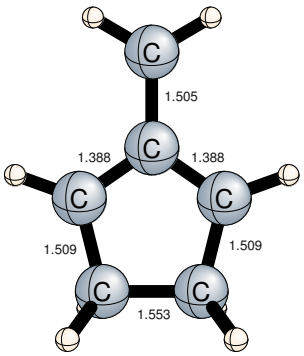

Figure 3.13: Selected interatomic distances (Å) for the **1a-p-*l*$_1$** (C_{2v}, $^1B_2$) structure.

Figure 3.15.

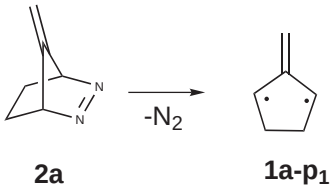

Figure 3.14: Formation of biradical **1a** from diazene **2a**.

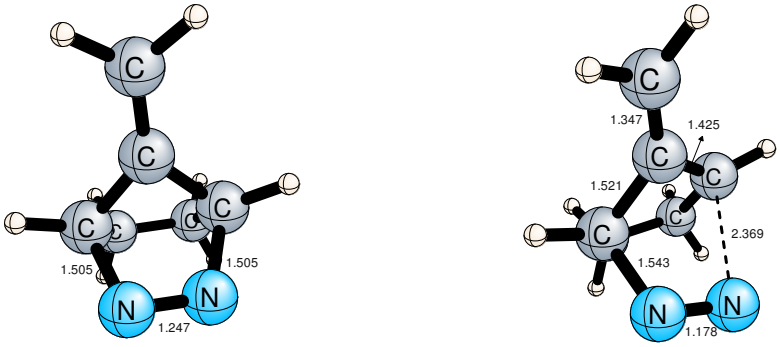

(a) **2a** (b) **2a/1a**

Figure 3.15: Selected interatomic distances (Å) for the **2a** and **2a/1a** structures.

Rearrangements among **1a**, **3a**, **4a**, and **12a** have been investigated next. In analogy with their monocyclic counterparts, the bicyclic MCPs **3a** and **12a** are expected to ring open to TMMs by a single step reaction path (Figure 3.16 on the next page). This anticipation is born out by **12a** which opens to **1a-o**$_1$ with C_1 acting as pivot carbon. The computed barrier

to the ring opening of **12a** is 23.7 − 5.2 = 18.5 kcal mol^{-1}, a value much smaller than 39.9 kcal mol^{-1} in parent MCP. The lowering in the barrier is expected in view of the large strain in the double bond of **12a**, a point that will be discussed below. We were unable to locate a TS for the direct path connecting **12a** with **1a-o**$_2$ in which C_2 would be the pivot carbon. Further, the activation energy for conversion of **12a** to **3a** (**12a** → **3a**) is calculated as 11.2 kcal mol^{-1} (23.7−5.2 = 18.5), which is close to the predicted upper limit of 16.8 kcal mol^{-1} for a trimethyl substituted analogue [8]. The computed geometries of the **12a** and **1a/12a** structures are shown in Figure 3.17 on the facing page.

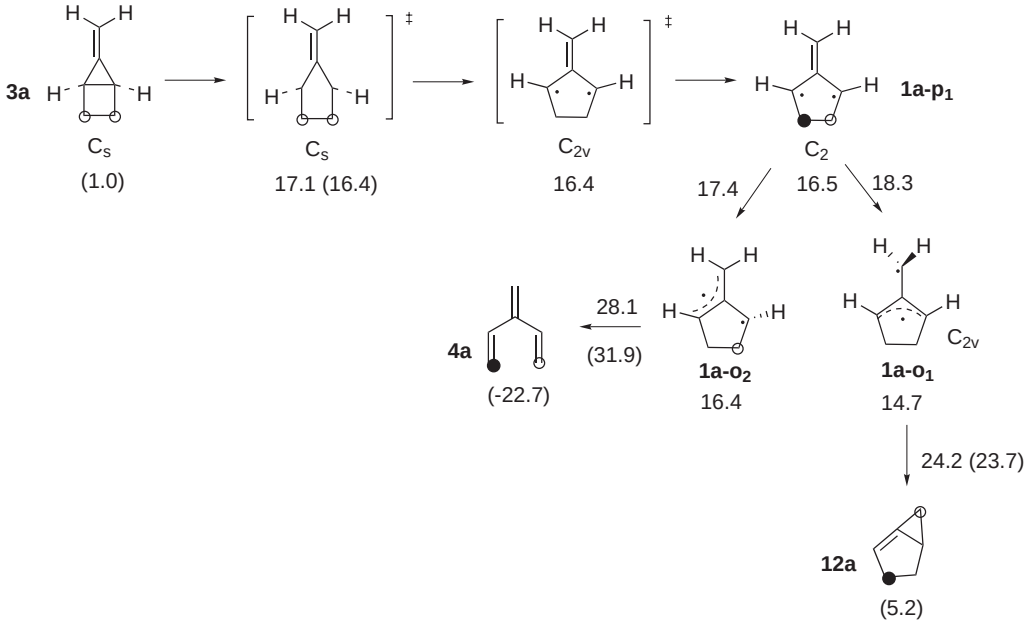

Figure 3.16: Reaction paths connecting the bicyclic MCPs, **3a**, **12a**, and species **4a** with TMMs. ZPVE corrected energies (in kcal mol^{-1}) relative to triplet **1a-T** at MRMP2//CASSCF and CCSD(T)//B3LYP (in parentheses) are indicated. A (4*e*,4*o*) active space is used except for the TS between **1a-o**$_2$ and **4a** where the active space employed is (6*e*,6*o*).

In the ring opening of **3a**, the expected immediate product is **1a-o**$_2$. Unlike the non-symmetric unique TS in the ring opening of monocyclic MCP derivatives, we have located four stationary points on the path connecting **3a** with **1a-o**$_2$. Proceeding along the forward direction from **3a**, as in Figure 3.16, there is a TS with C_s symmetry, lying at 17.1 kcal mol^{-1} above **3a** at MRMP2//CASSCF level. The TS mode (the vibration with the imaginary frequency) is totally symmetric, and it leads to a second TS with C_{2v} symmetry. The TS mode in this second structure is a non-totally symmetric (b_1) vibration, and it lowers the symmetry to give the C_2 symmetric **1a-p**$_1$ species. At the CASSCF level, **1a-p**$_1$ is a minimum; however, when

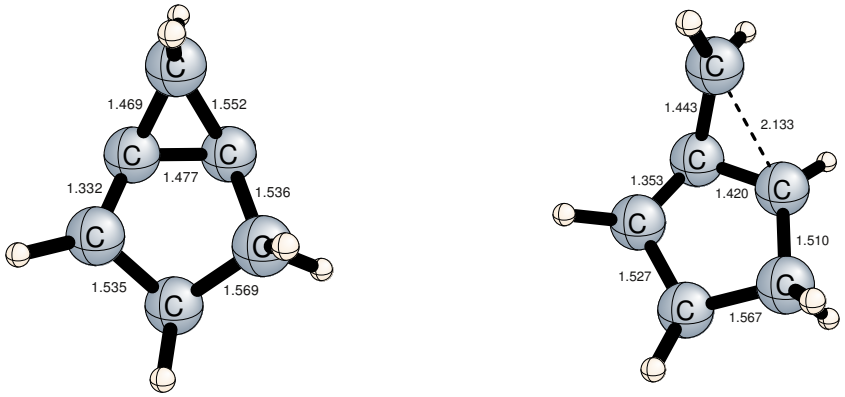

(a) **12a** (b) **1a/12a**

Figure 3.17: Selected interatomic distances (Å) for the **12a** and **1a/12a** structures.

dynamical correlation (MRMP2) and ZPVE are included, its enthalpy moves slightly (0.1 kcal mol^{-1}) above that of the C_{2v} TS. The region of the PES involving these three structures is considerably flat, and it is very likely that the exact PES has no minima in these planar or nearly-planar TMM regions. The fourth stationary point before reaching **1a-o**$_2$ is a TS with a geometry that qualitatively resembles the ring opening TS in the parent TMM (Figure 3.7 on page 39). It has the highest energy (17.4 kcal mol^{-1}) among the four, and therefore, the ring opening barrier of **3a** to **1a-o**$_2$ is 16.4 kcal mol^{-1} at the MRMP2//CASSCF level, which is 2.6 kcal mol^{-1} lower than the barrier between **12a** and **1a-o**$_1$. Furthermore, the computed barrier is in fair agreement with the experimental value of 13.7 kcal mol^{-1} [6]. The computed geometries of the **3a** and **1a/3a** structures are shown in Figure 3.18 on the next page. The orthogonal TMM species **1a-o**$_2$ is a minimum. Admittedly it is a shallow well, the barrier in the reverse direction to **1a-p**$_1$ from **1a-o**$_2$ being only 1.0 kcal mol^{-1}. Nevertheless, we believe that it is a true minimum.

Comparing to the parent TMM system, the activation energy for the ring opening of **3a** to **1a-o**$_2$ is 23.5 kcal mol^{-1} lower than that for the MCP $\rightarrow$ **o**$_1$ reaction. The substantial lowering in the activation energy can be attributed to the high ring strain of **3a**. At the CCSD(T)//B3LYP level, the ring strain energy of **3a** is calculated as 27.5 kcal mol^{-1} relative to strain energy of the MCP via an isodesmic reaction [97] (Figure 3.19 on the following page). Further, the computed strain energy for cyclobutane is 25.7 kcal mol^{-1} at the CCSD(T)//B3LYP level. Hence, our results show that the law barrier height of **3a** $\rightarrow$ **1a-o**$_2$ conversion can be traced to the high ring strain of cyclobutane moiety in **3a**. A similar situ-

(a) **3a** (b) **1a/3a**

Figure 3.18: Selected interatomic distances (Å) for the **3a** and **1a/3a** (C_s symmetry) structures.

ation is also valid for the ring opening of **12a** to **1a-o**$_1$, which is 21.4 kcal mol^{-1} lower than that for MCP. This small activation barrier may be attributed to the double bond strain in the 5-membered ring. At the CCSD(T)//B3LYP level, the double bond strain energy of **12a** is calculated as 32.2 kcal mol^{-1} relative to that of MCP via an isodesmic reaction (Figure 3.20). The computed strain energy is 10.8 kcal mol^{-1} higher than the activation energy barrier difference of 21.4 kcal mol^{-1}. That 10.8 kcal mol^{-1} difference is thought to be arising from somewhat stabilization of the double bond by alkyl groups in **12a**, since the more substituted alkenes (those with fewer hydrogens attached to the C=C) are more stable [208].

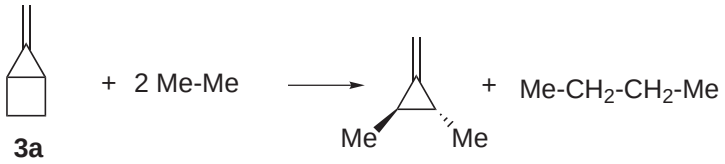

Figure 3.19: The isodesmic reaction for calculating relative strain energy of **3a**.

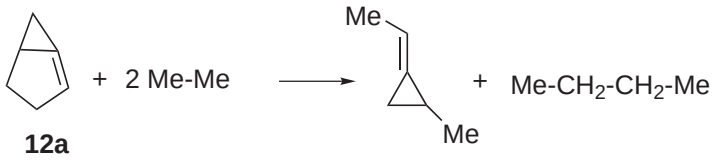

Figure 3.20: The isodesmic reaction for calculating relative strain energy of **12a**.

The planar TMM species **1a-p**$_1$ can also rearrange to the lowest orthogonal TMM **1a-o**$_1$ with an enthalpy barrier of 18.3 − 16.5 = 1.8 kcal mol^{-1}. Additionally, it is involved in the 180°

rotation of the methylene group in **1a-o**$_1$ about the C_1-C_4 bond, and can play an important role in racemization of optically active, substituted **3a** or **12a**. The TS geometry (Figure 3.21) is similar to that of **1a-p**$_2$ (or **1a-p**$_3$).

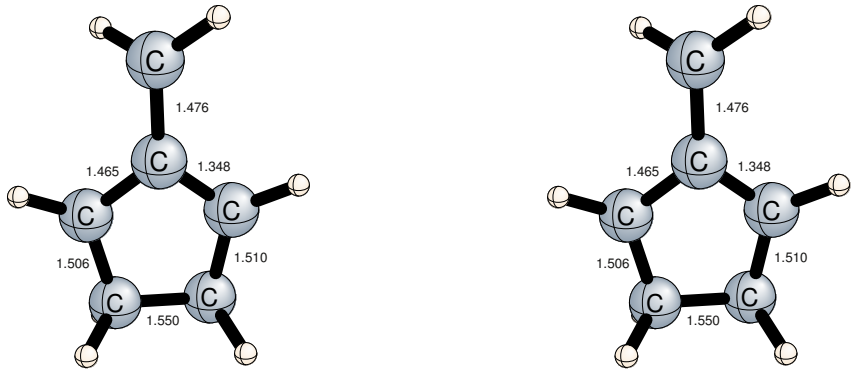

(a) **1a-p**$_1$**/1a-o**$_1$ (b) **1a-p**$_1$**/1a-o**$_2$

Figure 3.21: Selected interatomic distances (Å) for the **1a-p**$_1$**/1a-o**$_1$ and **1a-p**$_1$**/1a-o**$_2$ structures.

The rearrangement of **1a-o**$_2$ to **4a** takes place via simultaneous bond breaking between C_4-C_5 carbon atoms and bond formation between C_1-C_5 and C_3-C_4 carbon atoms with a radicalic mechanism. For this conversion, the reaction energy and barrier are computed as −39.1 and 15.7 kcal mol^{-1}, respectively. The computed geometries of **4a** and **1a/4a** are shown in Figure 3.22.

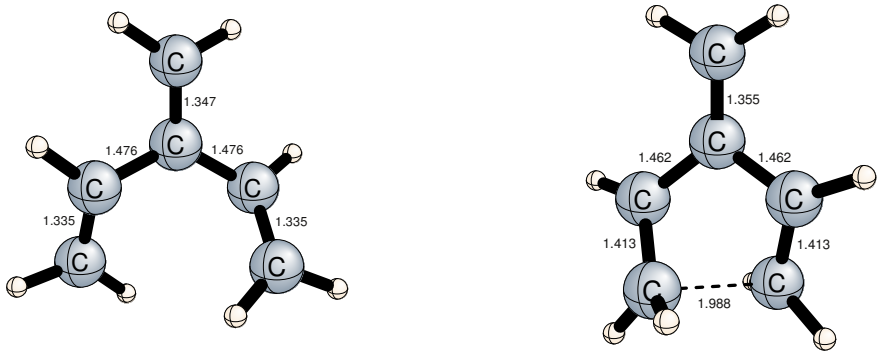

(a) **4a** (b) **1a/4a**

Figure 3.22: Selected interatomic distances (Å) for the **4a** and **1a/4a** structures.

3.2.2 Berson Scheme 1a

In previous section rearrangements involving TMMa structures were discussed. In this section the remaining part of Berson **Scheme 1a** will be discussed. Qualitative structures of the species that appear in our extended Berson **Schemes 1a** and **2a** are illustrated in Figure 3.23. ZPVE corrected relative energies of the minima are reported in Table 3.6 on page 106, while those for the transition states are given in Table 3.7 on page 107. The computational methods that have been employed are previously detailed in chapter 2, section 2.3 on page 31. Furthermore, the **11a** molecule has been chosen as the reference molecule for the Berson **Schemes 1a** and **2a**. Hereafter the relative energies of all stationary points will be presented with respect to the energy of **11a**.

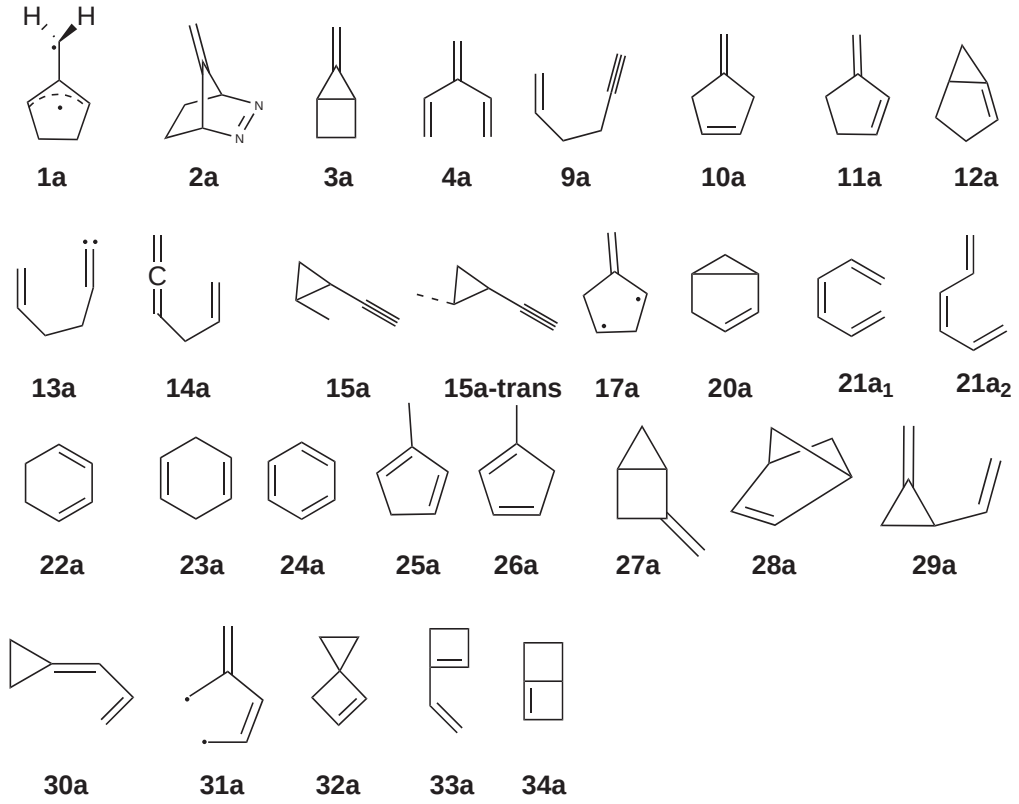

Figure 3.23: Qualitative structures of the species that appear in the extended Berson **Schemes 1a** and **2a**.

3.2.2.1 12a → 9a Conversion

The bicyclic **12a** molecule rearranges to the carbene **13a** via vinylidene cycloreversion reaction with a barrierless path (Figure 3.24). The reaction energy is calculated as 30.2 kcal mol^{-1} for this conversion (Figure 3.25 on the next page). The vinylidene **13a** further rearranges to enyne **9a** via well-known vinylidene-acetylene rearrangement [3,209-212]. This conversion again takes place with a barrierless 1,2-hydrogen shift, which is consistent with an experimentally proposed fast rearrangement for the vinylidene-acetylene rearrangement [209, 210]. Further, at the MRCI/4-31G+DZP level the calculated activation energy of 2.4 kcal mol^{-1} [3] for the vinylidene-acetylene conversion indicates that for such rearrangements the activation energy barrier is quite small. The computed reaction energy for the **13a** → **9a** reaction is −44.5 kcal mol^{-1}, which is consistent with −42.2 kcal mol^{-1} at MRCI/4-31G+DZP level [3] for the vinylidene-acetylene conversion. The computed geometries of the **13a** and **9a** species are shown in Figure 3.26 on the following page.

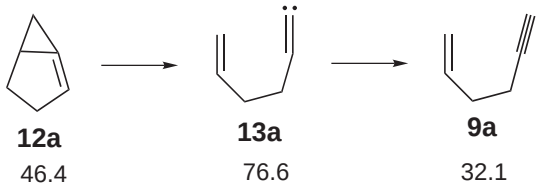

Figure 3.24: The reaction picture for **12a** → **9a** conversion with relative energies (in kcal mol^{-1}). Energy of TSs are not indicated since the reactions take place barrierlessly.

3.2.2.2 4a → 34a Conversion

The **4a** molecule rearranges to **33a** (Figure 3.27 on the next page) via well-known electrocyclic reaction [208] with a reaction energy of 4.9 kcal mol^{-1} and reaction barrier of 40.6 kcal mol^{-1} (Figure 3.29 on page 53). The **33a** molecule further rearranges to **34a** again via an electrocyclic reaction. The reaction energy and barrier are 31.4 and 55.4 kcal mol^{-1}, respectively. Another noticeable point is that the relative energy of the **33a/34a**, 78.8 kcal mol^{-1}, is very high (as high as the relative energy of the TS for decomposition of diazene **2a** to **1a**, 78.7 kcal mol^{-1}). Hence, the cyclization of **33a** to **34a** is not expected at low temperatures. The computed geometries of the **33a**, **34a**, and **33a/34a** structures are shown in Figure 3.28.

Considering the overall picture for the extended Berson **Scheme 1a**, closed-shell bicyclic

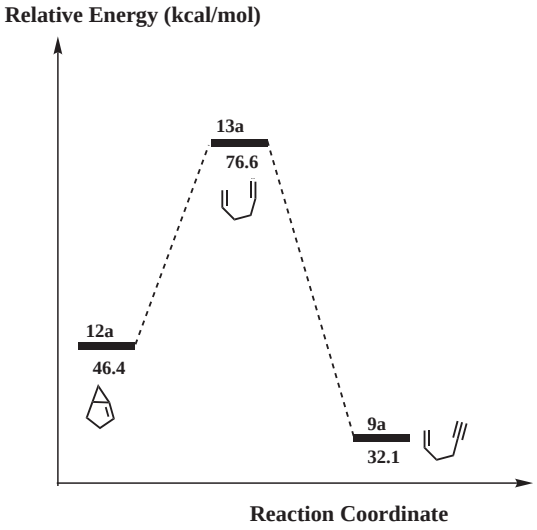

Figure 3.25: Relative energy profile for the **12a** → **9a** conversion.

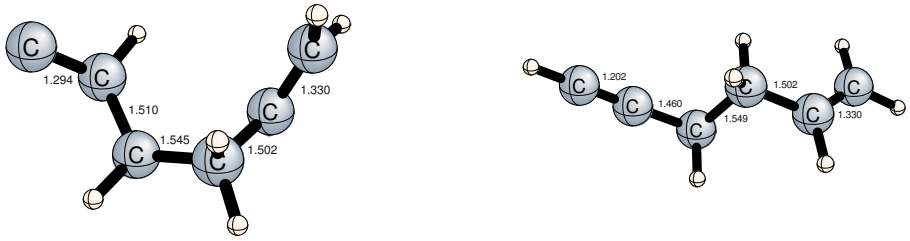

(a) **13a** (b) **9a**

Figure 3.26: Selected interatomic distances (Å) for the **13a** and **9a** structures.

Figure 3.27: The reaction picture for **4a** → **34a** conversion with relative energies (in kcal mol^{-1}). The values over arrows indicate relative energy of TSs.

structures (**3a**, **12a**, and **34a**) suffer from the high ring strain. On the other hand, open-chain structures **9a** and **4a**, and monocyclic **33a** are relatively more stable than those bicyclic struc-

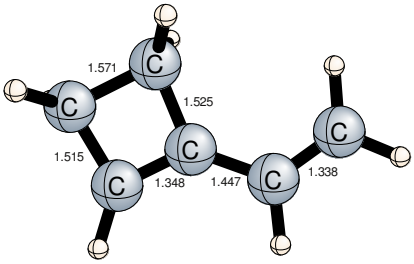

(a) **33a**

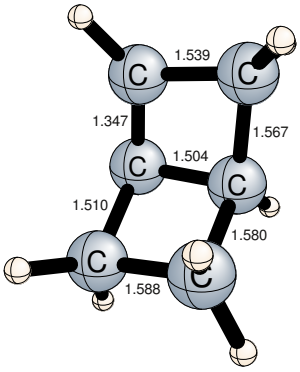

(b) **34a**

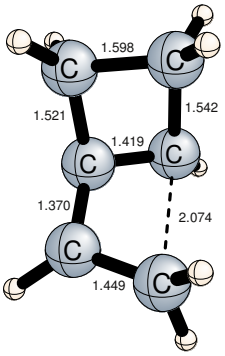

(c) **33a/34a**

Figure 3.28: Selected interatomic distances (Å) for the **33a**, **34a**, and **33a/34a** structures.

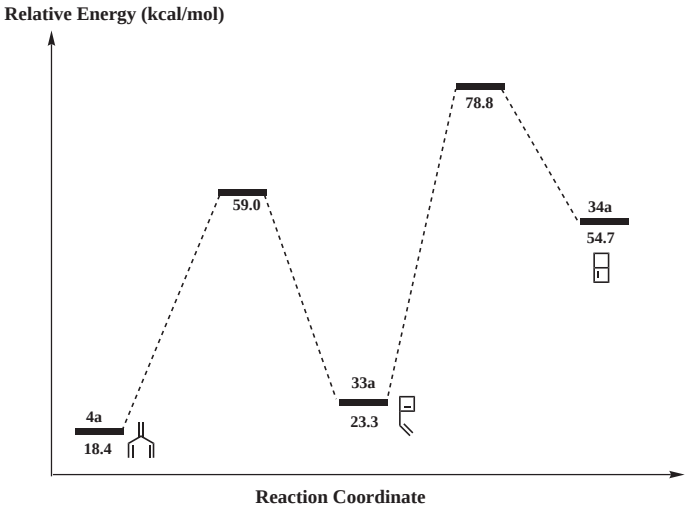

Figure 3.29: Relative energy profile for the **4a** → **34a** conversion.

tures. Hence, the **9a** and **4a** molecules are expected to be major products at high temperatures. Our that expectation is generally consistent with Berson *et al.* [51] observations.

3.2.3 Berson Scheme 2a

The overall picture for the extended Berson **Scheme 2a** is presented in Figure 3.30.

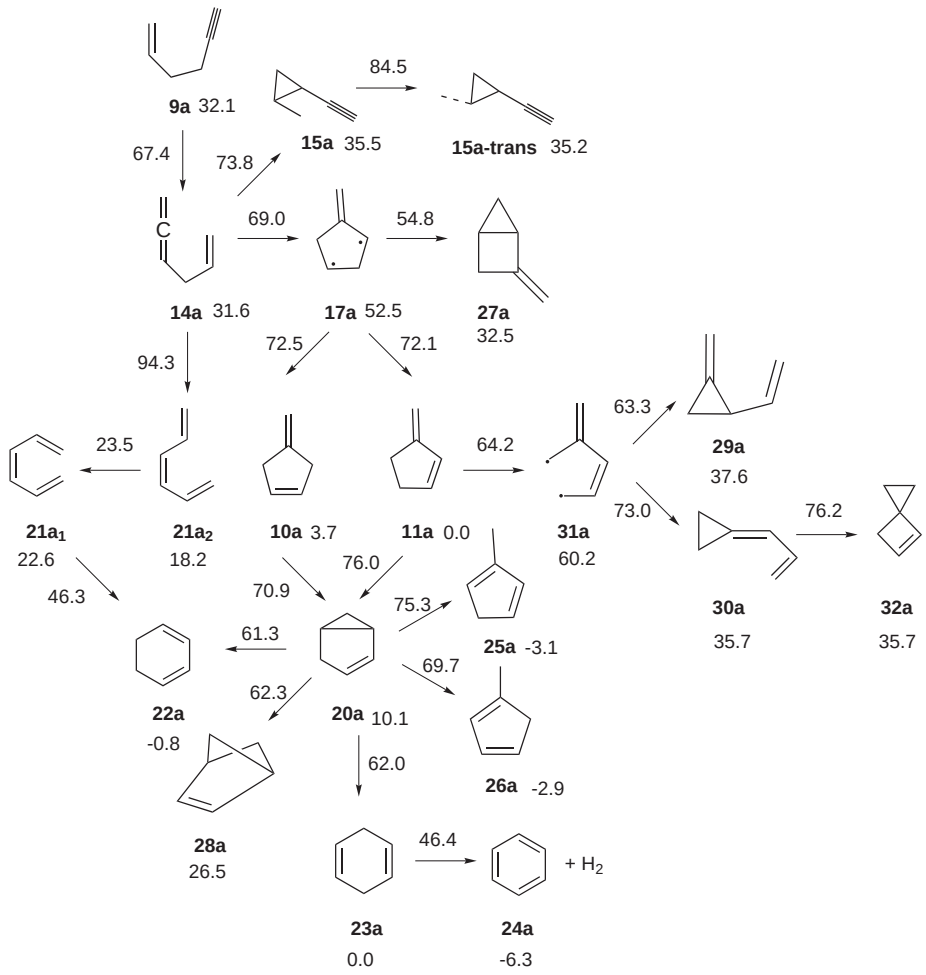

Figure 3.30: The overall picture with relative energies (in kcal mol^{-1}), with respect to **11a**, at CCSD(T)//B3LYP level for the extended Berson **Scheme 2a**. The values over arrows indicate relative energies of TSs. Energies of biradicals are computed according to Eq.(2.41).

3.2.3.1 Formation of Methelenecyclopentenes

Relative energy profile for the Huntsman mechanism (Figure 1.12 on page 8) is provided in Figure 3.31 on the next page.

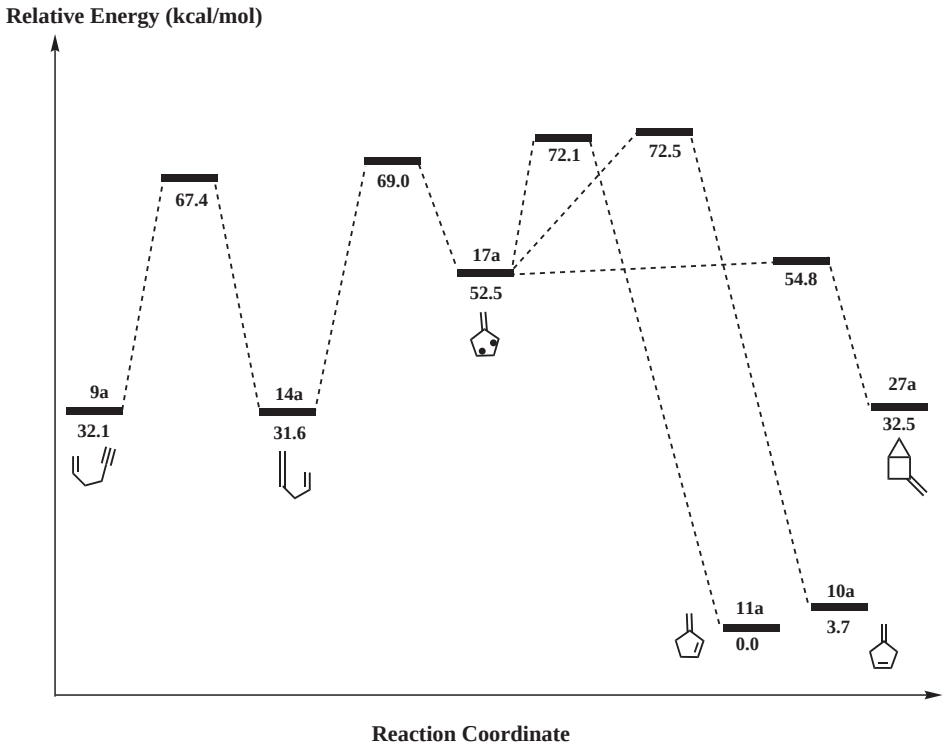

Figure 3.31: Relative energy profile for the Huntsman mechanism.

Roth *et al.* determined the activation parameters of all steps in the Huntsman mechanism (Figure 1.12 on page 8) by carrying out thermolyses experiments [69]. For the reaction **9a** → **14a** in the forward direction their value for the activation energy is 32.8 kcal mol^{-1}, whereas in the reverse direction it is 33.7 kcal mol^{-1}. These findings also mean that species **9a** is higher in enthalpy than **14a** by 0.9 kcal mol^{-1}. Even though the latter difference is within the generally accepted chemical accuracy (or error) of ±1.0 kcal mol^{-1}, it is remarkable that computations at appropriate levels can nearly reproduce it with the correct sign for we found 32.1 − 31.6 = 0.5 kcal mol^{-1} for it. On the other hand, the computed barrier heights, 35.3 and 35.8 kcal mol^{-1}, overestimate the experimental ones by 2.5 and 2.1 kcal mol^{-1} for the forward and reverse directions, respectively.

The interconversions among **14a**, **10a**, **11a**, and **27a** must be discussed together since the reaction paths in all of these rearrangements pass through the biradical **17a**. Based on a personal communication with Dowd, Roth stated that the biradical has a triplet ground state [69]. In this species the two radical centers, being at a distance of 2.35 Å (Figure 3.33 on page 58), should interact weakly, and we therefore expect the singlet to be close to the triplet. In order

to test this hypothesis, we optimized the lowest singlet and triplet states of the biradical at the $(8e, 8o)$CASSCF/6-311G(d,p) level. The triplet minimum was found to be lower in energy, but only by 0.5 kcal mol^{-1} at both the CASSCF and MRMP2//CASSCF levels, in agreement with our expectation.

The TS **17a/27a** is involved in the exo-endo interconversion of **27a**. Roth experimentally studied this geometric isomerization in the 5-methyl derivative of **27a**, and determined the activation energy for the exo-endo conversion as 24.5 kcal mol^{-1}, whereas for the reverse process it was 23.6 kcal mol^{-1} [69]. Our result, 54.8−32.5 = 22.3 kcal mol^{-1} agrees reasonably well with Roth's values. Further, for the **17a** → **27a** reaction the computed activation barrier, 2.3 kcal mol^{-1}, is in good agreement with the experimental value of 3.1 kcal mol^{-1}, which is obtained for rearrangement of dimethyl substituted analogue of **17a** (**17c** to **27c**) again by Roth [69]. In the same work, Roth also determined the activation energies for the three reactions **27a** → **14a**, **27a** → **10a**, and **27a** → **11a** as 36.5, 35.8, and 35.8 kcal mol^{-1}, respectively. According to our findings (Figure 3.31 on the preceding page), the rate determining barrier in the **27a** → **14a** transformation is the TS **14a/17a**. The theoretical barrier height in **27a** → **14a** is thus 69.0 − 32.5 = 36.5 kcal mol^{-1}, in excellent agreement with Roth.

For the rearrangements of **14a** to **10a** and **11a**, a two-step mechanism has been proposed [65] which involves rate-determining cyclization to the 1,3-biradical **17a** followed by 1,2-hydrogen migration in each of two possible directions giving the **10a** and **11a** molecules (Figure 1.12 on page 8). For the rearrangement of **14a** to **17a**, the reaction energy and barrier are calculated as 20.9 kcal mol^{-1} and 37.4 kcal mol^{-1}, respectively. The calculated reaction energy is consistent with Huntsman's crude estimation of 18 kcal mol^{-1} [65]. Further, for the rearrangement of **17a** to **10a**, the reaction energy and barrier are computed as −48.8 and 20.0 kcal mol^{-1}, respectively, while the corresponding results are −52.5 and 19.6 kcal mol^{-1} for the conversion of **17a** to **11a**. The reaction energy for the second step in the cyclization of **14a** is estimated to be approximately −50 kcal mol^{-1} [65]. Hence, our results, −48.8 and −52.5 kcal mol^{-1}, are again consistent with Huntsman's crude estimation of −50 kcal mol^{-1} [65]. On the other hand, Roth's measurements indicate that the barriers **17a/10a** and **17a/11a** have the same energy that is slightly lower (by 0.7 kcal mol^{-1}) than **14a/17a**. This means that the same barrier **14a/17a** is rate determining in the conversions of **14a** into **27a**, **10a**, and **11a**. Again in the same work, Roth also determined the activation energies for the individual reactions **14a** → **10a** and **14a** → **11a** as 36.6 and 36.8 kcal mol^{-1}, respectively [69]. There

is also the value 37.2 kcal mol^{-1}for **14a** → **10a + 11a**, reported by Huntsman *et al.* [65]. We have found that the enthalpy of **27a** is 0.9 kcal mol^{-1} higher than that of **14a**. Assuming that our computational result is correct, and combining with Roth's value for **14a** → **27a**, one would expect an activation energy of 36.5 + 0.9 = 37.4 kcal mol^{-1} for the reverse reaction. Furthermore, the computed barrier height is 69.0 – 31.6 = 37.6 kcal mol^{-1}, in good agreement with the expected value. It appears, therefore, that Huntsman's value of 37.2 kcal mol^{-1} is more reliable for the activation energy in **14a** → **17a**.

Additionally, we have also calculated the relative amounts of **10a** and **11a** using transition-state theory (TST) [213, 214] to compare our computations with the experimental values [65, 68, 70]. At temperatures 253, 385, and 530 °C the calculated [**11a**]/[**10a**] ratios are 1.5, 1.4, and 1.3, respectively, which are in very good agreement with the experimental values of 1.4 [68], 1.3 [65], and 1.3 [70]. Thus, these results indicate that relative barrier heights for the **17a** → **10a** and **17a** → **11a** reactions are computed very accurately.

Furthermore, Black *et al.* [215] calculated the activation energy for the **9a** → **14a** reaction as 30.7 and 33.0 kcal mol^{-1} at MP2/6-31G(d)//RHF/6-31G(d) and B3LYP/6-31G(d) levels, respectively, which are also consistent with our result. The computed geometries of **9a** and **14a** are similar to those of Black *et al.* [215], while the geometry of **9a/14a** is consistent with those reported for Cope rearrangements [216-218]. The computed geometries of **14a** and **9a/14a** are shown in Figure 3.32, **17a** and **14a/17a** in Figure 3.33 on the next page, **10a** and **11a** in Figure 3.34 on the following page, **17a/10a** and **17a/11a** in Figure 3.35 on the next page, and **27a** and **17a/27a** in Figure 3.36 on page 59.

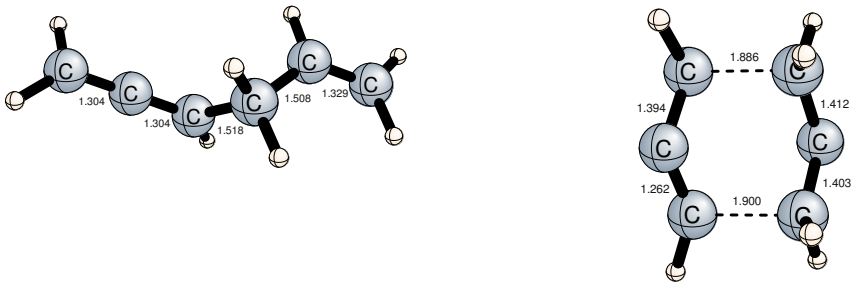

(a) **14a** (b) **9a/14a**

Figure 3.32: Selected interatomic distances (Å) for the **14a** and **9a/14a** structures.

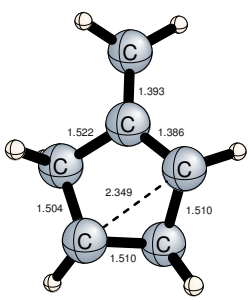

(a) **17a**

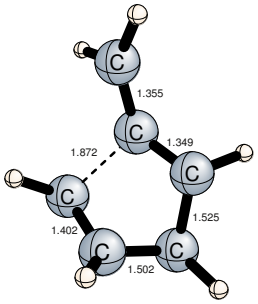

(b) **14a/17a**

Figure 3.33: Selected interatomic distances (Å) for the **17a** and **14a/17a** structures.

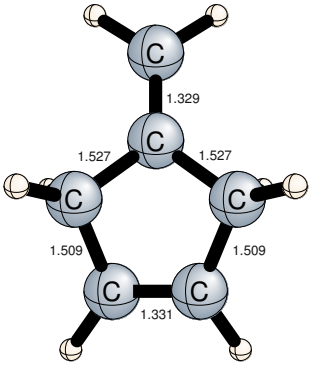

(a) **10a**

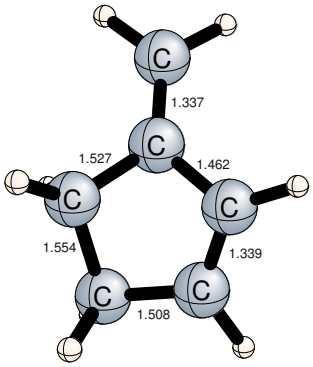

(b) **11a**

Figure 3.34: Selected interatomic distances (Å) for the **10a** and **11a** structures.

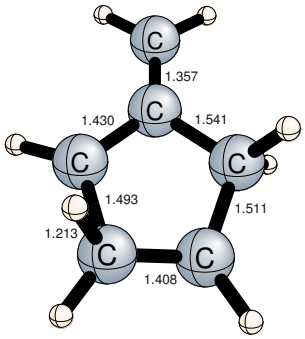

(a) **17a/10a**

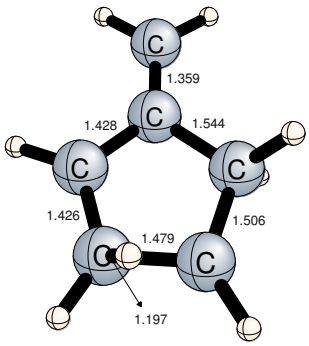

(b) **17a/11a**

Figure 3.35: Selected interatomic distances (Å) for the **17a/10a** and **17a/11a** structures.

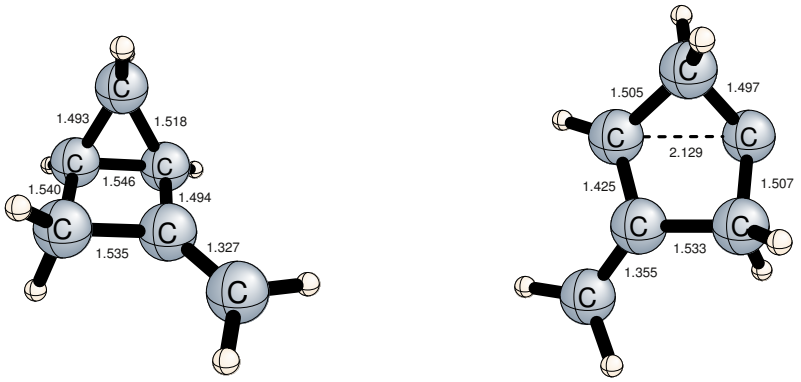

(a) **27a** (b) **17a/27a**

Figure 3.36: Selected interatomic distances (Å) for the **27a** and **17a/27a** structures.

Moreover, the **17a** molecule has two resonance structures as shown in Figure 3.37. The cyclization of **17a** via second resonance hybrid will yield a cyclic molecule with bridgehead double bond. However, it is well-known that formation of such a molecule is very difficult as expressed by Bredt's rule which states that "*A double bond cannot be placed with one terminus at the bridgehead of a bridged ring system unless the rings are large enough to accommodate the double bond without excessive strain*" [219, 220]. Indeed, a B3LYP/6-311G(d,p) optimization places the bicyclic molecule 69 kcal mol^{-1} above **27a**.

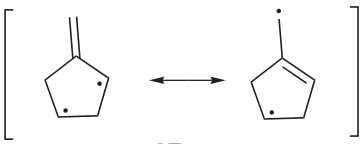

17a

Figure 3.37: Resonance structures of **17a**.

3.2.3.2 Hopf Mechanism

Relative energy profiles for Hopf *et al.*'s [70] suggested mechanism (Figure 1.14 on page 10) are provided in Figures 3.38 on the next page and 3.39 on page 61. Thermal rearrangement of **14a** to **15a** occurs via simultaneous 1,3-cyclization and 1,6-hydrogen shift. The conversion frame requires a *syn* orientation, thus only the *cis* isomer can be formed. The calculated reaction energy and barrier are 3.9 and 42.2 kcal mol^{-1}, respectively. The *cis* **15a** isomer transforms to the **15a-trans** molecule with a reaction energy of −0.3 and reaction barrier of 49.0

kcal mol^{-1}. The relative energy of **15a/15a-trans** is 84.5 kcal mol^{-1}, which is high compared with other relative energies. Thus, formation of the **15a-trans** molecule is not expected, except for very high temperatures. The computed geometries of the **15a** and **14a/15a** structures are shown in Figure 3.40 on the next page, while **15a-trans** and **15a/15a-trans** structures are shown in Figure 3.41 on page 62.

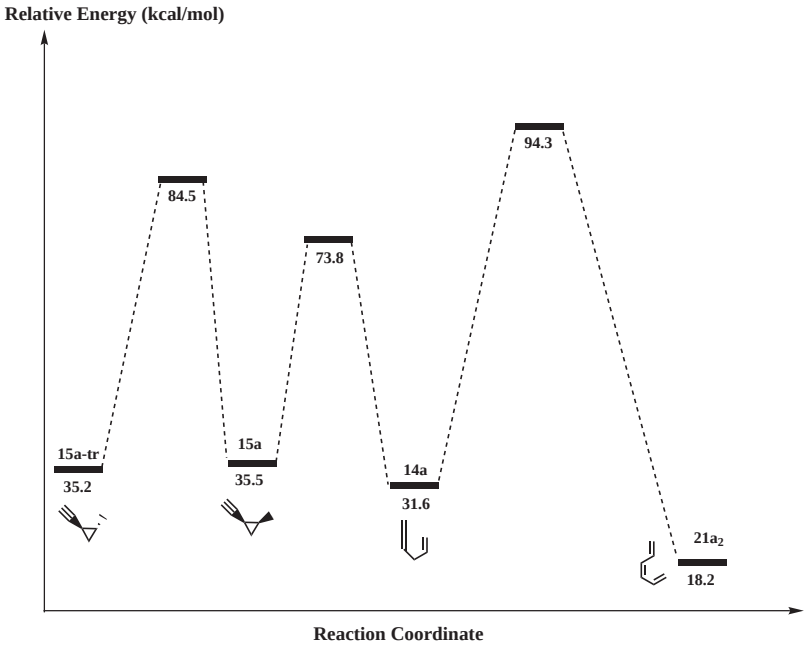

Figure 3.38: Relative energy profile for the Hopf mechanism (Part I).

Hopf *et al.* suggested that the triene **21a**$_1$ (Figure 1.14 on page 10) might be formed from **14a**. Then, triene can yield benzene by several consecutive reactions. At first, the possibility of formation of triene from **14a** has been investigated. The results obtained show that the allene **14a** rearranges to triene **21a**$_2$ by 1,3-hydrogen shift. The reaction energy and barrier are calculated as −9.0 and 62.7 kcal mol^{-1}, respectively. Further, the relative energy of TS that connects **14a** to **21a**$_2$, **14a/21a** is, 94.3 kcal mol^{-1}, too high compared with other relative energies. Thus, our results demonstrate that Hopf *et al.*'s [70] suggested mechanism for the formation of **21a**$_2$ from **14a** is kinetically unfavorable. Hence, in the following subsection an alternative path will be considered for the formation of benzene (**24a**). The computed geometries of the **21a**$_2$ and **14a/21a**, structures are shown in Figure 3.42 on page 62.

The triene **21a**$_2$ rearranges to **21a**$_1$ with a reaction energy of 4.4 kcal mol^{-1} and an activation barrier of 5.3 kcal mol^{-1}. Then, the triene **21a**$_1$ rearranges to 1,3-cyclohexadiene, **22a**, via a

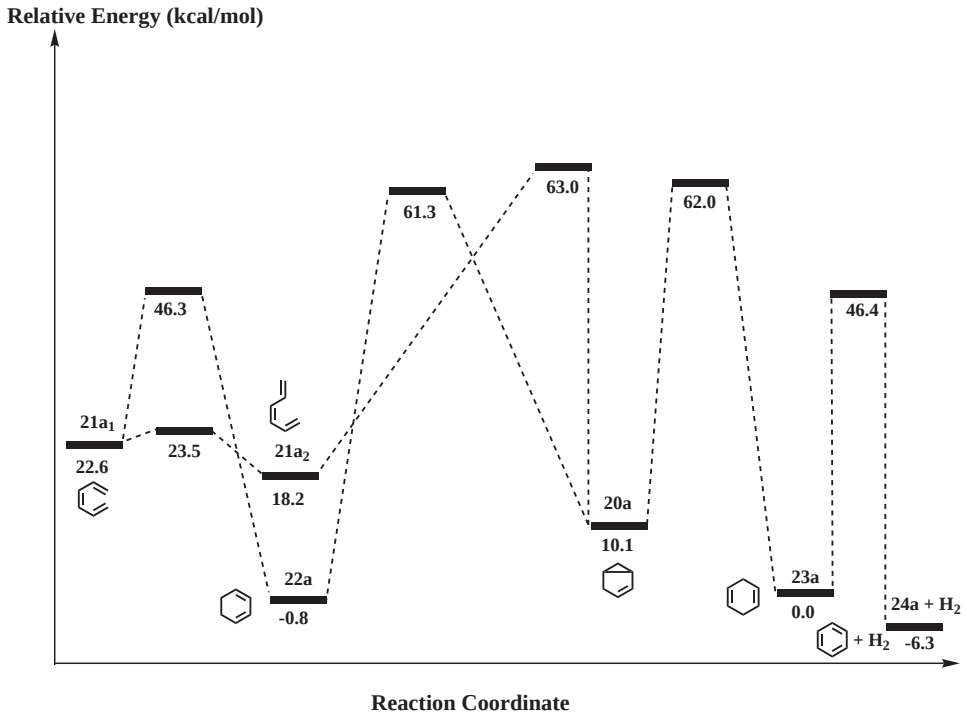

Figure 3.39: Relative energy profile for the Hopf mechanism (Part II).

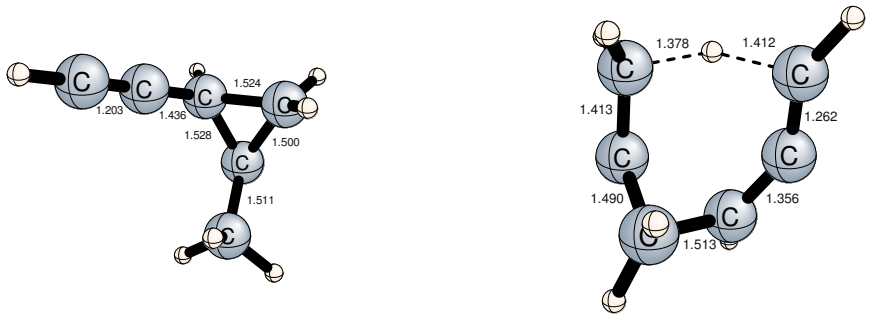

(a) **15a** (b) **14a/15a**

Figure 3.40: Selected interatomic distances (Å) for the **15a** and **14a/15a** structures.

well-known electrocyclic ring closure [208]. For the **21a**$_1$ → **22a** conversion, the calculated reaction energy and barrier are −23.4 and 23.7 kcal mol^{-1}, respectively. Our results, −23.4 and 23.7 kcal mol^{-1}, are consistent with Rodriguez-Otero's computation of −23.0 and 24.8 kcal mol^{-1} at the QCISD(T)/6-31G(d,p)//MP2/6-31G(d,p) level for the reaction energy and barrier, respectively [221]. The computed geometries of **21a**$_1$ and **21a**$_1$**/21a**$_2$ are shown in Figure 3.43, while **22a** and **21a/22a** are shown in Figure 3.44 on the next page.

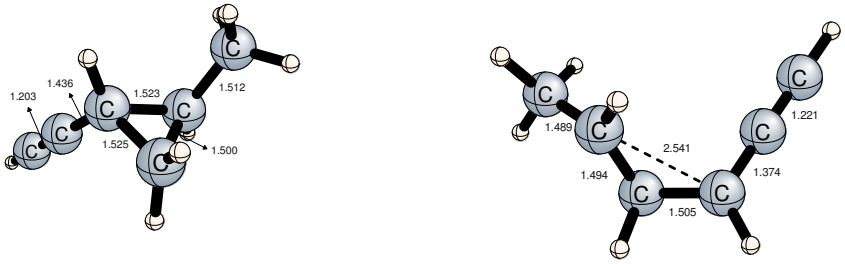

(a) **15a-trans** (b) **15a/15a-trans**

Figure 3.41: Selected interatomic distances (Å) for the **15a-trans** and **15a/15a-trans** structures.

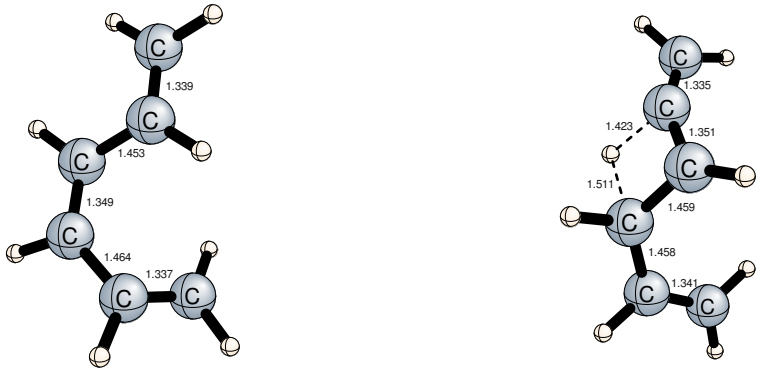

(a) **21a**$_2$ (b) **14a/21a**$_2$

Figure 3.42: Selected interatomic distances (Å) for the **21a**$_2$ and **14a/21a**$_2$ structures.

The **22a** molecule further rearranges to the bicyclic intermediate **20a** via an initial 1,2-hydrogen shift followed by ring closure. That bicyclic intermediate, **20a**, plays a prominent role for connecting methylenecyclopentenes **10a** and **11a** to the benzene molecule. For the process **22a** → **20a**, the reaction energy and barrier are calculated as 10.9 and 62.1 kcal mol^{-1}, respectively. The calculated activation energy for the reverse reaction (**20a** → **22a**) is 51.2 kcal mol^{-1}, which is in good agreement with the experimental value of 50.2 kcal mol^{-1} [73]. Further, Roth *et al.* [222] determined formation enthalpies of **20a** and **11a** as 37.8 and 27.6 kcal mol^{-1}, respectively, by calorimetry hydrogenation method. Hence, the experimental relative energy of **20a** is 10.2 kcal mol^{-1}, which is in excellent agreement with our result of 10.1 kcal mol^{-1}. Moreover, the experimental formation enthalpy of **22a** was reported as 25.4 kcal mol^{-1} [223],

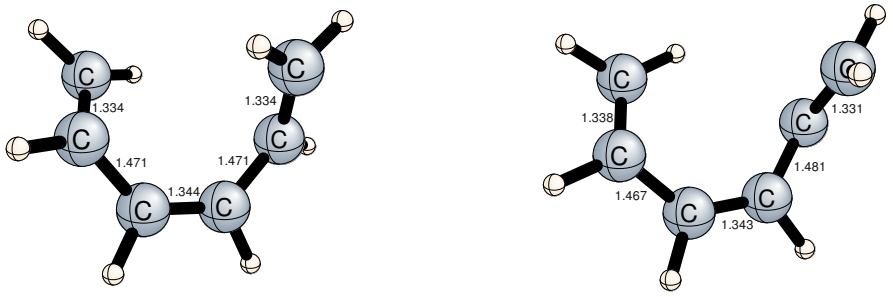

(a) **21a**$_1$ (b) **21a**$_1$**/21a**$_2$

Figure 3.43: Selected interatomic distances (Å) for the **21a**$_1$ and **21a**$_1$**/21a**$_2$ structures.

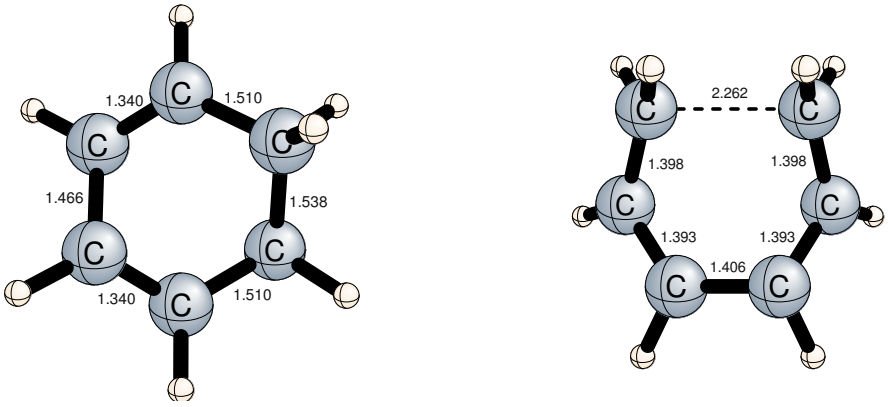

(a) **22a** (b) **21a/22a**

Figure 3.44: Selected interatomic distances (Å) for the **22a** and **21a/22a** structures.

thus experimental relative energy of **22a** is −2.2 kcal mol^{-1}. The computed relative energy is 1.4 kcal mol^{-1} higher than experiment. The computed geometries of the **20a** and **20a/22a** structures are shown in Figure 3.45 on the next page.

The **20a** intermediate rearranges to 1,4-cyclohexadiene (**23a**) via 1,2-hydrogen shift. The calculated values for the reaction energy and barrier are −10.1 and 51.9 kcal mol^{-1}, respectively. The experimental activation energy for this reaction is 50.2 kcal mol^{-1} [73]. Thus, the calculated value of 51.9 kcal mol^{-1} is in good agreement with experiment. Further, the experimental formation enthalpy of **23a** was reported as 26.1 kcal mol^{-1} by Roth *et al.* [222], thus experimental relative energy of **22a** is −1.5 kcal mol^{-1}. Hence, the computed relative energy is 1.5 kcal mol^{-1} higher than experiment. The **20a** molecule can also rearrange to **21a**$_2$ with

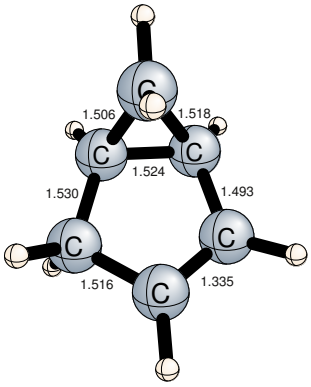

(a) **20a**

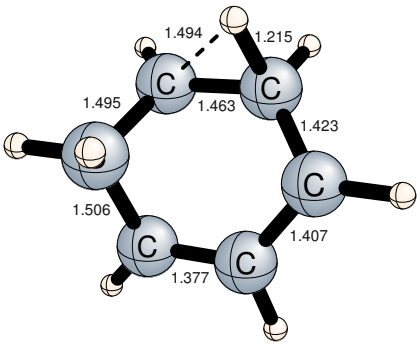

(b) **20a/22a**

Figure 3.45: Selected interatomic distances (Å) for the **20a** and **20a/22a** structures.

a reaction energy of 12.5 and reaction barrier of 52.9 kcal mol^{-1}, respectively. The computed geometries of the **23a**, **20a/21a**, and **20a/23a** structures are shown in Figure 3.46.

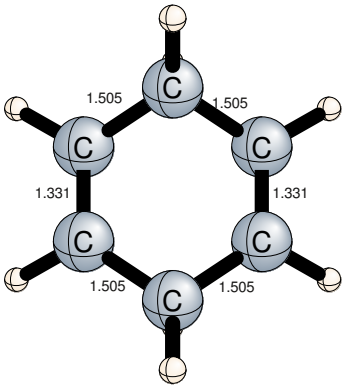

(a) **23a**

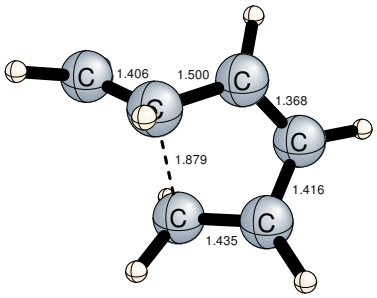

(b) **20a/21a**

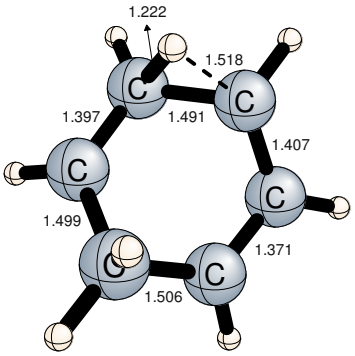

(c) **20a/23a**

Figure 3.46: Selected interatomic distances (Å) for the **23a**, **20a/21a**, and **20a/23a** structures.

The **23a** molecule decomposes to the benzene + H_2 via a *syn* elimination by a retro Diels-Alder like mechanism [74] (Figure 1.16 on page 11). The reaction energy and barrier are −6.3 and 46.4 kcal mol^{-1}, respectively. The experimental activation energy for this dissociation has been reported as 42.7 kcal mol^{-1} [73]. Hence, the calculated reaction barrier of is too high by 3.7 kcal mol^{-1}. The computed geometry of the **24a** and **23a/24a** structures are shown in Figure 3.47.

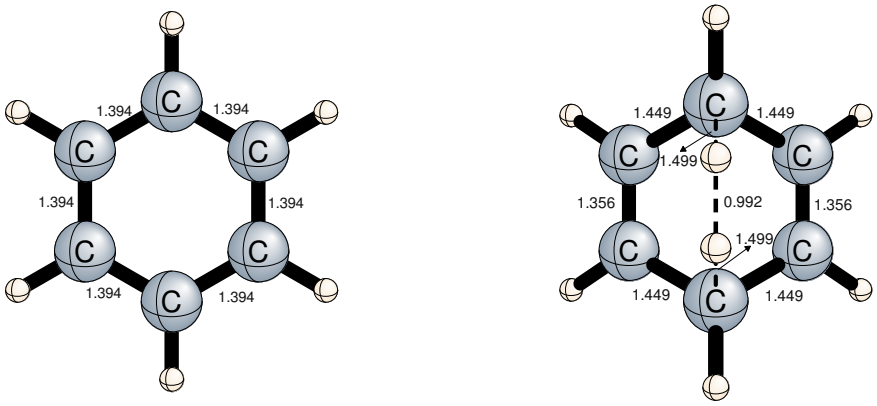

(a) **24a** (b) **23a/24a**

Figure 3.47: Selected interatomic distances (Å) for the **24a** and **23a/24a** structures.

3.2.3.3 An Alternative Path to Formation of Cyclohexadienes

Relative energy profile for the methylenecyclopentenes route (Figure 1.17 on page 12) is provided in Figure 3.48 on the next page. As discussed in previous subsection, the path connecting **14a** to **21a** has a high energy TS. In this subsection, an alternative path to formation of cyclohexadienes (thus benzene) has been investigated. For this purpose, Huntsman *et al.*'s [78] mechanism has been considered (Figure 1.17 on page 12). Formation of bicyclic intermediate **20a** from methylenecyclopentenes route has been studied. The **10a** molecule rearranges to **20a** via a radicalic mechanism (Figure 1.17 on page 12). First biradicalic intermediate **18a** is formed via 1,2-hydrogen shift, then **18a** cyclizes to **20a** (Figure 1.17 on page 12). As proposed by Huntsman *et al.* [78], first we consider formation of biradicalic intermediate **18a** (Figure 1.17 on page 12). However, the **18a** structure does not correspond to any stationary point. Since the **18a** structure includes a primary radicalic center, it is not stable. However, it still plays an important role in rearrangement of **10a**. When IRC computations are carried out, it is observed that the TS **10a/20a** connecting **10a** to **20a** pass through the **18a** structure.

For the **10a** → **20a** conversion, the reaction energy and barrier are calculated as 6.4 and 67.2 kcal mol^{-1}, respectively. Similarly, the **11a** molecule rearranges to **20a**. Again, IRC computations showed that the reaction path through TS **11a/20a** connecting **11a** to **20a** passes through the **19a** structure (Figure 1.17 on page 12). For this conversion, the reaction energy and barrier are calculated as 10.1 and 76.0 kcal mol^{-1}, respectively. Compared with the allene (**14a**) route to formation of **20a** (**14a** → **22a** → **20a**), the methylenecyclopentenes route includes lower energy TSs. The relative energy of **14a/21a** is 23.4 and 18.3 kcal mol^{-1} higher than that for **10a/20a** and **11a/20a** TSs, respectively. Therefore, the formation of **20a** (thus benzene) proceeds by methelenecyclopentenes route. The computed geometries of the **10a/20a** and **11a/20a** structures are shown in Figure 3.49 on the next page.

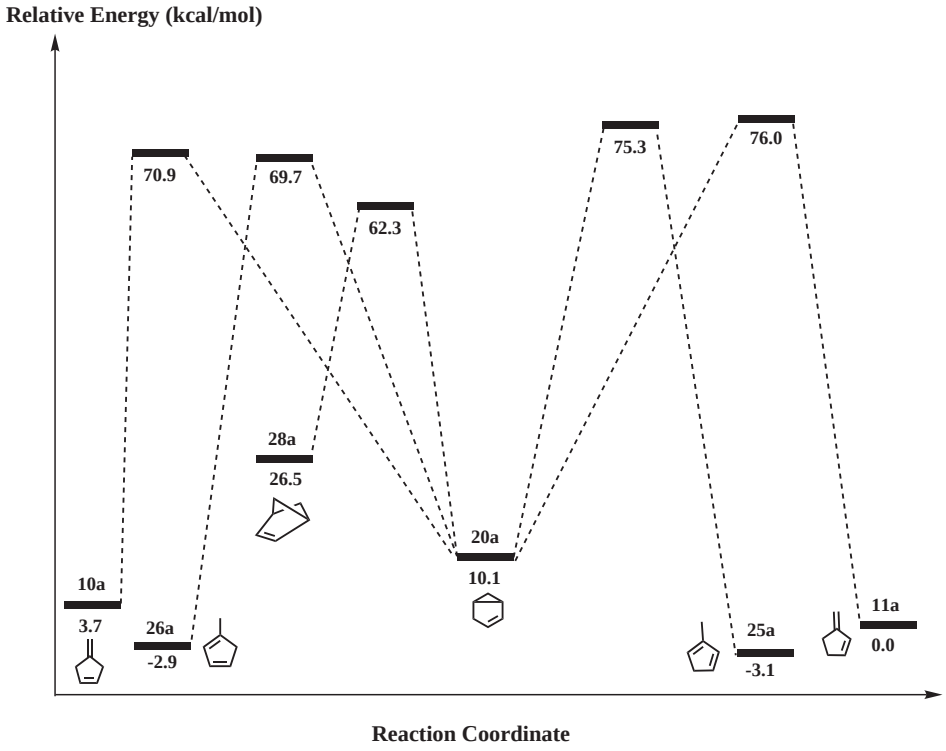

Figure 3.48: Relative energy profile for the methylenecyclopentenes route.

Another remarkable point is that **10a/20a** is 5.1 kcal mol^{-1} lower in energy than **11a/20a**. Since **18a** has two resonance hybrids (Figure 3.50 on page 68), while **19a** has only one (Figure 1.17 on page 12), the **10a** route proceeds via a relatively more stable biradicalic structure, **18a**, than **11a** route. Therefore, the **10a** route has a lower energy TS. One of the resonance hybrids of **18a** cyclizes to **20a**, while the other one cyclizes to bicyclic **28a** molecule. Hence, the **18a** structure also connects **28a** to **20a**. Since, **19a** has only one resonance structure, it

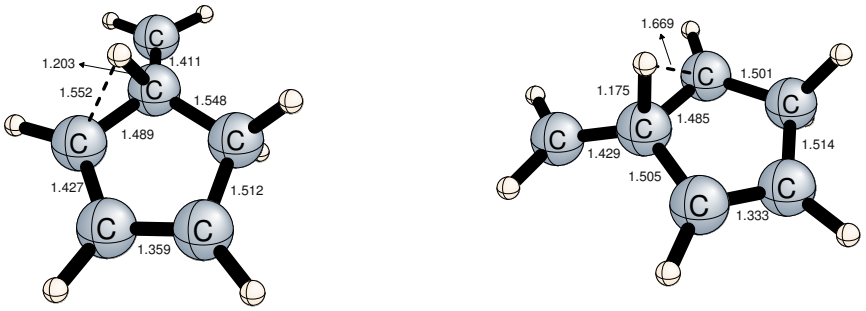

(a) **10a/20a** (b) **11a/20a**

Figure 3.49: Selected interatomic distances (Å) for the **10a/20a** and **11a/20a** structures.

can only cyclize to **20a** molecule. The calculated reaction energy and barrier, for conversion of **20a** to **28a**, via **18a** structure, are 16.4 and 52.2 kcal mol^{-1}, respectively. Further, the experimental value of activation energy for the **28a** → **20a** conversion was reported as 35.2 kcal mol^{-1} [224, 225]. Thus, our result, 62.3 − 26.5 = 35.8 kcal mol^{-1}, is in good agreement with experiment.

Moreover, the experimental formation enthalpy of **28a** was reported as 60.0 kcal mol^{-1} again by Roth *et al.* [222], thus experimental relative energy of **28a** is 32.4 kcal mol^{-1}. The computed relative energy of 26.5 kcal mol^{-1} is 5.9 kcal mol^{-1} lower than experiment. Apparently there is a discrepancy between our result and experiment. Altough the computed reaction barrier for the **28a** → **20a** conversion is in good agreement with experiment [224, 225], the reason why the computed relative energy of **28a** is so different is unclear. Further, we have carried out CCSD(T) computation at optimized MP2 geometries instead of B3LYP geometries in order to show whether that discrepancy is related to the computed geometries or not. However, we obtained almost the same result which indicates that the problem is not related to the geometries. Then, we have performed completely renormalized coupled-cluster lambda (CR-CCL) computations, which is much more expensive than CCSD(T) but it works better in problematic cases, at B3LYP geometries and calculated a relative energy of 26.3 kcal mol^{-1}, no improvement. Then, we have included core electrons in CCSD(T) computations and obtained a relative energy of 26.2 kcal mol^{-1}, again no improvement. Finally, we decided to use a much larger basis set, cc-pVTZ, to investigate whether the problem is related to the basis set, and we calculated the relative energy as 28.6 kcal mol^{-1} at the CCSD(T)/cc-pVTZ

level, which is somewhat better than the CCSD(T)/6-311G(d,p) result but still not in a good agreement with experiment. The computed geometries of **28a** and **20a/28a** are shown in Figure 3.51.

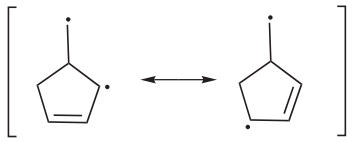

18a

Figure 3.50: Resonance structures of **18a**.

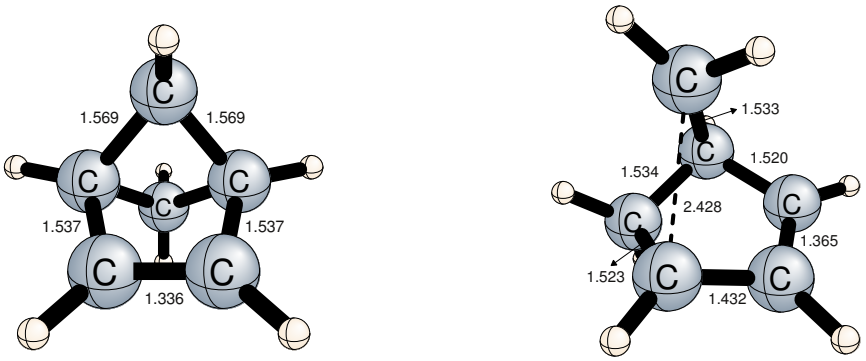

(a) **28a** (b) **20a/28a**

Figure 3.51: Selected interatomic distances (Å) for the **28a** and **20a/28a** structures.

The **20a** molecule also rearranges to **25a** via the **18a** structure, and to **26a** molecules via the **19a** structure. The calculated reaction energy and barrier are −13.2 and 65.2 kcal mol^{-1} for conversion to **25a**, while −13.0 and 59.6 kcal mol^{-1} for conversion to **26a**, respectively. The computed geometries of the **25a** and **20a/25a** structures are shown in Figure 3.52, while the **26a** and **20a/26a** structures are shown in Figure 3.53 on the next page.

3.2.3.4 Vinylmethylenecyclopropane Rearrangement

Relative energy profile for the vinylmethylenecyclopropane rearrangement (Figure 3.55 on page 70) is provided in Figure 3.54 on page 70. In this subsection, Shields *et al.*'s [79] mechanism has been studied. The **11a** molecule rearranges to biradicalic intermediate **31a** by a single bond cleavage process. Both radicalic centers in **31a** intermediate are allylic radicals, thus **31a** intermediate is stabilized by resonance effects. For the **11a** → **31a** conversion,

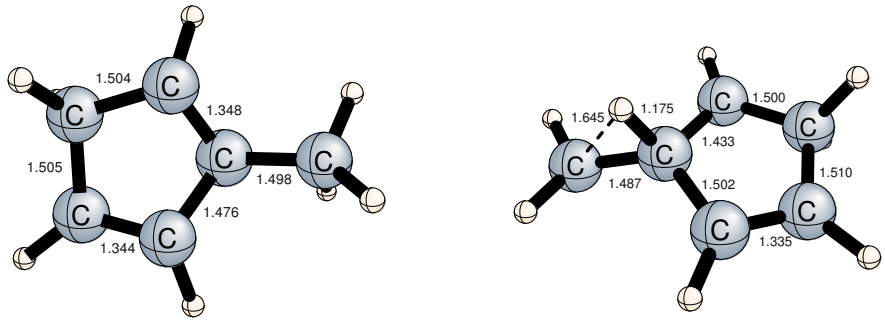

(a) **25a** (b) **20a/25a**

Figure 3.52: Selected interatomic distances (Å) for the **25a** and **20a/25a** structures.

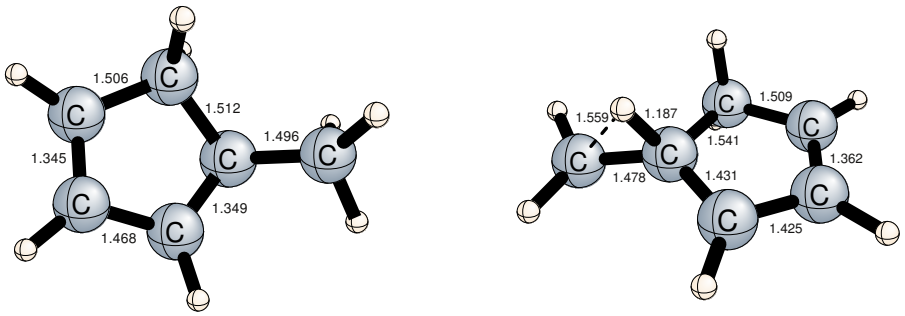

(a) **26a** (b) **20a/26a**

Figure 3.53: Selected interatomic distances (Å) for the **26a** and **20a/26a** structures.

the reaction energy and barrier are 60.2 and 64.2 kcal mol^{-1}, respectively. The computed geometries of the **31a** and **11a/31a** structures are shown in Figure 3.55 on the following page.

The biradical **31a** rearranges to **29a** by a well-known vinylcyclopropane rearrangement [3]. The reaction energy and barrier are −22.6 and 3.1 kcal mol^{-1}, respectively. Further, Billups *et al.* [80] determined the activation energy as 25.8 kcal mol^{-1} for the reverse reaction (**29a** → **31a**). For **29a** → **31a** reaction the calculated reaction barrier is 25.7 kcal mol^{-1}, which is in excellent agreement with the experimental value of 25.8 kcal mol^{-1}. The biradical **31a** also rearranges to **30a**. For the **31a** → **30a** conversion, the reaction energy and barrier are −24.5 and 12.8 kcal mol^{-1}, respectively. The **31a** molecule has three unique resonance hybrids as shown in Figure 3.56. The cyclization of **31a** via resonance structures I, II, and III yields

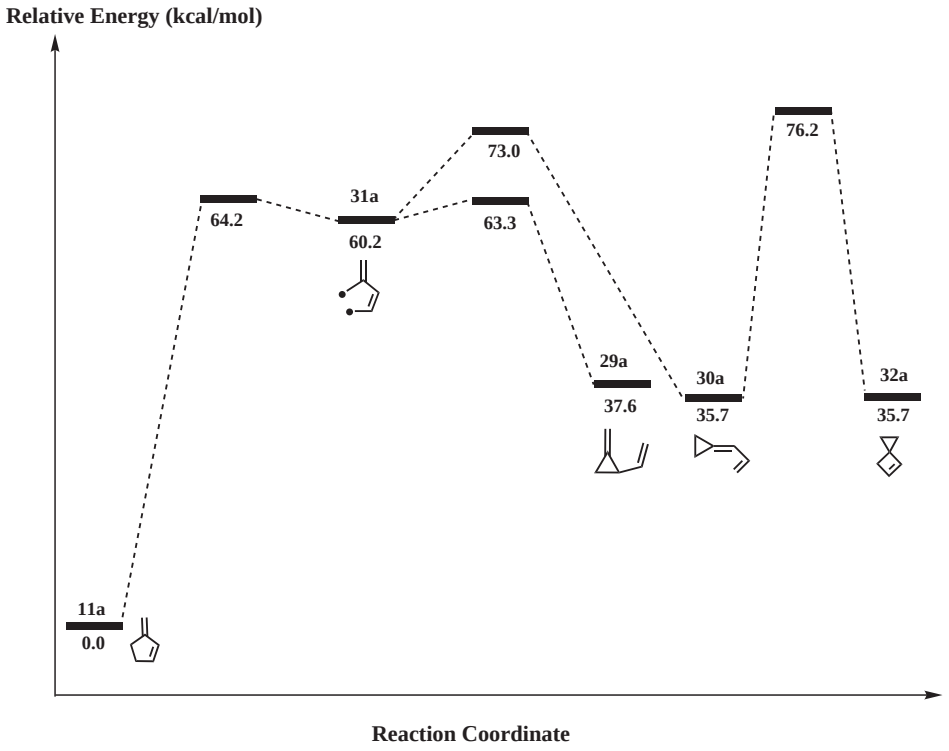

Figure 3.54: Relative energy profile for the vinylmethylenecyclopropane rearrangement.

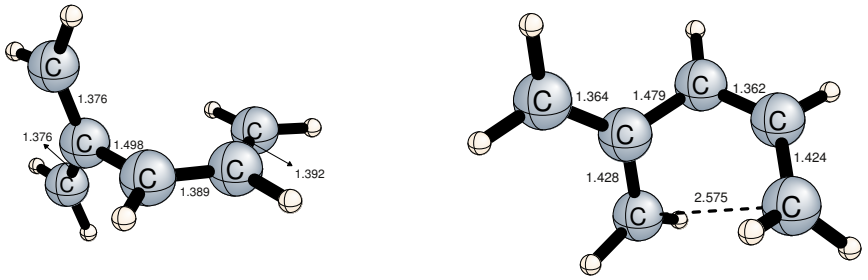

(a) **31a** (b) **11a/31a**

Figure 3.55: Selected interatomic distances (Å) for the **31a** and **11a/31a** structures.

11a, **29a**, and **30a**, respectively. Comparing the resonance hybrids, one can conclude that the structure II is more stable than the other two structures. Structure II has one primary and one secondary radicalic centers, while the other two structures have only primary radicalic centers. Thus, the TS **31a/29a** yielding **29a**, is more stabilized by resonance effects compared to **31a/30a**. Therefore, **31a/29a** is 9.7 kcal mol^{-1} lower in energy than **31a/30a**. The computed

geometries of the **29a** and **31a/29a** structures are shown in Figure 3.57, while those of **30a** and **31a/30a** are given in Figure 3.58 on the following page.

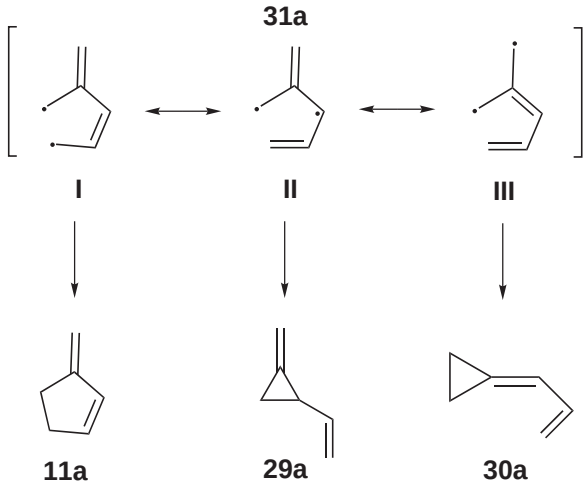

Figure 3.56: Resonance structures of **31a**.

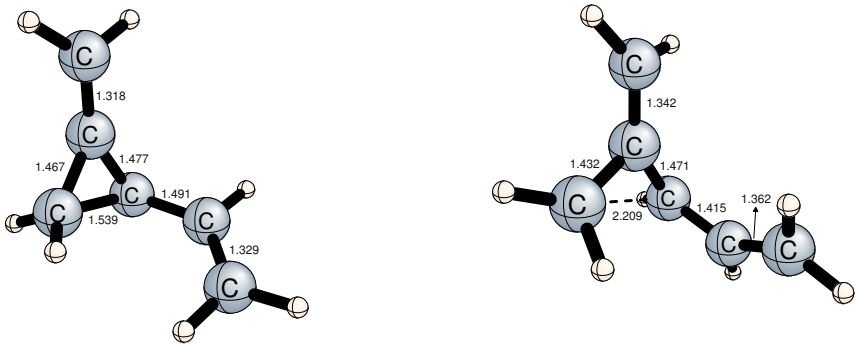

(a) **29a** (b) **31a/29a**

Figure 3.57: Selected interatomic distances (Å) for the **29a** and **31a/29a** structures.

The **30a** molecule further rearranges to **32a** via a well-known electrocyclic reaction [208]. The reaction energy and barrier are 0.0 and 40.5 kcal mol^{-1}, respectively. The computed geometries of the **32a** and **30a/32a** structures are shown in Figure 3.59 on the next page.

Considering the overall picture for the extended Berson **Scheme 2a**, the major product of both pyrolysis reactions (Figure 1.9 on page 7) is expected to be the **24a** (benzene) molecule. Since **24a** is a dissociation product, under experimental conditions (700 °C and 10^{-3} - 10^{-4} torr) [51] the recombination of **24a** and H_2 is not probable. Further, the **10a**, **11a**, **25a**, and

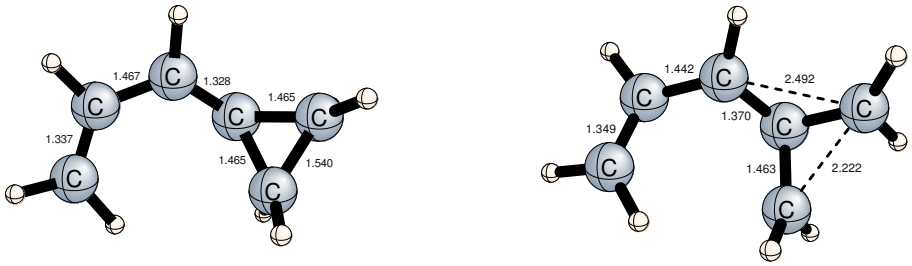

(a) **30a** (b) **31a/30a**

Figure 3.58: Selected interatomic distances (Å) for the **30a** and **31a/30a** structures.

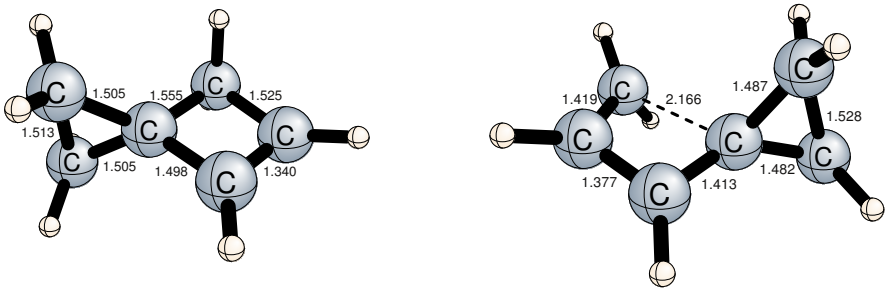

(a) **32a** (b) **30a/32a**

Figure 3.59: Selected interatomic distances (Å) for the **32a** and **30a/32a** structures.

26a molecules are relatively more stable isomers among the set of all minima considered. Therefore, under experimental conditions these molecules may also be observed as minor products. Consequently, our results are consistent with Berson and co-workers observations [51].

3.3 Thermal Rearrangements of 2-isopropylidenecyclopenta-1,3-diyl Biradical

Since Berson *et al.* [51] carried out their experiments with dimethyl-substituted analogous of the TMMa system, in this section we will investigate rearrangements of those dimethyl-substituted molecules, the TMMc system. In most of the reactions, the methyl groups are

not directly involved in the rearrangements, hence the methyl groups are just substituents. As can be expected, substituent effects do not change main aspects of the reactions, thus reaction energies and barriers are slightly different from those in the TMMa system. However, in several reactions the methyl groups are directly involved in the reactions, and those reactions do not occur in the TMMa system. In the following subsections, we will summarize the similarities with the TMMa system, but emphasize the main differences.

3.3.1 Rearrangements Involving Berson TMMc Structures

As in case of the TMMa system, biradical **1c** is generated from diazene **2c** by thermal denitrogenation reaction (Figure 3.60). The computed relative energies and reaction barrier are nearly same as in the TMMa system ($\Delta E \leq 1.0$ kcal mol^{-1}). The computed geometries of diazene **2c** and **2c/1c** structures are shown in Figure 3.61.

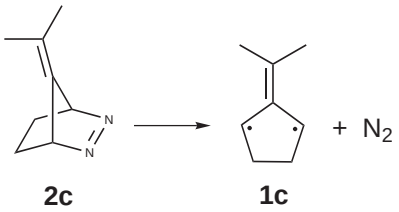

Figure 3.60: Formation of biradical **1c** from diazene **2c**.

(a) **2c** (b) **2c/1c**

Figure 3.61: Selected interatomic distances (Å) for the **2c** and **2c/1c** structures.

Rearrangements among **1c**, **3c**, **4c**, and **12c** have been investigated next (Figure 3.62 on page 74). Relative energies differ by not more than 1-2 kcal mol^{-1} from those for the TMMa system.

The computed geometries of the **12c** and **1c/12c** structures are shown in Figure 3.63, the **3c** and **1c/3c** structures are in Figure 3.64 on the facing page, and the **4c** and **1c/4c** structures are in Figure 3.65 on page 75.

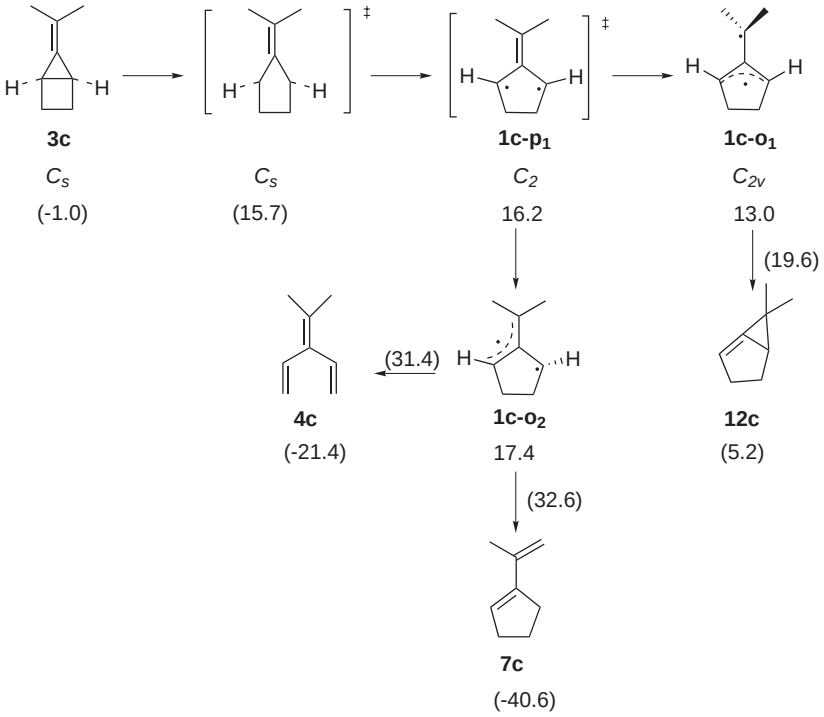

Figure 3.62: Reaction paths connecting the bicyclic MCPs, **3c**, **12c**, and species **4c** and **7c** with TMMs. ZPVE corrected energies (in kcal mol^{-1}) relative to triplet **1c-T** at MRMP2//CASSCF and CCSD(T)//B3LYP (in parentheses) are indicated. A (4*e*,4*o*) active space is used for biradicals.

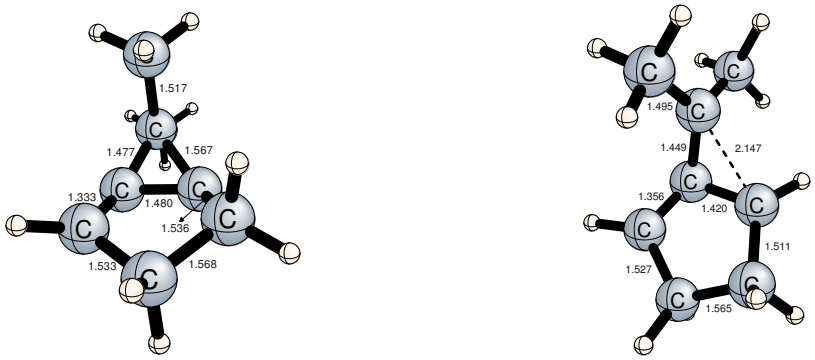

(a) **12c** (b) **1c/12c**

Figure 3.63: Selected interatomic distances (Å) for the **12c** and **1c/12c** structures.

As distinct from the TMMa system, biradical **1c** can also rearrange to **7c** by 1,4-hydrogen shift. The reaction proceeds via a five-membered cyclic transition state (Figure 3.66 on page

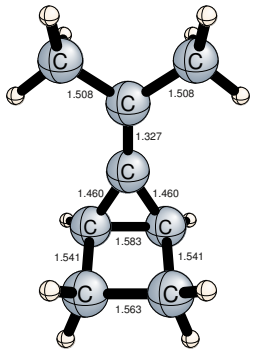

(a) **3c**

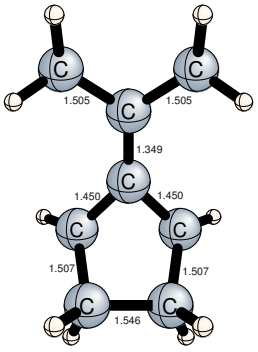

(b) **1c/3c**

Figure 3.64: Selected interatomic distances (Å) for the **3c** and **1c/3c** structures.

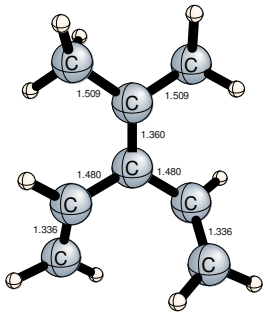

(a) **4c**

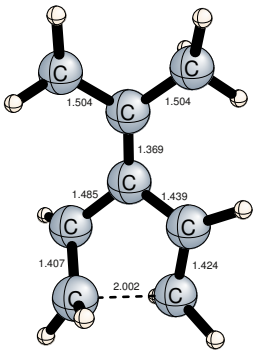

(b) **1c/4c**

Figure 3.65: Selected interatomic distances (Å) for the **4c** and **1c/4c** structures.

76). The calculated reaction energy and barrier are −58.0 and 15.2 kcal mol^{-1}, respectively. The **7c** molecule is one of the thermodynamically most stable isomers among the species involved in **Scheme 1c**. Thus, in high temperature thermal reactions, the **7c** molecule should be expected as one of the major products, which is consistent with Berson and co-workers observation [51]. The **7c** molecule is an observed product in the both pyrolysis reactions, as shown in Figure 1.9 on page 7. The computed geometries of the **7c** and **1c/7c** structures are shown in Figure 3.66 on the following page.

3.3.2 Berson Scheme 1c

In the previous section the rearrangements involving TMMc structures have been discussed. In this section the remaining part of Berson **Scheme 1c** will be discussed. Qualitative struc-

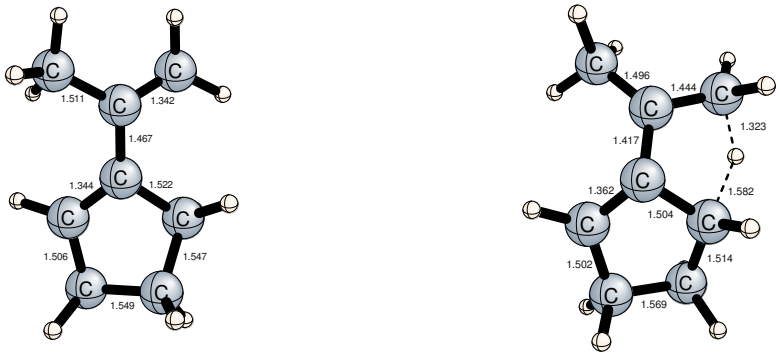

(a) **7c** (b) **1c/7c**

Figure 3.66: Selected interatomic distances (Å) for the **1c** and **1c/7c** structures.

tures of the species that appear in our extended Berson **Schemes 1c** and **2c** are illustrated in Figure 3.67 on page 78. The computational methods that have been employed are previously detailed in chapter 2 on page 14, section 2.3 on page 31. Furthermore, the **11c** molecule has been chosen as the reference molecule. Hence, the relative energies of all stationary points are presented with respect to the energy of **11c**. ZPVE corrected relative energies of the minima are reported in section 3.5 Table 3.8 on page 108, while those of the transition states are given in Table 3.9 on page 109.

For the remaining conversions in **Scheme 1c** (**12c** → **13c**, **13c** → **9c**, **4c** → **33c**, and **33c** → **34c**) again the computed relative energies are quite similar to those for the TMMa system, at most differing by 3.0 kcal mol^{-1} (Figures 3.68, 3.69 on page 79, 3.71 on page 80, and 3.73 on page 81). The computed geometries of the **13c** and **9c** species are shown in Figure 3.70 on page 79, while the **33c**, **34c**, and **33c/34c** structures are shown in Figure 3.72 on page 81.

As different from the TMMa system, the **4c** molecule can also rearrange to **6c** (Figure 3.71 on page 80) via 1,5-hydrogen shift. The calculated reaction energy and barrier are −1.0 and 34.9 kcal mol^{-1} for this conversion, respectively (Figure 3.73 on page 81). The stereochemistry of this conversion requires a cyclic TS (double bonds in *cis* position), hence **4c** can not rearrange to **5c** in this way. The **6c** molecule further rearranges to **35c** and **36c** via electrocyclic reactions (Figure 3.71 on page 80). For the **6c** → **35c** conversion the reaction energy and barrier are calculated as 2.3 and 37.5 kcal mol^{-1}, respectively, while the analogous results are 0.6 and 36.0 kcal mol^{-1} for the **6c** → **36c** reaction. The computed geometries of the **6c** and **4c** structures are shown in Figure 3.74 on page 82, while **35c** and **6c/35c** are in Figure 3.75 on page 82, and

36c and **6c/36c** are in Figure 3.76 on page 82.

The **35c** and **36c** molecules isomerize to **37c** and **38c**, respectively, again via electrocyclic reactions (Figure 3.71 on page 80). For the **35c** → **37c** conversion the reaction energy and barrier are calculated as 30.6 and 54.4 kcal mol^{-1}, respectively, while the analogous results are 33.5 and 56.6 kcal mol^{-1} for the **36c** → **38c** reaction. The computed geometries of the **35c/37c** and **36c/38c** structures are shown in Figure 3.77 on page 83.

Both **35c** and **36c** yield **5c** by conrotatory ring-opening reactions (Figure 3.71 on page 80). For the **35c** → **5c** conversion the reaction energy and barrier are calculated as −2.7 and 39.9 kcal mol^{-1}, respectively, while the analogous results are −1.0 and 40.6 kcal mol^{-1} for the **36c** → **5c** isomerization. The computed geometries of the **5c**, **35c/5c**, and **36c/5c** structures are shown in Figure 3.78 on page 83. Another remarkable point is that the relative energy of the **35c/37c**, 78.3 kcal mol^{-1}, and **36c/38c**, 78.8 kcal mol^{-1}, are high compared to other relative energies. Hence, the cyclization of **35c** to **37c** and **36c** to **38c** are not expected at ordinary temperatures.

Considering the overall picture for the extended Berson **Scheme 1c**, closed-shell bicyclic structures (**3c**, **12c**, **34c**, **37c** and **38c**) suffer from high ring strain. Open-chain structures, **4c**, **5c**, and **6c** and monocyclic structures **7c**, **33c**, **35c**, and **36c** are relatively more stable isomers since all these molecules are stabilized by conjugacy among the double bonds. Furthermore, relative energy profiles (Figures 3.69 on page 79 and 3.73 on page 81) demonstrate that at high temperatures the **4c**, **5c**, **6c**, **7c**, **33c**, **35c**, and **36c** molecules should be expected as a product for **Scheme 1c**. Berson *et al.* [51] observed the **4c**, **5c**, **6c**, and **7c** molecules as pyrolysis products (Figure 1.9 on page 7), however they did not observe the **33c**, **35c**, and **36c** molecules.

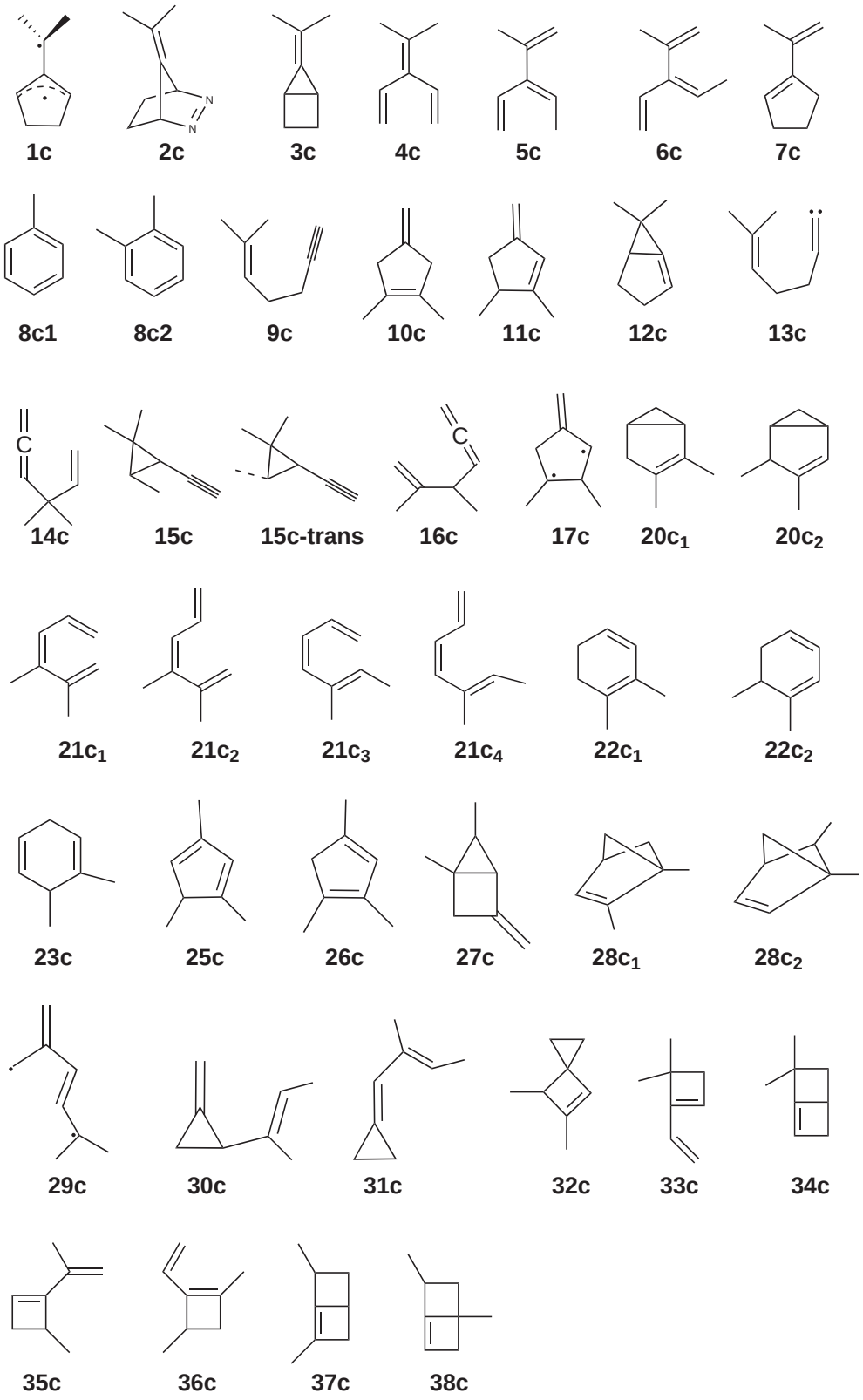

Figure 3.67: Qualitative structures of the species that appear in the extended Berson **Schemes 1c** and **2c**.

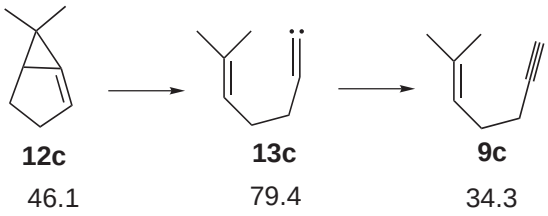

Figure 3.68: The reaction picture for the **12c** → **9c** conversion with relative energies (in kcal mol^{-1}). Energy of TSs are not indicated since the reactions take place barrierlessly.

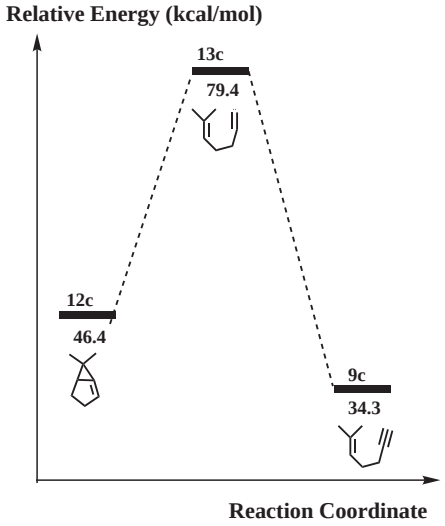

Figure 3.69: Relative energy profile for the **12c** → **9c** conversion.

(a) **13c** (b) **9c**

Figure 3.70: Selected interatomic distances (Å) for the **13c** and **9c** structures.

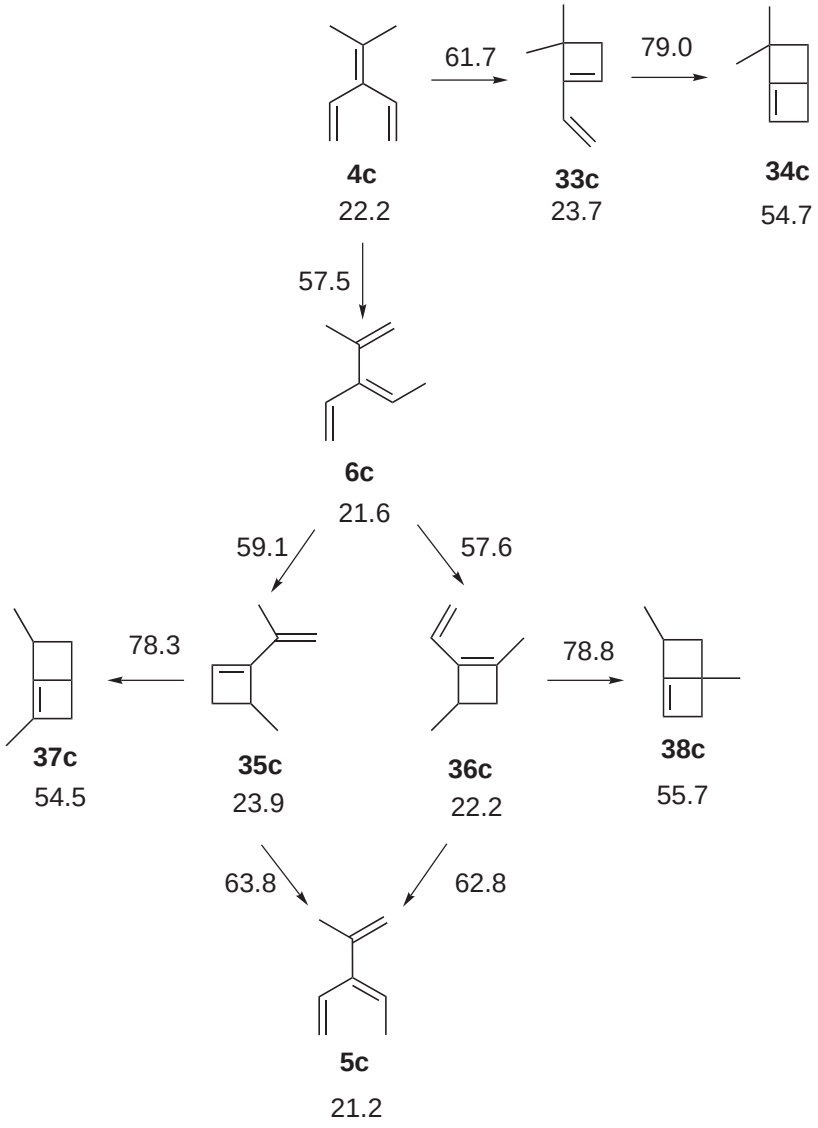

Figure 3.71: The reaction picture for the rearrangements of **4c** with relative energies (in kcal mol^{-1}). The values over arrows indicate relative energies of TSs.

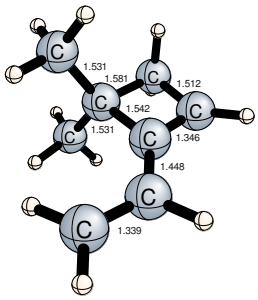

(a) **33c**

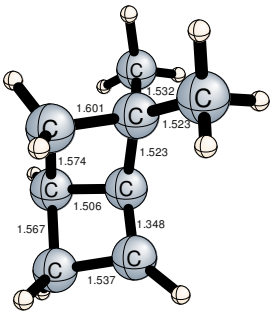

(b) **34c**

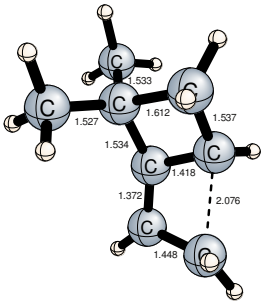

(c) **33c/34c**

Figure 3.72: Selected interatomic distances (Å) for the **33c**, **34c**, and **33c/34c** structures.

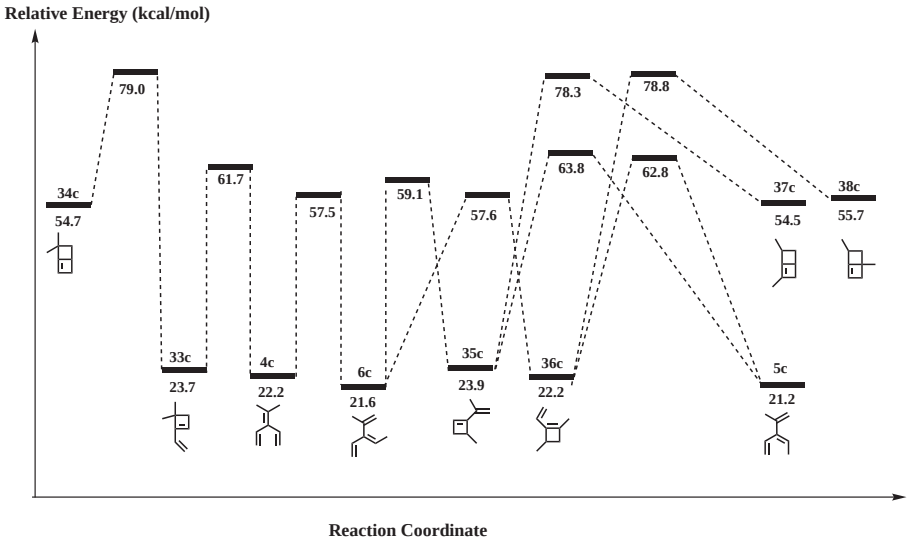

Figure 3.73: Relative energy profile for the rearrangements of **4c**.

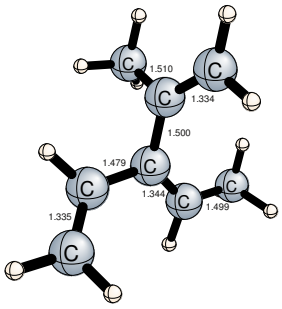

(a) **6c**

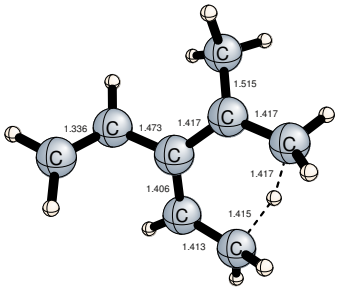

(b) **6c/4c**

Figure 3.74: Selected interatomic distances (Å) for the **6c** and **4c/6c** structures.

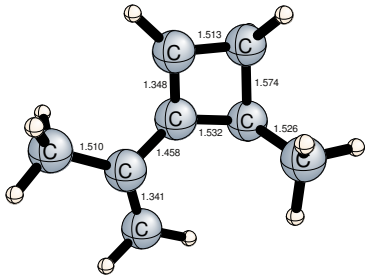

(a) **35c**

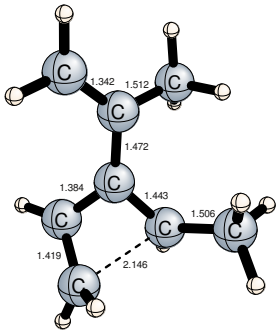

(b) **6c/35c**

Figure 3.75: Selected interatomic distances (Å) for the **35c** and **6c/35c** structures.

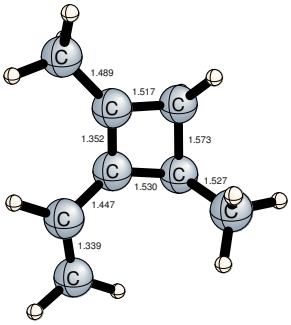

(a) **36c**

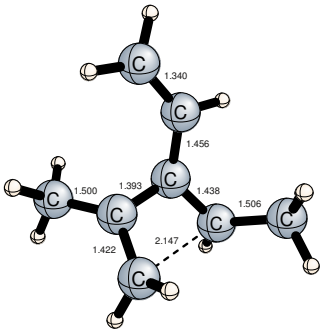

(b) **6c/36c**

Figure 3.76: Selected interatomic distances (Å) for the **36c** and **6c/36c** structures.

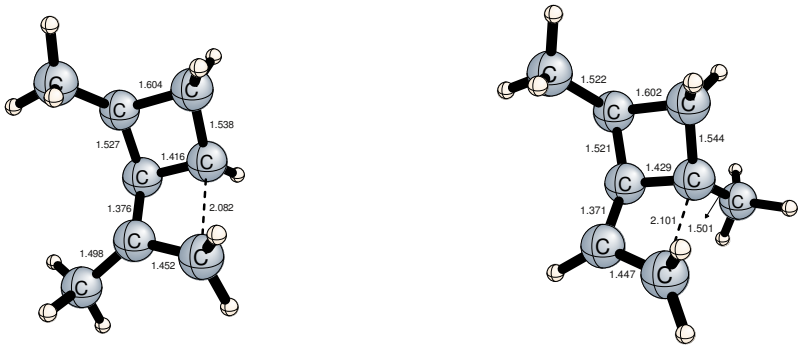

(a) **35c/37c** (b) **36c/38c**

Figure 3.77: Selected interatomic distances (Å) for the **35c/37c** and **36c/38c** structures.

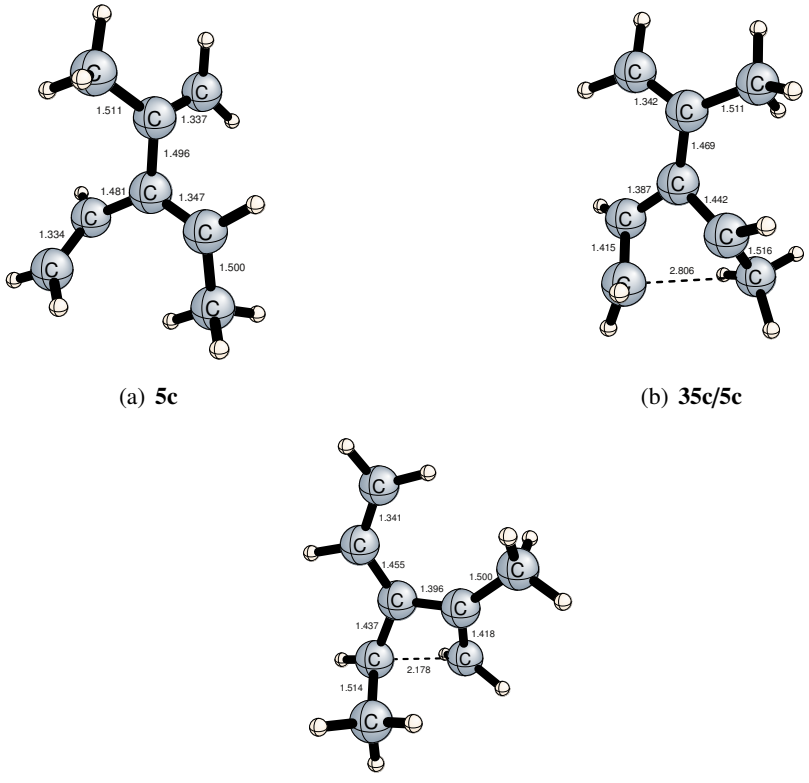

(a) **5c** (b) **35c/5c**

(c) **36c/5c**

Figure 3.78: Selected interatomic distances (Å) for the **5c**, **35c/5c**, and **36c/5c** structures.

3.3.3 Berson Scheme 2c

The overall picture for the extended Berson **Scheme 2c** is presented in Figure 3.79 on the facing page. For **Scheme 2c** the computed relative energies, reactions energies, and barriers are again quite similar ($\Delta E < 3.0$ kcal mol^{-1}) to those for the TMMa system, except for the TSs **9c/14c** and **15c/15c-trans**. Relative energies of both **9c/14c** and **15c/15c-trans** transition structures are 3.8 kcal mol^{-1} higher than those for **9a/14a** and **15a/15a-trans**, which can be attributed to steric hindrance of the methyl groups. Hence, the methyl groups are again just substituents for most of the reactions. However, in some reactions methyl groups lead to branching such as rearrangements of **10c** to **20c**$_1$ and **11c** to **20c**$_2$ (in the TMMa system both **10a** and **11a** yield **20a**).

As an important difference from the TMMa system, decomposition of **23c** yields both toluene (**8c**$_1$) and *o*-xylene (**8c**$_2$). The computation results for the reaction energy and barrier are −15.5 and 64.8 kcal mol^{-1} for the **23c** → **8c**$_1$ reaction, while analogous results are −6.5 and 45.2 kcal mol^{-1} for **23c** → **8c**$_2$. Activation energy for the *o*-xylene route is 19.6 kcal mol^{-1} lower than the toluene route. On the other hand, reaction energy of the toluene route is 9 kcal mol^{-1} lower than the *o*-xylene route. Hence, these two reactions are competitive considering both kinetic and thermodynamic stabilities. The *o*-xylene (**8c**$_2$) route is kinetically favored, while the toluene route is thermodynamically favored. Therefore, we conclude that under the experimental conditions both the toluene and *o*-xylene molecules should be expected as products. However, Berson *et al.* [51] reported only the toluene molecule as the dissociation product (Figure 1.9 on page 7). Relative energy profiles for **Scheme 2c** , Figures 3.82–3.86 (on pages 87- 90), indicate that at high temperature thermal reactions in addition to the dissociation products, the **10c**, **11c**, **22c**$_1$, **22c**$_2$, **23c**, **25c**, and **26c** molecules should be expected as products. But, Berson *et al.* [51] observed only the **10c**, **11c**, and **8c**$_1$ molecules considering **Scheme 2c**. The computed geometries of all remaining structures are shown in Figures 3.87–3.113 (on pages 91-101).

Moreover, bicyclic intermediates **20c**$_1$ and **20c**$_2$ can give degenerate rearrangements to interchange the positions of the methyl groups. The reaction picture for degenerate rearrangements of **20c**$_1$ and **20c**$_2$ is presented in Figures 3.80 and 3.81 on page 86.

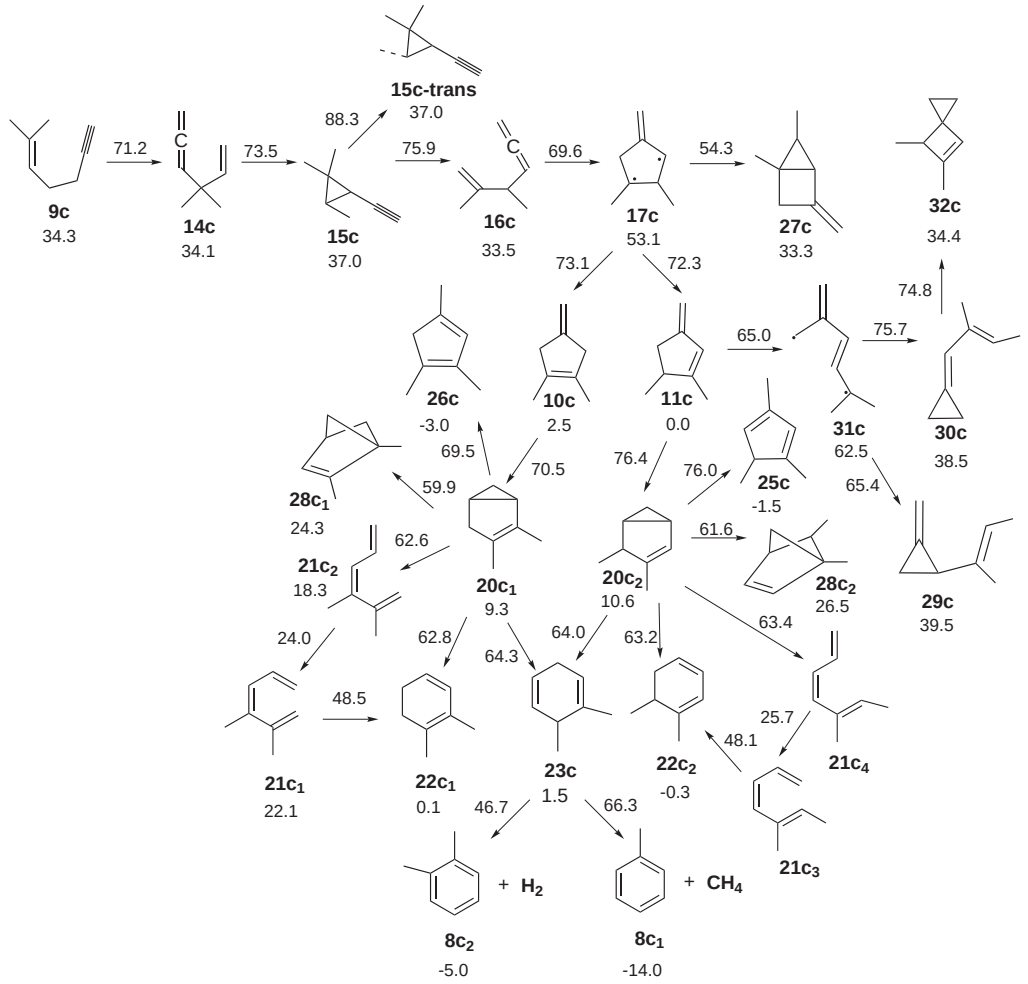

Figure 3.79: The overall picture with relative energies (in kcal mol^{-1}) for the extended Berson **Scheme 2c**. The values over arrows indicate relative energies of TSs.

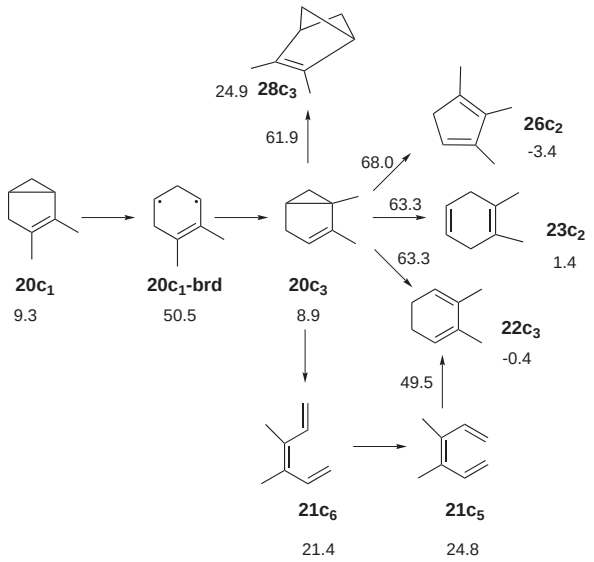

Figure 3.80: The reaction picture with relative energies (in kcal mol^{-1}) for degenerate rearrangement of **20c**$_1$. The values over arrows indicate relative energies of TSs.

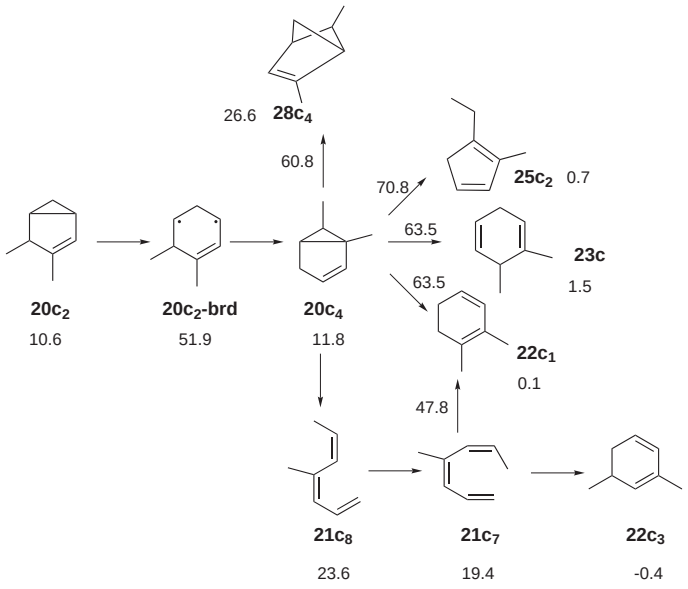

Figure 3.81: The reaction picture with relative energies (in kcal mol^{-1}) for degenerate rearrangement of **20c**$_2$. The values over arrows indicate relative energies of TSs.

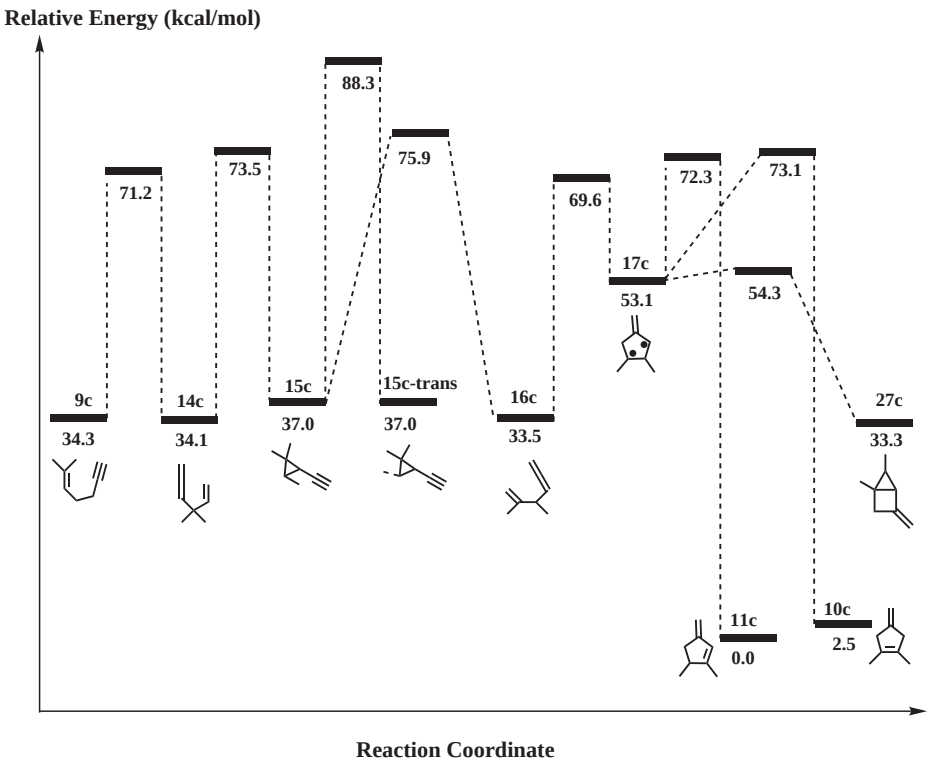

Figure 3.82: Relative energy profile for the **Scheme 2c** (Part I).

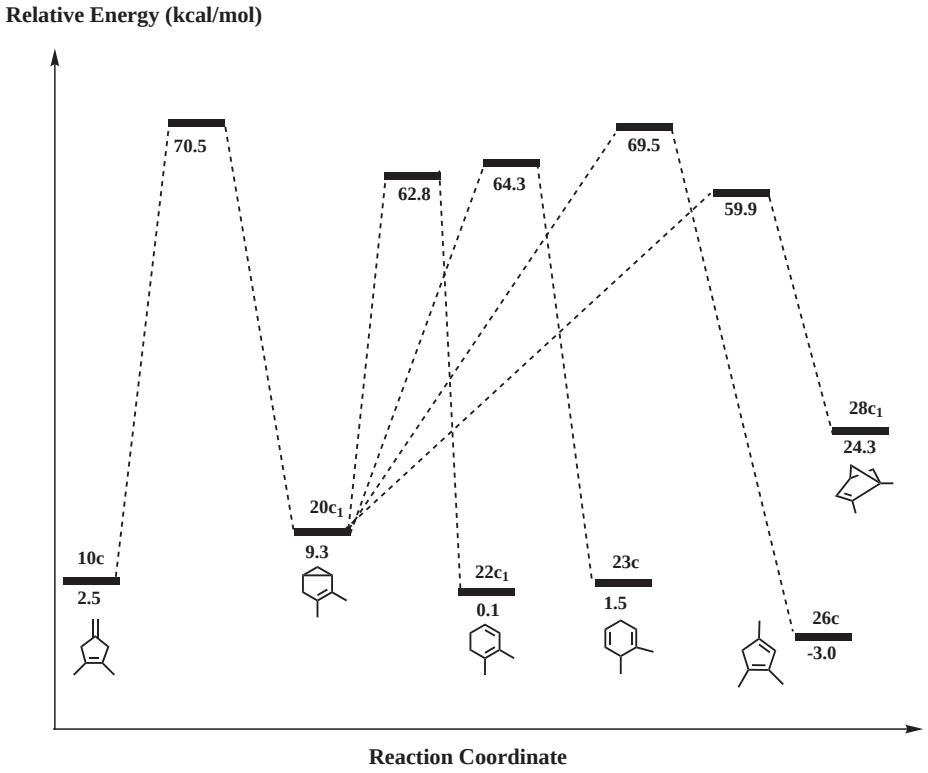

Figure 3.83: Relative energy profile for the **Scheme 2c** (Part II).

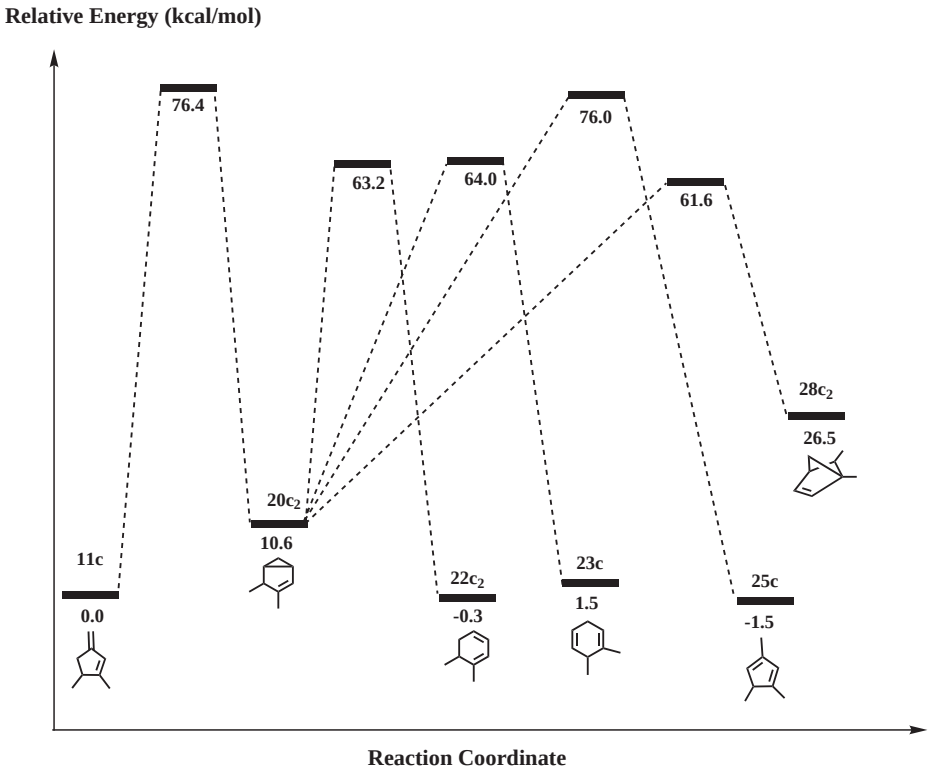

Figure 3.84: Relative energy profile for the **Scheme 2c** (Part III).

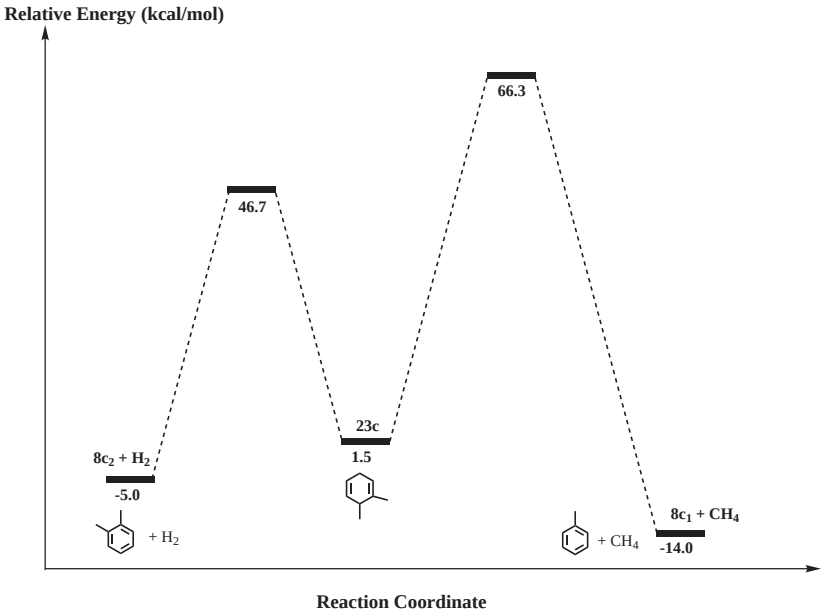

Figure 3.85: Relative energy profile for the **Scheme 2c** (Part IV).

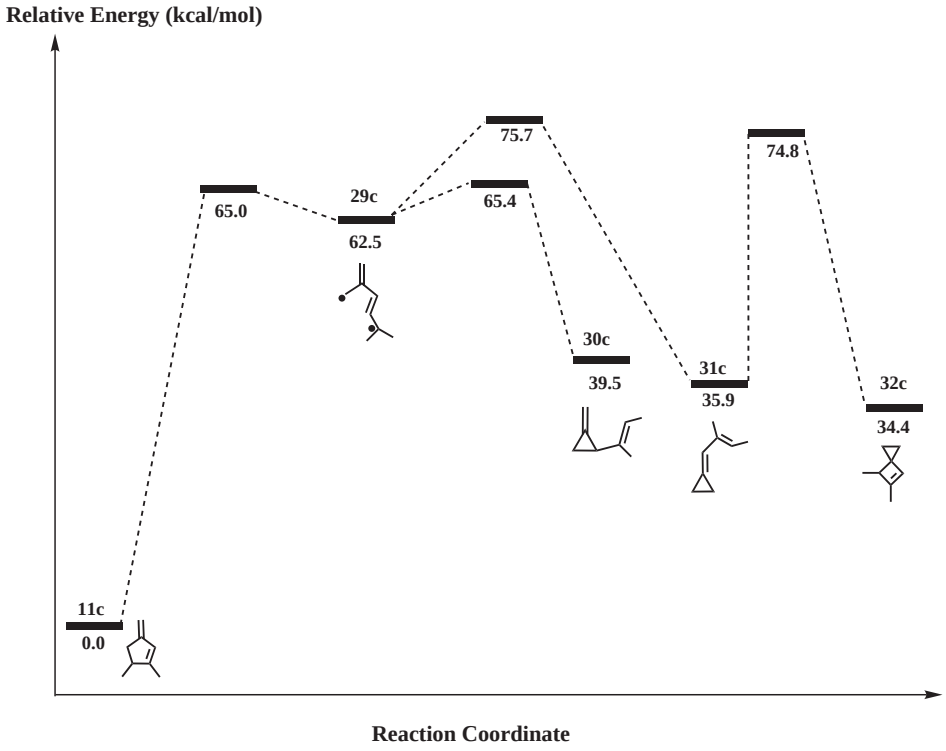

Figure 3.86: Relative energy profile for the **Scheme 2c** (Part V).

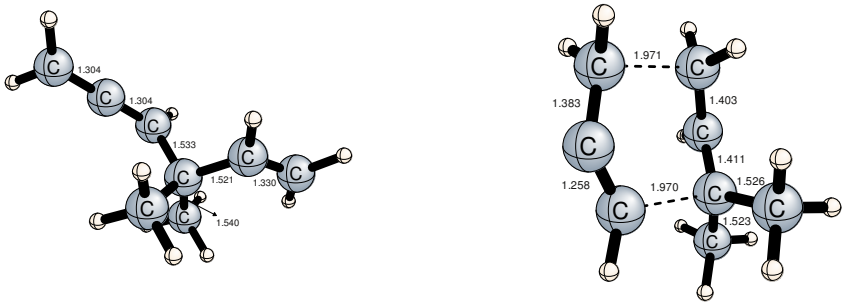

(a) **14c** (b) **9c/14c**

Figure 3.87: Selected interatomic distances (Å) for the **14c** and **9c/14c** structures.

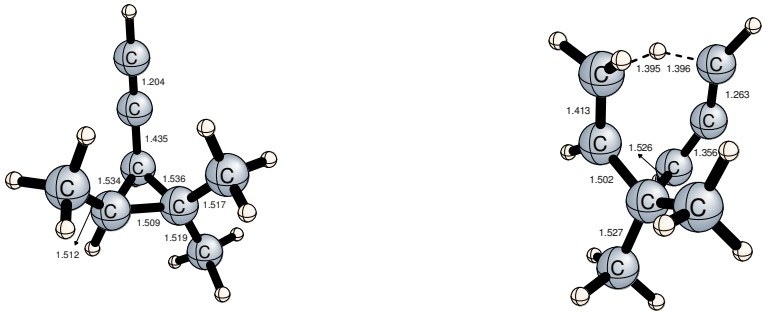

(a) **15c** (b) **14c/15c**

Figure 3.88: Selected interatomic distances (Å) for the **15c** and **14c/15c** structures.

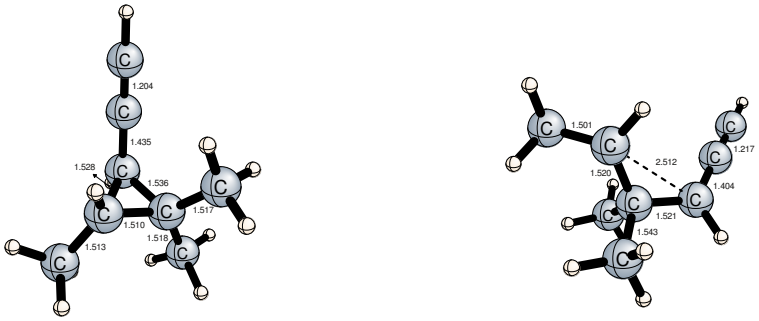

(a) **15c-trans** (b) **15c/15c-trans**

Figure 3.89: Selected interatomic distances (Å) for the **15c-trans** and **15c/15c-trans** structures.

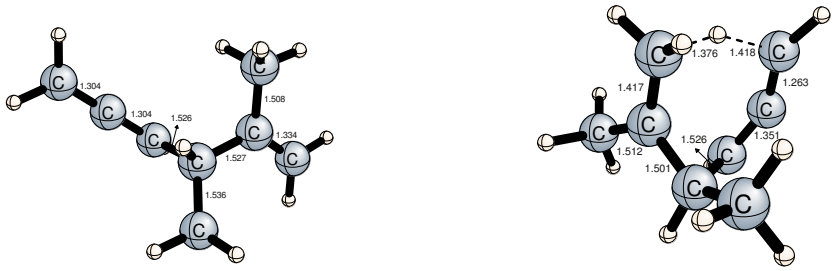

(a) **16c** (b) **15c/16c**

Figure 3.90: Selected interatomic distances (Å) for the **16c** and **15c/16c** structures.

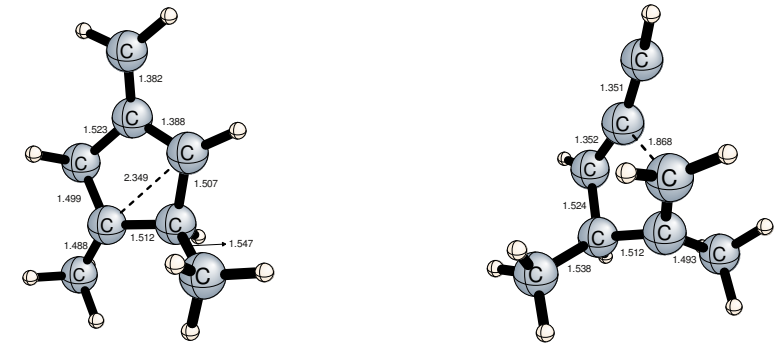

(a) **17c** (b) **16c/17c**

Figure 3.91: Selected interatomic distances (Å) for the **17c** and **16c/17c** structures.

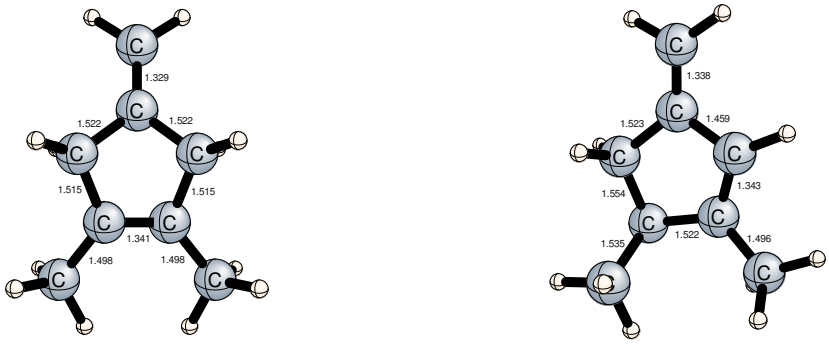

(a) **10c** (b) **11c**

Figure 3.92: Selected interatomic distances (Å) for the **10c** and **11c** structures.

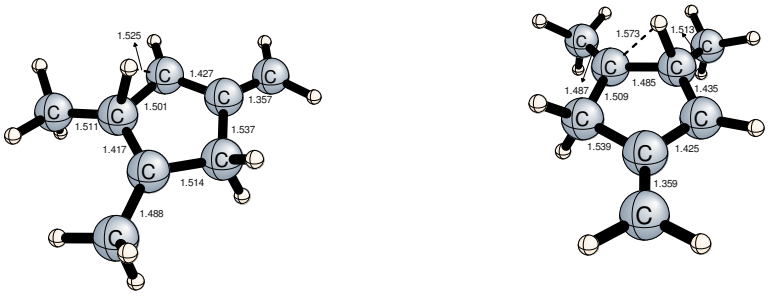

(a) **17c/10c** (b) **17c/11c**

Figure 3.93: Selected interatomic distances (Å) for the **17c/10c** and **17c/11c** structures.

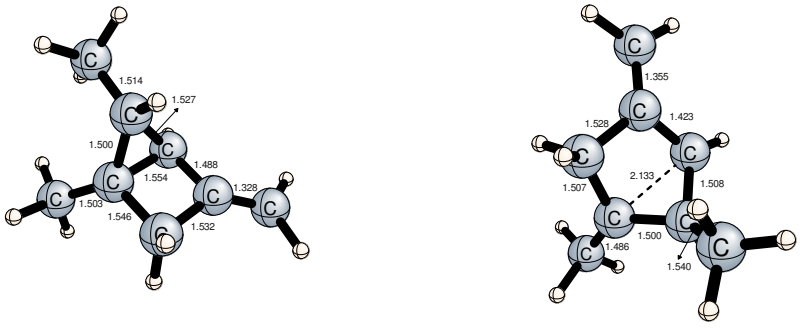

(a) **27c** (b) **17c/27c**

Figure 3.94: Selected interatomic distances (Å) for the **27c** and **17c/27c** structures.

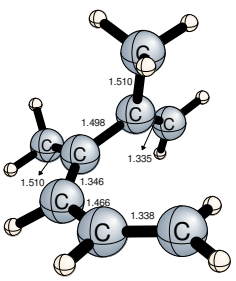

(a) **21c**$_1$

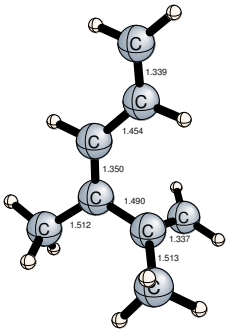

(b) **21c**$_2$

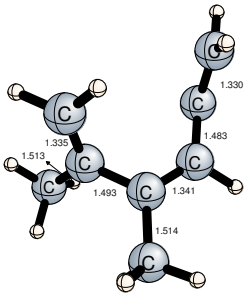

(c) **21c**$_1$**/21c**$_2$

Figure 3.95: Selected interatomic distances (Å) for the **21c**$_1$, **21c**$_2$, and **21c**$_1$**/21c**$_2$ structures.

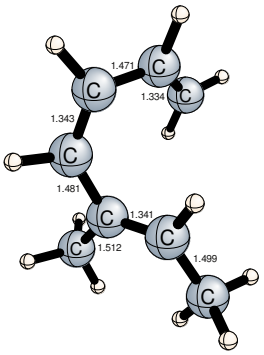

(a) **21c**$_3$

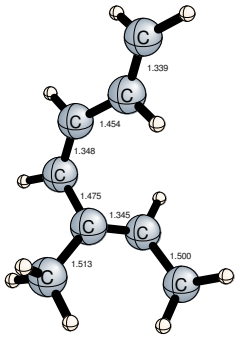

(b) **21c**$_4$

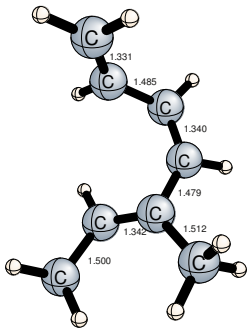

(c) **21c**$_3$**/21c**$_4$

Figure 3.96: Selected interatomic distances (Å) for the **21c**$_3$, **21c**$_4$, and **21c**$_3$**/21c**$_4$ structures.

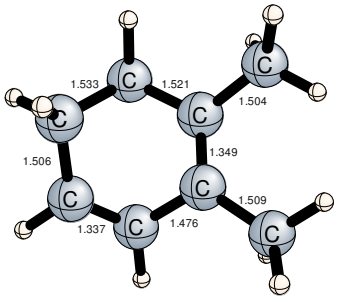

(a) **22c**$_1$

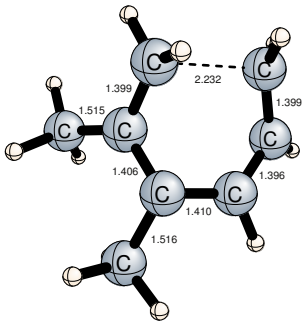

(b) **21c**$_1$**/22c**$_1$

Figure 3.97: Selected interatomic distances (Å) for the **22c**$_1$ and **21c**$_1$**/22c**$_1$ structures.

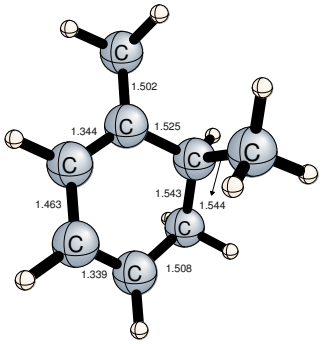

(a) **22c**$_2$

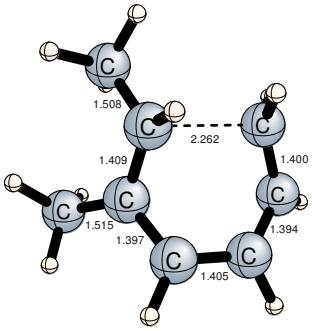

(b) **21c**$_3$**/22c**$_2$

Figure 3.98: Selected interatomic distances (Å) for the **22c**$_2$ and **21c**$_3$**/22c**$_2$ structures.

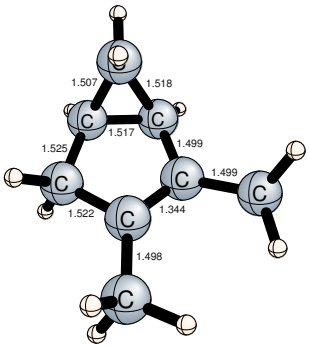

(a) **20c**$_1$

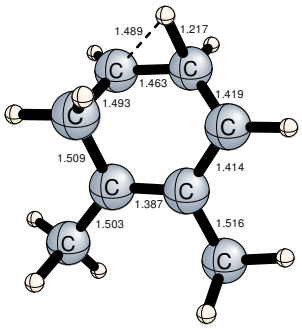

(b) **20c**$_1$**/22c**$_1$

Figure 3.99: Selected interatomic distances (Å) for the **20c**$_1$ and **20c**$_1$**/22c**$_1$ structures.

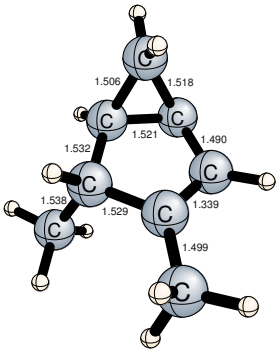

(a) **20c**$_2$

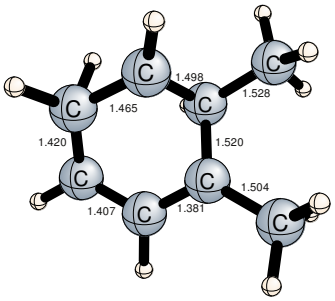

(b) **20c**$_2$**/22c**$_2$

Figure 3.100: Selected interatomic distances (Å) for the **20c**$_2$ and **20c**$_2$**/22c**$_2$ structures.

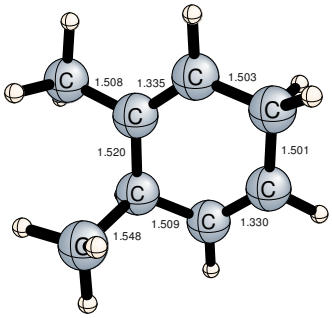

(a) **23c**

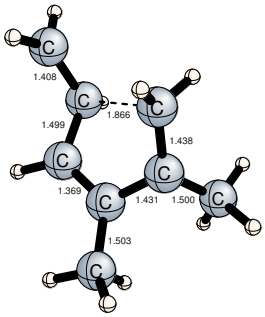

(b) **20c**$_1$**/21c**$_2$

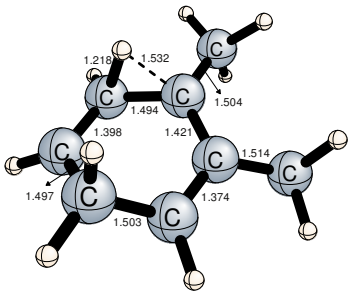

(c) **20c**$_1$**/23c**

Figure 3.101: Selected interatomic distances (Å) for the **23c**, **20c**$_1$**/21c**$_2$, and **20c**$_1$**/23c** structures.

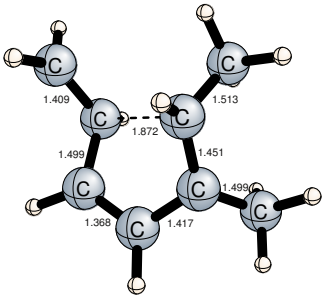

(a) **20c$_2$/21c$_4$**

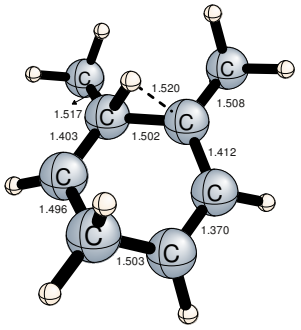

(b) **20c$_2$/23c**

Figure 3.102: Selected interatomic distances (Å) for the **20c$_2$/21c$_4$** and **20c$_2$/23c** structures.

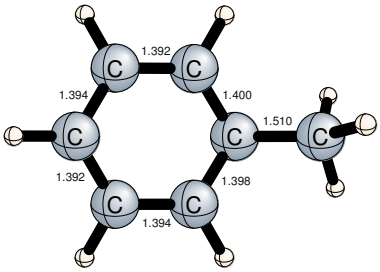

(a) **8c$_1$**

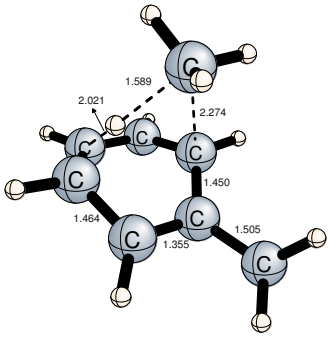

(b) **23c/8c$_1$**

Figure 3.103: Selected interatomic distances (Å) for the **8c$_1$** and **23c/8c$_1$** structures.

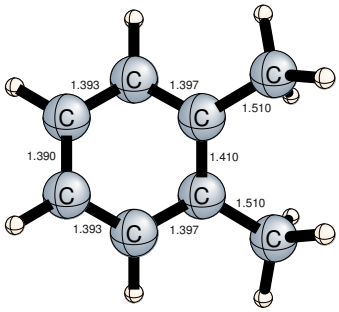

(a) **8c$_2$**

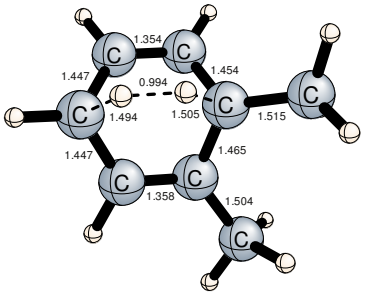

(b) **23c/8c$_2$**

Figure 3.104: Selected interatomic distances (Å) for the **8c$_2$** and **23c/8c$_2$** structures.

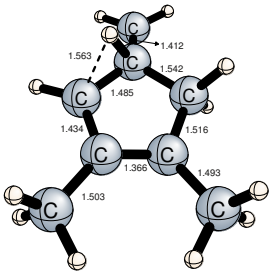

(a) **10c/20c**

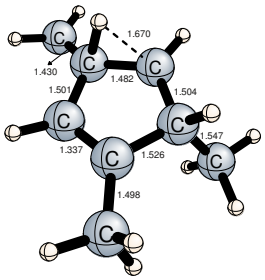

(b) **11c/20c**

Figure 3.105: Selected interatomic distances (Å) for the **10c/20c**$_1$ and **11c/20c**$_2$ structures.

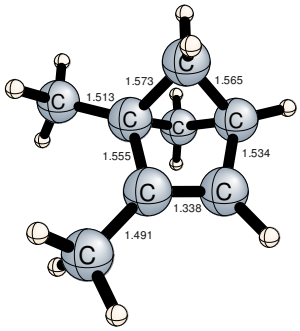

(a) **28c**$_1$

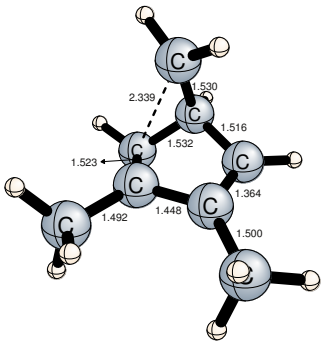

(b) **20c**$_1$**/28c**$_2$

Figure 3.106: Selected interatomic distances (Å) for the **28c**$_1$ and **20c**$_1$**/28c**$_2$ structures.

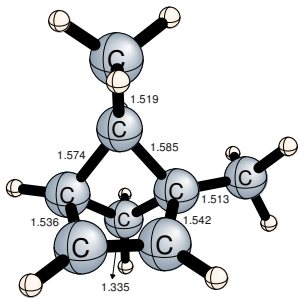

(a) **28c**$_2$

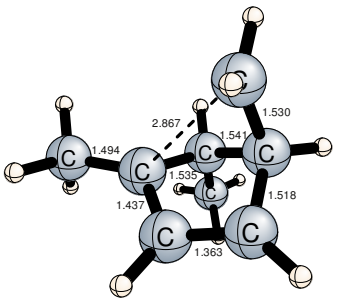

(b) **20c**$_2$**/28c**$_2$

Figure 3.107: Selected interatomic distances (Å) for the **28c**$_2$ and **20c**$_2$**/28c**$_2$ structures.

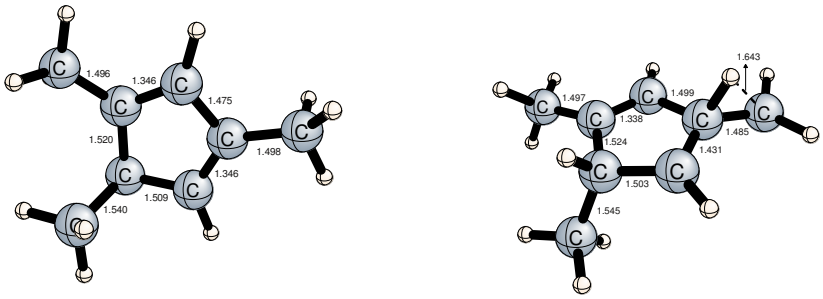

(a) **25c** (b) **20c$_2$/25c**

Figure 3.108: Selected interatomic distances (Å) for the **25c** and **20c$_2$/25c** structures.

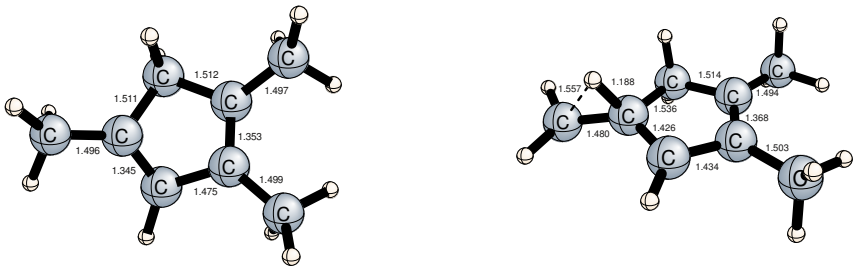

(a) **26c** (b) **20c$_1$/26c**

Figure 3.109: Selected interatomic distances (Å) for the **26c** and **20c$_1$/26c** structures.

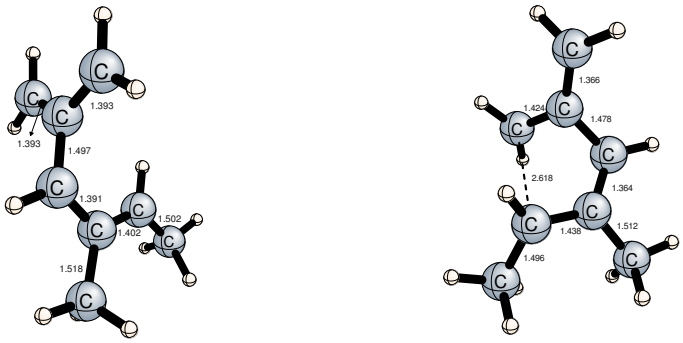

(a) **29c** (b) **11c/29c**

Figure 3.110: Selected interatomic distances (Å) for the **29c** and **11c/29c** structures.

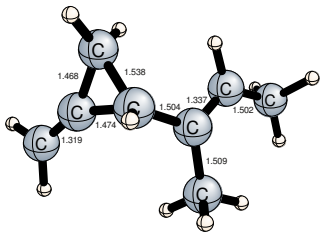

(a) **30c**

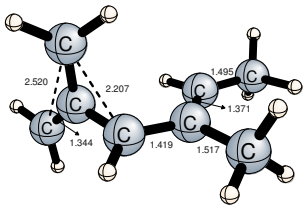

(b) **29c/30c**

Figure 3.111: Selected interatomic distances (Å) for the **30c** and **29c/30c** structures.

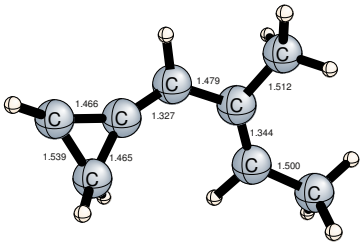

(a) **31c**

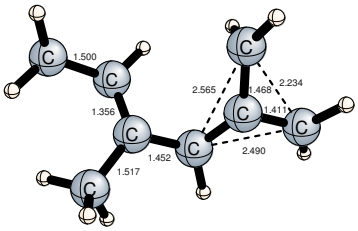

(b) **29c/31c**

Figure 3.112: Selected interatomic distances (Å) for the **31c** and **29c/31c** structures.

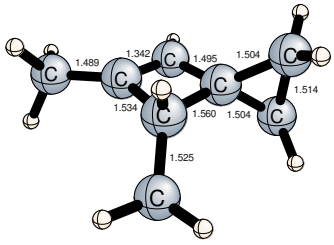

(a) **32c**

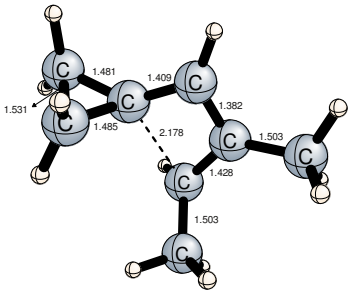

(b) **31c/32c**

Figure 3.113: Selected interatomic distances (Å) for the **32c** and **31c/32c** structures.

3.4 Kinetic Simulations

For the whole TMMa system we have written rate equations and solved the first-order kinetic equations with MATLAB 7.0.4 program [226] using TST rate constants. Our results for the kinetic simulation of Huntsman, Hopf, and Berson mechanisms (Figures 1.12 on page 8, 1.14 on page 10, 1.10, and 1.11 on page 8) are provided in Tables 3.3 on the facing page, 3.4 on page 104, and 3.5 on page 105, respectively, while relative free energies are reported in Section 3.6.

For the Huntsman mechanism our results are in general agreement with experiment [65]. As a major difference, the kinetic computation indicates that the **4a** molecule should also be observed under Huntsman's experimental conditions, however he did not observe that molecule. For the Hopf mechanism, our computations are again in general agreement with experiment [70]. However, our results are again pointed out that the **4a** molecule should also be observed. Further, in contrast to Hopf, observation of species **22a** in high percentages is not expected according to our computations. Moreover, with the same system at the same temperature (340 °C) Huntsman did not observe **22a** which supports our findings. Hence, reexamination of the Hopf mechanism is recommended.

For the TMMc system we considered the mechanism shown in Figure 3.114 on page 104. Our results are in general agreement with Berson *et al.*'s observations [51]. However, our computations are in disagreement with experiment for the toluene $\mathbf{8c}_1$ molecule. The kinetic simulations indicate that toluene is not expected as a product, while at longer reaction times, such as 100 s, only the *o*-xylene species can form in significant amounts.

Table 3.3: Product distribution for the Huntsman mechanism at 340 °C.

Reaction Time (s)	Molecule	% (Computation)	% (Experiment)[a]
62	**9a**	33.0	29
	14a	52.7	65
	10a	3.2	2
	11a	5.4	3
	4a	4.9	0
	15a	0.4	0
	27a	0.4	0
130	**9a**	28.1	24
	14a	44.9	62
	10a	6.5	6
	11a	10.9	8
	4a	8.9	0
	15a	0.3	0
	27a	0.3	0
150	**9a**	26.8	20
	14a	42.8	50
	10a	7.4	13
	11a	12.4	17
	4a	10.0	0
	15a	0.3	0
	27a	0.3	0

[a] Reference [65]

Table 3.4: Product distribution for the Hopf mechanism with a reaction time of 35 s.

Temperature (°C)	Molecule	% (Computation)	% (Experiment)[a]
340	**9a**	25.6	20
	14a	45.8	58
	10a	1.1	3
	11a	1.8	4
	4a	1.0	0
	15a	23.6	33
	15a-trans	0.9	
	22a	0.0	15
	24a	0.0	0
	27a	0.3	0
530	**9a**	0.0	0
	14a	0.0	0
	10a	35.0	29
	11a	54.9	38
	4a	9.9	0
	15a	0.3	0
	15a-trans	0.0	0
	22a	0.0	30
	24a	0.0	3

[a] Reference [70]

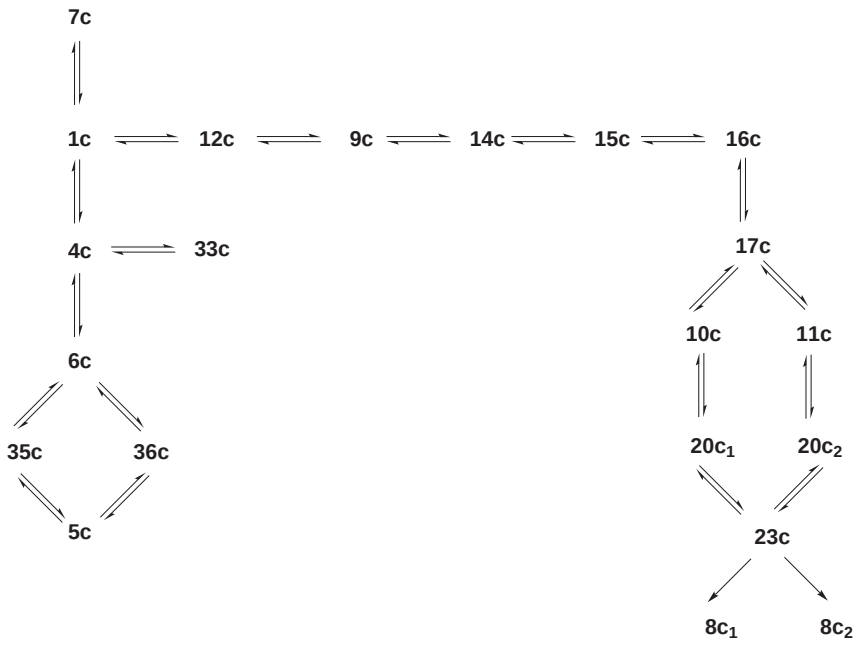

Figure 3.114: The mechanism which considered for kinetic simulation of the TMMc system.

Table 3.5: Product distribution for the Berson mechanism at 700 °C with a reaction time of 0.02 s.

Molecule	% (Computation)	% (Experiment)[a]
4c	65.0	31
5c	6.9	10
6c	13.5	10
7c	5.4	1
8c$_1$	0.0	32
9c[b]	0.1	
10c	3.2	6
11c	4.7	0
33c	0.1	0
35c	0.2	0
36c	0.8	0
2c[b]	0.0	
4c	65.6	10
5c	7.0	25
6c	13.6	30
7c	5.5	5
8c$_1$	0.0	10
9c	0.0	1
10c	2.9	0
11c	4.3	0
33c	0.1	0
35c	0.2	0
36c	0.1	0

[a] Reference [51].
[b] Starting material.

3.5 ZPVE Corrected Relative Energies

Table 3.6: ZPVE corrected relative energies (in kcal mol^{-1}) of the minima in extended Berson **Schemes 1a** and **2a** with respect to **11a** at CCSD(T)/6-311G(d,p)//B3LYP/6-311G(d,p) level. Energy of biradicals are computed according to Eq.(2.41) (on page 31).

Minimum	Relative Energy
1a-T	41.4
1a-o_1	56.5
1a-o_2	58.7
1a-p_1	58.2
2a	53.5[a]
3a	42.4
4a	18.4
9a	32.1
10a	3.7
11a	0.0
12a	46.4
13a	76.6
14a	31.6
15a	35.5
15a-trans	35.2
17a	52.5
20a	10.1
21a_1	22.6
21a_2	18.2
22a	−0.8
23a	0.0
24a	−6.3[b]
25a	−3.1
26a	−2.9
27a	32.5
28a	26.5
29a	37.6
30a	35.7
31a	60.2
32a	35.7
33a	23.3
34a	54.7

[a] Energy of **2a** relative to that of **11a** + N_2
[b] Energy of **24a** relative to that of **11a** - H_2

Table 3.7: ZPVE corrected relative energies (in kcal mol^{-1}) of the TSs in extended Berson **Schemes 1a** and **2a** with respect to **11a** at CCSD(T)/6-311G(d,p)//B3LYP/6-311G(d,p) level.

TS	**Relative Energy**
1a/2a	78.7[a]
1a/3a	57.6
1a/4a	73.1
1a/12a	64.9
4a/33a	59.0
9a/14a	67.4
10a/17a	72.5
10a/20a	70.9
11a/17a	72.1
11a/20a	76.0
11a/31a	64.2
14a/15a	73.8
14a/17a	69.0
15a/15a-trans	84.5
17a/27a	54.8
20a/21a_2	63.0
20a/22a	61.3
20a/23a	62.0
20a/25a	75.3
20a/26a	69.7
20a/28a	62.3
21a_1/21a_2	23.5
21a_1/22a	46.3
23a/24a	46.4
29a/31a	63.3
30a/31a	73.0
30a/32a	76.2
33a/34a	78.8

[a] Energy of **2a/1a** relative to that of **11a** + N_2

Table 3.8: ZPVE corrected relative energies (in kcal mol^{-1}) of the minima in extended Berson **Schemes 1c** and **2c** with respect to **11c** at CCSD(T)/6-311G(d,p)//B3LYP/6-311G(d,p) level. Energy of biradicals are computed according to Eq.(2.41) (on page 31).

Minimum	Relative Energy
1c-T	43.6
1c-o_1	56.6
1c-o_2	61.0
2c	54.2[a]
3c	42.6
4c	22.2
5c	21.2
6c	21.6
7c	3.0
$8c_1$	−14.0[b]
$8c_2$	−5.0[c]
9c	34.3
10c	2.5
11c	0.0
12c	46.1
13c	79.4
14c	34.1
15c	37.0
15c-trans	37.0
16c	33.5
17c	53.1
$20c_1$	9.3
$20c_2$	10.6
$21c_1$	22.1
$21c_2$	18.3
$21c_3$	24.5
$21c_4$	20.1
$22c_1$	0.1
$22c_2$	−0.3
23c	1.5
25c	−1.5
26c	−3.0
27c	33.3
$28c_1$	24.3
$28c_2$	26.5
29c	39.5
30c	38.5
31c	62.5
32c	34.4
33c	23.7
34c	54.7
35c	23.9
36c	22.2
37c	54.5
38c	55.7

[a] Energy of **2c** relative to that of **11c** + N_2
[b] Energy of $\mathbf{8c}_1$ relative to that of **11c** - CH_4
[c] Energy of $\mathbf{8c}_2$ relative to that of **11c** - H_2

Table 3.9: ZPVE corrected relative energies (in kcal mol^{-1}) of the TSs in extended Berson **Schemes 1c** and **2c** with respect to **11c** at CCSD(T)/6-311G(d,p)//B3LYP/6-311G(d,p) level.

TS	**Relative Energy**
1c/2c	79.2[a]
1c/3c	59.3
1c/4c	75.0
1c/7c	76.2
1c/12c	63.2
4c/6c	57.5
4c/33c	61.7
5c/35c	63.8
5c/36c	62.8
6c/35c	59.1
6c/36c	57.6
$8c_1$/23c	66.3
$8c_2$/23c	46.7
9c/14c	71.2
10c/17c	73.1
10c/$20c_1$	70.5
11c/17c	72.3
11c/$20c_1$	76.4
11c/31c	65.0
14c/15c	73.5
15c/15c-trans	88.3
15c/16c	75.9
16c/17c	69.6
16c/38c	68.2
17c/27c	54.4
$20c_1$/$21c_2$	62.6
$20c_1$/$22c_2$	62.8
$20c_1$/23c	64.3
$20c_1$/26c	69.5
$20c_1$/$28c_1$	59.9
$20c_2$/$21c_4$	63.4
$20c_2$/$22c_2$	63.2
$20c_2$/23c	64.0
$20c_2$/25c	76.0
$20c_2$/$28c_2$	61.6
$21c_1$/$21c_2$	24.0
$21c_1$/$22c_1$	48.5
$21c_3$/$21c_4$	25.7
$21c_3$/$22c_2$	48.1
29c/31c	65.4
30c/31c	75.7
30c/32c	74.8
33c/34c	79.0
35c/37c	78.3
36c/38c	78.8

[a] Energy of **2c/1c** relative to that of **11c** + N_2

3.6 Relative Free Energies

Table 3.10: Relative free energies (in kcal mol^{-1}) of the minima in extended Berson **Schemes 1a** and **2a** with respect to **11a** at CCSD(T)/6-311G(d,p)//B3LYP/6-311G(d,p) level. Energy of biradicals are computed according to Eq.(2.41) (on page 31).

Minimum	*G* (340 °C)	*G* (530 °C)
1a	57.24	56.50
3a	43.47	43.77
4a	16.53	15.50
9a	28.66	27.02
10a	3.71	3.72
11a	0.00	0.00
12a	48.31	49.01
13a	71.76	69.59
14a	28.08	26.44
15a	34.10	33.21
15a-trans	33.69	32.77
17a	52.25	51.80
20a	12.74	13.78
$21a_1$	19.34	17.83
$21a_2$	16.15	15.12
22a	0.97	1.68
23a	1.36	1.92
25a	−2.58	−2.49
26a	−2.47	−2.42
27a	33.91	34.33
28a	29.99	31.42
29a	36.00	35.10
30a	33.21	32.07
31a	57.00	55.24
32a	36.87	37.20
33a	23.09	22.87
34a	56.81	57.60

Table 3.11: Relative free energies (in kcal mol^{-1}) of the TSs in extended Berson **Schemes 1a** and **2a** with respect to **11a** at CCSD(T)/6-311G(d,p)//B3LYP/6-311G(d,p) level.

TS	*G* (340 °C)	*G* (530 °C)
1a/3a	58.63	59.01
1a/4a	72.47	72.06
1a/12a	66.21	66.65
4a/33a	58.55	58.30
9a/14a	67.80	67.79
14a/15a	74.76	74.94
14a/17a	69.52	69.54
14a/$21a_2$	92.67	91.81
10a/17a	73.13	73.15
10a/20a	71.73	71.84
11a/17a	72.50	72.44
11a/20a	76.48	76.43
11a/31a	64.04	63.70
15a/15a-trans	80.11	78.06
17a/27a	55.83	56.16
20a/$21a_2$	63.83	63.96
20a/22a	63.55	64.43
20a/23a	64.24	65.11
20a/25a	75.88	75.88
20a/26a	70.46	70.55
20a/28a	64.77	65.73
$21a_1$/$21a_2$	21.68	21.03
$21a_1$/22a	47.11	47.46
23a/24a	50.70	52.42
29a/31a	61.90	61.05
30a/31a	71.02	69.90
30a/32a	77.13	77.44
33a/34a	80.58	81.32

Table 3.12: Relative free energies (in kcal mol^{-1}) of the minima considered in kinetic simulations of the extended Berson **Schemes 1c** and **2c** with respect to **11c** at CCSD(T)/6-311G(d,p)//B3LYP/6-311G(d,p) level. Energy of biradicals are computed according to Eq.(2.41) (on page 31).

Minimum	G (700 °C)
1c	51.34
4c	11.84
5c	16.17
6c	14.88
7c	4.76
9c	25.68
10c	0.48
11c	0.00
12c	49.59
13c	68.41
14c	29.39
15c	33.74
16c	26.87
17c	50.03
$20c_1$	12.39
$20c_2$	14.58
23c	3.62
33c	23.75
35c	22.86
36c	20.28

Table 3.13: Relative free energies (in kcal mol^{-1}) of the TSs considered in kinetic simulations of the extended Berson **Schemes 1c** and **2c** with respect to **11c** at CCSD(T)/6-311G(d,p)//B3LYP/6-311G(d,p) level.

TS	G (700 °C)
1c/4c	73.35
1c/7c	78.72
1c/12c	65.48
4c/6c	58.48
4c/33c	60.73
5c/35c	62.97
5c/36c	61.51
6c/35c	57.58
6c/36c	54.07
$8c_1$/23c	68.97
$8c_2$/23c	52.22
9c/14c	71.48
10c/$20c_1$	68.66
10c/17c	72.10
11c/17c	71.37
11c/$20c_2$	75.99
14c/15c	76.07
15c/16c	77.21
16c/17c	68.60
$20c_1$/23c	66.53
$20c_2$/23c	66.29

CHAPTER 4

CONCLUSIONS

In this work, thermal rearrangements of the Berson's TMMs and numerous other isomers connected to them by chemical reaction pathways have been investigated employing the highest level of theory available within our computational facilities. The relevant portions of the lowest-energy, singlet-spin potential energy surface of the C_4H_6 (TMM), C_6H_8 (TMMa), and C_8H_{12} (TMMc) chemical systems have been explored in order to determine the reaction energies and activation parameters accurately, with the ultimate objective of providing a theoretical account of pyrolysis experiments by Huntsman, Baldwin, Hopf, and Roth on the TMMa system and by Berson on TMMc. For this purpose, a combination of DFT, CASSCF, MRMP2, and CCSD(T) methods have been employed, all with the triple-split valence 6-311G(d,p) basis set. Stationary points of closed-shell species (minima and TSs) have been located at the DFT level, while CASSCF has been used for the open-shell singlets (biradicals). Dynamical correlation is included by single-point CCSD(T) calculations for the former, and by MRMP2 for the latter species. ZPVE corrections are all at the DFT level.

The nature of the orthogonal and the planar structures of the parent tMM have been clarified in this work. We have concluded that the orthogonal TMM $^1B_1$ minimum has a C_{2v} symmetry structure, i.e. there is no pyramidalization in the unique methylene group. It lies at 13.9 kcal mol^{-1} above the triplet minimum $^3B_2$, at MRCI level. The closed-shell $^1A_1$ state of the planar TMM is not a true minimum, but a TS for 180° rotation of the unique methylene group in the orthogonal TMM minimum. It lies at 3.0 kcal mol^{-1} above $^1B_1$. The planar structures are also involved in the interchange of equivalent orthogonal TMMs ($\mathbf{o}_1$, $\mathbf{o}_2$, $\mathbf{o}_3$). the latter close the unique methylene group at the pivot carbon more or less maintains its orthogonal geometry. The activation energy from MCP has been calculated as 39.9 kcal mol^{-1}, in good agreement

with the experimental value of 41.2 kcal mol^{-1} (LeFevre and Crawford).

Many features of the parent TMM are retained in TMMa and TMMc, despite the constraints imposed by the five-membered ring in the latter species. Thus ring-closure to the bicyclic molecules **3a** (**3c**) and **12a** (**12c**) take place similarly to that in the parent TMM. Likewise, planar TMMa (TMMc) structures are TSs, while orthogonal ones are true minima. The adiabatic singlet-triplet gaps are also similar, being 14.7 (13.0) and 16.5 (16.2) kcal mol^{-1} in the orthogonal ($\mathbf{o}_1$) and planar TMMa (TMMc), respectively. It has been shown here that the substantial reductions in the ring opening barriers of MCP derivatives **3a (c)** and **12a (c)** can be largely attributed to ring strain in the former and π-bond strain in the latter species.

The computational results herein on the TMMa system fully support the mechanism experimentally studied by Huntsman, Baldwin, Hopf, and Roth (Figures 1.12 and 1.13 on page 9, 3.31 on page 55). In particular, we have verified that the reaction paths from **9a**, **14a**, and **15a** to **10a**, **11a**, and **27a** all go through the biradical species **17a**. Roth had measured the activation parameters for both the forward and reverse directions in each step in this mechanism. Our computed values are in good agreement with Roth's. We have found that direct formation of 1,3,5-hexatriene, **21a**, from **14a** as suggested by Hopf (Figure 1.14 on page 10) is not energetically feasible. Existence of an alternative path with much lower energetics demands and involving species **20a** has been demonstrated. Precursors to benzene is 1,4-cyclohexadiene, **23a**, according to our computational results. Species **22a** may also contribute to benzene formation, but only through the sequence **22a** $\rightarrow$ **20a** $\rightarrow$ **23a** $\rightarrow$ benzene.

In the extended Berson **Scheme 1a**, closed-shell bicyclic structures (**3a**, **12a**, and **34a**) suffer from high ring strain. On the other hand, open-chain structures **9a** and **4a**, and monocyclic **33a** are relatively more stable than those bicyclic structures. According to our kinetic simulations, the **9a** and **4a** molecules are expected to be major products, while **33a** to be a minor product at high temperatures. Our expectation is generally consistent with Berson *et al.* [51] observations.

Our results show that for the extended Berson **Scheme 2a**, the major product of both pyrolysis reactions (Figure 1.9 on page 7) is expected to be the **24a** (benzene) molecule. Since **24a** is a dissociation product, under experimental conditions (700 °C and 10^{-3} - 10^{-4} torr) [51] the recombination of **24a** and H_2 is not probable. Further, the **10a**, **11a**, **25a**, and **26a** molecules

are relatively more stable isomers among the set of all minima considered. Therefore, under experimental conditions these molecules may also be observed as minor products. Consequently, our results are consistent with Berson and co-workers observations [51] (Figure 1.9 on page 7).

Since Berson *et al.* [51] carried out their experiments with dimethyl-substituted analogous of the TMMa system, the rearrangements of those dimethyl-substituted molecules, the TMMc system, have also been investigated. In most of the reactions, the methyl groups are not directly involved in the rearrangements, hence the methyl groups are just substituents. As we expected, those substituent effects do not change the main aspects of reactions, thus reaction energies and barriers are slightly different than those in the TMMa system. However, in several reactions the methyl groups are directly involved in the reactions, and those reactions do not occur in the TMMa system.

Our results demonstrate that for the extended Berson **Scheme 1c**, closed-shell bicyclic structures (**3c**, **12c**, **34c**, **37c** and **38c**) are suffer from high ring strain. On the other hand, open-chain structures, **4c**, **5c**, and **6c** and monocyclic structures **7c**, **33c**, **35c**, and **36c** are relatively more stable isomers than the other molecules considered. Thus, at high temperatures, the **4c**, **5c**, **6c**, **7c**, **33c**, **35c**, and **36c** molecules should be expected as products for **Scheme 1c**. Berson *et al.* [51] observed the **4c**, **5c**, **6c**, and **7c** molecules as pyrolysis products (Figure 1.9 on page 7), however they did not observe the **33c**, **35c**, and **36c** molecules.

Our results indicate that at high temperature thermal reactions in addition to the dissociation products, the **10c**, **11c**, **22c**$_1$, **22c**$_2$, **23c**, **25c**, and **26c** molecules should be expected as a product. But, Berson *et al.* [51] observed only the **10c**, **11c**, and **8c**$_1$ molecules considering **Scheme 2c**.

It is verified that the enyne **9c** plays a central role in connecting the two portions of the reaction path (Berson Schemes 1 and 2), and bicyclic intermediates **20a**, **20c**$_1$, and **20c**$_2$ play prominent roles for connecting methylenecyclopentenes to the dissociation products. It is concluded that the proposed mechanisms are confirmed by the theoretical calculations. Computed activation energy and enthalpy of reaction values are in good agreement with the available experimental values, differing only by a few kcal mol^{-1} (Tables 4.1, 4.2, and 4.3 on page 118).

Table 4.1: Comparison of our computations (at CCSD(T)//CASSCF, MRCISD//CASSCF, and CCSD(T)//B3LYP levels for MCP, p_1, and TMMa species, respectively) with the experimental values for relative energies (in kcal mol^{-1}) with respect to triplet TMM (for MCP and p_1) and **11a** (for TMMa species) (Experimental formation enthalpy[b] of **11a** is 27.6 kcal mol^{-1}).

Molecule	**Computation**	**Experiment**
MCP	−22.5	−22.1[a]
p_1	16.9	16.1[a]
20a	10.1	10.2[b]
22a	−0.8	−2.2[c]
23a	0.0	−1.5[b]
28a	26.5	32.4[b]
28a	28.6[d]	

[a] References [38, 205, 20, 21]
[b] Reference [222]
[c] Reference [223]
[d] With the cc-pVTZ basis set

Table 4.2: Comparison of our computations (at CCSD(T)//B3LYP level) with the experimental values for activation energies (in kcal mol^{-1}).

Reaction	**Computation**	**Experiment**
MCP → TMM	39.9	41.2[a]
9a → 14a	35.3	32.7[b]
		32.8[c]
14a → 9a	35.8	33.7[c]
14a → 10a	40.9	36.6[c]
14a → 11a	40.5	36.8[c]
14a → 10a + 11a		37.2[b]
20a → 22a	51.2	50.2[d]
$21a_2$ → 22a	28.1	29.9[e]
23a → 24a	46.4	42.7[d]
27a → 10a	40.0	35.8[c]
27a → 11a	39.6	35.8[c]
27a → 14a	36.5	36.5[c]
28a → 20a	35.8	35.2[c]
9c → 14c	36.9	36.3[c]
14c → 9c	37.1	35.2[c]
17c → 27c	2.3	3.1[c]

[b] Reference [49]
[b] Reference [65]
[c] Reference [69]
[d] Reference [73]
[e] Reference [227]

Table 4.3: Comparison of our computations (using CCSD(T)//B3LYP energy results with transition-state theory (TST)) with the experimental observations for the [**11a**]/[**10a**] ratio at various temperatures.

Temperature (°C)	**Computation**	**Experiment**
235	1.5	1.4[a]
340	1.4	1.3[b]
340		1.3[b]
340		1.5[b]
340		1.3[c]
370	1.4	1.8[c]
385	1.4	1.3[b]
530	1.3	1.3[c]
700	1.2	

[a] References [68]
[b] Reference [65] (Table 1.1 on page 9)
[c] Reference [70] (Table 1.2 on page 10)

REFERENCES

[1] Dewar, M. J. S. *The molecular Orbital Theory of Organic Chemistry*; McGraw-Hill: New York, 1969.

[2] Berson, J. A. *Acc. Chem. Res.* **1997**, *30*, 238.

[3] Gajewski, J. J. *Hydrocarbon Thermal Isomerizations*, 2nd ed.; Academic Press, 2004.

[4] Dowd, P. *Acc. Chem. Res.* **1972**, *5*, 242.

[5] Berson, J. A. *Acc. Chem. Res.* **1978**, *11*, 446.

[6] Mazur, M. R.; Berson, J. A. *J. Am. Chem. Soc.* **1982**, *104*, 2217.

[7] Rule, M.; Mondo, J. A.; Berson, J. A. *J. Am. Chem. Soc.* **1982**, *104*, 2209.

[8] Salinaro, R. F.; Berson, J. A. *J. Am. Chem. Soc.* **1982**, *104*, 2228.

[9] Dowd, P. *J. Am. Chem. Soc.* **1966**, *88*, 2587.

[10] Baseman, R. J.; Pratt, D. W.; Chow, M.; Dowd, P. *J. Am. Chem. Soc.* **1976**, *98*, 5726.

[11] Dowd, P.; Chow, M. *J. Am. Chem. Soc.* **1977**, *99*, 2825.

[12] Dowd, P.; Chow, M. *J. Am. Chem. Soc.* **1977**, *99*, 6438.

[13] Dowd, P.; Chow, M. *Tetrahedron* **1982**, *38*, 799.

[14] Gajewski, J. J.; Paul, G. C. *J. Org. Chem.* **1997**, *62*, 7189.

[15] Dolbier, W. R.; Burkholder, J. R. *J. Am. Chem. Soc.* **1984**, *106*, 2139.

[16] Berson, J. A.; Turro, N. J.; Mircbach, M. J.; Harrit, N.; Platz, M. S. *J. Am. Chem. Soc.* **1978**, *100*, 7653.

[17] Baum, T.; Rossi, A.; Srinivasan, R. *J. Am. Chem. Soc.* **1985**, *107*, 4411.

[18] Leigh, W. J.; Srinivasan, R. *Acc. Chem. Res.* **1987**, *20*, 107.

[19] Wenthold, P. G.; Hu, J.; Squires, R. R.; Lineberger, W. C. *J. Am. Chem. Soc.* **1996**, *118*, 475.

[20] Wenthold, P. G.; Hu, J.; Squires, R. R.; Lineberger, W. C. *J. Am. Chem. Soc. Mass. Spec.* **1999**, *10*, 800.

[21] Wenthold, P. G.; Lineberger, W. C. *Acc. Chem. Res.* **1999**, *32*, 597.

[22] Schaefer, H. F.; Yarkony, D. R. *J. Am. Chem. Soc.* **1974**, *96*, 3754.

[23] Goddard, W. A.; Davis, J. H. *J. Am. Chem. Soc.* **1976**, *98*, 303.

[24] Goddard, W. A.; Davis, J. H. *J. Am. Chem. Soc.* **1977**, *99*, 4242.

[25] Dixon, D. A.; Foster, R.; Halgren, T. A.; Lipscomb, W. N. *J. Am. Chem. Soc.* **1978**, *100*, 1359.

[26] Davidson, E. R.; Borden, W. T. *J. Am. Chem. Soc.* **1977**, *99*, 2053.

[27] Davidson, E. R.; Borden, W. T. *J. Am. Chem. Soc.* **1977**, *99*, 4587.

[28] Schaefer, H. F.; Pitzer, R. M.; Hood, D. M. *J. Am. Chem. Soc.* **1978**, *100*, 2227.

[29] Schaefer, H. F.; Pitzer, R. M. *J. Am. Chem. Soc.* **1978**, *100*, 8009.

[30] Dixon, D. A.; Dunning, T. H.; Eades, R. A.; Kleier, D. A. *J. Am. Chem. Soc.* **1981**, *103*, 2878.

[31] Auster, S. B.; Pitzer, R. M.; Platz, M. S. *J. Am. Chem. Soc.* **1982**, *104*, 3812.

[32] Feller, D.; Tanaka, K.; Davidson, E. R.; Borden, W. T. *J. Am. Chem. Soc.* **1982**, *104*, 967.

[33] Davidson, E. R.; Borden, W. T. *J. Phys. Chem.* **1983**, *87*, 4783.

[34] Borden, W. T.; Du, P. *J. Am. Chem. Soc.* **1987**, *109*, 5330.

[35] Skancke, A.; Schaad, L. J.; Hess, B. D. *J. Am. Chem. Soc.* **1988**, *110*, 5315.

[36] Schaefer, H. F.; Ma, B. *Chem. Phys.* **1996**, *207*, 201.

[37] Davidson, E. R.; Gajewski, J. J.; Shook, C. A.; Cohe, T. *J. Am. Chem. Soc.* **1995**, *117*, 8495.

[38] Cramer, C. J.; Smith, B. A. *J. Phys. Chem.* **1996**, *100*, 9664.

[39] Lijser, H. J. P. D.; Arnold, D. R. *J. Phys. Chem.* **1996**, *100*, 3996.

[40] Schaad, L. J.; Hu, J. *J. Am. Chem. Soc.* **1998**, *120*, 1571.

[41] Borden, W. T.; Lewis, S. B.; Hrovat, D. A. *J. Chem. Soc. Perkin Trans.* **1999**, *2*, 2339.

[42] Slipchenko, L. V.; Krylov, A. I. *J. Chem. Phys.* **2002**, *117*, 4697.

[43] Slipchenko, L. V.; Krylov, A. I. *J. Chem. Phys.* **2003**, *118*, 6874.

[44] Datta, S. N.; Mukherjee, P.; Jha, P. P. *J. Phys. Chem. A* **2003**, *107*, 5049.

[45] Ikeda, H.; Namai, H.; Taki, H.; Miyashi, T. *J. Org. Chem.* **2005**, *70*, 3806.

[46] Pittner, J.; Brabec, J. *J. Phys. Chem. A* **2006**, *110*, 11765.

[47] Borden, W. T.; Lewis, S. B.; Hrovat, D. A. *J. Am. Chem. Soc.* **2006**, *128*, 16676.

[48] Chesick, J. P. *J. Am. Chem. Soc.* **1962**, *85*, 2720.

[49] LeFevre, G. N.; Crawford, R. J. *J. Org. Chem.* **1986**, *51*, 747.

[50] Jahn, H. A.; Teller, E. *Proc. R. Soc. London* **1937**, *A161*, 220.

[51] Mazur, M. R.; Potter, S. E.; Pinhas, A. R.; Berson, J. A. *J. Am. Chem. Soc.* **1982**, *104*, 6823.

[52] Adam, W.; Finzel, R. *J. Am. Chem. Soc.* **1992**, *114*, 4563.

[53] Paul, G. C.; Gajewski, J. J. *J. Org. Chem.* **1996**, *61*, 1399.

[54] Kelley, D. F.; Rentzepis, P. M.; Mazur, M. R.; Berson, J. A. *J. Am. Chem. Soc.* **1982**, *104*, 3764.

[55] Lazzara, M. G.; Harrison, J. J.; Rule, M.; Hilinski, E. F.; Berson, J. A. *J. Am. Chem. Soc.* **1982**, *104*, 2233.

[56] Schmidt, S. P.; Pinhas, A. R.; Hammons, J. H.; Berson, J. A. *J. Am. Chem. Soc.* **1982**, *104*, 6822.

[57] Salinaro, R. F.; Berson, J. A. *J. Am. Chem. Soc.* **1979**, *101*, 7094.

[58] Rule, M.; Lazzara, M. G.; Berson, J. A. *J. Am. Chem. Soc.* **1979**, *101*, 7091.

[59] Lazzara, M. G.; Harrison, J. J.; Rule, M.; Berson, J. A. *J. Am. Chem. Soc.* **1979**, *101*, 7092.

[60] Osterman, V. M.; Schulte, G.; Berson, J. A. *J. Am. Chem. Soc.* **1989**, *111*, 8727.

[61] Rule, M.; Salinaro, R. F.; Pratt, D. R.; Berson, J. A. *J. Am. Chem. Soc.* **1982**, *104*, 2223.

[62] Borden, W. T.; Davidson, E. R. *Acc. Chem. Res.* **1981**, *14*, 69.

[63] Abe, M.; Kawanami, S.; Masuyama, A.; Hayashi, T. *J. Org. Chem.* **2006**, *71*, 6607.

[64] Platz, M. S.; Berson, J. A. *J. Am. Chem. Soc.* **1977**, *99*, 5178.

[65] Huntsman, W. D. In *The Chemistry of Ketenes, Allenes and Related Compounds, Part 2*; Patai, S., Ed.; John Wiley & Sons: New York, 1972; pp 521–667.

[66] Huntsman, W. D.; Dykstra, K. A. unpublished results; K. A. Dykstra, *PhD Dissertation*, Ohio University (1972).

[67] Huntsman, W. D.; Boer, J. A. D.; Woosley, M. H. *J. Am. Chem. Soc.* **1966**, *88*, 5846.

[68] Andrews, G. D.; Baldwin, J. E. *J. Org. Chem.* **1988**, *53*, 4624.

[69] Roth, W. R.; Bauer, F.; Braun, K.; Offerhaus, R. *Angew. Chem. Int. Ed. Engl.* **1989**, *28*, 1056.

[70] Dalacker, V.; Hopf, H. *Tetrahedron Lett.* **1974**, 15.

[71] Hopf, H.; Wolff, J. *Eur. J. Org. Chem.* **2001**, 4009.

[72] Viola, A.; Collins, J. J.; Filipp, N. *Tetrahedron* **1981**, *37*, 3765.

[73] Ellis, R. J.; Frey, H. M. *J. Chem. Soc. A* **1966**, 553.

[74] Fleming, I.; Wildsmith, E. *Chem. Comm.* **1970**, 223.

[75] Orchard, S. W.; Thrush, B. A. *J. Chem. Soc. Chem. Commun.* **1973**, 14.

[76] Benson, S. W.; Shaw, R. *Trans. Faraday Soc.* **1967**, *63*, 985.

[77] Benson, S. W.; Shaw, R. *J. Am. Chem. Soc.* **1967**, *89*, 5351.

[78] Huntsman, W. D.; Chen, J. P.; Yelekci, K.; Yin, T.-K.; Zhang, L. J. *J. Org. Chem.* **1988**, *53*, 4357.

[79] Shields, T. C.; Billups, W. E.; Lepley, A. R. *J. Am. Chem. Soc.* **1968**, *90*, 4749.

[80] Billups, W. E.; Leavell, K. H.; Lewis, E. S.; Vanderpool, S. *J. Am. Chem. Soc.* **1973**, *95*, 8096.

[81] Schrödinger, E. *Ann. Physik.* **1926**, *79*, 361.

[82] Born, M.; Oppenheimer, J. R. *Ann. Physik.* **1927**, *84*, 457.

[83] Szabo, A.; Ostlund, N. S. *Modern Quantum Chemistry*; McGraw-Hill: New York, 1989.

[84] C. D. Sherrill, *The Born-Oppenheimer Approximation* (lecture notes), School of Chemistry and Biochemistry, Georgia Institue of Technology, USA (2005), http://vergil.chemistry.gatech.edu/notes/index.html, last visited on 26/12/2010.

[85] Özkan, I. unpublished notes; Middle East Technical University (2011).

[86] Levine, I. N. *Quantum Chemistry*, 5th ed.; Prentice Hall: New Jersey, 2000.

[87] Pauli, W. *Phys. Rev.* **1940**, *58*, 716.

[88] Slater, J. C. *Phys. Rev.* **1930**, *35*, 210.

[89] Hartree, D. R. *Proc. Camb. Phil. Soc.* **1928**, *24*, 89.

[90] Fock, V. Z. *Phys.* **1930**, *61*, 161.

[91] Roothaan, C. C. J. *Rev. Mod. Phys.* **1951**, *23*, 69.

[92] Cramer, C. J. *Essentials of Computational Chemistry: Theories and Models*; John Wiley & Sons: New York, 2002.

[93] H. F. Schaefer III, *Advanced Quantum Chemistry Lecture Notes*, University of Georgia, USA (2010).

[94] Helgaker, T.; Jørgensen, P.; Olsen, J. *Molecular Electronic Structure Theory*; John Wiley & Sons: New York, 2000.

[95] The spin-orbital formalism is 16 times slower than closed-shell spin-adapted formalism (RHF) and requires 16 times more storage. The situation will be even worser for correlated methods.

[96] Pople, J. A.; Nesbet, R. K. *J. Chem. Phys.* **1954**, *22*, 571.

[97] Jensen, F. *Introduction to Computational Chemistry*; John Wiley & Sons: New York, 1999.

[98] C. D. Sherrill, *Basis Sets in Quantum Chemistry* (lecture notes), School of Chemistry and Biochemistry, Georgia Institue of Technology (USA), http://vergil.chemistry.gatech.edu/notes/index.html, last visited on 26/12/2010.

[99] E. Valeev, *Basis Sets in Quantum Chemistry* (lecture notes), Department of Chemistry, Virginia Tech, USA (2007), http://www.files.chem.vt.edu/chem-dept/valeev/docs/basisset_notes.11082007.pdf, last visited on 26/12/2010.

[100] Slater, J. C. *Phys. Rev.* **1930**, *36*, 57.

[101] Boys, S. F. *Proc. R. Soc. London* **1950**, *200*, 542.

[102] Rienstra-Kiracofe, J. C.; Tschumper, G. S.; Schaefer, H. F.; Nandi, S.; Ellison, G. B. *Chem. Rev.* **2002**, *102*, 231.

[103] Bozkaya, U.; Schaefer, H. F. *Mol. Phys.* **2010**, *108*, 2491.

[104] Hehre, W. J.; Stewart, R. F.; Pople, J. A. *J. Chem. Phys.* **1969**, *51*, 2657.

[105] Hehre, W. J.; Ditchfield, R.; Pople, J. A. *J. Chem. Phys.* **1972**, *56*, 2257.

[106] Hariharan, P. C.; Pople, J. A. *Theor. Chem. Acc.* **1973**, *28*, 213.

[107] McLean, A. D.; Chandler, G. S. *J. Chem. Phys.* **1980**, *72*, 5639.

[108] Raghavachari, K.; Binkley, J. S.; Seeger, R.; Pople, J. A. *J. Chem. Phys.* **1980**, *72*, 650.

[109] Binkley, J. S.; Pople, J. A. *J. Am. Chem. Soc.* **1980**, *102*, 939.

[110] Frisch, M. J.; Pople, J. A.; Binkley, J. S. *J. Chem. Phys.* **1984**, *80*, 3265.

[111] Gaussian 03, Revision D.01, M. J. Frisch and G. W. Trucks and H. B. Schlegel and G. E. Scuseria and M. A. Robb and J. R. Cheeseman and Montgomery and Jr. and J. A. and T. Vreven and K. N. Kudin and J. C. Burant and J. M. Millam and S. S. Iyengar and J. Tomasi and V. Barone and B. Mennucci and M. Cossi and G. Scalmani and N. Rega and G. A. Petersson and H. Nakatsuji and M. Hada and M. Ehara and K. Toyota and R. Fukuda and J. Hasegawa and M. Ishida and T. Nakajima and Y. Honda and O. Kitao and H. Nakai and M. Klene and X. Li and J. E. Knox and H. P. Hratchian and J. B. Cross and V. Bakken and C. Adamo and J. Jaramillo and R. Gomperts and R. E. Stratmann and O. Yazyev and A. J. Austin and R. Cammi and C. Pomelli and J. W. Ochterski and P. Y. Ayala and K. Morokuma and G. A. Voth and P. Salvador and J. J. Dannenberg and V. G. Zakrzewski and S. Dapprich and A. D. Daniels and M. C. Strain and O. Farkas and D. K. Malick and A. D. Rabuck and K. Raghavachari and J. B. Foresman and J. V. Ortiz and Q. Cui and A. G. Baboul and S. Clifford and J. Cioslowski and B. B. Stefanov and G. Liu and A. Liashenko and P. Piskorz and I. Komaromi and R. L. Martin and D. J. Fox and T. Keith and M. A. Al-Laham and C. Y. Peng and A. Nanayakkara and M. Challacombe and P. M. W. Gill and B. Johnson and W. Chen and M. W. Wong and C. Gonzalez and J. A. Pople, Gaussian, Inc., Wallingford, CT, 2004.

[112] Dunning, T. H. *J. Chem. Phys.* **1989**, *90*, 1007.

[113] Kendall, R. A.; Dunning, T. H.; Harrison, R. J. *J. Chem. Phys.* **1992**, *96*, 6796.

[114] Woon, D. E.; Dunning, T. H. *J. Chem. Phys.* **1993**, *98*, 1358.

[115] Woon, D. E.; Dunning, T. H. *J. Chem. Phys.* **1995**, *103*, 4572.

[116] Wilson, A. K.; van Mourik, T.; Dunning, T. H. *J. Mol. Struct.* **1996**, *388*, 339.

[117] East, A. L. L.; Allen, W. D. *J. Chem. Phys.* **1993**, *99*, 4638.

[118] Schuurman, M. S.; Muir, S. R.; Allen, W. D.; Schaefer, H. F. *J. Chem. Phys.* **2004**, *120*, 11586.

[119] Gonzales, J. M.; Pak, C.; Cox, R. S.; Allen, W. D.; Schaefer, H. F.; Császár, A. G.; Tarczay, G. *Chem. Eur. J.* **2003**, *9*, 2173.

[120] Császár, A. G.; Allen, W. D.; Schaefer, H. F. *Chem. Phys.* **1998**, *108*, 9751.

[121] Császár, A. G.; Tarczay, G.; Leininger, M. L.; Polyansky, O. L.; Tennyson, J.; Allen, W. D. *Spectroscopy From Space*, Dordrecht, 2007; pp 317–340.

[122] Bozkaya, U.; Turney, J. M.; Yamaguchi, Y.; Schaefer, H. F. *J. Chem. Phys.* **2010**, *132*, 064308.

[123] Löwdin, P.-O. *Adv. Chem. Phys.* **1959**, *2*, 207.

[124] Roos, B. O. *Adv. Chem. Phys.* **1987**, *69*, 399.

[125] Mok, D. K. W.; Neumann, R.; Handy, N. C. *J. Phys. Chem.* **1996**, *100*, 6225.

[126] C. D. Sherrill, *An Introduction to Configuration Interaction Theory* (lecture notes), School of Chemistry and Biochemistry, Georgia Institue of Technology, USA (1995), http://vergil.chemistry.gatech.edu/notes/index.html, last visited on 26/12/2010.

[127] Sherrill, C. D. *Ph.D. thesis*, The University of Georgia (USA), 1996.

[128] C. D. Sherrill, *Computational Scaling of the Configuration Interaction Method with System Size* (lecture notes), Department of Chemistry, University of California, Berkeley, USA (1996), http://vergil.chemistry.gatech.edu/notes/index.html, last visited on 26/12/2010.

[129] C. D. Sherrill, *Derivation of the Configuration Interaction Singles (CIS) Method for Various Single Determinant References and Extensions to Include Selected Double Substitutions (XCIS)* (lecture notes), School of Chemistry and Biochemistry, Georgia Institue of Technology, USA (1996), http://vergil.chemistry.gatech.edu/notes/index.html, last visited on 26/12/2010.

[130] C. D. Sherrill, *Analytic Gradients of Configuration Interaction Energies* (lecture notes), School of Chemistry and Biochemistry, Georgia Institue of Technology, USA (2009), http://vergil.chemistry.gatech.edu/notes/index.html, last visited on 26/12/2010.

[131] C. D. Sherrill, *Some Comments on the Davidson Correction* (lecture notes), Department of Chemistry, University of California, Berkeley, USA (1996), http://vergil.chemistry.gatech.edu/notes/index.html, last visited on 26/12/2010.

[132] Langhoff, S. R.; Davidson, E. R. *Int. J. Quant. Chem.* **1974**, *8*, 61.

[133] Shepard, R. *Adv. Chem. Phys.* **1987**, *69*, 63.

[134] Olsen, J.; Yeager, D. L.; Jørgensen, P. *Adv. Chem. Phys.* **1983**, *54*, 1.

[135] Shepard, R.; Shavitt, I.; Simons, J. *J. Chem. Phys.* **1982**, *76*, 543.

[136] Dalgaard, E.; Jørgensen, P. *J. Chem. Phys.* **1978**, *69*, 3833.

[137] Dalgaard, E. *Chem. Phys. Lett.* **1979**, *65*, 559.

[138] Yeager, D. L.; Jørgensen, P. *J. Chem. Phys.* **1979**, *71*, 755.

[139] Werner, H.-J. *Adv. Chem. Phys.* **1987**, *69*, 1.

[140] Chaban, G.; Schmidt, M. W.; Gordon, M. S. *Theor. Chem. Acc.* **1997**, *97*, 88.

[141] Shepard, R. In *Modern Electronic Structure Theory Part I*; Yarkony, D. R., Ed., 1st ed.; Advanced Series in Physical Chemistry Vol.2; World Scientific Publishing Company: London, 1995; pp 345–458.

[142] Y. Yamaguchi, *Complete Active Space SCF (CASSCF) and Multiconfiguration SCF (MCSCF) Wavefunctions* (lecture notes), Center for Computational Chemistry, University of Georgia, USA (1996), http://www.ccqc.uga.edu/lec_top/casscf/casscf.html, last visited on 26/12/2010.

[143] Yamaguchi, Y.; Osamura, Y.; Goddard, J. D.; Schaefer, H. F. *A New Dimension to Quantum Chemistry: Analytic Derivative Methods in Ab Initio Molecular Electronic Structure Theory*; Oxford University Press: USA, 1994.

[144] Roos, B. O.; Taylor, P.; Siegbahn, P. E. *Chem. Phys.* **1980**, *48*, 157.

[145] Schmidt, M. W.; Gordon, M. S. *Annu. Rev. Phys. Chem.* **1998**, *49*, 233.

[146] Sherrill, C. D.; Schaefer, H. F. In *Advances in Quantum Chemistry*; Löwdin, P.-O., Ed.; Academic Press: New York, 1999; Vol. 34, pp 143–269.

[147] Shavitt, I.; Bartlett, R. J. *Many-Body Methods in Chemistry and Physics*; Cambridge Press: New York, 2009.

[148] Harris, F. E.; Monkhorst, H. J.; Freeman, D. L. *Algebraic and Diagrammatic Methods in Many-Fermion Theory*; Oxford Press: New York, 1992.

[149] Crawford, T. D. *Ph.D. thesis*, The University of Georgia, 1996.

[150] Wilson, S. *Electron Correlation in Molecules*; Dover Publications: New York, 2007.

[151] Hubač, I.; Wilson, S. *Brillouin-Wigner Methods for Many-Body Systems*; Dordrecht: New York, 2010.

[152] Lindgren, I.; Morrison, J. *Atomic Many-Body Theory*, 1st ed.; Springer: New York, 1982.

[153] Møller, C.; Plesset, M. S. *Phys. Rev.* **1934**, *46*, 618.

[154] Binkley, J. S.; Pople, J. A. *Int. J. Quant. Chem.* **1975**, *9*, 229.

[155] Andersson, K.; Malmqvist, P.-A.; Roos, B. O.; Sadlej, A. J.; Wolinski, K. *J. Phys. Chem.* **1990**, *94*, 5483.

[156] Andersson, K.; Malmqvist, P.-A.; Roos, B. O. *J. Chem. Phys.* **1990**, *96*, 1218.

[157] Andersson, K.; Roos, B. O. In *Modern Electronic Structure Theory Part II*; Yarkony, D. R., Ed.; Advanced Series in Physical Chemistry Vol.2; World Scientific Publishing Company: London, 1995; pp 55–109.

[158] Roos, B. O. In *Theory and Applications of Computational Chemistry: The First Forty Years*; Dykstra, C., Ed.; Elsevier, 2005; pp 725–764.

[159] Hoffmann, M. R. In *Modern Electronic Structure Theory Part II*; Yarkony, D. R., Ed.; Advanced Series in Physical Chemistry Vol.2; World Scientific Publishing Company: London, 1995; pp 1166–1190.

[160] Čížek, J. *J. Chem. Phys.* **1966**, *45*, 4256.

[161] Čížek, J. *Adv. Chem. Phys.* **1969**, *14*, 35.

[162] Purvis, G. D.; Bartlett, R. J. *J. Chem. Phys.* **1982**, *76*, 1910.

[163] Bartlett, R. J. *J. Chem. Phys.* **1989**, *93*, 1697.

[164] Pople, J. A.; Head-Gordon, M.; Raghavachari, K. *J. Chem. Phys.* **1987**, *87*, 5968.

[165] Scuseria, G. E.; Scheiner, A. C.; Lee, T. J.; Rice, J. E.; Schaefer, H. F. *J. Chem. Phys.* **1987**, *86*, 2881.

[166] Scuseria, G. E.; Janssen, C. L.; Schaefer, H. F. *J. Chem. Phys.* **1988**, *89*, 7382.

[167] Scuseria, G. E.; Schaefer, H. F. *J. Chem. Phys.* **1989**, *90*, 3700.

[168] Crawford, T. D.; Schaefer, H. F. *Rev. Comp. Chem.* **2000**, *14*, 33.

[169] Bartlett, R. J. In *Modern Electronic Structure Theory Part II*; Yarkony, D. R., Ed.; Advanced Series in Physical Chemistry Vol.2; World Scientific Publishing Company: London, 1995; pp 1047–1131.

[170] Bartlett, R. J.; Musial, M. *Rev. Mod. Phys.* **2007**, *291*, 1910.

[171] Gauss, J. In *Modern Methods and Algorithms of Quantum Chemistry, Molecular Properties*; NIC Series, Vol. 3; John von Neumann Institute for Computing: London, 2000; pp 541–542.

[172] Thomas, L. H. *Proc. Camb. Phil. Soc.* **1927**, *23*, 542.

[173] Fermi, E. *Rend. Accad. Lincei.* **1927**, *6*, 602.

[174] Hohenberg, P.; Kohn, W. *Phys. Rev. B* **1964**, *136*, 864.

[175] Kohn, W.; Sham, L. J. *Phys. Rev. A* **1965**, *140*, 1133.

[176] Parr, R. G.; Yang, W. *Density-Functional Theory of Atoms and Molecules*; Oxford University Press: New York, 1989.

[177] Levy, M. *Proc. Natl Acad. Sci. USA* **1979**, *76*, 6062.

[178] Levy, M. *Phys. Rev. A* **1982**, *26*, 1200.

[179] McQuarrie, D. A. *Statistical Mechanics*; Harper & Row: New York, 1976.

[180] Slater, J. C. *The Self-Consistent Field for Molecular and Solids, Quantum Theory of Molecular and Solids, Vol. 4*; McGraw-Hill: New York, 1974.

[181] Vosko, S. H.; Wilk, L.; Nusair, M. *Can. J. Phys.* **1980**, *58*, 1200.

[182] Perdew, J. P.; Wang, Y. *Phys. Rev. B* **1986**, *33*, 8800.

[183] Perdew, J. P.; Chevary, J. A.; Vosko, S. H.; Jackson, K. A.; Pederson, M. R.; Singh, D. J.; Fiolhais, C. *Phys. Rev. B* **1992**, *46*, 6671.

[184] Perdew, J. P.; Wang, Y. *Phys. Rev. B* **1992**, *45*, 13244.

[185] Perdew, J. P.; Chevary, J. A.; Vosko, S. H.; Jackson, K. A.; Pederson, M. R.; Singh, D. J.; Fiolhais, C. *Phys. Rev. B* **1993**, *48*, 4978.

[186] Becke, A. D. *Phys. Rev. A* **1988**, *38*, 3098.

[187] Becke, A. D. *Phys. Rev. A* **1989**, *39*, 3761.

[188] Becke, A. D. *J. Chem. Phys.* **1992**, *96*, 2155.

[189] Becke, A. D. *J. Chem. Phys.* **1992**, *97*, 9173.

[190] Becke, A. D. *J. Chem. Phys.* **1996**, *104*, 1040.

[191] Becke, A. D. *J. Chem. Phys.* **1997**, *107*, 8554.

[192] Lee, C.; Yang, W.; Parr, R. G. *Phys. Rev. B* **1988**, *37*, 785.

[193] Miehlich, B.; Savin, A.; Stoll, H.; Preuss, H. *Chem. Phys. Lett.* **1989**, *157*, 200.

[194] Becke, A. D. *J. Chem. Phys.* **1993**, *98*, 5648.

[195] Becke, A. D. *J. Chem. Phys.* **1993**, *98*, 1372.

[196] Koch, W.; Holthausen, M. C. *A Chemist's Guide to Density Functional Theory*, 2nd ed.; Wiley-VCH: New York, 2001.

[197] Gill, P. M. W.; Johnson, B. G.; Pople, J. A.; Frisch, M. J. *Chem. Phys. Lett.* **1992**, *197*, 499.

[198] Scuseria, G. E. *J. Chem. Phys.* **1992**, *97*, 7528.

[199] Sosa, C.; Lee, C. *J. Chem. Phys.* **1993**, *98*, 8004.

[200] Schmidt, M. W.; Baldridge, K. K.; Boatz, J. A.; Elbert, S. T.; Gordon, M. S.; Jensen, J. H.; Koseki, S.; Matsunaga, N.; Nguyen, K. A.; Su, S. J.; Windus, T. L.; Dupuis, M.; Montgomery, J. A. *J. Comp. Chem.* **1993**, *14*, 1347.

[201] cheMVP is free, open-source software designed to make clean, simple molecule drawings suitable for publications and presentations. The program is written in C++, using the QT library and some icons from the SVG icons project by A. Simmonett (andysim@ccc.uga.edu) and J. M. Turney (jturney@ccc.uga.edu), Center for Computational Quantum Chemistry (CCQC), University of Geoergia (USA), 2008.

[202] Ishida, K.; Morokuma, K.; Komornicki, A. *J. Chem. Phys.* **1977**, *66*, 2153.

[203] Neumark, D. M. *Acc. Chem. Res.* **1993**, *26*, 33.

[204] Polanyi, J. C.; Zewail, A. H. *Acc. Chem. Res.* **1995**, *28*, 119.

[205] Cox, J. D.; Pilcher, G. *Thermochemistry of Organic and Organometallic Compounds*; Academic: New York, 1970.

[206] Gajewski, J. J. *J. Am. Chem. Soc.* **1968**, *90*, 7178.

[207] Gajewski, J. J. *J. Am. Chem. Soc.* **1971**, *93*, 4450.

[208] Solomons, T. W. G.; Fryhle, C. B. *Organic Chemistry*, 9th ed.; John Wiley & Sons: New York, 2007.

[209] Dykstra, C. E.; Schaefer, H. F. *J. Am. Chem. Soc.* **1978**, *100*, 1378.

[210] Hartzier, H. D. In *Carbenes, Vol. II*; Moss, R. A., Jones, M., Eds.; Wiley: New York, 1975; p 52.

[211] Brown, R. F. C. *Recl. Trav. Chim. Pays. Bas.* **1988**, *107*, 655.

[212] Walsh, R.; Wolf, C.; Untiedt, S.; de Meijere, A. *J. Chem. Soc., Chem. Commun.* **1992**, 421.

[213] Holbrook, K. A.; Pilling, M. J.; Robertson, S. H. *Unimolecular Reactions*, 2nd ed.; John Wiley & Sons: New York, 1996.

[214] Steinfeld, J. I.; Francisco, J. S.; Hase, W. L. *Chemical Kinetics and Dynamics*, 2nd ed.; Prentice Hall: New Jersey, 1999; pp 287–382.

[215] Black, K. A.; Wilsey, S.; Houk, K. N. *J. Am. Chem. Soc.* **1998**, *120*, 5622.

[216] Zora, M.; Özkan, I. *J. Mol. Struct.* **2003**, *625*, 251.

[217] Zora, M.; Özkan, I.; Danışman, M. F. *J. Mol. Struct.* **2003**, *636*, 9.

[218] Özkan, I.; Zora, M. *J. Org. Chem.* **2003**, *68*, 9635.

[219] IUPAC. *Compendium of Chemical Terminology*, 2nd ed. (the "Gold Book"). Compiled by McNaught, A.D. and Wilkinson, A. Blackwell Scientific Publications, Oxford, 1997.

[220] Balcı, M. *Organic Chemistry, Reaction Mechanism*; TUBA,: Ankara, 2008.

[221] Rodriguez-Otero, J. *J. Org. Chem.* **1999**, *64*, 6842.

[222] Roth, W. R.; Adamczak, O.; Breuckmann, R.; Lennartz, H. W.; Boese, R. *Chem. Ber.* **1991**, *124*, 2499.

[223] Frenkel, M.; Marsh, K. N.; Wilhoit, R. C.; Kabo, G. J.; Roganov, G. N. *Thermodynamics of Organic Compounds in the Gas State*; 1994.

[224] Bond, F. T.; Scerbo, L. *Tetrahedron Lett.* **1968**, 2789.

[225] Frey, H. M.; Hopkins, R. G.; O'Neal, H. E.; Bond, F. T. *Tetrahedron Lett.* **1969**, 1069.

[226] MATLAB 7.0.4, The Language of Technical Computing, The MathWorks Inc., 2005.

[227] Lewis, K. E.; Steiner, H. *J. Chem. Soc.* **1964**, 3080.

APPENDIX A

ELECTRONIC AND ZERO POINT ENERGIES OF ALL STATIONARY STRUCTURES

Table A.1: Electronic energies (in a.u.) and ZPVEs (in kcal mol^{-1}) of the parent TMM species, MCP, TS (MCP/o_1) structures at optimized (4*e*,4*o*)CASSCF/6-311G(d,p) geometries.

Structure	**(4*e*,4*o*)CASSCF**	**(4*e*,4*o*)MRMP2**	**ZPVE**
triplet	−154.943234	−155.466171	52.4
o_1	−154.920105	−155.441106	51.6
s_1	−154.912389	−155.434082	50.3
l_1	−154.911772	−155.434713	49.3
MCP	−154.969332	−155.497372	55.7
MCP/o_1	−154.914599	−155.437286	51.6

Table A.2: Electronic energies (in a.u.) and ZPVEs (in kcal mol^{-1}) of the TMMa species at optimized (4*e*,4*o*)CASSCF/6-311G(d,p) geometries.

Structure	**(4*e*,4*o*)CASSCF**	**(4*e*,4*o*)MRMP2**	**ZPVE**
1a-T	−231.867311	−232.675312	76.9
1a-o_1	−231.844365	−232.650575	76.2
1a-o_2	−231.839496	−232.647068	77.0
1a-p_1	−231.839056	−232.647805	76.2

Table A.3: Electronic energies (in a.u.) and ZPVEs (in kcal mol^{-1}) of minima in the TMMa system at optimized B3LYP/6-311G(d,p) geometries.

Structure	**B3LYP**	**CCSD(T)**	**ZPVE**
2a	−342.952655	−342.054118	83.4
3a	−233.409783	−232.754161	75.2
4a	−233.452329	−232.790787	74.2
9a	−233.426528	−232.768428	73.9
10a	−233.472368	−232.816337	75.5
11a	−233.480446	−232.822672	75.8
12a	−233.400198	−232.748411	75.6
13a	−233.350906	−232.695194	72.4
14a	−233.432933	−232.768616	73.5
15a	−233.419319	−232.763655	74.3
15a-trans	−233.419964	−232.764121	74.2
17a	−233.398474	−232.737097	72.4
20a	−233.458888	−232.807647	76.4
$21a_1$	−233.445759	−232.783724	74.0
$21a_2$	−233.455532	−232.791492	74.4
22a	−233.481358	−232.825052	76.5
23a	−233.481080	−232.823514	76.3
24a	−232.308550	−231.653848	62.9
25a	−233.483692	−232.826638	75.2
26a	−233.483414	−232.826311	75.2
27a	−233.424446	−232.770063	75.3
28a	−233.425075	−232.781860	76.6
29a	−233.419916	−232.759722	73.9
30a	−233.425597	−232.763148	74.1
31a	−233.390259	−232.711940	71.3
32a	−233.417924	−232.764714	75.1
33a	−233.443017	−232.784105	74.9
34a	−233.385377	−232.734991	75.5

Table A.4: Electronic energies (in a.u.) and ZPVEs (in kcal mol^{-1}) of TSs in the TMMa system at optimized B3LYP/6-311G(d,p) geometries.

Structure	**B3LYP**	**CCSD(T)**	**ZPVE**
1a/2a	−342.912834	−342.009263	80.5
1a/3a	−233.384285	−232.726865	73.2
1a/4a	−233.363928	−232.699957	71.9
1a/12a	−233.369315	−232.714851	73.0
4a/33a	−233.384928	−232.724451	73.1
9a/14a	−233.369845	−232.710813	73.0
14a/15a	−233.358534	−232.697358	70.9
14a/17a	−233.363593	−232.707138	72.3
15a/15a-trans	−233.347622	−232.678632	69.9
10a/17a	−233.360899	−232.698951	70.7
10a/20a	−233.362640	−232.702029	71.0
11a/17a	−233.362396	−232.699751	70.8
11a/20a	−233.350664	−232.693363	70.6
11a/31a	−233.377312	−232.713820	71.6
17a/27a	−233.385523	−232.730852	72.9
14a/$21a_2$	−233.330606	−232.663224	70.0
20a/$21a_2$	−233.375785	−232.716738	72.4
20a/22a	−233.379668	−232.720344	72.9
20a/23a	−233.378544	−232.718949	72.7
20a/25a	−233.351813	−232.694565	70.7
20a/26a	−233.364726	−232.704124	71.1
20a/28a	−233.366436	−232.719750	73.5
$21a_1$/$21a_2$	−233.443970	−232.782111	73.8
$21a_1$/22a	−233.412739	−232.746559	74.4
23a/24a	−233.402180	−232.742021	71.6
29a/31a	−233.377333	−232.714881	71.5
30a/31a	−233.363577	−232.698585	70.9
30a/32a	−233.355285	−232.697192	73.2
33a/34a	−233.348662	−232.693904	73.8

Table A.5: Electronic energies (in a.u.) and ZPVEs (in kcal mol^{-1}) of the TMMc species at optimized (4*e*,4*o*)CASSCF/6-311G(d,p) geometries.

Structure	**(4*e*,4*o*)CASSCF**	**(4*e*,4*o*)MRMP2**	**ZPVE**
1c-T	−309.956919	−311.074100	114.4
1c-o_1	−309.939568	−311.053281	114.4
1c-o_2	−309.930286	−311.046424	114.4
1c-p_1	−309.927664	−311.046424	113.2

Table A.6: Electronic energies (in a.u.) and ZPVEs (in kcal mol^{-1}) of minima in the TMMc system at optimized B3LYP/6-311G(d,p) geometries.

Structure	B3LYP	CCSD(T)	ZPVE
2c	−421.609002	−420.488504	118.5
3c	−312.067484	−311.189208	110.2
4c	−312.103108	−311.219952	109.0
5c	−312.103696	−311.221536	109.0
6c	−312.103014	−311.220551	108.8
7c	−312.132071	−311.254365	111.4
$8c_1$	−271.636048	−270.870052	79.9
$8c_2$	−310.962910	−310.086496	97.4
9c	−312.082379	−311.200508	108.9
10c	−312.132120	−311.252979	110.0
11c	−312.136399	−311.257882	110.6
12c	−312.055943	−311.184232	110.5
13c	−312.006341	−311.126403	107.5
14c	−312.080324	−311.200147	108.5
15c	−312.071193	−311.196478	109.1
15c-trans	−312.071491	−311.196434	109.0
16c	−312.084875	−311.201362	108.6
17c	−312.054631	−311.168272	107.5
$20c_1$	−312.118041	−311.243760	111.1
$20c_2$	−312.114252	−311.242010	111.3
$20c_3$	−312.116375	−311.244544	111.1
$20c_4$-endo	−312.111034	−311.239982	111.2
$20c_4$-exo	−312.111681	−311.240435	111.1
$21c_1$	−312.102632	−311.220228	109.1
$21c_2$	−312.110477	−311.226317	109.1
$21c_3$	−312.101245	−311.216246	109.0
$21c_4$	−312.110604	−311.223644	109.3
$21c_5$	−312.096621	−311.215080	108.6
$21c_6$	−312.105000	−311.221347	109.1
$21c_7$	−312.111990	−311.225033	109.4
$21c_8$	−312.104969	−311.218405	109.5
$22c_1$	−312.136561	−311.258427	111.1
$22c_2$	−312.135692	−311.259645	111.4
$22c_3$	−312.136878	−311.259555	111.2
$22c_4$	−312.135050	−311.258338	111.3
$23c_1$	−312.133726	−311.256529	111.3
$23c_2$	−312.135500	−311.256031	110.9
25c	−312.137609	−311.259650	110.2
$25c_2$	−312.135231	−311.256501	110.5
26c	−312.141582	−311.261360	109.8
$26c_2$	−312.141392	−311.262000	109.9
27c	−312.079258	−311.204006	110.1
$28c_1$	−312.084550	−311.219920	111.1
$28c_2$-endo	−312.079852	−311.216518	111.1
$28c_2$-exo	−312.078006	−311.214725	111.2
$28c_3$	−312.086107	−311.219323	111.4
$28c_4$-endo	−312.082285	−311.216723	111.4
$28c_4$-exo	−312.080358	−311.214538	111.4
29c	−312.075410	−311.192301	108.9
30c	−312.079693	−311.193852	109.0
31c	−312.044471	−311.151107	106.1
32c	−312.077399	−311.201957	109.9
33c	−312.094583	−311.218672	109.7
34c	−312.038898	−311.170019	110.2
35c	−312.097447	−311.218658	109.9
36c	−312.101729	−311.221006	109.7
37c	−312.043442	−311.170590	110.3
38c	−312.038565	−311.168628	110.3

Table A.7: Electronic energies (in a.u.) and ZPVEs (in kcal mol^{-1}) of TSs in the TMMc system at optimized B3LYP/6-311G(d,p) geometries.

Structure	B3LYP	CCSD(T)	ZPVE
1c/2c	−421.569855	−420.443793	115.4
1c/3c	−312.038596	−311.159028	107.9
1c/4c	−312.017866	−311.132129	106.7
1c/7c	−312.011736	−311.129550	106.3
1c/12c	−312.031220	−311.153415	108.3
4c/6c	−312.047780	−311.160142	106.8
4c/33c	−312.035660	−311.154986	107.8
5c/35c	−312.032931	−311.152136	108.1
5c/36c	−312.035899	−311.153601	107.9
6c/35c	−312.041556	−311.159604	108.1
6c/36c	−312.045150	−311.161571	107.7
$8c_1$/23c	−312.029619	−311.146143	106.8
$8c_2$/23c	−312.057160	−311.176476	106.2
9c/14c	−312.018418	−311.139701	107.7
10c/17c	−312.017965	−311.133400	105.6
10c/$20c_1$	−312.020936	−311.137487	105.6
11c/$20c_2$	−312.006161	−311.128112	105.6
11c/17c	−312.019793	−311.134787	105.7
11c/31c	−312.034741	−311.147766	106.5
14c/15c	−312.011478	−311.133071	105.8
15c/15c-trans	−311.993759	−311.108351	105.1
15c/16c	−312.009558	−311.129159	105.8
16c/17c	−312.020469	−311.141594	107.3
17c/27c	−312.044014	−311.166780	107.8
$20c_1$/$21c_2$	−312.033850	−311.152196	106.9
$20c_1$/$22c_1$	−312.033000	−311.152646	107.4
$20c_1$/23c	−312.030363	−311.150087	107.3
$20c_1$/26c	−312.022565	−311.139142	105.6
$20c_1$/$28c_1$	−312.027706	−311.158358	108.0
$20c_2$/$21c_4$	−312.032565	−311.151237	107.1
$20c_2$/$22c_2$	−312.031977	−311.152457	107.7
$20c_2$/23c	−312.030266	−311.150661	107.4
$20c_2$/25c	−312.006925	−311.128859	105.6
$20c_2$/$28c_2$	−312.023595	−311.155784	108.2
$20c_3$/$22c_3$	−312.032312	−311.151888	107.4
$20c_3$/$23c_2$	−312.032250	−311.151529	107.2
$20c_3$/$26c_2$	−312.024083	−311.141842	105.8
$20c_3$/$28c_3$	−312.025053	−311.154953	107.9
$20c_4$/$22c_1$	−312.031436	−311.151644	107.5
$20c_4$/$23c_1$	−312.031712	−311.151704	107.5
$20c_4$/$25c_2$	−312.021636	−311.137435	105.9
$20c_4$/$28c_4$	−312.028388	−311.157753	108.6
$21c_1$/$21c_2$	−312.097588	−311.216367	108.5
$21c_1$/$22c_1$	−312.064245	−311.177913	108.9
$21c_3$/$21c_4$	−312.098176	−311.213809	108.7
$21c_3$/$22c_2$	−312.066195	−311.179018	109.2
$21c_5$/$22c_3$	−312.062791	−311.176192	108.9
$21c_7$/$22c_4$	−312.067181	−311.179050	108.9
29c/31c	−312.032594	−311.146852	106.4
30c/31c	−312.016237	−311.129424	105.7
30c/32c	−312.015971	−311.134135	107.8
33c/34c	−312.001671	−311.128553	108.5
35c/37c	−312.006705	−311.129653	108.5
36c/38c	−312.004293	−311.129238	108.7

APPENDIX B

OPTIMIZED GEOMETRIES OF ALL MINIMA

Table B.1: Triplet TMM (D_{3h}, $^3A_2'$) at (4e,4o)CASSCF/6-311G(d,p) level.

Atom	x (Å)	y (Å)	z (Å)
C	0.000000	0.000000	0.000000
C	−1.225487	0.707535	0.000000
C	1.225487	0.707535	0.000000
C	0.000000	−1.415070	0.000000
H	−2.165307	0.188046	0.000000
H	2.165307	0.188046	0.000000
H	−1.245505	1.781187	0.000000
H	1.245505	1.781187	0.000000
H	−0.919801	−1.969234	0.000000
H	0.919801	−1.969234	0.000000

Table B.2: Singlet TMM $\mathbf{s}_1$ (C_{2v}, $^1A_1$) at (4e,4o)CASSCF/6-311G(d,p) level.

Atom	x (Å)	y (Å)	z (Å)
C	0.000000	0.048246	0.000000
C	1.260110	−0.717458	0.000000
C	−1.260110	−0.717458	0.000000
C	0.000000	1.393942	0.000000
H	2.204312	−0.208209	0.000000
H	−2.204312	−0.208209	0.000000
H	1.255251	−1.789990	0.000000
H	−1.255251	−1.789990	0.000000
H	0.917644	1.954909	0.000000
H	−0.917644	1.954909	0.000000

Table B.3: Singlet TMM $\mathbf{o}_1$ (C_s, $^1A''$) at (4e,4o)CASSCF/6-311G(d,p) level.

Atom	x (Å)	y (Å)	z (Å)
C	0.034660	0.001747	0.000000
C	−1.450091	0.178704	0.000000
C	0.568213	−1.287258	0.000000
C	0.852943	1.128855	0.000000
H	−1.999780	0.092319	−0.919831
H	−1.999780	0.092319	0.919831
H	−0.063743	−2.155593	0.000000
H	1.632057	−1.443624	0.000000
H	0.439220	2.119594	0.000000
H	1.923864	1.032468	0.000000

Table B.4: MCP at (4e,4o)CASSCF/6-311G(d,p) level.

Atom	x (Å)	y (Å)	z (Å)
C	−0.298933	0.000000	0.000000
C	0.937678	−0.782434	0.000000
C	0.937678	0.782434	0.000000
C	−1.624764	0.000000	0.000000
H	1.235232	−1.280695	−0.907795
H	1.235232	−1.280695	0.907795
H	1.235232	1.280695	−0.907795
H	1.235232	1.280695	0.907795
H	−2.182679	−0.920308	0.000000
H	−2.182679	0.920308	0.000000

Table B.5: **1a-T** at (4e,4o)CASSCF/6-311G(d,p) level.

Atom	x (Å)	y (Å)	z (Å)
C	0.823950	0.000000	0.000000
C	−0.000343	1.150782	0.000000
C	−0.000343	−1.150782	0.000000
C	−1.460408	0.776696	0.000000
C	−1.460408	−0.776696	0.000000
C	2.232065	0.000000	0.000000
H	−1.973210	1.176917	−0.871237
H	−1.973210	1.176917	0.871237
H	−1.973210	−1.176917	−0.871237
H	−1.973210	−1.176917	0.871237
H	2.785918	0.920042	0.000000
H	2.785918	−0.920042	0.000000
H	0.359698	2.162098	0.000000
H	0.359698	−2.162098	0.000000

Table B.6: **1a-p**$_1$ at (4*e*,4*o*)CASSCF/6-311G(d,p) level.

Atom	x (Å)	y (Å)	z (Å)
C	0.000000	0.000000	−0.879657
C	−1.165723	0.063219	0.020781
C	1.165723	−0.063219	0.020781
C	−0.768761	−0.084699	1.459934
C	0.768761	0.084699	1.459934
C	0.000000	0.000000	−2.221881
H	−1.044266	−1.069406	1.835947
H	1.044266	1.069406	1.835947
H	−1.263608	0.640655	2.099689
H	1.263608	−0.640655	2.099689
H	−0.917893	0.037317	−2.781065
H	0.917893	−0.037317	−2.781065
H	−2.183307	0.078214	−0.320460
H	2.183307	−0.078214	−0.320460

Table B.7: **1a-o**$_1$ at (4*e*,4*o*)CASSCF/6-311G(d,p) level.

Atom	x (Å)	y (Å)	z (Å)
C	0.795738	0.007715	0.000000
C	−0.010865	1.144380	0.000000
C	−1.472851	0.770043	0.000000
C	0.001895	−1.140401	0.000000
C	−1.464268	−0.782340	0.000000
C	2.280541	0.020055	0.000000
H	−1.985480	1.169262	0.871593
H	−1.985480	1.169262	−0.871593
H	−1.972396	−1.187287	−0.871597
H	−1.972396	−1.187287	0.871597
H	2.822098	−0.101537	−0.920111
H	2.822098	−0.101537	0.920111
H	0.349149	2.155577	0.000000
H	0.372259	−2.148063	0.000000

Table B.8: **1a-o**$_2$ at (4*e*,4*o*)CASSCF/6-311G(d,p) level.

Atom	x (Å)	y (Å)	z (Å)
C	0.846672	−0.002083	0.009514
C	−0.071557	1.197331	0.146193
C	0.034196	−1.132056	0.021703
C	−1.462067	0.729965	−0.207533
C	−1.431535	−0.791940	0.085811
C	2.227004	0.033317	−0.080962
H	−1.648329	0.889126	−1.267887
H	−2.239324	1.248961	0.341302
H	−2.024045	−1.371566	−0.616232
H	−1.829327	−0.996118	1.078737
H	2.799116	−0.874723	−0.138427
H	2.762398	0.964187	−0.102039
H	0.076076	1.870570	0.975700
H	0.404197	−2.141621	0.029782

Table B.9: **2a** at B3LYP/6-311G(d,p) level.

Atom	x (Å)	y (Å)	z (Å)
C	−0.496693	0.575000	−0.698996
C	−0.497213	0.575849	0.810353
C	1.035042	0.574014	1.111616
C	0.287154	−0.710479	−0.805116
C	1.588921	−0.333391	−0.029470
C	−0.983884	1.410452	−1.600785
N	−0.904376	−0.845862	1.086901
N	−0.461059	−1.571911	0.175576
H	−1.104060	1.289792	1.359115
H	1.235815	0.179376	2.108479
H	1.429756	1.589435	1.054563
H	0.413287	−1.199227	−1.766539
H	2.273335	0.206480	−0.685410
H	2.094778	−1.226195	0.340379
H	−1.520961	2.306793	−1.310146
H	−0.863865	1.229286	−2.663389

Table B.10: **3a** at B3LYP/6-311G(d,p) level.

Atom	x (Å)	y (Å)	z (Å)
C	0.131276	−0.793530	0.579842
C	1.350122	−0.781045	−0.358880
C	0.131133	0.793657	0.579681
C	1.350214	0.781015	−0.358840
C	−0.963770	−0.000132	0.031791
C	−2.225185	−0.000011	−0.363176
H	−0.009980	−1.481857	1.406314
H	1.207184	−1.278074	−1.321662
H	2.245047	−1.186204	0.115621
H	−0.010258	1.482134	1.405998
H	2.245186	1.186163	0.115588
H	1.207275	1.277972	−1.321648
H	−2.763723	−0.926844	−0.531427
H	−2.763464	0.926993	−0.531295
H	−1.520961	2.306793	−1.310146
H	−0.863865	1.229286	−2.663389

Table B.11: **4a** at B3LYP/6-311G(d,p) level.

Atom	x (Å)	y (Å)	z (Å)
C	−0.000541	2.028637	0.000090
C	0.000053	0.681544	−0.000212
C	1.284139	−0.023939	0.174848
C	1.594637	−1.265025	−0.208036
C	−1.284000	−0.024611	−0.175023
C	−1.594183	−1.265578	0.208167
H	−0.911821	2.594805	−0.154222
H	0.910196	2.595547	0.154942
H	2.068734	0.583516	0.620570
H	2.597573	−1.649799	−0.063664
H	−2.068621	0.582611	−0.620964
H	−2.597055	−1.650618	0.063902
H	−0.884925	−1.921331	0.696538
H	0.885280	−1.920902	−0.696098
H	−1.520961	2.306793	−1.310146
H	−0.863865	1.229286	−2.663389

Table B.12: **9a** at B3LYP/6-311G(d,p) level.

Atom	x (Å)	y (Å)	z (Å)
C	2.832092	−0.322739	−0.314682
C	1.811593	0.260395	0.306714
C	0.423683	−0.305475	0.407456
C	−0.632384	0.612447	−0.257369
C	−1.993529	0.100574	−0.128897
C	−3.105178	−0.340431	−0.011777
H	3.813419	0.136580	−0.353324
H	2.724244	−1.286328	−0.803976
H	1.967252	1.227465	0.783933
H	0.383959	−1.295106	−0.055361
H	0.149650	−0.433866	1.460846
H	−0.579581	1.612537	0.188417
H	−0.386272	0.734686	−1.317662
H	−4.090329	−0.724589	0.088459
H	−1.520961	2.306793	−1.310146
H	−0.863865	1.229286	−2.663389

Table B.13: **10a** at B3LYP/6-311G(d,p) level.

Atom	x (Å)	y (Å)	z (Å)
C	0.808314	0.000001	0.000433
C	−0.083378	−1.239160	0.001056
C	−0.083377	1.239160	0.001054
C	−1.479636	−0.665565	−0.000865
C	−1.479635	0.665565	−0.000861
C	2.136953	−0.000001	−0.001060
H	−2.366861	−1.287925	−0.001858
H	−2.366860	1.287925	−0.001852
H	0.100003	−1.871039	0.879417
H	0.101899	−1.873392	−0.875153
H	0.101900	1.873393	−0.875155
H	0.100003	1.871039	0.879416
H	2.707232	−0.923166	−0.001677
H	2.707235	0.923163	−0.001679

Table B.14: **11a** at B3LYP/6-311G(d,p) level.

Atom	x (Å)	y (Å)	z (Å)
C	0.836250	0.009734	0.000412
C	−0.100154	−1.195968	0.002034
C	−1.536552	−0.602180	−0.001924
C	−0.008200	1.203611	0.001130
C	−1.309799	0.888948	0.000044
C	2.172865	−0.017515	−0.001409
H	0.074253	−1.819522	0.882470
H	0.077618	−1.825778	−0.873186
H	−2.118382	−0.918809	0.871345
H	−2.112410	−0.916662	−0.879981
H	0.395359	2.209116	0.001979
H	−2.123875	1.604333	−0.000109
H	2.726280	−0.949948	−0.002202
H	2.754705	0.897487	−0.002039

Table B.15: **12a** at B3LYP/6-311G(d,p) level.

Atom	x (Å)	y (Å)	z (Å)
C	−0.627014	0.744691	−0.278713
C	−0.648804	−0.729665	−0.367707
C	0.691244	−1.131504	0.267141
C	0.574176	1.245352	0.005333
C	1.600232	0.105904	−0.055164
C	−1.814649	0.074261	0.267120
H	−0.914778	−1.187677	−1.318267
H	1.081704	−2.072162	−0.130296
H	0.598988	−1.243461	1.353197
H	0.799181	2.234591	0.389116
H	2.406261	0.245843	0.671901
H	2.074142	0.009678	−1.041216
H	−2.743195	0.040206	−0.296681
H	−1.953411	0.118739	1.344193

Table B.16: **13a** at B3LYP/6-311G(d,p) level.

Atom	x (Å)	y (Å)	z (Å)
C	2.163647	−0.931659	0.114959
C	1.537703	0.156542	−0.325524
C	0.519339	0.942890	0.449454
C	−0.881868	0.921705	−0.201661
C	−1.495268	−0.458274	−0.210709
C	−2.614624	−0.944229	0.220181
H	1.753632	0.520171	−1.329731
H	0.449963	0.565841	1.473569
H	0.838276	1.990723	0.510232
H	−1.547403	1.604764	0.329758
H	−0.812526	1.281200	−1.234323
H	−0.923578	−1.296871	−0.642033
H	2.887384	−1.458719	−0.496491
H	1.980681	−1.328960	1.108818

Table B.17: **14a** at B3LYP/6-311G(d,p) level.

Atom	x (Å)	y (Å)	z (Å)
C	1.813192	−0.050636	−0.195238
C	0.594764	−0.418915	−0.480025
C	−0.552713	−0.460888	0.513568
C	−1.662423	0.487615	0.136728
C	−2.905571	0.124818	−0.163786
C	3.030079	0.313800	0.098232
H	0.358986	−0.706151	−1.503332
H	−0.949712	−1.481023	0.566458
H	−0.168322	−0.208785	1.506974
H	−1.388608	1.540411	0.105007
H	−3.662157	0.853744	−0.431626
H	−3.213833	−0.916576	−0.148464
H	3.346106	1.349999	0.020939
H	3.773568	−0.406381	0.427168

Table B.18: **15a** at B3LYP/6-311G(d,p) level.

Atom	x (Å)	y (Å)	z (Å)
C	−0.158123	−0.770183	−0.471710
C	0.845597	−1.140737	0.614144
C	1.183413	−0.047192	−0.355775
C	−1.389641	−0.114318	−0.131322
C	−2.426944	0.431040	0.142290
H	−0.242140	−1.470886	−1.296189
H	1.341474	−2.099960	0.526242
H	0.588838	−0.852110	1.626515
H	−3.343828	0.909068	0.384461
C	1.263842	1.395445	0.085694
H	0.512532	1.620358	0.845435
H	2.249877	1.613936	0.506693
H	1.097378	2.074002	−0.755919
H	1.886995	−0.318732	−1.137165

Table B.19: **15a-trans** at B3LYP/6-311G(d,p) level.

Atom	x (Å)	y (Å)	z (Å)
C	0.510361	1.284704	−0.102407
C	0.903102	−0.119658	−0.453983
C	−0.234867	0.115093	0.531267
C	2.207883	−0.708971	0.031129
C	−1.593311	−0.166237	0.160504
C	−2.731512	−0.402925	−0.150036
H	−0.028515	1.872821	−0.834286
H	1.167099	1.853150	0.546606
H	0.579811	−0.461284	−1.431896
H	0.001011	−0.082904	1.572673
H	2.460305	−0.339608	1.029421
H	2.155808	−1.800526	0.081026
H	3.030599	−0.441222	−0.639063
H	−3.736054	−0.612462	−0.423324

Table B.20: **17a** at (4*e*,4*o*)CASSCF/6-311G(d,p) level.

Atom	x (Å)	y (Å)	z (Å)
C	−0.802954	−0.059250	0.010748
C	0.054571	−1.148721	0.011316
C	−0.000356	1.233372	0.009171
C	1.509625	−0.746575	0.009962
C	1.423489	0.757943	0.103568
C	−2.195280	−0.104108	0.004126
H	2.268748	1.404562	−0.040583
H	−0.276023	1.878301	0.842187
H	−0.184460	1.805916	−0.900457
H	−2.719636	−1.042282	−0.002422
H	−2.783705	0.794965	0.005721
H	2.057899	−1.180884	0.845392
H	2.018822	−1.078038	−0.896386
H	−0.273767	−2.172067	−0.002291

Table B.21: **17a** at B3LYP/6-311G(d,p) level.

Atom	x (Å)	y (Å)	z (Å)
C	−0.809811	−0.062221	−0.000026
C	0.054116	−1.149352	−0.000044
C	0.003329	1.230651	0.000135
C	1.502503	−0.741263	0.000111
C	1.421605	0.757726	−0.000132
C	−2.191136	−0.104168	−0.000055
H	2.282218	1.413484	−0.000954
H	−0.238172	1.853446	0.875899
H	−0.238376	1.853914	−0.875209
H	−2.722778	−1.048400	−0.000237
H	−2.785122	0.801631	0.000081
H	2.045854	−1.139880	0.874098
H	2.046300	−1.140192	−0.873427
H	−0.273557	−2.182243	−0.000189

Table B.22: **20a** at B3LYP/6-311G(d,p) level.

Atom	x (Å)	y (Å)	z (Å)
C	1.460749	−0.020869	0.632479
C	0.647056	−0.772701	−0.387748
C	−0.791068	−1.156290	−0.033814
C	0.712131	0.749358	−0.440061
C	−1.467905	0.179527	0.204586
C	−0.654983	1.206948	−0.053309
H	2.539478	−0.085019	0.541560
H	1.093029	0.050937	1.650635
H	1.180812	−1.369727	−1.116720
H	−0.844992	−1.809665	0.845351
H	−1.271844	−1.701248	−0.855892
H	1.277596	1.281440	−1.196438
H	−2.487504	0.263959	0.562319
H	−0.922458	2.253488	0.036386

Table B.23: **21a**$_1$ at B3LYP/6-311G(d,p) level.

Atom	x (Å)	y (Å)	z (Å)
C	−1.595898	0.030874	0.315472
C	−1.691013	−1.056643	−0.451031
C	−0.654813	1.149121	0.152184
C	0.654570	1.149168	−0.152208
C	1.595606	0.030906	−0.315808
C	1.691502	−1.056073	0.451347
H	−2.331098	0.167876	1.107576
H	−2.454158	−1.804351	−0.267712
H	−1.014647	−1.234069	−1.278948
H	−1.108973	2.127857	0.299633
H	1.108746	2.127937	−0.299417
H	2.330010	0.167448	−1.108733
H	2.454466	−1.803913	0.267815
H	1.015929	−1.232902	1.280044

Table B.24: **21a**$_2$ at B3LYP/6-311G(d,p) level.

Atom	x (Å)	y (Å)	z (Å)
C	0.560084	0.899632	0.101956
C	−0.772552	1.105405	0.048630
C	−1.835890	0.134516	−0.214811
C	−1.903018	−1.127748	0.221855
C	1.273740	−0.334322	−0.177343
C	2.593449	−0.482886	−0.004907
H	1.186402	1.756931	0.339110
H	−1.116929	2.127552	0.190323
H	−2.676605	0.520374	−0.789812
H	−2.748177	−1.759784	−0.025448
H	−1.139567	−1.557121	0.860122
H	0.694132	−1.164818	−0.568309
H	3.097258	−1.410676	−0.248009
H	3.208610	0.319958	0.389743

Table B.25: **22a** at B3LYP/6-311G(d,p) level.

Atom	x (Å)	y (Å)	z (Å)
C	−1.256543	−0.725184	−0.107049
C	−0.113504	−1.422725	−0.064079
C	1.192593	−0.729244	0.243764
C	−1.256467	0.725313	0.107050
C	1.192671	0.729121	−0.243761
C	−0.113357	1.422738	0.064070
H	−2.203838	−1.225303	−0.280361
H	−0.116225	−2.501085	−0.186556
H	2.034279	−1.271871	−0.195633
H	1.349300	−0.753858	1.333626
H	−2.203708	1.225529	0.280375
H	1.349389	0.753720	−1.333622
H	2.034411	1.271659	0.195644
H	−0.115966	2.501097	0.186552

Table B.26: **23a** at B3LYP/6-311G(d,p) level.

Atom	x (Å)	y (Å)	z (Å)
C	1.497255	0.000015	0.000615
C	0.665444	1.254343	−0.000410
C	−0.665471	1.254332	−0.000417
C	−1.497255	−0.000015	0.000622
C	0.665471	−1.254332	−0.000407
C	−0.665444	−1.254344	−0.000419
H	2.170886	0.000024	0.870685
H	2.172654	0.000019	−0.868050
H	1.202389	2.199106	−0.000692
H	−1.202434	2.199085	−0.000709
H	−2.172665	−0.000019	−0.868031
H	−2.170877	−0.000025	0.870703
H	1.202435	−2.199084	−0.000690
H	−1.202391	−2.199106	−0.000716

Table B.27: **24a** at B3LYP/6-311G(d,p) level.

Atom	x (Å)	y (Å)	z (Å)
C	−1.207278	−0.696977	0.000000
C	−1.207192	0.696988	0.000000
C	0.000000	1.393893	0.000000
C	1.207308	0.696926	0.000000
C	1.207221	−0.696937	0.000000
C	−0.000059	−1.393893	0.000000
H	−2.146411	−1.239141	0.000000
H	−2.146374	1.239096	0.000000
H	−0.000032	2.478300	0.000000
H	2.146370	1.239213	0.000000
H	2.146334	−1.239165	0.000000
H	0.000113	−2.478300	0.000000
H	1.202435	−2.199084	−0.000690
H	−1.202391	−2.199106	−0.000716

Table B.28: **25a** at B3LYP/6-311G(d,p) level.

Atom	x (Å)	y (Å)	z (Å)
C	−0.094854	−1.126326	0.000056
C	0.707268	−0.042507	−0.000028
C	−0.143912	1.163108	0.000045
C	−1.440129	0.807056	−0.000020
H	0.226353	−2.159874	−0.000155
H	0.240670	2.176323	−0.000149
H	−2.295683	1.468898	−0.000026
C	2.205130	−0.004346	0.000003
H	2.587304	0.525279	−0.879620
H	2.587187	0.524831	0.879951
H	2.629283	−1.010381	−0.000243
C	−1.535676	−0.694759	0.000033
H	−2.080793	−1.069203	−0.877381
H	−2.081285	−1.069223	0.877085

Table B.29: **26a** at B3LYP/6-311G(d,p) level.

Atom	x (Å)	y (Å)	z (Å)
C	0.690628	0.063650	−0.000174
C	−0.104007	1.153673	−0.000135
C	−1.513533	0.744285	0.000049
C	−1.588969	−0.598739	−0.000076
H	0.236544	2.182272	0.000139
H	−2.350565	1.431230	0.000302
H	−2.487271	−1.200733	0.000359
C	2.185235	0.005047	0.000065
H	2.619461	1.007226	0.000020
H	2.567305	−0.526318	0.879623
H	2.567898	−0.526705	−0.878974
C	−0.193075	−1.163376	−0.000087
H	−0.005399	−1.797561	−0.877117
H	−0.005643	−1.796645	0.877802

Table B.30: **27a** at B3LYP/6-311G(d,p) level.

Atom	x (Å)	y (Å)	z (Å)
C	0.849229	−0.056070	−0.005387
C	0.078307	1.267024	0.093874
C	−1.179511	0.513314	−0.376004
C	−0.369823	−0.802297	−0.439937
C	−1.489053	−0.603484	0.565857
C	2.133641	−0.373449	0.093250
H	0.440426	1.995747	−0.635315
H	0.014935	1.746945	1.075700
H	−1.898611	0.884150	−1.094632
H	−0.407233	−1.601492	−1.170133
H	−1.258317	−0.513255	1.623771
H	−2.390380	−1.167051	0.350245
H	2.876876	0.361422	0.383175
H	2.485558	−1.376698	−0.122728

Table B.31: **28a** at B3LYP/6-311G(d,p) level.

Atom	x (Å)	y (Å)	z (Å)
C	−0.809529	−0.000073	−1.065917
C	−0.279879	1.022844	−0.000068
C	1.215352	0.667915	−0.000021
C	−0.279881	−1.022842	0.000067
C	1.215352	−0.667916	0.000020
C	−0.809528	0.000073	1.065919
H	−0.328223	−0.000140	−2.045650
H	−1.899132	−0.000082	−1.162128
H	−0.570693	2.072411	−0.000139
H	2.042387	1.363610	−0.000046
H	−0.570694	−2.072410	0.000137
H	2.042385	−1.363612	0.000049
H	−1.899131	0.000085	1.162131
H	−0.328218	0.000139	2.045650

Table B.32: **29a** at B3LYP/6-311G(d,p) level.

Atom	x (Å)	y (Å)	z (Å)
C	1.165189	0.007478	0.004174
C	0.482627	1.303976	−0.065542
C	−0.107027	0.134992	0.742670
C	2.174494	−0.756871	−0.361189
C	−1.330821	−0.598915	0.310123
C	−2.270147	−0.138484	−0.510208
H	−0.003327	1.577024	−0.997152
H	0.885750	2.144954	0.490777
H	−0.002769	0.224127	1.823996
H	2.966042	−0.379261	−1.000726
H	2.247837	−1.790279	−0.037995
H	−1.432681	−1.601599	0.721886
H	−3.125241	−0.745816	−0.783986
H	−2.221501	0.857794	−0.936975

Table B.33: **30a** at B3LYP/6-311G(d,p) level.

Atom	x (Å)	y (Å)	z (Å)
C	2.175639	−0.285522	0.000000
C	1.358619	1.019508	0.000001
C	0.711157	−0.294116	−0.000003
C	−0.409405	−1.006841	0.000000
C	−1.779075	−0.481415	0.000000
C	−2.154156	0.802302	0.000000
H	2.703242	−0.551253	0.911892
H	2.703246	−0.551246	−0.911891
H	1.344981	1.610597	−0.911996
H	1.344977	1.610594	0.912001
H	−0.317504	−2.090582	0.000001
H	−2.558009	−1.240543	0.000003
H	−3.202573	1.075761	0.000001
H	−1.435035	1.613179	−0.000003

Table B.34: **31a** at (4*e*,4*o*)CASSCF/6-311G(d,p) level.

Atom	x (Å)	y (Å)	z (Å)
C	−0.508274	1.411525	1.200938
C	−0.508274	1.411525	−1.200938
C	−0.050865	0.920901	0.000000
C	1.010332	−0.135890	0.000000
C	0.754315	−1.500911	0.000000
C	−0.508274	−2.085872	0.000000
H	−1.214755	2.221653	1.232350
H	−1.214755	2.221653	−1.232350
H	−0.162098	1.014433	2.136746
H	−0.162098	1.014433	−2.136746
H	2.030641	0.204830	0.000000
H	1.609058	−2.157980	0.000000
H	−1.402858	−1.492343	0.000000
H	−0.616891	−3.154355	0.000000

Table B.35: **31a** at B3LYP/6-311G(d,p) level.

Atom	x (Å)	y (Å)	z (Å)
C	−0.508274	1.411525	1.200938
C	−0.508274	1.411525	−1.200938
C	−0.050865	0.920901	0.000000
C	1.010332	−0.135890	0.000000
C	0.754315	−1.500911	0.000000
C	−0.508274	−2.085872	0.000000
H	−1.214755	2.221653	1.232350
H	−1.214755	2.221653	−1.232350
H	−0.162098	1.014433	2.136746
H	−0.162098	1.014433	−2.136746
H	2.030641	0.204830	0.000000
H	1.609058	−2.157980	0.000000
H	−1.402858	−1.492343	0.000000
H	−0.616891	−3.154355	0.000000

Table B.36: **32a** at B3LYP/6-311G(d,p) level.

Atom	x (Å)	y (Å)	z (Å)
C	0.019738	0.232589	0.000000
C	−1.061822	−0.884143	0.000000
C	0.126814	−1.838832	0.000000
C	1.042895	−0.860935	0.000000
C	0.019738	1.533273	0.756391
C	0.019738	1.533273	−0.756391
H	−1.694617	−0.913196	−0.892507
H	−1.694617	−0.913196	0.892507
H	0.185370	−2.920031	0.000000
H	2.127188	−0.845533	0.000000
H	0.929880	1.825078	1.268560
H	−0.892846	1.825224	1.264227
H	−0.892846	1.825224	−1.264227
H	0.929880	1.825078	−1.268560

Table B.37: **33a** at B3LYP/6-311G(d,p) level.

Atom	x (Å)	y (Å)	z (Å)
C	−0.583500	−1.140999	0.000000
C	0.000000	0.267423	0.000000
C	−1.987505	−0.435831	0.000000
C	−1.209063	0.863521	0.000000
C	1.361323	0.756877	0.000000
C	2.446521	−0.025650	0.000000
H	−0.370485	−1.740171	0.889808
H	−0.370485	−1.740171	−0.889808
H	−2.598106	−0.627349	0.888081
H	−2.598106	−0.627349	−0.888081
H	−1.521785	1.902249	0.000000
H	1.480996	1.838565	0.000000
H	3.447031	0.389787	0.000000
H	2.364283	−1.107616	0.000000

Table B.38: **34a** at B3LYP/6-311G(d,p) level.

Atom	x (Å)	y (Å)	z (Å)
C	1.514065	0.656697	−0.045758
C	0.049673	0.703449	−0.411930
C	1.149032	−0.817122	0.419960
C	−0.163683	−0.784950	−0.458803
C	−1.145874	0.991920	0.137495
C	−1.585057	−0.482764	0.128360
H	1.883370	1.358515	0.703716
H	2.189347	0.642894	−0.905506
H	0.934929	−0.851541	1.489593
H	1.874686	−1.590567	0.159405
H	−0.094965	−1.354664	−1.386957
H	−1.526212	1.851221	0.679042
H	−1.733663	−0.880085	1.138094
H	−2.436427	−0.779161	−0.493331

Table B.39: **1c-T** at (4*e*,4*o*)CASSCF/6-311G(d,p) level.

Atom	x (Å)	y (Å)	z (Å)
C	−0.009123	0.019128	0.024393
C	0.949596	1.064948	0.031059
C	0.688386	−1.216090	0.030459
C	2.355630	0.526455	0.082960
C	2.180401	−1.011331	0.010827
C	−1.420607	0.164909	0.016079
H	2.855558	0.826915	1.001409
H	2.962355	0.904561	−0.736076
H	2.667318	−1.514859	0.842162
H	2.618942	−1.419752	−0.897228
H	0.731004	2.113548	0.054630
H	0.233679	−2.185983	−0.005446
C	−2.101971	1.502174	−0.092518
C	−2.330462	−1.036983	0.002271
H	−1.408392	2.329066	−0.159822
H	−2.746460	1.676291	0.767869
H	−2.739886	1.533606	−0.975101
H	−1.937202	−1.859021	0.589005
H	−2.490203	−1.402272	−1.012320
H	−3.305169	−0.781357	0.407455

Table B.40: **1c-o**$_1$ at (4*e*,4*o*)CASSCF/6-311G(d,p) level.

Atom	x (Å)	y (Å)	z (Å)
C	−0.009123	0.019128	0.024393
C	0.949596	1.064948	0.031059
C	0.688386	−1.216090	0.030459
C	2.355630	0.526455	0.082960
C	2.180401	−1.011331	0.010827
C	−1.420607	0.164909	0.016079
H	2.855558	0.826915	1.001409
H	2.962355	0.904561	−0.736076
H	2.667318	−1.514859	0.842162
H	2.618942	−1.419752	−0.897228
H	0.731004	2.113548	0.054630
H	0.233679	−2.185983	−0.005446
C	−2.101971	1.502174	−0.092518
C	−2.330462	−1.036983	0.002271
H	−1.408392	2.329066	−0.159822
H	−2.746460	1.676291	0.767869
H	−2.739886	1.533606	−0.975101
H	−1.937202	−1.859021	0.589005
H	−2.490203	−1.402272	−1.012320
H	−3.305169	−0.781357	0.407455

Table B.41: **1c-o**$_2$ at (4*e*,4*o*)CASSCF/6-311G(d,p) level.

Atom	x (Å)	y (Å)	z (Å)
C	−0.060481	0.048433	0.758098
C	0.040038	−1.227463	−0.063560
C	−0.151819	1.093822	−0.158332
C	−0.488276	−0.905062	−1.438411
C	−0.213819	0.611288	−1.584892
C	−0.037956	0.107377	2.149701
H	−1.561586	−1.081595	−1.473085
H	−0.032130	−1.497301	−2.223223
H	−0.974064	1.126513	−2.165415
H	0.736629	0.778669	−2.090257
H	0.935100	−1.824035	0.028646
H	−0.139099	2.137962	0.089681
C	−0.064203	1.404362	2.914272
H	−0.109645	2.274163	2.272617
H	−0.923886	1.438702	3.581456
H	0.823389	1.499378	3.538424
C	0.057355	−1.138673	2.990593
H	−0.154125	−2.034314	2.419634
H	1.051852	−1.245608	3.424294
H	−0.644837	−1.095367	3.820510

Table B.42: **2c** at B3LYP/6-311G(d,p) level.

Atom	x (Å)	y (Å)	z (Å)
C	−0.324074	−0.000011	−0.081622
C	0.709856	−1.101901	−0.133676
C	1.571658	−0.778930	1.128290
C	0.709866	1.101864	−0.133933
C	1.571452	0.779268	1.128251
C	−1.653234	−0.000001	−0.007797
C	−2.465193	−1.270852	0.039011
C	−2.465196	1.270859	0.038703
N	1.575911	−0.623132	−1.269164
N	1.576193	0.622761	−1.269089
H	0.418292	−2.138967	−0.264559
H	2.571457	−1.207218	1.041113
H	1.096423	−1.188272	2.021266
H	0.418311	2.138890	−0.265154
H	1.095918	1.188563	2.021088
H	2.571156	1.207814	1.041236
H	−3.183275	−1.295967	−0.788338
H	−1.849071	−2.167785	−0.020357
H	−3.051196	−1.320798	0.963998
H	−3.182945	1.295993	−0.788936
H	−3.051571	1.320793	0.963453
H	−1.849041	2.167785	−0.020403

Table B.43: **3c** at B3LYP/6-311G(d,p) level.

Atom	x (Å)	y (Å)	z (Å)
C	1.046376	−0.791364	0.627804
C	2.130378	−0.781201	−0.466825
C	1.046352	0.791152	0.627964
C	2.130033	0.781404	−0.466939
C	−0.114403	−0.000050	0.228915
C	−1.418578	−0.000013	−0.016655
C	−2.198903	−1.281965	−0.160255
C	−2.198868	1.281978	−0.160110
H	1.032245	−1.468173	1.475862
H	1.860210	−1.277057	−1.402746
H	3.081699	−1.186286	−0.117618
H	1.032308	1.467784	1.476165
H	3.081216	1.186892	−0.117844
H	1.859540	1.277104	−1.402863
H	−2.707098	−1.323969	−1.131037
H	−1.552768	−2.156796	−0.071939
H	−2.980968	−1.354996	0.605495
H	−2.707258	1.324045	−1.130788
H	−2.980774	1.355015	0.605801
H	−1.552677	2.156778	−0.071883

Table B.44: **4c** at B3LYP/6-311G(d,p) level.

Atom	x (Å)	y (Å)	z (Å)
C	1.255709	−0.000016	0.000093
C	−0.104054	−0.000012	−0.000006
C	−0.854909	−1.263120	0.178859
C	−2.066286	−1.556924	−0.302584
C	−0.854827	1.263127	−0.178951
C	−2.066297	1.556943	0.302251
H	−0.352915	−2.032312	0.757356
H	−2.513598	−2.526422	−0.114954
H	−0.352665	2.032348	−0.757266
H	−2.513530	2.526471	0.114596
H	−2.639830	0.859549	0.900368
H	−2.639661	−0.859553	−0.900876
C	2.093525	1.252780	−0.079535
H	2.891665	1.210771	0.670500
H	2.592417	1.330052	−1.054076
H	1.532712	2.169143	0.092635
C	2.093553	−1.252791	0.079835
H	2.592268	−1.330080	1.054466
H	1.532817	−2.169170	−0.092482
H	2.891836	−1.210719	−0.670045

Table B.45: **5c** at B3LYP/6-311G(d,p) level.

Atom	x (Å)	y (Å)	z (Å)
C	−1.416824	−0.194632	−0.023405
C	0.075709	−0.110380	−0.086318
C	0.622457	1.166039	−0.601167
C	1.625759	1.872135	−0.076791
C	0.827025	−1.163373	0.287651
C	2.316831	−1.318126	0.208572
C	−2.081873	−1.223246	−0.558292
C	−2.131616	0.941099	0.670721
H	0.115988	1.563542	−1.480229
H	1.955890	2.800266	−0.530081
H	2.136366	1.559066	0.826923
H	0.291199	−2.025843	0.676652
H	2.569435	−2.297545	−0.211788
H	2.785850	−0.545520	−0.401322
H	2.774888	−1.283452	1.204586
H	−3.162498	−1.293816	−0.490013
H	−1.567080	−2.017407	−1.086153
H	−3.212434	0.788838	0.669981
H	−1.793118	1.034756	1.708189
H	−1.919305	1.900021	0.187426

Table B.46: **6c** at B3LYP/6-311G(d,p) level.

Atom	x (Å)	y (Å)	z (Å)
C	0.973907	−0.620898	0.178731
C	−0.346469	0.043475	−0.075824
C	−1.510789	−0.866536	−0.139026
C	−2.745789	−0.591979	0.286480
C	−0.474074	1.367267	−0.270879
C	0.607084	2.404443	−0.229693
C	1.590413	−0.512994	1.356647
C	1.553536	−1.419622	−0.964697
H	−1.314366	−1.860921	−0.534705
H	−3.545037	−1.318274	0.194499
H	−2.995569	0.357165	0.748482
H	−1.468509	1.738278	−0.509724
H	0.624895	2.981494	−1.161248
H	0.421677	3.125248	0.575869
H	1.593572	1.969726	−0.067363
H	2.543138	−0.998380	1.543498
H	1.158214	0.057133	2.171001
H	2.486077	−1.908446	−0.675990
H	0.858127	−2.191602	−1.310238
H	1.750865	−0.770359	−1.824512

Table B.47: **7c** at B3LYP/6-311G(d,p) level.

Atom	x (Å)	y (Å)	z (Å)
C	0.048115	0.003286	−0.017238
C	−0.662678	−1.137114	−0.036689
C	−2.148285	−0.901504	−0.116576
C	−0.881208	1.206512	−0.079665
C	−2.279362	0.607880	0.204207
C	1.510996	0.113358	0.005478
C	2.314692	−1.164192	0.078527
C	2.125068	1.305524	−0.043941
H	−0.235054	−2.132662	−0.039168
H	−2.718822	−1.530471	0.574686
H	−2.520030	−1.137859	−1.123498
H	−0.829458	1.669111	−1.073590
H	−0.612071	1.983425	0.641373
H	−3.072424	1.095863	−0.365956
H	−2.517629	0.731389	1.264137
H	3.384438	−0.951468	0.105334
H	2.058694	−1.741926	0.972286
H	2.116913	−1.805193	−0.786510
H	3.206555	1.380798	−0.032006
H	1.574862	2.236496	−0.101706

Table B.48: **8c**$_1$ at B3LYP/6-311G(d,p) level.

Atom	x (Å)	y (Å)	z (Å)
C	−1.196671	−1.204230	0.001774
C	0.195505	−1.199170	−0.007501
C	0.912303	0.002838	−0.009849
C	−1.901705	−0.001952	0.007192
C	−1.201515	1.201638	0.001796
C	0.192072	1.201087	−0.007511
H	−1.731828	−2.147617	0.001257
H	0.735146	−2.141255	−0.015030
H	−2.985862	−0.004039	0.011730
H	−1.739456	2.143415	0.001373
H	0.728686	2.144673	−0.015067
C	2.422483	0.001228	0.007932
H	2.826074	0.958395	−0.329135
H	2.804228	−0.179514	1.018744
H	2.828175	−0.782690	−0.636875

Table B.49: **8c**$_2$ at B3LYP/6-311G(d,p) level.

Atom	x (Å)	y (Å)	z (Å)
C	0.477207	−0.704801	−0.000025
C	0.477194	0.704836	−0.000033
C	−0.744983	1.381497	0.000009
C	−1.957094	0.695168	0.000063
C	−1.957084	−0.695190	0.000006
C	−0.744959	−1.381496	−0.000066
H	−0.744903	2.467023	−0.000035
H	−2.891921	1.244614	0.000076
H	−2.891906	−1.244646	−0.000057
H	−0.744858	−2.467020	−0.000124
C	1.772510	−1.480222	0.000057
H	2.383696	−1.246872	−0.878297
H	2.382370	−1.248664	0.879814
H	1.584803	−2.555345	−0.001214
C	1.772509	1.480228	−0.000039
H	2.382877	1.247895	0.879175
H	2.383190	1.247556	−0.878923
H	1.584848	2.555352	−0.000240

Table B.50: **9c** at B3LYP/6-311G(d,p) level.

Atom	x (Å)	y (Å)	z (Å)
C	1.902489	0.022673	−0.042692
C	0.778388	−0.634160	−0.353495
C	−0.593471	−0.072635	−0.602337
C	−1.614351	−0.538915	0.467704
C	−2.969240	−0.058003	0.213045
C	−4.074777	0.353049	−0.017938
H	0.843012	−1.719173	−0.433600
H	−0.588581	1.018013	−0.630818
H	−0.954235	−0.406591	−1.581954
H	−1.621647	−1.634117	0.511395
H	−1.283733	−0.195270	1.453817
H	−5.055011	0.711117	−0.215489
C	3.197507	−0.722169	0.172717
H	3.072271	−1.799782	0.051576
H	3.965106	−0.386055	−0.534494
H	3.595252	−0.534475	1.177023
C	2.012752	1.518301	0.115698
H	1.066020	2.039767	−0.020615
H	2.395493	1.769513	1.111643
H	2.730275	1.928220	−0.604691

Table B.51: **10c** at B3LYP/6-311G(d,p) level.

Atom	x (Å)	y (Å)	z (Å)
C	1.562471	−0.000003	0.000444
C	0.668706	1.231483	0.001737
C	0.668713	−1.231477	0.001735
C	−0.738206	0.670326	0.000086
C	−0.738202	−0.670312	0.000124
C	2.891553	−0.000006	−0.002121
H	0.851428	1.868750	−0.874255
H	0.849972	1.865620	0.880381
H	0.850049	−1.865816	0.880196
H	0.851301	−1.868551	−0.874445
H	3.461384	0.923567	−0.003225
H	3.461365	−0.923591	−0.003184
C	−1.910821	−1.602412	−0.000877
H	−2.866812	−1.076851	−0.001792
H	−1.887323	−2.258471	−0.879319
H	−1.888816	−2.258362	0.877680
C	−1.910823	1.602393	−0.000888
H	−2.866796	1.076823	−0.001501
H	−1.888680	2.258615	0.877480
H	−1.887426	2.258309	−0.879457

Table B.52: **11c** at B3LYP/6-311G(d,p) level.

Atom	x (Å)	y (Å)	z (Å)
C	−1.547147	0.080085	−0.033533
C	−0.747511	−1.196108	0.193016
C	0.720374	−0.736369	0.416563
C	−0.574194	1.160228	−0.161401
C	0.682515	0.745369	0.069594
C	−2.878928	0.187819	−0.098956
H	−0.808121	−1.830536	−0.697939
H	−1.135730	−1.782113	1.029265
H	0.979054	−0.827207	1.481822
H	−0.856206	2.181881	−0.392044
H	−3.527678	−0.672497	0.022094
H	−3.358971	1.143909	−0.276543
C	1.918345	1.588095	0.062196
H	2.626106	1.256365	−0.705675
H	1.686179	2.638323	−0.124897
H	2.444648	1.519381	1.021929
C	1.747759	−1.551397	−0.381074
H	2.770415	−1.214784	−0.189949
H	1.694158	−2.609792	−0.110379
H	1.558867	−1.469266	−1.456115

Table B.53: **12c** at B3LYP/6-311G(d,p) level.

Atom	x (Å)	y (Å)	z (Å)
C	0.103933	−0.096060	−0.842330
C	0.124517	−0.798654	0.460555
C	1.434300	−0.313246	1.100103
C	1.271407	0.462397	−1.162183
C	2.327693	0.006399	−0.148411
C	−1.119155	0.023269	−0.022542
C	−2.340059	−0.820618	−0.349361
C	−1.451090	1.383629	0.560972
H	−0.070378	−1.869508	0.479501
H	1.873685	−1.061537	1.765169
H	1.286013	0.599738	1.687560
H	1.447676	1.238305	−1.899485
H	3.068243	0.788959	0.045495
H	2.884001	−0.880373	−0.481345
H	−2.057723	−1.790386	−0.763784
H	−2.941981	−0.988983	0.548951
H	−2.966894	−0.310576	−1.087503
H	−1.990507	1.996006	−0.168411
H	−2.091298	1.268942	1.442032
H	−0.550114	1.926704	0.851011

Table B.54: **13c** at B3LYP/6-311G(d,p) level.

Atom	x (Å)	y (Å)	z (Å)
C	1.849986	0.024440	0.018740
C	0.766089	−0.710577	0.297147
C	−0.601564	−0.236110	0.703864
C	−1.657187	−0.521663	−0.387379
C	−3.053631	−0.119245	0.038639
C	−3.877306	0.750266	−0.456574
C	3.147692	−0.635350	−0.378556
C	1.908575	1.530044	0.072865
H	0.863283	−1.792609	0.213664
H	−0.904836	−0.752517	1.623643
H	−0.611127	0.830877	0.932639
H	−1.392181	0.009456	−1.303794
H	−1.661452	−1.589606	−0.629268
H	−3.511381	−0.590920	0.920121
H	3.949069	−0.375427	0.323081
H	3.059797	−1.723008	−0.406950
H	3.475571	−0.292386	−1.366900
H	2.668751	1.858199	0.791209
H	2.206628	1.935258	−0.900898
H	0.961954	1.991844	0.350983

Table B.55: **14c** at B3LYP/6-311G(d,p) level.

Atom	x (Å)	y (Å)	z (Å)
C	−1.975901	−0.366769	−0.367850
C	−0.729411	−0.312568	−0.747391
C	0.439331	0.289783	0.040541
C	1.363767	−0.865277	0.394166
C	2.615863	−1.056497	−0.011354
C	−3.224995	−0.422524	0.003152
H	−0.462760	−0.743165	−1.711689
H	0.907882	−1.603942	1.051578
H	3.178035	−1.926161	0.310301
H	3.130766	−0.365810	−0.669270
H	−3.612896	−1.267516	0.564666
H	−3.924628	0.372590	−0.237678
C	−0.045827	0.946185	1.347010
H	−0.758996	1.747026	1.135469
H	−0.540844	0.220208	1.996310
H	0.801508	1.369944	1.891626
C	1.124464	1.345704	−0.845920
H	1.995123	1.773133	−0.341043
H	1.456587	0.919270	−1.796181
H	0.426477	2.156200	−1.068221

Table B.56: **15c** at B3LYP/6-311G(d,p) level.

Atom	x (Å)	y (Å)	z (Å)
C	−0.319586	−0.322643	−0.865948
C	0.901751	−0.247820	0.062309
C	0.346414	1.020074	−0.537433
C	−1.626259	−0.644677	−0.369185
C	−2.725911	−0.919824	0.036720
H	−0.122113	−0.712057	−1.860340
H	−3.696162	−1.167146	0.390650
C	−0.368606	2.089878	0.256585
H	−1.046902	1.669911	0.999672
H	0.348884	2.734252	0.774155
H	−0.965704	2.721315	−0.407758
H	0.932284	1.414698	−1.363737
C	0.726177	−0.542410	1.539585
H	0.820248	−1.617083	1.724046
H	1.499724	−0.034096	2.124673
H	−0.247499	−0.232354	1.917552
C	2.205787	−0.773847	−0.511304
H	3.062875	−0.313812	−0.007650
H	2.283580	−1.858037	−0.379786
H	2.292186	−0.557984	−1.579451

Table B.57: **15c-trans** at B3LYP/6-311G(d,p) level.

Atom	x (Å)	y (Å)	z (Å)
C	−0.512840	0.624253	0.014904
C	−0.526433	−0.783504	0.559640
C	0.448550	−0.425811	−0.561840
C	−1.640171	−1.781718	0.330943
C	1.864702	−0.378450	−0.335130
C	3.054255	−0.341765	−0.153491
H	−0.047654	−0.879620	1.530098
H	0.170197	−0.799783	−1.543817
H	−2.055957	−1.715509	−0.676357
H	−1.272587	−2.803024	0.467649
H	−2.459562	−1.625735	1.039961
H	4.103784	−0.312026	0.005528
C	0.060487	1.714741	0.900326
H	0.448329	2.542542	0.298004
H	−0.715839	2.114632	1.561141
H	0.879106	1.345218	1.519808
C	−1.630442	1.106308	−0.892589
H	−2.480235	1.466643	−0.302849
H	−1.282560	1.937116	−1.514417
H	−1.995674	0.325217	−1.561327

Table B.58: **16c** at B3LYP/6-311G(d,p) level.

Atom	x (Å)	y (Å)	z (Å)
C	−2.115456	−0.031511	−0.280601
C	−0.910897	0.344424	−0.609169
C	0.248514	0.531119	0.364916
C	1.362903	−0.459893	0.036134
C	2.529416	−0.098541	−0.499638
C	−3.318000	−0.406030	0.057677
H	−0.690364	0.557218	−1.654755
H	−0.125653	0.274960	1.363038
H	3.290792	−0.836487	−0.729125
H	2.774298	0.931739	−0.725892
H	−3.603571	−1.453828	0.071127
H	−4.079768	0.316809	0.334842
C	1.052736	−1.901302	0.354223
H	0.873878	−2.031414	1.427942
H	0.143606	−2.230973	−0.157922
H	1.872129	−2.560674	0.062830
C	0.682048	2.004289	0.383371
H	1.519556	2.157903	1.068540
H	0.987364	2.346067	−0.609519
H	−0.149855	2.633350	0.707409

Table B.59: **17c** at (4*e*,4*o*)CASSCF/6-311G(d,p) level.

Atom	x (Å)	y (Å)	z (Å)
C	1.511133	−0.032133	−0.012612
C	0.747447	1.070509	−0.370548
C	0.591096	−1.227409	0.201175
C	−0.730578	0.782208	−0.421049
C	−0.785299	−0.672200	−0.010129
C	2.885500	−0.078194	0.126568
H	0.724069	−1.670126	1.200619
H	0.827918	−2.038065	−0.509266
H	3.494637	0.801480	−0.045222
H	3.395511	−0.990761	0.410428
H	−1.106471	0.907129	−1.455147
H	1.163214	2.047742	−0.590865
C	−2.004185	−1.520986	−0.094190
H	−2.081062	−2.031367	−1.069975
H	−2.003475	−2.310168	0.666114
H	−2.921613	−0.938404	0.029673
C	−1.572063	1.730326	0.465116
H	−1.474272	2.766215	0.126348
H	−2.632728	1.466826	0.424944
H	−1.244037	1.676777	1.506363

Table B.60: **17c** at B3LYP/6-311G(d,p) level.

Atom	x (Å)	y (Å)	z (Å)
C	1.511133	−0.032133	−0.012612
C	0.747447	1.070509	−0.370548
C	0.591096	−1.227409	0.201175
C	−0.730578	0.782208	−0.421049
C	−0.785299	−0.672200	−0.010129
C	2.885500	−0.078194	0.126568
H	0.724069	−1.670126	1.200619
H	0.827918	−2.038065	−0.509266
H	3.494637	0.801480	−0.045222
H	3.395511	−0.990761	0.410428
H	−1.106471	0.907129	−1.455147
H	1.163214	2.047742	−0.590865
C	−2.004185	−1.520986	−0.094190
H	−2.081062	−2.031367	−1.069975
H	−2.003475	−2.310168	0.666114
H	−2.921613	−0.938404	0.029673
C	−1.572063	1.730326	0.465116
H	−1.474272	2.766215	0.126348
H	−2.632728	1.466826	0.424944
H	−1.244037	1.676777	1.506363

Table B.61: **20c**$_1$ at B3LYP/6-311G(d,p) level.

Atom	x (Å)	y (Å)	z (Å)
C	1.945092	0.265234	0.792320
C	1.592375	−0.645655	−0.355348
C	0.357982	−1.531888	−0.222626
C	1.104342	0.790364	−0.356807
C	−0.793276	−0.553420	−0.041076
C	−0.379463	0.720156	−0.154513
H	2.975851	0.596855	0.855663
H	1.454147	0.119273	1.749026
H	2.392462	−0.956614	−1.015792
H	0.432942	−2.234388	0.617516
H	0.208561	−2.143523	−1.122681
H	1.524504	1.547394	−1.010958
C	−2.172668	−1.064784	0.242318
H	−2.203856	−1.616564	1.189595
H	−2.911980	−0.264240	0.300691
H	−2.497585	−1.765140	−0.536782
C	−1.188094	1.978322	−0.057809
H	−2.252860	1.783203	0.079431
H	−0.846794	2.598720	0.779217
H	−1.073135	2.585042	−0.963676

Table B.62: **20c**$_2$ at B3LYP/6-311G(d,p) level.

Atom	x (Å)	y (Å)	z (Å)
C	−2.067997	−0.237636	0.723881
C	−1.175658	0.769847	0.048176
C	0.317514	0.795643	0.391210
C	−1.470246	−0.557720	−0.634025
C	0.794679	−0.604446	0.004825
C	−0.179723	−1.301272	−0.593028
H	−3.126255	−0.003195	0.764595
H	−1.689162	−0.785247	1.580440
H	−1.632409	1.685403	−0.310087
H	0.463663	0.953428	1.468993
H	−2.128327	−0.637906	−1.491827
H	−0.073828	−2.315555	−0.963319
C	2.179839	−1.083741	0.317372
H	2.367294	−1.075067	1.397678
H	2.337838	−2.102836	−0.042244
H	2.942696	−0.443360	−0.138844
C	1.065150	1.909368	−0.360214
H	0.678924	2.893187	−0.076929
H	2.135137	1.897227	−0.136577
H	0.943081	1.793653	−1.441059

Table B.63: **21c**$_1$ at B3LYP/6-311G(d,p) level.

Atom	x (Å)	y (Å)	z (Å)
C	−0.815424	−0.698459	−0.021000
C	−1.398513	−1.243253	−1.091299
C	−0.469502	0.758861	0.021374
C	0.783560	1.245278	0.099694
C	2.068546	0.541200	0.070204
C	2.357809	−0.632078	−0.503752
H	−1.682649	−2.290270	−1.107213
H	−1.599119	−0.668210	−1.988816
H	0.875240	2.324714	0.206257
H	2.883170	1.081477	0.550011
H	3.363243	−1.035075	−0.460227
H	1.616462	−1.210856	−1.040653
C	−0.549922	−1.486090	1.240217
H	−1.110404	−1.061427	2.080230
H	−0.844484	−2.531175	1.123993
H	0.508266	−1.448144	1.510702
C	−1.656990	1.692151	0.026448
H	−2.339071	1.454453	0.850646
H	−1.349934	2.735984	0.119170
H	−2.238102	1.582870	−0.895415

Table B.64: **21c**$_2$ at B3LYP/6-311G(d,p) level.

Atom	x (Å)	y (Å)	z (Å)
C	−1.011640	0.714959	−0.028032
C	0.333324	0.680952	−0.137914
C	1.131687	−0.576057	−0.099761
C	0.899302	−1.580350	−0.951050
C	−1.912856	−0.399633	0.214565
C	−3.246074	−0.280751	0.253908
H	−1.491896	1.689986	−0.094492
H	1.492673	−2.488679	−0.925860
H	0.122873	−1.518259	−1.704140
H	−1.463329	−1.373045	0.382929
H	−3.885652	−1.131762	0.455224
H	−3.738149	0.671948	0.082970
C	2.248873	−0.648523	0.917734
H	2.724713	−1.630592	0.905656
H	3.021171	0.101849	0.720987
H	1.870352	−0.459336	1.927744
C	1.117835	1.963751	−0.294062
H	1.757547	2.153510	0.574788
H	1.776065	1.918347	−1.168644
H	0.450938	2.819938	−0.409487

Table B.65: **21c**$_3$ at B3LYP/6-311G(d,p) level.

Atom	x (Å)	y (Å)	z (Å)
C	2.303605	−0.489494	−0.113316
C	1.978044	−1.186997	0.976806
C	1.740540	0.796500	−0.551283
C	0.477835	1.252927	−0.504124
C	−0.765396	0.567923	−0.079992
C	−1.108267	−0.618759	−0.600969
H	3.125272	−0.856132	−0.727312
H	2.491691	−2.109155	1.223611
H	1.196581	−0.862055	1.653659
H	2.478362	1.473884	−0.978753
H	0.330108	2.286498	−0.819134
H	−0.416841	−1.058592	−1.315288
C	−1.605278	1.360202	0.895799
H	−1.803239	2.364194	0.503316
H	−2.564694	0.890656	1.111102
H	−1.073400	1.495675	1.844038
C	−2.326433	−1.444873	−0.314448
H	−3.020451	−0.970958	0.380346
H	−2.872961	−1.664876	−1.238465
H	−2.038331	−2.413711	0.112038

Table B.66: **21c**$_4$ at B3LYP/6-311G(d,p) level.

Atom	x (Å)	y (Å)	z (Å)
C	1.528825	−0.819281	−0.347535
C	0.245550	−1.210938	−0.478828
C	−0.981743	−0.490949	−0.088674
C	−1.158779	0.805706	−0.396943
C	2.021012	0.389780	0.292304
C	3.309206	0.755204	0.302345
H	2.296448	−1.490708	−0.726880
H	0.076237	−2.202571	−0.896974
H	−0.365578	1.291011	−0.959845
H	1.290450	1.009087	0.803617
H	3.641673	1.651414	0.812383
H	4.070143	0.168470	−0.203234
C	−2.008522	−1.352718	0.611875
H	−2.952351	−0.837393	0.786335
H	−2.220842	−2.248000	0.016773
H	−1.627763	−1.701612	1.577747
C	−2.336346	1.682560	−0.088861
H	−2.019665	2.562202	0.483834
H	−2.788958	2.063125	−1.011898
H	−3.115011	1.178791	0.484042

Table B.67: **22c**$_1$ at B3LYP/6-311G(d,p) level.

Atom	x (Å)	y (Å)	z (Å)
C	0.608193	0.677141	−0.026222
C	0.561059	−0.671279	−0.042078
C	−0.778266	−1.360242	−0.252835
C	−0.644257	1.442424	−0.178894
C	−1.963350	−0.574150	0.318574
C	−1.851716	0.886915	−0.029698
H	−0.753176	−2.364345	0.182248
H	−0.921697	−1.502969	−1.335715
H	−0.556273	2.504702	−0.390318
H	−1.985630	−0.677107	1.414805
H	−2.905320	−0.994571	−0.045572
H	−2.753786	1.485365	−0.106326
C	1.743649	−1.596364	0.037511
H	2.703022	−1.080940	0.054913
H	1.685439	−2.228330	0.932141
H	1.747290	−2.279780	−0.821191
C	1.858409	1.510694	0.116380
H	2.763473	0.917183	0.235419
H	1.993387	2.154364	−0.760802
H	1.780939	2.175591	0.983971

Table B.68: **22c**$_2$ at B3LYP/6-311G(d,p) level.

Atom	x (Å)	y (Å)	z (Å)
C	−0.127534	−1.463976	−0.266496
C	−0.894878	−0.434658	0.130422
C	−0.251286	0.929738	0.351264
C	1.320657	−1.327125	−0.425520
C	1.204646	0.786117	0.840102
C	1.967479	−0.267051	0.075818
H	−0.581193	−2.425994	−0.487473
H	−0.816277	1.457996	1.127991
H	1.862733	−2.115916	−0.937236
H	1.208598	0.511584	1.906182
H	1.709202	1.755945	0.776660
H	3.045414	−0.177595	−0.010370
C	−2.383276	−0.539761	0.298726
H	−2.751249	−1.531161	0.025861
H	−2.676283	−0.342122	1.336941
H	−2.908680	0.199245	−0.317824
C	−0.338567	1.769515	−0.941147
H	−1.371074	1.863913	−1.286932
H	0.050138	2.778513	−0.771030
H	0.245224	1.308787	−1.741783

Table B.69: **23c** at B3LYP/6-311G(d,p) level.

Atom	x (Å)	y (Å)	z (Å)
C	−0.506208	0.814617	−0.389038
C	0.936062	1.255291	−0.430485
C	1.967936	0.478528	−0.113945
C	1.813441	−0.959320	0.289646
C	−0.654361	−0.672229	−0.111325
C	0.392789	−1.440902	0.198029
H	−0.950002	1.012151	−1.378133
H	1.110296	2.289509	−0.718520
H	2.977448	0.879286	−0.147440
H	2.198243	−1.104874	1.310800
H	2.458087	−1.592248	−0.338093
H	0.230480	−2.500353	0.384367
C	−2.044235	−1.245662	−0.226066
H	−2.036640	−2.329760	−0.096695
H	−2.724315	−0.824167	0.521530
H	−2.478847	−1.023672	−1.208140
C	−1.293284	1.682396	0.622974
H	−1.157018	2.744798	0.401504
H	−2.364872	1.472866	0.590241
H	−0.935704	1.500152	1.639839

Table B.70: **25c** at B3LYP/6-311G(d,p) level.

Atom	x (Å)	y (Å)	z (Å)
C	0.738505	1.069916	−0.357114
C	1.424382	−0.039020	−0.021238
C	0.462579	−1.145122	0.142422
C	−0.791967	−0.714123	−0.088549
H	1.155863	2.051734	−0.543711
H	0.743153	−2.158885	0.407659
C	2.903467	−0.189012	0.163961
H	3.141366	−0.541721	1.173701
H	3.316750	−0.925414	−0.534294
H	3.423495	0.757669	0.004155
C	−0.736806	0.763884	−0.437184
H	−1.078828	0.889790	−1.476633
C	−1.607618	1.657396	0.465222
H	−1.509706	2.708474	0.181116
H	−2.664972	1.388752	0.388838
H	−1.302554	1.558149	1.510119
C	−2.061422	−1.503234	−0.039150
H	−1.866657	−2.548042	0.212740
H	−2.757953	−1.103027	0.707231
H	−2.586677	−1.481594	−1.001136

Table B.71: **26c** at B3LYP/6-311G(d,p) level.

Atom	x (Å)	y (Å)	z (Å)
C	−1.460811	0.056852	−0.000046
C	−0.640733	1.123535	−0.000086
C	0.770872	0.695414	0.000027
C	0.816919	−0.656437	−0.000043
H	−0.956148	2.161536	−0.000154
C	−2.956111	0.030533	0.000094
H	−3.368578	1.042035	−0.001294
H	−3.350808	−0.493917	−0.878284
H	−3.350672	−0.491400	0.880048
C	−0.600183	−1.185033	−0.000077
H	−0.800317	−1.815577	0.877406
H	−0.800273	−1.815253	−0.877808
C	2.005599	−1.566119	0.000048
H	2.009697	−2.222079	−0.879008
H	2.945846	−1.011399	−0.000021
H	2.009663	−2.221776	0.879332
C	1.906885	1.673941	0.000033
H	2.879371	1.179116	−0.000030
H	1.863748	2.326324	−0.879479
H	1.863848	2.326268	0.879598

Table B.72: **27c** at B3LYP/6-311G(d,p) level.

Atom	x (Å)	y (Å)	z (Å)
C	1.536929	−0.170501	−0.046972
C	0.913880	1.013759	0.698877
C	−0.451279	0.640525	0.076308
C	0.222746	−0.576849	−0.615669
C	−0.801902	−0.754416	0.502284
C	2.787963	−0.573230	−0.234037
H	1.298717	1.969485	0.331849
H	0.963427	1.007519	1.792999
H	0.043505	−1.006099	−1.595622
H	−0.425303	−1.094259	1.466404
H	3.619822	−0.082613	0.259821
H	3.022173	−1.400479	−0.895724
C	−2.140020	−1.355766	0.127171
H	−2.092042	−2.447869	0.164603
H	−2.927496	−1.032907	0.815452
H	−2.447006	−1.076850	−0.884002
C	−1.412714	1.665830	−0.455477
H	−1.841954	2.253514	0.364419
H	−0.906917	2.362596	−1.131281
H	−2.240547	1.211850	−1.003830

Table B.73: **28c**$_1$ at B3LYP/6-311G(d,p) level.

Atom	x (Å)	y (Å)	z (Å)
C	−1.180877	0.204039	−1.065326
C	−0.120842	0.668536	−0.000004
C	0.810299	−0.576330	−0.000005
C	−1.426163	−0.916362	0.000001
C	−0.052220	−1.598706	−0.000002
C	−1.180862	0.204033	1.065330
H	−0.808491	−0.105636	−2.044330
H	−2.017286	0.903324	−1.167093
H	−2.321808	−1.535853	−0.000003
H	0.141788	−2.662847	0.000012
H	−2.017267	0.903322	1.167117
H	−0.808476	−0.105647	2.044334
C	2.301344	−0.548372	−0.000004
H	2.711354	−1.560927	−0.000074
H	2.695001	−0.024026	−0.878695
H	2.694993	−0.024158	0.878773
C	0.484143	2.055376	0.000002
H	1.108897	2.218885	0.884082
H	1.108771	2.218944	−0.884158
H	−0.296408	2.821330	0.000083

Table B.74: **28c**$_2$ at B3LYP/6-311G(d,p) level.

Atom	x (Å)	y (Å)	z (Å)
C	−0.728715	−0.037485	−1.076552
C	−0.278038	1.033587	0.001906
C	1.232467	0.733956	0.080465
C	−0.179355	−1.021287	0.022741
C	1.295453	−0.599387	0.094144
C	−0.793365	−0.015463	1.054229
H	−1.823923	−0.084696	−1.100554
H	2.027272	1.467173	0.110459
H	−0.423611	−2.083207	0.026031
H	2.155013	−1.253321	0.138725
H	−1.884994	−0.062524	1.117986
H	−0.341851	0.014950	2.047641
C	−0.745417	2.472173	−0.026065
H	−0.418806	3.009961	0.869953
H	−0.343367	3.001950	−0.895793
H	−1.836563	2.533284	−0.072499
C	−0.190416	−0.031099	−2.496878
H	−0.489556	−0.941879	−3.025682
H	−0.592409	0.817852	−3.059318
H	0.899397	0.031320	−2.518786

Table B.75: **29c** at B3LYP/6-311G(d,p) level.

Atom	x (Å)	y (Å)	z (Å)
C	−1.882495	−0.106316	−0.116828
C	−1.422472	−1.445695	0.270465
C	−0.710779	−0.178722	0.774583
C	−2.725999	0.632016	−0.811053
C	0.658048	0.236308	0.310947
C	1.568501	−0.668557	−0.063272
H	−0.921090	−2.049952	−0.479098
H	−2.003384	−2.016220	0.989272
H	−0.914015	0.071997	1.817085
H	−3.512742	0.180987	−1.407816
H	−2.665224	1.715736	−0.810912
H	1.277498	−1.715565	−0.014522
C	0.873750	1.729117	0.337294
H	1.890969	2.019690	0.076191
H	0.188831	2.226516	−0.357982
H	0.655703	2.130229	1.333805
C	2.968952	−0.431686	−0.551122
H	3.695775	−0.931038	0.099870
H	3.106816	−0.855528	−1.552513
H	3.235817	0.624359	−0.599467

Table B.76: **30c** at B3LYP/6-311G(d,p) level.

Atom	x (Å)	y (Å)	z (Å)
C	3.052724	0.194268	0.000428
C	2.224669	−1.103194	0.000298
C	1.587114	0.215978	0.000013
C	0.483872	0.953955	0.000012
C	−0.923248	0.497222	−0.000109
C	−1.254659	−0.805568	−0.000248
H	3.584160	0.453381	−0.911327
H	3.583635	0.453622	0.912419
H	2.207994	−1.695020	0.912008
H	2.208607	−1.695143	−0.911342
H	0.618602	2.034513	0.000074
H	−0.438596	−1.522941	−0.000265
C	−2.622976	−1.419227	−0.000368
H	−2.758882	−2.063070	0.876947
H	−3.429651	−0.685927	−0.000698
H	−2.758531	−2.063465	−0.877442
C	−1.927846	1.627717	−0.000063
H	−1.786851	2.266472	0.879021
H	−1.787270	2.266191	−0.879422
H	−2.961110	1.284490	0.000247

Table B.77: **31c** at (4*e*,4*o*)CASSCF/6-311G(d,p) level.

Atom	x (Å)	y (Å)	z (Å)
C	−1.747436	0.031979	0.090153
C	−2.252254	−0.573665	1.238973
C	−0.551867	0.924866	0.204680
C	−2.360786	−0.122470	−1.151236
C	0.770212	0.512132	0.071477
C	1.093297	−0.826462	−0.191770
H	−1.765754	−0.458279	2.189146
H	−3.159754	−1.150209	1.206961
H	−0.755245	1.962161	0.407404
H	−3.271387	−0.685979	−1.251880
H	−1.957378	0.338721	−2.032980
H	0.283770	−1.526069	−0.294504
C	2.474858	−1.390507	−0.362201
H	2.467249	−2.469345	−0.222786
H	2.844703	−1.205369	−1.369032
H	3.190786	−0.972566	0.334092
C	1.866189	1.551268	0.220998
H	2.525119	1.315599	1.051569
H	2.476753	1.615888	−0.674601
H	1.443690	2.532134	0.403595

Table B.78: **31c** at B3LYP/6-311G(d,p) level.

Atom	x (Å)	y (Å)	z (Å)
C	−1.749599	0.041014	0.037787
C	−2.099863	−0.701518	1.159543
C	−0.555772	0.933107	0.116262
C	−2.509729	0.025539	−1.123775
C	0.766102	0.509143	0.044157
C	1.092897	−0.832766	−0.158736
H	−1.497554	−0.676099	2.058140
H	−2.999960	−1.306982	1.168836
H	−0.759932	1.993272	0.233129
H	−3.430140	−0.545508	−1.180150
H	−2.213452	0.591819	−1.997394
H	0.274686	−1.534403	−0.281801
C	2.471933	−1.403414	−0.237265
H	2.599592	−2.223558	0.480864
H	2.664689	−1.836759	−1.227982
H	3.251998	−0.665892	−0.042283
C	1.861664	1.551151	0.183177
H	2.508111	1.340335	1.040503
H	2.500085	1.584488	−0.704747
H	1.436076	2.545762	0.325985

Table B.79: **32c** at B3LYP/6-311G(d,p) level.

Atom	x (Å)	y (Å)	z (Å)
C	0.843904	−0.302495	0.028734
C	−0.299223	0.645155	0.505632
C	−1.230943	−0.470866	0.016603
C	−0.224574	−1.264249	−0.382492
C	2.166084	−0.577877	0.691333
C	2.119338	0.062650	−0.680038
H	−0.311056	0.761340	1.596690
H	−0.185072	−2.252527	−0.829407
H	2.495871	−1.608442	0.765283
H	2.455949	0.044368	1.531244
H	2.378924	1.113093	−0.757727
H	2.416717	−0.534064	−1.535483
C	−2.716679	−0.570097	0.022726
H	−3.054305	−1.512534	−0.415528
H	−3.112680	−0.507167	1.043071
H	−3.172778	0.250084	−0.543599
C	−0.418255	2.006178	−0.172256
H	−1.356139	2.500660	0.100098
H	0.399133	2.671043	0.124725
H	−0.392485	1.903765	−1.260810

Table B.80: **33c** at B3LYP/6-311G(d,p) level.

Atom	x (Å)	y (Å)	z (Å)
C	0.727968	−0.339562	0.000006
C	−0.412924	0.698245	−0.000030
C	1.686789	0.917309	−0.000248
C	0.425877	1.751022	−0.000153
C	−1.857393	0.594925	0.000091
C	−2.561137	−0.543765	−0.000111
H	2.320134	1.007462	−0.889392
H	2.320457	1.007620	0.888644
H	0.262658	2.823669	−0.000135
H	−2.392596	1.543226	0.000342
H	−3.644608	−0.536463	−0.000033
H	−2.080740	−1.515224	−0.000407
C	0.832479	−1.193465	−1.266639
H	1.788712	−1.726511	−1.293696
H	0.034410	−1.940262	−1.312181
H	0.761678	−0.574669	−2.165189
C	0.832514	−1.192942	1.267017
H	0.033096	−1.938203	1.313979
H	1.787787	−1.727755	1.293195
H	0.763975	−0.573484	2.165282

Table B.81: **34c** at B3LYP/6-311G(d,p) level.

Atom	x (Å)	y (Å)	z (Å)
C	0.965692	0.050749	−0.000058
C	−0.404363	0.206157	−0.646144
C	0.110185	−0.750447	1.090927
C	−1.077972	−0.932226	0.074014
C	−1.469305	1.032414	−0.611852
C	−2.351476	−0.018796	0.080087
H	−0.153040	−0.107239	1.933195
H	0.570986	−1.672598	1.455106
H	−1.163440	−1.931292	−0.354693
H	−1.580177	2.106364	−0.715608
H	−2.662392	0.290175	1.083801
H	−3.225201	−0.410088	−0.451671
C	1.671647	1.318177	0.464862
H	2.511989	1.076151	1.123848
H	2.070269	1.878082	−0.387022
H	0.987110	1.973427	1.009330
C	1.915610	−0.881576	−0.758781
H	2.333333	−0.378143	−1.635453
H	2.747216	−1.188019	−0.116248
H	1.403235	−1.783534	−1.102918

Table B.82: **35c** at B3LYP/6-311G(d,p) level.

Atom	x (Å)	y (Å)	z (Å)
C	−0.040617	−0.310821	−0.114987
C	1.311968	0.353776	−0.392352
C	0.495067	−1.537994	0.038608
C	1.916717	−1.089528	−0.221689
C	−1.402303	0.206810	−0.066104
C	−1.673128	1.480543	−0.387058
C	−2.485723	−0.760663	0.345639
C	1.806866	1.404643	0.597875
H	1.405936	0.725486	−1.419004
H	0.070477	−2.512854	0.251930
H	2.391626	−1.501221	−1.118478
H	2.612912	−1.191195	0.617797
H	−2.685449	1.867864	−0.361119
H	−0.893805	2.168192	−0.692900
H	−3.465914	−0.281071	0.348001
H	−2.524643	−1.615999	−0.336763
H	−2.293934	−1.158818	1.347112
H	1.730568	1.035074	1.625037
H	2.854512	1.656250	0.404911
H	1.224617	2.327688	0.533883

Table B.83: **36c** at B3LYP/6-311G(d,p) level.

Atom	x (Å)	y (Å)	z (Å)
C	−0.108919	−0.352619	−0.091863
C	−0.318709	1.123218	−0.434825
C	1.236851	−0.243291	−0.018796
C	1.247931	1.235833	−0.354247
C	−1.024712	−1.461498	0.065902
C	−2.346229	−1.406616	−0.143628
C	2.357322	−1.184609	0.256143
C	−1.102763	1.982283	0.553964
H	−0.694495	1.281185	−1.452460
H	1.744259	1.507175	−1.292908
H	1.614769	1.900587	0.436409
H	−0.582108	−2.408129	0.371147
H	−2.976436	−2.278397	−0.014740
H	−2.836069	−0.491023	−0.456098
H	3.044615	−1.234543	−0.596669
H	2.948777	−0.850845	1.116840
H	1.999868	−2.196263	0.461979
H	−0.727250	1.841755	1.572245
H	−1.014309	3.044099	0.302803
H	−2.166254	1.728188	0.555553

Table B.84: **37c** at B3LYP/6-311G(d,p) level.

Atom	x (Å)	y (Å)	z (Å)
C	−1.240686	−0.578980	0.378174
C	0.020983	−0.259558	−0.409460
C	−1.096034	0.938735	0.838457
C	−0.124423	1.238931	−0.366751
C	1.359468	−0.268770	−0.225862
C	1.434144	1.270144	−0.221740
H	−0.602795	1.018578	1.809192
H	−2.027924	1.511134	0.849709
H	−0.573529	1.807124	−1.182838
H	1.776681	1.663680	0.742073
H	1.985558	1.779261	−1.020326
C	−2.506840	−0.865463	−0.425401
H	−2.470535	−1.864319	−0.868901
H	−3.392700	−0.811830	0.214923
H	−2.633098	−0.143990	−1.237894
H	−1.119597	−1.319547	1.174005
C	2.352051	−1.297276	0.197537
H	1.887622	−2.283593	0.279937
H	3.179891	−1.376693	−0.517182
H	2.798448	−1.046381	1.167573

Table B.85: **38c** at B3LYP/6-311G(d,p) level.

Atom	x (Å)	y (Å)	z (Å)
C	−1.295652	−0.658726	0.215947
C	0.031438	−0.710003	−0.519140
C	−0.456460	0.232438	1.236653
C	0.674221	0.484194	0.155064
C	1.138691	−1.478427	−0.507920
C	1.986103	−0.381412	0.152344
H	−0.111919	−0.352640	2.090991
H	−0.966891	1.134988	1.585250
H	2.317695	−0.669853	1.155900
H	2.840154	0.037645	−0.390819
C	−2.466382	0.056630	−0.453955
H	−2.885721	−0.557061	−1.256078
H	−3.262730	0.253507	0.270363
H	−2.162866	1.011013	−0.890651
H	−1.625571	−1.620170	0.618934
C	0.756523	1.883176	−0.426176
H	1.300100	2.550121	0.253332
H	1.287851	1.876080	−1.382624
H	−0.231434	2.319898	−0.595132
H	1.290440	−2.550744	−0.576369

APPENDIX C

OPTIMIZED GEOMETRIES OF ALL SADDLE POINTS

Table C.1: Singlet TMM $\boldsymbol{l}_1$ (C_{2v}, $^1B_2$) at (4e,4o)CASSCF/6-311G(d,p) level.

Atom	**x (Å)**	**y (Å)**	**z (Å)**
C	−0.044223	0.000000	0.000000
C	−0.717205	−1.213231	0.000000
C	−0.717205	1.213231	0.000000
C	1.472811	0.000000	0.000000
H	−0.189975	−2.149111	0.000000
H	−0.189975	2.149111	0.000000
H	−1.791208	−1.246990	0.000000
H	−1.791208	1.246990	0.000000
H	2.015848	−0.924382	0.000000
H	2.015848	0.924382	0.000000

Table C.2: MCP/$\mathbf{o}_1$ at (4e,4o)CASSCF/6-311G(d,p) level.

Atom	**x (Å)**	**y (Å)**	**z (Å)**
C	0.089702	0.011763	−0.062523
C	−0.977157	1.040902	0.033736
C	−0.474881	−1.315999	0.001000
C	1.411340	0.289813	−0.008801
H	−1.637109	1.211915	−0.800721
H	−1.375049	1.258127	1.010153
H	−1.436700	−1.509389	−0.436590
H	−0.045023	−2.082821	0.620874
H	1.767053	1.304404	−0.004872
H	2.143345	−0.497513	0.046794

Table C.3: **1a/3a** B3LYP/6-311G(d,p) level.

Atom	x (Å)	y (Å)	z (Å)
C	−0.030171	1.038937	−0.323791
C	−0.030887	−1.039090	−0.324901
C	0.914699	−0.000639	0.016512
C	2.240722	0.000100	0.238629
H	0.235097	1.906140	−0.919970
H	0.233747	−1.906789	−0.920549
H	2.793351	0.928284	0.315990
H	2.796161	−0.926689	0.314171
C	−1.420509	0.772560	0.183984
C	−1.420277	−0.772205	0.185348
H	−2.185939	1.158800	−0.493148
H	−1.604586	1.229709	1.167180
H	−2.188009	−1.160311	−0.488459
H	−1.601282	−1.227118	1.170106

Table C.4: **1a/4a** B3LYP/6-311G(d,p) level.

Atom	x (Å)	y (Å)	z (Å)
C	0.849575	−0.000007	−0.000025
C	−0.034773	−1.157860	−0.122782
C	−0.034709	1.157864	0.122619
C	2.204990	−0.000026	0.000061
H	2.767617	−0.925107	−0.010415
H	2.767638	0.925042	0.010602
H	0.272749	2.051365	0.654424
H	0.272527	−2.051208	−0.654929
C	−1.374936	−0.954807	0.276474
C	−1.374970	0.954813	−0.276360
H	−1.608716	−0.654349	1.293838
H	−2.136997	−1.614957	−0.139228
H	−1.608966	0.654314	−1.293659
H	−2.136914	1.615044	0.139437

Table C.5: **1a/12a** B3LYP/6-311G(d,p) level.

Atom	x (Å)	y (Å)	z (Å)
C	−0.761807	0.341056	−0.281708
C	−0.294205	−0.999698	−0.249758
C	1.127757	−0.975499	0.258105
C	0.226299	1.246040	−0.096007
C	1.559270	0.503405	−0.030467
C	−2.087145	0.058656	0.214334
H	−0.776743	−1.837301	−0.733931
H	1.746490	−1.728126	−0.241182
H	0.101269	2.288860	0.162171
H	2.208193	0.896036	0.756907
H	2.129855	0.566199	−0.967982
H	−2.832502	−0.430537	−0.402039
H	−2.377842	0.386131	1.204599
H	1.180266	−1.185028	1.334463

Table C.6: **1a/2a** B3LYP/6-311G(d,p) level.

Atom	x (Å)	y (Å)	z (Å)
C	1.019706	−0.206683	0.010226
C	0.016551	0.488398	0.918013
C	−1.097184	−0.566821	1.063686
C	0.194694	−0.851105	−0.956710
C	−1.112148	−1.281506	−0.324508
C	2.357884	−0.131884	0.145683
N	−0.602534	1.592579	0.035481
N	−0.687258	1.342133	−1.112302
H	0.382644	0.932193	1.840325
H	−2.055793	−0.121185	1.334946
H	−0.812071	−1.262094	1.857271
H	0.543645	−1.218725	−1.911863
H	−1.166080	−2.369856	−0.202051
H	−1.977919	−0.995646	−0.930108
H	2.814542	0.475359	0.918409
H	3.022559	−0.685429	−0.507522

Table C.7: **4a/33a** B3LYP/6-311G(d,p) level.

Atom	x (Å)	y (Å)	z (Å)
C	−1.013104	1.252078	−0.056594
C	0.013538	0.252768	−0.136683
C	−0.710418	−0.923006	−0.260423
C	−1.990291	−0.612368	0.268814
C	1.448276	0.483393	−0.019757
C	2.371642	−0.471800	0.139240
H	−1.689933	1.371369	−0.890588
H	−0.908142	2.146532	0.563522
H	−0.432863	−1.842546	−0.767123
H	−2.072093	−0.288515	1.297863
H	1.772601	1.519396	−0.089034
H	3.428743	−0.236709	0.173577
H	2.096388	−1.516884	0.237094
H	−2.912555	−1.039029	−0.132890

Table C.8: **33a/34a** B3LYP/6-311G(d,p) level.

Atom	x (Å)	y (Å)	z (Å)
C	−1.406105	0.851328	0.100675
C	0.043875	0.602771	−0.287509
C	−1.502516	−0.739071	0.226253
C	−0.122229	−0.795986	−0.458073
C	1.371069	0.816778	−0.021251
C	1.805350	−0.536383	0.262630
H	−2.042051	1.224334	−0.706170
H	−1.593490	1.434349	1.005535
H	−2.336815	−1.228518	−0.284504
H	−1.498979	−1.050385	1.273936
H	0.121454	−1.387045	−1.331119
H	1.974063	1.718347	−0.023415
H	2.772523	−0.932095	−0.064844
H	1.466627	−0.975610	1.194231

Table C.9: **9a/14a** B3LYP/6-311G(d,p) level.

Atom	x (Å)	y (Å)	z (Å)
C	0.744784	1.402212	−0.036913
H	1.543114	2.115217	−0.133217
C	−0.516352	1.360498	−0.030970
H	−2.029879	0.304952	−1.032439
C	−1.541347	0.416601	−0.064289
H	−2.273593	0.445192	0.742225
C	1.508924	−0.321021	0.198394
H	2.474197	−0.244943	−0.295879
C	0.565372	−1.206699	−0.343711
H	0.689421	−1.524831	−1.375511
H	−0.763976	−1.240308	1.314686
C	−0.725005	−1.258085	0.227599
H	−1.438836	−1.956965	−0.201797
H	1.581287	−0.259350	1.281273

Table C.10: **10a/20a** B3LYP/6-311G(d,p) level.

Atom	x (Å)	y (Å)	z (Å)
C	−0.792476	0.049339	0.089213
C	0.145663	1.202086	−0.007490
C	0.112562	−1.204538	0.024371
C	1.485409	0.713865	−0.061751
C	1.514607	−0.644735	−0.058606
C	−2.185532	0.014927	−0.129686
H	2.354795	1.359083	−0.074173
H	2.403927	−1.259319	−0.030429
H	−0.607638	0.534663	1.174585
H	−0.177646	2.233139	−0.010866
H	−0.148475	−1.802171	−0.854720
H	−0.018637	−1.861650	0.893514
H	−2.762601	0.927850	−0.205890
H	−2.725127	−0.917255	−0.028325

Table C.11: **11a/20a** B3LYP/6-311G(d,p) level.

Atom	x (Å)	y (Å)	z (Å)
C	−0.814871	−0.060973	0.103777
C	0.158216	−1.176377	−0.010866
C	1.556281	−0.632171	−0.053299
C	0.040381	1.175268	0.035941
C	1.334347	0.865132	−0.047726
C	−2.218920	−0.024791	−0.158963
H	−0.113482	−2.220628	0.043761
H	−0.719331	−0.449909	1.208358
H	2.090149	−0.953307	−0.963656
H	2.194473	−0.960347	0.782903
H	−0.381300	2.171922	0.055426
H	2.149228	1.576833	−0.098292
H	−2.792498	−0.938743	−0.247951
H	−2.759845	0.897648	0.006266

Table C.12: **11a/31a** B3LYP/6-311G(d,p) level.

Atom	x (Å)	y (Å)	z (Å)
C	−0.866950	−0.031849	−0.124840
C	−0.468503	1.275993	−0.536859
C	1.747339	0.564608	0.566120
C	0.184194	−1.047940	−0.351663
C	1.463869	−0.675498	−0.072876
C	−2.073912	−0.306549	0.447183
H	−1.071801	2.139284	−0.271431
H	0.247344	1.402211	−1.335530
H	1.119387	0.934819	1.363998
H	2.716986	1.037129	0.452370
H	−0.066055	−2.032975	−0.727803
H	2.293488	−1.307453	−0.382982
H	−2.836564	0.456714	0.544074
H	−2.319007	−1.302310	0.794906

Table C.13: **14a/15a** B3LYP/6-311G(d,p) level.

Atom	x (Å)	y (Å)	z (Å)
C	0.091342	−1.218407	−0.326038
C	1.211977	−0.730060	0.566017
C	1.122175	0.477927	−0.300975
C	−1.181420	−0.813982	−0.092467
C	−1.918643	0.192755	0.095597
H	0.356769	−1.785967	−1.210155
H	2.132826	−1.305982	0.495065
H	0.922717	−0.567961	1.602478
H	−2.833836	0.489912	0.575131
C	0.346891	1.621908	−0.007230
H	−0.954785	1.194785	−0.153408
H	0.274726	1.919722	1.037633
H	0.450963	2.459415	−0.692523
H	1.616692	0.415229	−1.263644

Table C.14: **14a/17a** B3LYP/6-311G(d,p) level.

Atom	x (Å)	y (Å)	z (Å)
C	−0.852039	−0.245508	−0.072018
C	0.127596	−1.172908	−0.069480
C	0.145598	1.326455	−0.270413
C	1.549019	−0.623231	−0.110384
C	1.239679	0.756500	0.396523
C	−2.187519	−0.114678	0.118377
H	1.434025	0.993263	1.436759
H	−0.363602	2.172191	0.182342
H	0.153623	1.365036	−1.359769
H	−2.781927	0.551144	−0.497664
H	−2.682558	−0.575040	0.967405
H	2.236778	−1.183642	0.529250
H	1.959465	−0.644393	−1.130066
H	−0.089807	−2.238348	−0.083881

Table C.15: **14a/21a**$_2$ B3LYP/6-311G(d,p) level.

Atom	x (Å)	y (Å)	z (Å)
H	0.751784	−0.861297	−0.828259
C	−0.513994	−0.844314	−0.002871
C	0.440066	−0.116302	0.826354
C	1.567383	−0.133371	0.082304
C	2.693552	0.430134	−0.360582
H	3.435399	−0.142587	−0.904163
H	2.857993	1.500593	−0.275935
C	−1.865158	−0.364344	−0.267720
C	−2.244619	0.913050	−0.118741
H	−0.385806	−1.922871	−0.019342
H	0.269667	0.304526	1.813916
H	−2.590447	−1.095128	−0.618090
H	−3.267555	1.226287	−0.289744
H	−1.534416	1.681358	0.169152

Table C.16: **15a/15a-trans** B3LYP/6-311G(d,p) level.

Atom	x (Å)	y (Å)	z (Å)
C	−2.360495	−0.792622	−0.193250
H	−2.009376	−1.479149	−0.981557
H	−2.957671	−1.388580	0.501717
H	−3.027878	−0.075989	−0.688069
C	−1.229573	−0.109907	0.494001
H	−0.817697	−0.540354	1.399791
C	−0.532629	1.070678	−0.099566
H	−0.828118	1.180677	−1.155697
H	−0.884703	1.999526	0.380437
C	0.970051	1.056503	−0.011410
C	1.733271	−0.086329	−0.036264
C	2.422338	−1.094205	−0.058070
H	3.021574	−1.970567	−0.082951
H	1.486088	2.009730	0.053683

Table C.17: **10a/17a** B3LYP/6-311G(d,p) level.

Atom	x (Å)	y (Å)	z (Å)
C	0.821701	−0.033896	0.001069
C	−0.032305	−1.179682	−0.047969
C	−0.076333	1.218053	0.036629
C	−1.451177	−0.714867	−0.025639
C	−1.487904	0.691545	−0.074689
C	2.178730	−0.031202	−0.018161
H	−2.379591	1.298966	−0.059337
H	0.173293	1.913861	−0.774894
H	0.081673	1.781639	0.968467
H	2.742583	−0.956507	−0.027923
H	2.743268	0.892979	−0.046801
H	−2.281441	−1.366036	−0.275750
H	−1.060780	−1.047664	1.073045
H	0.264724	−2.216951	−0.084247

Table C.18: **11a/17a** B3LYP/6-311G(d,p) level.

Atom	x (Å)	y (Å)	z (Å)
C	0.823159	−0.048632	−0.019543
C	−0.031291	−1.191633	−0.065219
C	−0.065922	1.213594	−0.027680
C	−1.396968	−0.785021	−0.004662
C	−1.478747	0.690975	−0.031728
C	2.180498	−0.028525	0.034903
H	−2.393530	1.260694	−0.070969
H	0.108555	1.806732	−0.937653
H	0.157228	1.881352	0.812590
H	2.752357	−0.948837	0.042512
H	2.737149	0.900724	0.059286
H	−2.235130	−1.421250	−0.270134
H	−1.615705	−0.365968	1.094614
H	0.304702	−2.217999	−0.046663

Table C.19: **17a/27a** B3LYP/6-311G(d,p) level.

Atom	x (Å)	y (Å)	z (Å)
C	1.275082	0.724077	−0.359297
C	0.188021	−1.086679	−0.094308
H	1.667293	1.006128	−1.327800
H	−0.004300	−2.066136	−0.520330
C	−0.042252	1.234052	0.167040
H	−0.496674	2.011410	−0.448596
H	0.032931	1.614000	1.195922
C	−0.813746	−0.086628	0.069713
C	−2.157541	−0.225776	−0.030216
H	−2.826646	0.611491	0.127013
H	−2.605451	−1.179266	−0.288356
C	1.566513	−0.603361	0.268882
H	1.772561	−0.564050	1.348745
H	2.363822	−1.167686	−0.217480

Table C.20: **20a/21a**$_2$ B3LYP/6-311G(d,p) level.

Atom	x (Å)	y (Å)	z (Å)
C	−0.860918	−0.078451	0.392485
C	0.305737	1.274631	−0.188940
C	1.546596	0.591232	0.040648
C	0.075438	−1.182947	0.000702
C	1.385196	−0.806423	−0.119371
C	−2.161055	0.016057	−0.134647
H	−0.815646	0.101317	1.471372
H	0.137448	2.238097	0.290732
H	−0.043255	1.266906	−1.215746
H	2.394702	1.035236	0.550382
H	−0.282728	−2.200613	−0.102076
H	2.203293	−1.511678	−0.214856
H	−2.378305	−0.297346	−1.149715
H	−2.961475	0.483485	0.424644

Table C.21: **20a/22a** B3LYP/6-311G(d,p) level.

Atom	x (Å)	y (Å)	z (Å)
C	0.551872	1.295347	−0.071988
C	−0.802236	1.102521	−0.229929
C	−1.380002	−0.139140	0.395494
C	1.407619	0.220832	0.234757
C	−0.549684	−1.173777	−0.294349
C	0.894831	−1.067150	−0.087529
H	0.988590	2.269918	−0.273548
H	−1.433340	1.812000	−0.751637
H	−2.442737	−0.275038	0.192862
H	−1.231379	−0.151619	1.488459
H	2.458074	0.359108	0.450627
H	−0.959722	−1.912609	−0.974015
H	0.343297	−1.739694	0.761537
H	1.542816	−1.793862	−0.573020

Table C.22: **20a/23a** B3LYP/6-311G(d,p) level.

Atom	x (Å)	y (Å)	z (Å)
C	−0.544635	−1.222572	−0.265281
C	−0.813269	1.096716	−0.218689
C	0.533787	1.309130	−0.080870
C	0.838427	−1.121219	−0.094388
C	1.408673	0.233552	0.156098
C	−1.390912	−0.162184	0.372874
H	−1.297498	−0.167256	1.476216
H	1.047896	−0.907362	1.089920
H	−0.981046	−2.025096	−0.843978
H	−1.456933	1.837850	−0.679381
H	0.964376	2.291013	−0.251990
H	1.510955	−1.878494	−0.485800
H	2.467326	0.335636	0.344086
H	−2.447497	−0.286834	0.132456

Table C.23: **20a/25a** B3LYP/6-311G(d,p) level.

Atom	x (Å)	y (Å)	z (Å)
C	0.141082	−1.162810	0.016859
C	−0.773925	−0.062890	0.096881
C	0.081127	1.169903	0.024275
C	1.373115	0.841927	−0.042723
H	−0.138001	−2.206785	0.041188
H	−0.328212	2.172519	0.031680
H	2.199620	1.539383	−0.096200
C	−2.231153	−0.016697	−0.195727
H	−1.291809	−0.145164	1.148098
H	−2.761139	0.896846	0.043743
H	−2.795827	−0.941085	−0.199329
C	1.552251	−0.657449	−0.038923
H	2.173538	−0.991382	0.807716
H	2.086851	−0.996232	−0.940750

Table C.24: **20a/26a** B3LYP/6-311G(d,p) level.

Atom	x (Å)	y (Å)	z (Å)
C	−0.742247	0.065292	0.082411
C	0.139385	1.189523	−0.006962
C	1.488909	0.732679	−0.029418
C	1.549625	−0.628013	−0.016971
H	−0.176859	2.223776	−0.009099
H	2.347210	1.393642	−0.039162
H	2.441794	−1.236461	0.022112
C	−2.202429	0.010154	−0.141010
H	−2.773737	0.927187	−0.198126
H	−2.722626	−0.917582	0.054264
H	−1.303445	0.139637	1.126285
C	0.148054	−1.188371	−0.019196
H	−0.026458	−1.908328	0.787937
H	−0.073660	−1.709453	−0.957332

Table C.25: **20a/28a** B3LYP/6-311G(d,p) level.

Atom	x (Å)	y (Å)	z (Å)
C	−1.286525	−0.432892	0.870532
C	−0.747207	−0.379747	−0.563734
C	0.603663	−1.072714	−0.491902
C	0.661967	0.966546	0.497065
C	1.385730	−0.247219	0.264014
C	−0.359616	1.103544	−0.623598
H	−0.924305	−1.198540	1.547839
H	−2.299869	−0.074287	1.054753
H	−1.431164	−0.759200	−1.330214
H	0.808891	−2.087269	−0.802751
H	1.038551	1.791900	1.090743
H	2.353210	−0.482411	0.689342
H	−1.196913	1.763525	−0.391876
H	0.103534	1.421169	−1.572096

Table C.26: **21a$_1$/21a$_2$** B3LYP/6-311G(d,p) level.

Atom	x (Å)	y (Å)	z (Å)
C	0.523750	1.134315	−0.157884
C	−0.791290	1.120179	0.112780
C	−1.731526	−0.003405	0.189963
C	−1.550968	−1.275763	−0.181276
C	1.412730	−0.012406	−0.454768
C	2.078288	−0.718998	0.455416
H	1.007989	2.109675	−0.187185
H	−1.245580	2.088237	0.310030
H	−2.708285	0.267158	0.585484
H	−2.354578	−1.996030	−0.077790
H	−0.617266	−1.639136	−0.589437
H	1.554470	−0.248196	−1.510720
H	2.741614	−1.527184	0.167635
H	1.975730	−0.518051	1.516599

Table C.27: **21a$_1$/22a** B3LYP/6-311G(d,p) level.

Atom	x (Å)	y (Å)	z (Å)
C	0.702793	1.235505	0.155918
C	1.477346	0.127875	−0.181499
C	1.130943	−1.205663	0.056114
C	−0.702979	1.235473	0.155735
C	−1.130840	−1.205718	0.056499
C	−1.477392	0.127662	−0.181658
H	1.173860	2.213247	0.098963
H	2.339493	0.326879	−0.817518
H	0.929665	−1.509290	1.067826
H	1.624356	−1.976023	−0.532808
H	−1.174068	2.213170	0.098273
H	−0.928741	−1.508632	1.068230
H	−1.624414	−1.976562	−0.531662
H	−2.339379	0.326406	−0.817963

Table C.28: **23a/24a** B3LYP/6-311G(d,p) level.

Atom	x (Å)	y (Å)	z (Å)
C	0.000000	−1.290707	0.243191
C	1.230117	−0.677789	−0.216533
C	1.230117	0.677789	−0.216533
C	0.000000	1.290707	0.243191
C	−1.230117	0.677789	−0.216533
C	−1.230117	−0.677789	−0.216533
H	0.000000	−2.361408	0.424139
H	2.115034	−1.274426	−0.399819
H	2.115034	1.274426	−0.399819
H	0.000000	2.361408	0.424139
H	−2.115034	1.274426	−0.399819
H	−2.115034	−1.274426	−0.399819
H	0.000000	−0.495983	1.514755
H	0.000000	0.495983	1.514755

Table C.29: **30a/32a** B3LYP/6-311G(d,p) level.

Atom	x (Å)	y (Å)	z (Å)
C	0.406145	0.163992	−0.122265
C	−1.429349	−0.960618	−0.358464
C	−1.772866	0.294213	0.208866
C	−0.651270	1.081424	0.072372
C	1.835658	0.216148	−0.508057
C	1.383053	−0.584776	0.712158
H	−1.803278	−1.907515	0.035887
H	−1.132248	−0.997700	−1.397369
H	−2.702833	0.526897	0.720120
H	−0.577292	2.163639	−0.001526
H	2.379292	1.144908	−0.352873
H	2.162247	−0.342877	−1.379930
H	1.437013	−1.666128	0.651904
H	1.608869	−0.183522	1.696128

Table C.30: **29a/31a** B3LYP/6-311G(d,p) level.

Atom	x (Å)	y (Å)	z (Å)
C	0.934573	−0.039334	0.006513
C	0.982971	1.371060	−0.237596
C	−0.220650	−0.077874	0.916867
C	1.844701	−0.996128	−0.234142
C	−1.567183	−0.090464	0.483107
C	−1.952917	−0.242390	−0.813815
H	0.082414	1.905563	−0.503863
H	1.891991	1.947287	−0.092157
H	−0.002890	−0.027548	1.977872
H	2.748825	−0.780747	−0.793438
H	1.708496	−2.004154	0.139075
H	−2.333677	0.031046	1.244442
H	−2.998787	−0.229188	−1.094314
H	−1.225348	−0.391482	−1.603217

Table C.31: **30a/31a** B3LYP/6-311G(d,p) level.

Atom	x (Å)	y (Å)	z (Å)
C	0.854457	−0.120897	−0.110010
C	0.884021	1.339634	−0.031103
C	−0.213373	−0.972203	−0.006788
C	2.219127	−0.433992	0.061180
C	−1.611907	−0.625886	−0.058237
C	−2.192192	0.584842	0.068182
H	1.432533	1.929035	−0.756267
H	0.538912	1.838619	0.866036
H	0.019890	−2.031355	0.058249
H	2.984870	0.157914	−0.424086
H	2.553320	−1.231076	0.720023
H	−2.274253	−1.470031	−0.243038
H	−3.260479	0.698861	−0.074793
H	−1.635593	1.479042	0.314532

Table C.32: **1c/3c** B3LYP/6-311G(d,p) level.

Atom	x (Å)	y (Å)	z (Å)
C	0.895989	−1.044812	−0.373470
C	0.895964	1.044776	−0.373491
C	−0.073003	−0.000027	−0.105849
C	−1.413856	−0.000016	0.043380
C	2.239340	−0.773103	0.252724
C	2.239310	0.773124	0.252735
C	−2.200089	−1.281015	0.109746
C	−2.200024	1.281055	0.109738
H	3.060871	−1.159787	−0.354833
H	2.339079	−1.225654	1.250042
H	3.060848	1.159860	−0.354779
H	2.338982	1.225657	1.250068
H	−2.904047	−1.267366	0.951435
H	−2.803504	−1.443466	−0.794584
H	−1.549008	−2.150910	0.229499
H	−1.548868	2.150886	0.229528
H	−2.803419	1.443559	−0.794606
H	−2.904005	1.267410	0.951416
H	0.705653	−1.888506	−1.028097
H	0.705619	1.888431	−1.028167

Table C.33: **1c/4c** B3LYP/6-311G(d,p) level.

Atom	x (Å)	y (Å)	z (Å)
C	0.009854	0.029686	−0.060421
C	−0.885615	−1.142666	−0.233031
C	−0.857116	1.174729	0.032179
C	1.376559	0.004495	0.009104
H	−0.503435	2.130638	0.402407
H	−0.727001	−1.858786	−1.031408
C	−2.152808	−0.971708	0.352866
C	−2.246740	0.953776	−0.187567
H	−2.231329	−0.715015	1.406056
H	−2.980785	−1.587666	0.005178
H	−2.603542	0.642945	−1.164669
H	−2.944063	1.639307	0.297403
C	2.225630	1.245444	0.025775
H	2.842854	1.291491	0.932994
H	2.926382	1.253814	−0.820372
H	1.642361	2.165308	−0.030742
C	2.125868	−1.298739	0.038898
H	1.473748	−2.133804	0.307633
H	2.581060	−1.537457	−0.933450
H	2.949955	−1.260877	0.762153

Table C.34: **1c/7c** B3LYP/6-311G(d,p) level.

Atom	x (Å)	y (Å)	z (Å)
C	−0.051967	−0.165202	−0.272566
C	0.799170	−1.226779	−0.220073
C	2.218787	−0.796082	0.016402
C	0.751616	1.105063	−0.210412
C	2.086571	0.721430	0.392429
C	−1.450825	−0.004872	−0.111253
C	−2.408484	−1.111708	0.198451
C	−1.763129	1.396617	0.040901
H	−0.546801	1.757544	0.414830
H	2.812272	−0.882986	−0.903537
H	2.722800	−1.413886	0.769352
H	0.792184	1.695165	−1.128256
H	2.077559	0.809714	1.485165
H	2.923074	1.318813	0.023662
H	−3.069622	−0.826068	1.025408
H	−3.062826	−1.342745	−0.652286
H	−1.894744	−2.035489	0.478860
H	−2.642161	1.640543	0.643714
H	−1.718632	2.038681	−0.845184
H	0.516465	−2.270093	−0.315010

Table C.35: **1c/12c** B3LYP/6-311G(d,p) level.

Atom	x (Å)	y (Å)	z (Å)
C	0.043523	0.039999	−0.513972
C	0.502733	−1.039138	0.287212
C	1.902483	−0.700660	0.745784
C	1.019159	0.936025	−0.802343
C	2.347947	0.387977	−0.285975
C	−1.318165	0.056262	−0.019756
H	0.033075	−2.007806	0.371630
H	2.547874	−1.584968	0.766737
H	0.881252	1.943062	−1.171302
H	2.961645	1.162384	0.182094
H	2.960135	−0.058309	−1.083304
H	1.905144	−0.284248	1.763080
C	−1.791730	1.212672	0.801571
H	−2.265881	1.977106	0.165628
H	−2.542474	0.903782	1.537007
H	−0.955397	1.700240	1.308343
C	−2.327322	−0.929028	−0.517720
H	−3.086597	−1.157236	0.236302
H	−2.853322	−0.519796	−1.394633
H	−1.857221	−1.858859	−0.850390

Table C.36: **1c/2c** B3LYP/6-311G(d,p) level.

Atom	x (Å)	y (Å)	z (Å)
C	0.314278	0.169011	−0.089995
C	−0.689878	−0.890089	−0.509007
C	−1.782789	−0.073722	−1.223532
C	−0.521011	1.236180	0.355589
C	−1.806676	1.275008	−0.442230
C	1.667239	0.032785	−0.072790
N	−1.358138	−1.346909	0.822077
N	−1.468956	−0.512504	1.645518
H	−0.343774	−1.769656	−1.042625
H	−2.743774	−0.591684	−1.230758
H	−1.476297	0.080359	−2.261499
H	−0.202655	2.050620	0.990250
H	−1.835579	2.126547	−1.133171
H	−2.688463	1.367962	0.199477
C	2.385752	−1.242022	−0.420056
H	3.058559	−1.091403	−1.273120
H	3.019705	−1.556774	0.418244
H	1.715856	−2.067198	−0.656747
C	2.569395	1.173194	0.313971
H	2.025251	2.103713	0.469862
H	3.115928	0.934920	1.234899
H	3.327038	1.346417	−0.459665

Table C.37: **4c/6c** B3LYP/6-311G(d,p) level.

Atom	x (Å)	y (Å)	z (Å)
C	0.805532	−0.749234	0.127937
C	−0.347341	0.070805	0.051950
C	−1.693544	−0.522634	−0.025627
C	−2.830056	0.122217	0.253422
C	−0.184984	1.432012	−0.261003
C	1.026648	2.151236	−0.160289
C	2.081574	−0.173678	0.345310
C	0.730361	−2.210919	−0.263721
H	−1.757297	−1.571748	−0.296869
H	−3.790992	−0.371758	0.169416
H	−2.836752	1.154222	0.587638
H	−0.992383	1.865742	−0.845536
H	1.109921	3.039383	−0.785999
H	1.477879	2.306329	0.816133
H	2.250903	0.396309	1.254732
H	1.901895	1.054303	−0.338275
H	2.941519	−0.792406	0.090843
H	0.063280	−2.399183	−1.108655
H	0.378271	−2.822522	0.574843
H	1.724618	−2.577503	−0.526142

Table C.38: **4c/33c** B3LYP/6-311G(d,p) level.

Atom	x (Å)	y (Å)	z (Å)
C	−0.888266	−0.366068	−0.008279
C	0.463427	0.138788	0.137799
C	0.326127	1.511763	0.022505
C	−0.878904	1.716737	−0.691584
C	1.667954	−0.673448	0.243995
C	2.918589	−0.226632	0.066206
H	0.946988	2.287836	0.463931
H	−0.995989	1.267247	−1.669072
H	1.527339	−1.715790	0.523875
H	3.777332	−0.865654	0.235164
H	3.117323	0.792386	−0.249149
H	−1.526022	2.579655	−0.520389
C	−1.138557	−1.607273	−0.835849
H	−1.069514	−2.509636	−0.210552
H	−2.150867	−1.599182	−1.250970
H	−0.427194	−1.708573	−1.657275
C	−1.914679	−0.173905	1.094637
H	−2.932468	−0.091588	0.702064
H	−1.901250	−1.058213	1.750755
H	−1.699832	0.701743	1.705026

Table C.39: **6c/35c** B3LYP/6-311G(d,p) level.

Atom	x (Å)	y (Å)	z (Å)
C	−1.088994	0.738177	−0.289614
C	−0.130442	−0.337432	−0.201444
C	−0.921643	−1.467155	−0.310230
C	−2.226622	−1.048548	0.057250
C	1.322232	−0.253370	0.018913
C	1.981006	−1.262053	0.609021
H	−0.648377	−2.435043	−0.721762
H	−2.391092	−0.638840	1.045246
H	3.061149	−1.252921	0.707584
H	1.454152	−2.119458	1.011149
H	−3.127752	−1.459589	−0.403781
C	−1.036692	2.020722	0.498804
H	−0.597623	2.837143	−0.089432
H	−2.048360	2.343137	0.763763
H	−0.464069	1.914713	1.422699
C	2.053046	0.967584	−0.491431
H	1.862496	1.119618	−1.558693
H	1.723079	1.875509	0.022119
H	3.130161	0.873577	−0.342058
H	−1.665112	0.794596	−1.204447

Table C.40: **6c/36c** B3LYP/6-311G(d,p) level.

Atom	x (Å)	y (Å)	z (Å)
C	−1.393818	−0.353702	−0.384739
C	−0.092575	0.221794	−0.174031
C	0.724842	−0.886611	0.035119
C	−0.171915	−1.906649	0.454918
C	0.198764	1.648156	−0.129496
C	1.335048	2.212163	0.302820
H	−0.765423	−1.761306	1.347937
H	−0.584491	2.303351	−0.506395
H	1.481984	3.284802	0.256689
H	2.147843	1.625054	0.714765
H	−0.005258	−2.957909	0.200978
C	−2.682437	0.268186	0.084748
H	−3.075665	0.966562	−0.667426
H	−3.452589	−0.494362	0.230312
H	−2.560223	0.817128	1.021213
C	2.183250	−1.085933	−0.255134
H	2.790428	−1.038730	0.656572
H	2.345657	−2.081334	−0.683964
H	2.568148	−0.338149	−0.952065
H	−1.497381	−1.029525	−1.223851

Table C.41: **33c/34c** B3LYP/6-311G(d,p) level.

Atom	x (Å)	y (Å)	z (Å)
C	−0.970194	0.081881	0.016120
C	0.474556	0.170480	−0.492628
C	−0.423348	−1.179877	0.856802
C	0.861289	−1.094702	0.017272
C	1.616359	0.923221	−0.602706
C	2.540512	0.117312	0.168327
H	−1.007210	−2.104060	0.793946
H	−0.291866	−0.915935	1.909796
H	1.319677	−1.912802	−0.522435
H	1.823715	1.853339	−1.121038
H	3.585213	−0.035172	−0.122627
H	2.396681	0.095866	1.242728
C	−2.000046	−0.344826	−1.035620
H	−2.941044	−0.638728	−0.559245
H	−2.215114	0.478908	−1.722928
H	−1.637726	−1.189615	−1.626962
C	−1.470676	1.267806	0.838222
H	−1.665637	2.129974	0.192341
H	−2.403951	1.020829	1.355223
H	−0.733452	1.569637	1.586469

Table C.42: **5c/35c** B3LYP/6-311G(d,p) level.

Atom	x (Å)	y (Å)	z (Å)
C	−0.980067	0.700976	0.454667
C	0.010044	−0.232724	−0.021057
C	−0.735240	−1.350353	−0.366933
C	−1.918733	−1.265064	0.403806
C	1.468112	−0.057248	−0.001127
C	2.295501	−1.109919	−0.096808
H	−0.522688	−2.093746	−1.130939
H	−1.844211	−1.199111	1.481120
H	3.370288	−0.981721	−0.161485
H	1.918504	−2.125897	−0.110329
H	−2.884883	−1.628224	0.046153
C	−1.977231	1.410036	−0.440003
H	−2.913226	1.630040	0.081728
H	−1.558775	2.376970	−0.754608
H	−2.202803	0.831759	−1.336549
C	1.999509	1.353896	0.096879
H	1.639565	1.971622	−0.732317
H	1.662824	1.836932	1.020327
H	3.090755	1.368663	0.091527
H	−0.726709	1.315111	1.328828

Table C.43: **5c/36c** B3LYP/6-311G(d,p) level.

Atom	x (Å)	y (Å)	z (Å)
C	−1.166407	−0.957646	−0.319419
C	0.158953	−0.435681	−0.127601
C	−0.016089	0.949629	−0.125865
C	−1.213003	1.152480	−0.857948
C	1.362785	−1.252429	−0.103209
C	2.629357	−0.823892	−0.002567
H	−1.295205	0.769093	−1.866180
H	1.190813	−2.326652	−0.150022
H	3.453999	−1.525390	0.038680
H	2.882896	0.228371	0.048269
H	−1.888655	1.984845	−0.639705
C	−2.260567	−0.916594	0.726641
H	−3.256682	−0.863053	0.277489
H	−2.231077	−1.843681	1.317311
H	−2.140362	−0.076207	1.411369
H	−1.271789	−1.835488	−0.972006
C	0.775103	2.033590	0.543761
H	1.514626	2.469741	−0.139051
H	0.111556	2.850768	0.846094
H	1.309098	1.670912	1.424998

Table C.44: **35c/37c** B3LYP/6-311G(d,p) level.

Atom	x (Å)	y (Å)	z (Å)
C	−1.400750	0.418373	−0.431799
C	0.044415	−0.071197	−0.485386
C	−1.726641	−1.068166	0.076424
C	−0.288727	−1.438532	−0.325609
C	1.337666	0.093244	−0.046319
C	1.540029	−1.173967	0.633887
H	−2.546451	−1.600301	−0.416459
H	−1.904039	−1.068526	1.155972
H	−0.006515	−2.267344	−0.961430
H	2.495464	−1.711356	0.590607
H	1.017080	−1.323823	1.571688
C	−1.760759	1.590890	0.470407
H	−1.377806	2.531158	0.062305
H	−2.845776	1.690952	0.573768
H	−1.333957	1.461050	1.469271
H	−1.835992	0.555343	−1.427498
C	2.337470	1.197422	−0.204338
H	2.559495	1.694056	0.746818
H	3.288349	0.796168	−0.576054
H	1.993934	1.954218	−0.912598

Table C.45: **36c/38c** B3LYP/6-311G(d,p) level.

Atom	x (Å)	y (Å)	z (Å)
C	−1.346252	−0.413704	−0.398848
C	−0.081338	0.418069	−0.549789
C	−0.475813	−1.257959	0.647756
C	0.769857	−0.520746	0.111023
C	0.474149	1.660810	−0.390080
C	1.454616	1.394153	0.640395
H	−0.493777	−2.349580	0.550613
H	−0.745674	−0.986892	1.672225
H	0.259915	2.610663	−0.869422
H	2.447510	1.855759	0.652636
H	1.075453	1.187793	1.635419
C	−2.630616	0.249194	0.078257
H	−3.055197	0.884636	−0.704773
H	−3.385085	−0.496727	0.346929
H	−2.443154	0.877702	0.953722
C	1.994847	−1.237005	−0.379003
H	2.620179	−1.579186	0.450868
H	1.706652	−2.130121	−0.951579
H	2.599084	−0.591127	−1.018689
H	−1.542609	−1.039784	−1.276215

Table C.46: **9c/14c** B3LYP/6-311G(d,p) level.

Atom	x (Å)	y (Å)	z (Å)
C	−0.092872	1.501561	−0.061865
H	0.625763	2.297281	−0.136447
C	−1.332310	1.303742	0.026362
H	−2.828851	0.220427	−0.973744
C	−2.276601	0.295206	−0.038173
H	−2.915649	0.132552	0.828077
C	0.940862	−0.175086	−0.029433
C	0.016061	−1.050575	−0.637621
H	0.100081	−1.171429	−1.715733
H	−1.252611	−1.528477	1.020624
C	−1.218346	−1.368055	−0.051702
H	−1.873559	−2.039490	−0.599250
C	1.212564	−0.275738	1.469312
H	1.683932	0.636233	1.844453
H	0.306103	−0.438228	2.051218
H	1.899604	−1.108173	1.662984
C	2.196677	0.152525	−0.827298
H	2.659870	1.079624	−0.477719
H	2.940621	−0.642826	−0.709988
H	1.978481	0.261025	−1.891963

Table C.47: **10c/20c**$_1$ B3LYP/6-311G(d,p) level.

Atom	x (Å)	y (Å)	z (Å)
C	−1.554729	0.058375	0.094953
C	−0.596986	1.190044	0.015116
C	−0.664168	−1.199093	0.025196
C	0.749093	0.696798	−0.034808
C	0.754853	−0.669179	−0.044869
C	−2.944075	0.040074	−0.154557
H	−1.385551	0.525869	1.189724
H	−0.902326	2.227764	0.014119
H	−0.924044	−1.789618	−0.859742
H	−0.803610	−1.863640	0.888994
H	−3.510494	0.959891	−0.230650
H	−3.496065	−0.885135	−0.054058
C	1.920425	−1.601935	−0.012191
H	2.875196	−1.078872	−0.087890
H	1.937022	−2.189083	0.916306
H	1.871579	−2.327968	−0.833670
C	1.936066	1.619518	−0.031420
H	2.869570	1.086896	−0.217210
H	1.835522	2.391047	−0.800962
H	2.030331	2.135230	0.930520

Table C.48: **11c/20c**$_2$ B3LYP/6-311G(d,p) level.

Atom	x (Å)	y (Å)	z (Å)
C	1.529922	−0.056508	0.101138
C	0.701651	1.142873	0.366872
C	−0.752996	0.766363	0.434012
C	0.522563	−1.152031	−0.093043
C	−0.729383	−0.720192	0.090587
C	2.876122	−0.172669	−0.366485
H	1.106410	2.118967	0.596523
H	1.638393	0.089680	1.262473
H	−1.174470	0.901385	1.445886
H	0.812320	−2.165589	−0.343041
H	3.552819	0.672046	−0.331057
H	3.305445	−1.158649	−0.487017
C	−1.982604	−1.536451	0.015199
H	−2.655562	−1.168861	−0.766837
H	−1.761568	−2.584486	−0.196582
H	−2.540175	−1.490368	0.957972
C	−1.624854	1.612317	−0.524072
H	−2.676468	1.316979	−0.463622
H	−1.561491	2.671916	−0.262872
H	−1.288182	1.494772	−1.557075

Table C.49: **11c/31c** B3LYP/6-311G(d,p) level.

Atom	x (Å)	y (Å)	z (Å)
C	−1.668319	0.014718	0.108311
C	−1.314573	−1.177822	0.800947
C	0.940558	−0.712040	−0.444360
C	−0.607385	1.043466	0.140675
C	0.683780	0.645848	−0.046295
C	−2.855225	0.182181	−0.546386
H	−1.944523	−2.060017	0.731818
H	−0.587526	−1.151220	1.599287
H	0.256218	−1.166653	−1.148372
H	−0.862421	2.083699	0.313188
H	−3.634916	−0.568569	−0.497020
H	−3.065729	1.082806	−1.109578
C	2.246482	−1.408532	−0.224191
H	2.131885	−2.491000	−0.316067
H	2.996216	−1.105755	−0.971567
H	2.676950	−1.193265	0.758194
C	1.840672	1.590234	0.189850
H	2.468303	1.246392	1.018924
H	2.487611	1.665039	−0.689870
H	1.481984	2.590217	0.439747

Table C.50: **14c/15c** B3LYP/6-311G(d,p) level.

Atom	x (Å)	y (Å)	z (Å)
C	−0.059572	−0.918138	−0.752343
C	0.913853	−0.068482	0.059433
C	0.097537	1.031715	−0.555891
C	−1.315812	−1.184834	−0.316537
C	−2.383144	−0.655077	0.102551
C	−1.035244	1.659613	0.008094
C	0.845171	−0.208310	1.575431
C	2.349663	−0.150637	−0.452981
H	0.255470	−1.200834	−1.751157
H	−3.250577	−0.871702	0.700062
H	−2.030839	0.684809	−0.068753
H	−1.062776	1.792025	1.087257
H	−1.428624	2.510083	−0.542719
H	0.380219	1.305147	−1.567282
H	1.326540	−1.139516	1.885376
H	1.368826	0.624421	2.053952
H	−0.181446	−0.225620	1.940694
H	2.959378	0.644775	−0.015045
H	2.797487	−1.112610	−0.188024
H	2.391629	−0.046092	−1.540894

Table C.51: **15c/15c-trans** CASSCF/6-311G(d,p) level.

Atom	x (Å)	y (Å)	z (Å)
C	2.790774	0.563086	−0.772028
C	1.605076	0.157520	0.054718
C	0.883958	−1.163466	−0.156875
C	−0.559828	−1.088909	0.316098
C	−1.425493	−0.019883	0.033499
C	−2.200397	0.893726	−0.180084
C	1.596517	−2.268715	0.650328
C	0.877773	−1.552875	−1.655528
H	2.502132	0.891373	−1.771693
H	3.318272	1.387771	−0.299330
H	3.498677	−0.254172	−0.897050
H	1.090848	0.928868	0.599787
H	−2.872269	1.684905	−0.362801
H	−1.004182	−1.981549	0.718101
H	1.675027	−1.997106	1.698476
H	1.054969	−3.209839	0.582580
H	2.600179	−2.436084	0.271327
H	0.272508	−2.437801	−1.820497
H	0.473677	−0.752820	−2.266972
H	1.882904	−1.769355	−2.002958

Table C.52: **15c/16c** B3LYP/6-311G(d,p) level.

Atom	x (Å)	y (Å)	z (Å)
C	0.401347	0.160733	−1.244364
C	−0.321009	1.115592	−0.298208
C	−0.921463	−0.142544	0.258119
C	1.493675	−0.523617	−0.838996
C	1.976017	−1.275658	0.054385
C	−0.343742	−0.857114	1.336374
C	−2.192903	−0.662550	−0.374633
C	0.515263	2.009892	0.602614
H	−0.079332	−0.064514	−2.189229
H	−1.057735	1.707296	−0.844157
H	2.915070	−1.538049	0.508595
H	0.787896	−1.437393	0.811565
H	0.156223	−0.284817	2.114442
H	−0.938655	−1.680956	1.725463
H	−2.212025	−1.755070	−0.403764
H	−3.057877	−0.335909	0.215948
H	−2.337744	−0.292011	−1.391730
H	0.963950	2.815165	0.015591
H	−0.107967	2.457829	1.381744
H	1.325086	1.460028	1.083786

Table C.53: **16c/17c** B3LYP/6-311G(d,p) level.

Atom	x (Å)	y (Å)	z (Å)
C	1.374625	−0.403409	−0.083082
C	0.371949	−0.986394	−0.777318
C	0.396529	0.621593	1.134658
C	−1.038783	−0.519909	−0.437472
C	−0.641012	0.788683	0.206014
C	2.716827	−0.247906	−0.079831
H	0.946386	1.504106	1.451961
H	0.317987	−0.129606	1.916655
H	3.279941	−0.203215	0.845365
H	3.259272	−0.057423	−0.999915
H	−1.615175	−0.331879	−1.353530
H	0.561642	−1.768820	−1.509049
C	−0.941358	2.093535	−0.454767
H	−1.914659	2.485289	−0.128783
H	−0.191689	2.850972	−0.209339
H	−0.997624	1.991025	−1.544376
C	−1.830486	−1.516722	0.426081
H	−2.810234	−1.108058	0.693404
H	−1.988950	−2.453514	−0.117068
H	−1.296641	−1.755708	1.348971

Table C.54: **10c/17c** B3LYP/6-311G(d,p) level.

Atom	x (Å)	y (Å)	z (Å)
C	−1.571593	0.026569	−0.002744
C	−0.715543	1.166246	0.069950
C	−0.672361	−1.220288	0.000635
C	0.713098	0.709323	0.124725
C	0.748696	−0.699776	−0.018961
C	−2.926220	0.020187	−0.090525
H	−0.879545	−1.872095	−0.859098
H	−0.863409	−1.839914	0.891698
H	−3.495455	0.942118	−0.070318
H	−3.482075	−0.902669	−0.204910
H	0.245254	0.912278	1.226106
H	−1.006996	2.206003	0.097311
C	1.938648	−1.593616	−0.003750
H	2.875690	−1.033470	−0.040050
H	1.970151	−2.229555	0.895211
H	1.935766	−2.282296	−0.859675
C	1.859124	1.655954	−0.146833
H	2.805167	1.266799	0.234312
H	1.965621	1.815371	−1.223796
H	1.686728	2.629835	0.318231

Table C.55: **11c/17c** B3LYP/6-311G(d,p) level.

Atom	x (Å)	y (Å)	z (Å)
C	1.569088	0.043887	0.035005
C	0.699937	1.172215	0.004935
C	0.689160	−1.218786	0.046605
C	−0.663538	0.755949	−0.158532
C	−0.728453	−0.726713	−0.108006
C	2.927968	0.029243	0.029877
H	0.771239	−1.737580	1.016409
H	0.988884	−1.953193	−0.710048
H	3.496767	0.951398	0.011082
H	3.488347	−0.897677	0.060140
H	−0.729327	0.326656	−1.276053
H	1.024431	2.201665	−0.060500
C	−1.943957	−1.570319	0.035700
H	−2.079473	−1.889238	1.083031
H	−2.852698	−1.037714	−0.253310
H	−1.885256	−2.486196	−0.562732
C	−1.846857	1.655486	0.126184
H	−2.764024	1.299568	−0.348746
H	−2.024596	1.708417	1.204068
H	−1.654384	2.668121	−0.233947

Table C.56: **17c/27c** B3LYP/6-311G(d,p) level.

Atom	x (Å)	y (Å)	z (Å)
C	−0.826424	−0.614440	0.074006
C	0.554694	0.682697	−0.906276
C	0.429664	−0.831693	0.877446
C	1.390724	−0.047160	−0.014940
C	2.738137	−0.185726	−0.041396
C	−0.868976	0.799527	−0.424383
C	−1.168904	1.916959	0.591442
C	−1.775876	−1.690766	−0.311420
H	0.896356	1.093810	−1.851064
H	0.718036	−1.885063	0.933082
H	0.374711	−0.452292	1.908165
H	3.260097	−0.778048	0.700478
H	3.336480	0.281893	−0.815604
H	−1.565363	0.895031	−1.266029
H	−1.043811	2.899568	0.125666
H	−2.196764	1.843068	0.962558
H	−0.491556	1.866553	1.447680
H	−2.534781	−1.851809	0.471489
H	−2.319866	−1.436618	−1.225751
H	−1.271772	−2.652479	−0.457543

Table C.57: **20c**$_1$**/21c**$_2$ B3LYP/6-311G(d,p) level.

Atom	x (Å)	y (Å)	z (Å)
C	−1.584714	0.014590	−0.416323
C	−0.536587	−1.241960	0.480640
C	0.761038	−0.700295	0.180711
C	−0.599541	1.120539	−0.188088
C	0.682172	0.725510	0.086133
C	−2.911464	0.104353	0.045796
H	−1.510390	−0.372460	−1.437651
H	−0.741550	−2.274675	0.195095
H	−0.925953	−1.011592	1.466190
H	−0.900781	2.157203	−0.296165
H	−3.147516	0.613149	0.973884
H	−3.717681	−0.414706	−0.456817
C	1.929916	−1.519952	−0.278636
H	2.636518	−1.710390	0.540870
H	1.597036	−2.499943	−0.633020
H	2.496857	−1.039119	−1.082478
C	1.868529	1.647170	0.137095
H	2.356315	1.615001	1.116330
H	2.622341	1.358265	−0.603114
H	1.578715	2.679535	−0.067103

Table C.58: **20c$_1$/22c$_1$** B3LYP/6-311G(d,p) level.

Atom	x (Å)	y (Å)	z (Å)
C	0.563071	−0.696312	0.122679
C	0.490515	0.687977	0.080424
C	−0.795700	1.287218	0.594576
C	−0.625942	−1.459897	0.166100
C	−1.775535	0.645967	−0.331910
C	−1.809358	−0.816056	−0.280169
H	−0.819024	2.375372	0.510482
H	−0.985043	1.020862	1.649424
H	−0.600642	−2.534443	0.293135
H	−2.368523	1.196361	−1.053395
H	−2.560287	−0.289035	0.520186
H	−2.501246	−1.348744	−0.928982
C	1.625528	1.591847	−0.311237
H	2.138387	2.005181	0.570606
H	2.377498	1.088867	−0.922679
H	1.257994	2.450321	−0.882576
C	1.887832	−1.424434	0.011917
H	2.275856	−1.389914	−1.012121
H	2.652422	−0.995444	0.665189
H	1.770136	−2.477253	0.276454

Table C.59: **20c$_1$/23c** B3LYP/6-311G(d,p) level.

Atom	x (Å)	y (Å)	z (Å)
C	−1.873087	−0.699984	−0.340422
C	−0.768022	1.334399	−0.071044
C	0.475931	0.753442	−0.012301
C	−0.670046	−1.403491	−0.233483
C	0.583991	−0.659095	0.092130
C	−1.963278	0.577250	0.435388
H	−1.901600	0.403126	1.529608
H	−0.400866	−1.455497	0.953701
H	−2.700271	−1.077711	−0.925102
H	−0.876727	2.360186	−0.408808
H	−0.543445	−2.372187	−0.710242
H	−2.896918	1.108026	0.242989
C	1.734312	1.581024	−0.169319
H	2.310925	1.604931	0.761725
H	2.396630	1.192028	−0.949012
H	1.482753	2.612412	−0.422250
C	1.885148	−1.407142	0.187483
H	2.469613	−1.282401	−0.734114
H	2.516137	−1.072677	1.016025
H	1.714074	−2.478651	0.314879

Table C.60: **20c$_1$/26c** B3LYP/6-311G(d,p) level.

Atom	x (Å)	y (Å)	z (Å)
C	−1.506606	0.068075	0.085237
C	−0.604832	1.170267	0.011788
C	0.750637	0.702776	−0.017466
C	0.783375	−0.665201	−0.024321
C	−2.968346	0.035172	−0.147242
C	−0.636087	−1.192307	−0.032605
C	1.957332	−1.587765	0.011211
C	1.923325	1.642487	−0.019654
H	−0.900276	2.211811	0.019271
H	−3.527903	0.960605	−0.185684
H	−3.500632	−0.887161	0.041863
H	−2.076568	0.135746	1.125392
H	−0.817770	−1.919586	0.767792
H	−0.863809	−1.703296	−0.975546
H	2.906064	−1.048183	−0.007889
H	1.952923	−2.212373	0.915027
H	1.954174	−2.280025	−0.840998
H	1.944336	2.245091	0.894759
H	2.875669	1.115844	−0.094852
H	1.861011	2.340500	−0.860814

Table C.61: **20c$_1$/28c$_1$** B3LYP/6-311G(d,p) level.

Atom	x (Å)	y (Å)	z (Å)
C	−1.665517	−0.064730	1.194359
C	−1.594862	−0.441522	−0.286493
C	−0.426608	−1.402187	−0.392398
C	0.289946	0.727154	−0.056670
C	0.689670	−0.662614	−0.130160
C	−1.002492	0.853081	−0.852718
H	−1.260282	−0.746629	1.934795
H	−2.491504	0.563652	1.530416
H	−2.535557	−0.797271	−0.721230
H	−0.501989	−2.480215	−0.444227
H	−1.595991	1.734072	−0.598608
H	−0.821382	0.839964	−1.941409
C	1.214484	1.869729	0.200392
H	2.003457	1.611595	0.910688
H	1.704047	2.188605	−0.733785
H	0.674859	2.737765	0.586769
C	2.077164	−1.169679	0.132728
H	2.812310	−0.715724	−0.539988
H	2.394415	−0.938197	1.155684
H	2.126903	−2.253015	0.006666

Table C.62: **20c$_2$/21c$_4$** B3LYP/6-311G(d,p) level.

Atom	x (Å)	y (Å)	z (Å)
C	−1.347204	−0.143844	0.407513
C	0.110767	0.678708	−0.430674
C	1.093833	−0.366901	−0.218414
C	−0.885774	−1.530667	0.075021
C	0.450607	−1.629028	−0.200357
C	−2.603866	0.339882	−0.008589
H	−1.116577	0.099726	1.450251
H	−0.334049	0.625160	−1.421257
H	−1.571772	−2.369300	0.103461
H	0.975366	−2.574644	−0.291593
H	−3.034811	0.035739	−0.956050
H	−3.136767	1.088640	0.563431
C	0.381209	2.103340	0.000352
H	1.154418	2.560571	−0.627421
H	−0.521465	2.710085	−0.097458
H	0.719825	2.160719	1.038392
C	2.503909	−0.135959	0.233450
H	3.023080	0.604952	−0.383525
H	2.545608	0.231376	1.268797
H	3.076258	−1.066211	0.203160

Table C.63: **20c$_2$/22c$_2$** B3LYP/6-311G(d,p) level.

Atom	x (Å)	y (Å)	z (Å)
C	−0.827330	1.332154	−0.243968
C	0.424309	0.781361	−0.048903
C	0.536933	−0.687360	−0.423199
C	−1.990858	0.542236	−0.297883
C	−0.510084	−1.239895	0.495214
C	−1.873135	−0.745849	0.287546
H	−0.934300	2.413993	−0.273296
H	0.219054	−0.814793	−1.473758
H	−2.959940	0.958233	−0.537466
H	−0.272741	−1.907706	1.317195
H	−1.599352	−1.716315	−0.395793
H	−2.671710	−1.127718	0.919791
C	1.614123	1.589470	0.391105
H	2.396427	1.630787	−0.378326
H	1.319397	2.614738	0.625755
H	2.083932	1.176905	1.290126
C	1.903140	−1.348362	−0.242710
H	1.853026	−2.402530	−0.528403
H	2.661959	−0.869432	−0.865485
H	2.241659	−1.298689	0.796444

Table C.64: **20c$_2$/23c** B3LYP/6-311G(d,p) level.

Atom	x (Å)	y (Å)	z (Å)
C	0.866785	1.295601	−0.021400
C	1.804989	−0.796765	−0.370048
C	0.580584	−1.407608	−0.312210
C	−0.433873	0.781402	0.094546
C	−0.576909	−0.713292	0.102413
C	2.001078	0.443700	0.454868
H	1.930473	0.221098	1.538529
H	−0.466939	0.303557	1.226453
H	1.035855	2.278490	−0.441646
H	2.626180	−1.230539	−0.930245
H	0.454428	−2.426240	−0.669184
H	2.968224	0.916274	0.277808
C	−1.923223	−1.377835	0.245421
H	−2.548589	−0.902462	1.004198
H	−2.487150	−1.353928	−0.696356
H	−1.808212	−2.424246	0.535754
C	−1.633207	1.623678	−0.298674
H	−1.880161	1.461010	−1.352129
H	−2.520482	1.379482	0.288737
H	−1.420976	2.684225	−0.151422

Table C.65: **20c$_2$/25c** B3LYP/6-311G(d,p) level.

Atom	x (Å)	y (Å)	z (Å)
C	0.710910	1.118584	0.383641
C	1.494694	−0.045197	0.103730
C	0.500515	−1.149266	−0.096631
C	−0.750713	−0.715895	0.094339
C	2.890838	−0.158088	−0.390752
C	−0.750047	0.768247	0.438784
C	−2.008408	−1.523260	0.008472
C	−1.622795	1.624180	−0.505434
H	1.107331	2.105468	0.581546
H	0.788591	−2.162343	−0.352949
H	2.139698	−0.231749	1.069192
H	3.331062	−1.146740	−0.427798
H	3.558128	0.688841	−0.286265
H	−1.156008	0.897759	1.457712
H	−2.677215	−1.143761	−0.771898
H	−1.793816	−2.570798	−0.213211
H	−2.568908	−1.483490	0.949578
H	−2.677494	1.340419	−0.439669
H	−1.546215	2.682248	−0.241400
H	−1.295128	1.508322	−1.541729

Table C.66: **20c$_2$/28c$_2$** B3LYP/6-311G(d,p) level.

Atom	x (Å)	y (Å)	z (Å)
C	1.376655	−0.880681	−1.186798
C	1.329620	0.340070	−0.266308
C	1.255172	−0.255243	1.127976
C	−0.712826	−0.506114	0.006975
C	0.028444	−0.847172	1.190100
C	−0.116612	0.803279	−0.528275
H	1.702062	−1.833627	−0.784832
H	1.567951	−0.721322	−2.249235
H	2.126851	1.074663	−0.425453
H	2.080423	−0.354429	1.818615
H	−0.323594	−1.529568	1.955045
H	−0.282128	0.907135	−1.604359
C	−2.097406	−0.975874	−0.298567
H	−2.290043	−1.967099	0.118759
H	−2.845830	−0.288428	0.122921
H	−2.275663	−1.015867	−1.376358
C	−0.606917	2.075069	0.181163
H	−0.099093	2.957494	−0.220134
H	−1.681084	2.220226	0.031460
H	−0.416629	2.030813	1.255976

Table C.67: **21c$_1$/21c$_2$** B3LYP/6-311G(d,p) level.

Atom	x (Å)	y (Å)	z (Å)
C	−0.859409	1.051583	0.211453
C	0.399794	0.719011	−0.109780
C	0.915533	−0.682029	−0.102864
C	0.411962	−1.626701	−0.899720
C	−1.961084	0.162189	0.653452
C	−2.856857	−0.417894	−0.140214
H	−1.106145	2.114052	0.211853
H	0.802043	−2.639526	−0.886819
H	−0.398314	−1.418952	−1.586193
H	−2.065430	0.036149	1.731887
H	−3.662130	−1.021346	0.264292
H	−2.817398	−0.310190	−1.219220
C	2.065636	−0.971318	0.836888
H	2.331343	−2.029673	0.813270
H	2.958096	−0.394376	0.573730
H	1.805521	−0.703430	1.866623
C	1.406453	1.792333	−0.464651
H	2.220747	1.839093	0.265918
H	1.864263	1.589019	−1.438504
H	0.935236	2.776135	−0.504218

Table C.68: **21c$_1$/22c$_1$** B3LYP/6-311G(d,p) level.

Atom	x (Å)	y (Å)	z (Å)
C	0.619875	−1.378747	−0.050406
C	1.837937	−0.844810	0.375512
C	2.351352	0.426712	0.097910
C	−0.576954	−0.659095	−0.244223
C	0.503488	1.497212	−0.551781
C	−0.600776	0.743029	−0.139354
H	0.489522	−2.448356	0.102163
H	2.344679	−1.429467	1.144554
H	2.586936	0.710006	−0.912114
H	3.052606	0.846648	0.819348
H	0.909467	1.272292	−1.523481
H	0.548744	2.550999	−0.287757
C	−1.767844	1.424324	0.545664
H	−2.651256	1.441034	−0.103295
H	−2.062911	0.924447	1.474154
H	−1.522538	2.462648	0.777371
C	−1.874437	−1.440589	−0.193092
H	−2.355192	−1.365947	0.789782
H	−2.594876	−1.072915	−0.929379
H	−1.701027	−2.499601	−0.392730

Table C.69: **21c$_3$/21c$_4$** B3LYP/6-311G(d,p) level.

Atom	x (Å)	y (Å)	z (Å)
C	−1.587909	−0.796405	−0.611664
C	−0.323991	−1.236726	−0.544788
C	0.888277	−0.525160	−0.084672
C	1.140511	0.741538	−0.448277
C	−2.108629	0.543266	−0.237928
C	−2.752763	0.807941	0.895997
H	−2.336522	−1.498321	−0.976600
H	−0.159303	−2.278913	−0.817756
H	0.420463	1.220958	−1.105694
H	−1.987987	1.344364	−0.965749
H	−3.137488	1.799274	1.108712
H	−2.907826	0.046600	1.653816
C	1.799865	−1.367723	0.778402
H	1.293439	−1.657851	1.705456
H	2.064392	−2.296847	0.260896
H	2.725864	−0.859841	1.045227
C	2.309143	1.604091	−0.073706
H	2.844126	1.943777	−0.968116
H	1.966524	2.508141	0.443571
H	3.027291	1.103731	0.576054

Table C.70: **21c$_3$/22c$_2$** B3LYP/6-311G(d,p) level.

Atom	x (Å)	y (Å)	z (Å)
C	1.833748	−0.895209	−0.158417
C	2.088211	0.376818	0.352127
C	1.306415	1.520195	0.150414
C	0.547927	−1.414238	−0.387906
C	−0.703530	0.679439	−0.458594
C	−0.640638	−0.704070	−0.200734
H	2.626537	−1.633233	−0.066496
H	2.865757	0.424305	1.115224
H	1.181738	1.912549	−0.843096
H	1.361321	2.304563	0.905432
H	0.483563	−2.499542	−0.414153
H	−0.307279	0.960582	−1.420882
C	−1.854305	1.535960	0.007739
H	−1.637575	2.595580	−0.144818
H	−2.771237	1.309855	−0.553118
H	−2.074245	1.387579	1.067441
C	−1.810089	−1.420294	0.443087
H	−1.882104	−1.177732	1.510364
H	−2.768315	−1.153567	−0.012796
H	−1.684598	−2.502550	0.370597

Table C.71: **23c/8c$_1$** B3LYP/6-311G(d,p) level.

Atom	x (Å)	y (Å)	z (Å)
C	−0.619635	1.756872	−1.072003
C	1.050443	−0.248476	0.111069
C	0.165573	0.688410	0.775132
C	−1.085715	0.193417	1.285970
C	−1.711694	−0.732327	0.519811
C	−1.035391	−1.023487	−0.740831
C	0.417743	−1.173881	−0.650727
C	2.543105	−0.091096	0.216024
H	0.626390	1.522721	1.295643
H	−1.526380	0.626506	2.175926
H	−2.710362	−1.099056	0.723552
H	−1.553684	−1.673333	−1.441277
H	0.947032	−1.870613	−1.290850
H	−1.682337	1.996090	−1.142529
H	−0.153185	1.635465	−2.051837
H	−0.117308	2.568836	−0.552387
H	2.858625	0.899921	−0.130233
H	2.889257	−0.195598	1.249520
H	3.060746	−0.838755	−0.388699
H	−0.985370	0.211220	−1.113505

Table C.72: **23c/8c**$_2$ B3LYP/6-311G(d,p) level.

Atom	x (Å)	y (Å)	z (Å)
C	−0.372077	0.709532	0.138718
C	−0.564586	−0.724331	−0.093953
C	0.567958	−1.465253	0.019777
C	1.777113	−0.740766	0.348424
C	1.957163	0.523237	−0.332708
C	0.833185	1.270005	−0.449528
H	0.556775	−2.549273	0.014454
H	2.661782	−1.314934	0.607331
H	2.944250	0.889369	−0.586729
H	0.836640	2.293650	−0.807177
C	−1.580553	1.613066	0.278905
H	−1.277967	2.620148	0.572469
H	−2.126549	1.690725	−0.667879
H	−2.279347	1.241183	1.030717
C	−1.934110	−1.320150	−0.273951
H	−2.567446	−1.157289	0.605199
H	−2.459356	−0.883615	−1.129924
H	−1.863355	−2.397343	−0.437068
H	1.147151	−0.086890	1.534306
H	0.322868	0.462222	1.450200

Table C.73: **30c/32c** B3LYP/6-311G(d,p) level.

Atom	x (Å)	y (Å)	z (Å)
C	−1.166321	−0.288604	−0.163709
C	0.731234	0.701941	−0.563872
C	1.027131	−0.635667	−0.160134
C	−0.184209	−1.298628	−0.207462
C	−2.632648	−0.170828	−0.332212
C	−1.922544	0.480438	0.857082
H	0.285021	0.824634	−1.542718
H	−0.365714	−2.359898	−0.368032
H	−3.249748	−1.048424	−0.153501
H	−3.023168	0.488089	−1.102686
H	−1.867516	1.565308	0.876902
H	−2.054541	0.028754	1.836739
C	1.384233	1.933869	−0.003527
H	2.187341	2.302423	−0.656111
H	0.653143	2.746409	0.072322
H	1.802815	1.768249	0.991881
C	2.352195	−1.138394	0.339991
H	3.179725	−0.861230	−0.320122
H	2.580414	−0.732351	1.332836
H	2.337801	−2.226726	0.435545

Table C.74: **29c/31c** B3LYP/6-311G(d,p) level.

Atom	x (Å)	y (Å)	z (Å)
C	−1.747858	−0.088195	−0.038195
C	−1.817917	−0.074693	1.390003
C	−0.626674	0.844579	−0.224269
C	−2.634406	−0.517455	−0.952245
C	0.743992	0.484779	−0.142399
C	1.098369	−0.838923	−0.094049
H	−0.918964	−0.192156	1.977340
H	−2.748639	0.115308	1.916672
H	−0.892849	1.886297	−0.369582
H	−3.529815	−1.053219	−0.655556
H	−2.490320	−0.317940	−2.007463
H	0.299403	−1.570984	−0.168027
C	1.772702	1.598301	−0.093822
H	2.603755	1.418380	−0.779840
H	1.320161	2.554032	−0.364720
H	2.193677	1.709791	0.910842
C	2.482140	−1.388482	0.039967
H	2.560245	−2.032111	0.925050
H	2.736230	−2.023201	−0.818315
H	3.245037	−0.613663	0.123666

Table C.75: **30c/31c** B3LYP/6-311G(d,p) level.

Atom	x (Å)	y (Å)	z (Å)
C	1.685817	0.041280	0.079258
C	1.732881	−1.417754	0.235214
C	0.610971	0.854213	−0.160675
C	3.050065	0.356903	−0.091959
C	−0.800115	0.520710	−0.075576
C	−1.278080	−0.739593	−0.219860
H	2.184131	−1.871942	1.110570
H	1.569951	−2.054535	−0.625448
H	0.843432	1.898778	−0.356676
H	3.805229	−0.137890	0.505876
H	3.398796	1.045654	−0.857222
H	−0.580119	−1.509619	−0.525141
C	−1.697244	1.708685	0.217697
H	−1.568162	2.054089	1.249283
H	−1.432643	2.548621	−0.432391
H	−2.753941	1.493623	0.063956
C	−2.686232	−1.218103	−0.021561
H	−3.101545	−1.622472	−0.953138
H	−2.710164	−2.038557	0.705483
H	−3.363342	−0.443799	0.339622

CURRICULUM VITAE

Surname: Bozkaya

Name: Uğur

Date and place of birth: September 21th 1982, Kars

E-mail address: ubozkaya@ccqc.uga.edu

Education:

Ph.D: Middle East Technical University, Department of Chemistry, 2004-2011.

B.S.: Gazi University, Department of Chemistry, 1999-2003.

Awards and Degrees:

B.S. graduation with 1st rank, 2003.

TUBITAK undergraduate scholarship, 2001-2003.

TUBITAK Ph.D. scholarship, 2005-2009.

TUBITAK Ph.D. scholarship, 2009-2010.

Publications:

T. Çaykara, U. Bozkaya, and Ö. Kantoğlu, *Journal of Polymer Science: Part B: Polymer Physics*, **41**, 1656 (2003).

U. Bozkaya, J. M. Turney, Y. Yamaguchi, H. F. Schaefer III, *J. Chem. Phys.*, **132**, 064308 (2010).

U. Bozkaya and H. F. Schaefer III, *Mol. Phys.*, **108**, 2491 (2010).